Universidad de Concepción
Dirección de Postgrado
Facultad de Farmacia - Programa de Ciencias y Tecnología Analítica.

INCIDENCIA DEL ESTRÉS HÍDRICO SOBRE LA BIOSÍNTESIS DE METABOLITOS SECUNDARIOS Y LA PREDISPOSICIÓN A LA DEFOLIACIÓN: UN ANÁLISIS METABOLÓMICO EN ESPECIES FORESTALES DE INTERÉS COMERCIAL PARA CHILE

Tesis para optar al grado de Doctor en Ciencias y Tecnología Analítica

por

Jasna Valentina Campos Rivera

Profesor Guía: Dr. Andy Jorge Pérez de Armas
Profesor Co-Guía: Dr. Rafael Alejandro Rubilar Pons

Mayo 2023
Concepción, Chile.

AGRADECIMIENTOS

En esta oportunidad quisiera agradecer a todos quienes me acompañaron en este importante proceso de formación profesional y personal. Quisiera agradecerles a mis queridos padres, Guísela y Víctor, por siempre apoyar mi educación y siempre creer en mi. Este pequeño logro también es de ustedes. A mis hermanos, Carla, Martin y Matías, por su alegría y apoyo, siempre brindando una sonrisa. Quiero agradecer a quien ha sido mi compañero de vida, mi pilar fundamental en estos últimos años, Damián, gracias por tu compañía incondicional y por apoyarme con tanto amor en los momentos más difíciles.

No puedo dejar de mencionar a las hermosas personas que fui conociendo a lo largo de este proceso, compañeros y amigos. Gracias por la alegría y palabras de optimismo, Barbarita, Pedro, Silenne, Mario, Seba, Dani, Cami y Lia. A mi amigo de la vida, Ariel, por tantos años de cariño y amistad.

Mis agradecimientos también son a quienes participaron de este proceso formativo, a mi profesor guía Dr. Andy Pérez por su apoyo, disposición y compromiso en el desarrollo de está tesis doctoral. Agradecer al Departamento de Análisis Instrumental, a todos quienes allí trabajan por brindar un ambiente tan acogedor y en especial a la profesora Dr. Claudia Mardones, por siempre brindar apoyo a los alumnos del programa de doctorado.

Finalmente agradecer a Dios por darme la fortaleza para sobrellevar todas las dificultades, por todos los momentos alegres y por todo lo aprendido.

TABLA DE CONTENIDO

ÍNDICE DE FIGURAS

ÍNDICE DE TABLAS

RESUMEN

Las especies de *Eucalyptus* son ampliamente plantadas en Chile debido a su rápido crecimiento y adaptabilidad. Sin embargo, la producción y sostenibilidad de plantaciones se ven amenazadas por factores como la escasa disponibilidad de agua y su susceptibilidad a plagas. En esta tesis doctoral se realizó el estudio de la incidencia de la sequía y defoliación por el insecto *Gonipterus platensis* sobre el metabolismo especializado de árboles de distintas especies de *Eucalyptus* a través de un enfoque metabolómico basado en UHPLC-QTOF-MS/MS. Se incluyeron las especies de mayor interés comercial, *E. globulus*, *E. nitens*, y la especie híbrida *E. nitens* × *E. globulus*. Los resultados sugieren que existe una diferencia constitutiva entre *E. globulus* y *E. nitens*, predisponia la susceptibilidad frente al ataque de *G. platensis*. Se evidenció la ausencia de enzimas claves en la especie susceptible *E. globulus*, como la estilbeno sintasa (STS) y la galato 1-β-glucosiltransferasa. Por otra parte, los resultados metabolómicos del ensayo de estrés hídrico en especies de *Eucalyptus*, demostró efectos negativos en la biosíntesis de fenilpropanoides, como flavonoles y estilbenos. Pero también se observó que la sequía inducia la regulación de fitoanticipinas en plantas estresadas sugiriendo la preparación para el ataque de plagas.

ABSTRACT

Eucalyptus species are widely planted in Chile due to their rapid growth and adaptability. However, the production and sustainability of plantations are threatened by factors such as low water availability and susceptibility to pests.

In this doctoral thesis, the incidence of drought and defoliation by the insect *Gonipterus platensis* on the specialized metabolism of trees of different *Eucalyptus* species was studied through a metabolomic approach based on UHPLC-QTOF-MS/MS. The species of significant commercial interest, *E. globulus*, *E. nitens*, and the hybrid species *E. nitens* × *E. globulus* were included. The results showed that the constitutive difference between *E. globulus* and *E. nitens* predisposes susceptibility to *G. platensis* attack. The absence of key enzymes in the susceptible *E. globulus* species, such as stilbene synthase (STS) and gallate 1-β-glucosyltransferase, was evidenced. On the other hand, metabolomic results of the water stress assay of six *Eucalyptus* species showed adverse effects on the biosynthesis of phenylpropanoids, such as flavonols and stilbenes. However, it was observed that up-regulation of phytoanticipins was induced upon drought stress, suggesting preparation for possible pest attacks.

xi

CAPITULO 1: INTRODUCCIÓN GENERAL

1.1. Indicadores macroeconómicos de la industria forestal en Chile referentes a *Eucalyptus spp.*

La industria forestal es de gran importancia para la economía chilena, el PIB forestal del año 2021 alcanzó a los 3.602 millones de pesos, lo que representa una contribución del 1,7% al PIB nacional (Álvarez *et al.*, 2022).

Según información del Instituto Forestal (INFOR) del Ministerio de Agricultura, en el año 2020 la superficie forestal con plantaciones alcanzó un total de 2.3 millones de hectáreas, lo que representa un crecimiento de 0.4% con respecto al año anterior, atribuible al aumento de las plantaciones de eucalipto (5,4%). Por el contrario, la superficie plantada con *Pinus radiata* disminuyó en 0,5%, mientras que las otras especies, entre las que destacan *Pinus ponderosa*, *Pinus contorta* lo hicieron en un 19,1% (Álvarez *et al.*, 2022). La superficie de plantaciones forestales de eucalipto en términos porcentuales referente al total, a diciembre de 2020, fue de un 25.1% para la especie *Eucalyptus globulus* Labill. ssp. *globulus* y un 12.0% para la especie *Eucalyptus nitens* (Dean & Maiden). A nivel regional, la Región del Biobío

lidera el rubro, con el 27,2% del total de las plantaciones de eucalipto del país (Aguirre *et al.*, 2021).

La industria nacional derivada de la actividad forestal de mayor consumo de trozas en el año 2021 fue la industria del aserrío, con el 38,1% de la producción total (Álvarez *et al.*, 2022). Le sigue de cerca la industria de pulpa para la producción de papel con el 36,7%. En la industria de la pulpa, las especies del género *Eucalyptus* aportan el 48,2% de la materia prima, destacándose en estos últimos años la participación de *E. nitens* con el 28% por sobre la de *E. globulus* con el 20% en el consumo de madera para pulpa. El exitoso desarrollo de especies de *Eucalyptus* de rápido crecimiento en Chile no ha quedado exento de problemas. Estas especies forestales crecen bajo duras condiciones de adaptación, expuestas a periodos de sequía (Berenguer *et al.*, 2018), heladas (Navarrete-Campos *et al.*, 2013) y ataques por insectos patágenos (Lanfranco & Dungey, 2001; Estay et al., 2002). Por estos motivos es que los nuevos desafíos de la industria forestal están enfocados a encontrar materiales genéticos resilientes a factores ambientales, para mejorar la productividad de las plantaciones comerciales de *Eucalyptus* spp.

1.2. Estrés hídrico en plantaciones de *Eucalyptus spp.*

El déficit hídrico es uno de los factores más importantes que afecta el ecosistema productivo, el cual es acrecentado por recurrentes períodos de sequía generados por el cambio climático (Jofré Filgueira *et al.*, 2013). Este es el principal factor ambiental limitante del crecimiento y productividad de las plantaciones comerciales de *Eucalyptus* spp. (White *et al.*, 1996; Berenguer *et al.*, 2018). En Chile las plantaciones forestales se distribuyen en una amplia zona entre la región de Coquimbo y la región de Aysen, zona que dada su amplitud latitudinal posee condiciones de clima y suelo muy variadas. Plantaciones establecidas en la zona central están expuestas a una distribución temporal de períodos estivales de altas temperaturas y bajas precipitaciones correspondiente al clima mediterráneo (Jofré Filgueira *et al.*, 2013).

Existe una gran preocupación sobre la distribución de plantaciones hacia ambientes más restrictivos, como son el secano costero y el valle de la Cordillera de los Andes. Ambos lugares presentan una gran sequedad durante el verano y bajas temperaturas en invierno (Coopman *et al.*, 2008). Esto afecta el crecimiento de las plantas y reduce las áreas de forestación, en particular en países donde estas especies han sido ampliamente cultivadas

(Chile, Brasil, y Estados Unidos). En este escenario, la productividad de las plantaciones comerciales de eucalipto solo se puede mantener mediante la selección de especies o genotipos más adaptables a condiciones de baja disponibilidad de agua.

Las respuestas de tolerancia a la sequía difieren segun la especie. Se ha evidenciado que *E. globulus* muestra una mayor capacidad de tolerar limitaciones hídricas estacionales moderadas (White *et al.*, 1996). En cambio, *E. nitens* muestra mayor tolerancia a zonas de heladas (Navarrete-Campos *et al.*, 2013). En los últimos años ha adquirido gran importancia las especies híbridas en silvicultura, especialmente en regiones subtropicales y tropicales, donde el objetivo es mejorar la adaptabilidad (Madhibha *et al.*, 2013; de Oliveira *et al.*, 2022; Romão *et al.*, 2023). Los híbridos interespecíficos de *Eucalyptus* spp., con frecuencia, presentan mayor plasticidad ambiental ante factores abióticos y buena supervivencia (Volker *et al.*, 2008). En la última década, los programas de reproducción y mejoramiento forestal en Chile han implementado el uso del híbrido *E. nitens* × *E. globulus*, debido a su productividad aceptable para la industria y resistencia a climas fríos y heladas frecuentes (Madhibha *et al.*, 2013; González *et al.*, 2018). Adicionalmente, otros híbridos y especies puras como

E. camaldulensis × *E. globulus*, *E. badjensis* y *E. smithii*, resultan atractivas por su potencial capacidad de adaptación a distintos escenarios ambientales (Garcia *et al.*, 2022).

Las plantas utilizan mecanismos morfológicos y fisiológicos para garantizar su supervivencia en condiciones ambientales adversas, como variaciones de temperaturas, salinidad del suelo y cambios estacionales en la disponibilidad de recursos hídricos (McDowell *et al.*, 2008). A nivel fisiológico se ha reportado que una forma en que las plantas compensan la restricción hídrica es mediante el cierre de estomas, lo cual reduce la pérdida de agua por transpiración (Lincoln, 2019). Sin embargo, el cierre de estomas también disminuye la captación de CO_2, reduciendo la capacidad fotosintética y suprimiendo el crecimiento (Chaves *et al.*, 2009). Durante la respuesta de la planta al estrés, los azúcares solubles totales y los carotenoides son actores clave bien conocidos por sus funciones de osmorregulación y antioxidantes, respectivamente (Berenguer *et al.*, 2018). La adaptación fisiológica al estrés hídrico implica un compromiso entre el desarrollo vegetativo y el reproductivo, ya que en condiciones de estrés el crecimiento vegetativo de la planta puede terminar prematuramente, influyendo en la producción de biomasa y en la distribución de esta (Lincoln, 2019).

A medida que se agudiza el estrés hídrico, la supervivencia de la planta depende del mantenimiento de la integridad del xilema (tejido vegetal encargado de transportar agua, sales y otros minerales) como principal sistema transportador de agua (Nardini & Pitt, 1999; Sperry & Hacke, 2002). Particularmente, en el caso de *Eucalyptus* se han reportado varios trabajos que han abordado los cambios fisiológicos del árbol frente a la restricción hídrica, como cambios en la distribución de biomasa (Spokevicius *et al.*, 2017), disminución en el potencial hídrico foliar (Costa E Silva *et al.*, 2004), cierre estomático (White *et al.*, 1996), y ajuste osmótico; junto con el aumento de la elasticidad de la pared celular para mantener la turgencia celular, estado de rigidez celular que se ocasiona por la absorción de agua (Coopman *et al.*, 2008).

Por otra parte, cambios a nivel metabólico como aumento de pigmentos (clorofila y carotenoides), y la activación de fitohormonas (Correia *et al.*, 2018). El ácido abscísico (ABA) es la fitohormona clave implicada en la respuesta al estrés por sequía, está actúa como una señal química regulando la apertura y cierre de estomas (Lim *et al.*, 2015). ABA se sintetiza principalmente en raíces deshidratadas y es transportada a través del xilema desde raíces a hojas. Por su parte, la fitohormona de ácido jasmónico (JA)

participa de la regulación de procesos como crecimiento celular y defensa contra patógenos (Wasternack & Song, 2017). Estas fitohormonas juegan importantes roles en la regulación de respuestas defensivas de las plantas y se ha demostrado que están involucrados en la respuesta a la sequía en la especie *Eucalyptus* (Correia *et al.*, 2014).

1.3. Relación entre estrés hídrico e incidencia de ataque de insectos defoliadores

Los eventos de estrés hídrico a veces coinciden con brotes de insectos o patógenos. Se ha postulado en literatura que los ataques de insectos suelen ocurrir en árboles debilitados por sequía o déficit hídrico, lo que puede provocar una mayor mortalidad en las plantas afectadas (Anderegg *et al.*, 2015). Son escasos los modelos o estudios que incluyen la respuesta de los árboles tanto al estrés hídrico (Harfouche *et al.*, 2018) como al daño por insectos (Loch & Matsuki, 2010), y la relación bioquímica entre ambas.

Se sabe que una sequía moderada, pero no letal, puede hacer que los árboles sean más vulnerables a la muerte por defoliación o más susceptibles al posterior ataque de patógenos (Anderegg *et al.*, 2015). Las características de los árboles hospederos también son de gran relevancia, como su tamaño, la

densidad foliar, así como su distribución en campo influyen en la capacidad de crecimiento y propagación de las poblaciones de insectos (McDowell *et al.,* 2008). Por ejemplo, un estudio experimental de sequía reveló que el estrés hídrico severo predisponía a los árboles de pino piñonero maduros (*Pinus edulis*) al ataque de los escarabajos del pino (*Ips confusus*). Luego de un año de tratamiento de sequía se encontró que en el 92% de los árboles muertos se encontraba una alta incidencia de escarabajos (Gaylord *et al.*, 2013).

Procesos similares ocurren con la mortalidad de árboles inducida por insectos defoliadores. El consumo foliar por parte de estos insectos depende de la calidad nutricional y la palatabilidad de las hojas, que están influenciada principalmente por metabolitos secundarios (Gessler *et al.*, 2017). Durante períodos de sequías los ataques de herbívoros podrían ser el resultado de la acumulación de compuestos de nitrógeno en el tejido vegetal, que mejoran el crecimiento y la reproducción de los herbívoros (Hamann *et al.*, 2021). Por otra parte, debido al cierre estomático durante la sequía se produce una menor fijación de carbono y, por tanto, una menor producción de compuestos defensivos, lo que puede amplificar los ataques de organismos oportunistas (McDowell *et al.*, 2008).

Los defoliadores reducen la biomasa foliar de la planta y con ello su crecimiento, pero a diferencia de los escarabajos de la corteza, se necesita una defoliación severa y prolongada para provocar la muerte de un árbol (Anderegg *et al.*, 2015).

En el caso específico de *Eucalyptus* spp., esta se ve amenazada por el insecto especialista *Gonipterus platensis* Marelli (Reis *et al.*, 2012); el cual es un defoliador que se alimenta exclusivamente del follaje joven de árboles de *Eucalyptus* afectando el crecimiento de plantaciones comerciales (Reis *et al.*, 2012; Gonçalves et al., 2019). Un conjunto de factores son los que propician el ataque de esta plaga, principalmente factores medioambientales y de disponibilidad del árbol hospedero. Cambios en los patrones climáticos pueden aumentar las poblaciones de insecto y reducir la vitalidad del hospedador y su resistencia al patógeno (Adame *et al.*, 2022).

1.4. Ataque de *Gonipterus platensis* Marelli en plantaciones de *Eucalyptus*

Junto con el exitoso plan de producción forestal de *Eucalyptus*, se han propagado de forma accidental por todo el mundo patógenos nocivos e insectos especializados que amenazan dicha productividad (EPPO, 2005;

Mapondera *et al.,* 2012). *Gonipterus platensis Marelli* (Coleoptera: curculionidae) es una de las principales plagas del eucalipto en el mundo, y tanto larvas como los insectos adultos se alimentan de las hojas del árbol (Estay *et al.*, 2002).

Este insecto defoliador, conocido comúnmente como el gorgojo del eucalipto es nativo del sureste de Australia (Mapondera *et al*., 2012; Reis *et al*., 2012) y amenaza las plantaciones produciendo una severa defoliación principalmente en árboles jóvenes (Lanfranco & Dungey, 2001).

En su lugar de origen este insecto causa bajo impacto en las plantaciones de *Eucalyptus* debido a que cuenta con la presencia de depredadores naturales que actúan como controladores biológicos, como lo es, *Anaphes nitens* (Hymenoptera: Mymaridae) que parasita los huevos del gorgojo haciéndolos infértiles (Santolamazza & Fernández, 2004). Distinto es el escenario reportado en otras partes del mundo donde ha sido accidentalmente introducido, como lo es Chile (Estay *et al.*, 2002).

Este insecto fue detectado por primera vez en Chile en febrero del año 1998 por el Servicio Agrícola y Ganadero (SAG). Por consiguiente, en diciembre de 1999, se publicó un reporte para la detección y control obligatorio del

gorgojo del *Eucalyptus*, que se aplica hasta la fecha (Beéche Cisternas *et al.*, 1999). De forma paralela se publicaron las resoluciones, Nº 1293/1998 y Nº 199/1999, declarando este insecto como una plaga de control obligatorio en Chile, incluyéndolo dentro de la lista A-2 de las plagas cuarentenarias (Beéche Cisternas *et al.*, 1999). Sin embargo, los esfuerzos para detener su expansión no han dado resultados positivos, ya que en el año 2006 el área entre la IV Región (Coquimbo) y la IX región (Araucanía) fue invadida por el gorgojo, afectando más de 525 mil hectáreas de plantaciones de *Eucalyptus* (Huerta-Fuentes *et al.*, 2008). Lo anterior ha sido atribuido a su potencial reproductivo y también a las condiciones climáticas favorables que ha encontrado en Chile. Se ha reportado que *G. platensis* puede llegar a tener cuatro generaciones anuales superpuestas, en las cuales se pueden encontrar adultos activos durante todo el año (Clarke *et al.*, 1998). Por el contrario, en otros países como Sudáfrica (Bouwer *et al.,* 2014), Francia (Pinet, 1984), España (Rivera *et al.*, 1999) y Estados Unidos (California) solo dos generaciones han sido reportadas, haciendo su control más sencillo (Cowles & Downer, 1995).

Aunque las pérdidas de la industria chilena causadas por *G. platensis* aún no han sido cuantificadas, en parte debido a la duración de la rotación de las

plantaciones de *Eucalyptus* spp., se han estimado daños por la disminución del incremento volumétrico anual y de las tasas de crecimiento, así como del porcentaje de defoliación. El grado de defoliación en la copa de los árboles de *Eucalyptus glóbulus* causado por *Gonipterus* en Australia se ha cuantificado entre el 18% y el 33%, mostrando un claro impacto en la tasa de crecimiento del árbol después de dos años y medio (Loch & Matsuki, 2010). El efecto negativo sobre el crecimiento del *Eucalyptus* se ha estimado en torno a un 30% de pérdida de la tasa de crecimiento anual en Chile, siendo por lejos la especie más afectada *E. globulus* (Valente *et al*., 2018).

Otro estudio realizado por investigadores australianos, en el que defoliaron artificialmente árboles de *E. globulus* durante dos años consecutivos, mostró una disminución del 17% del diámetro de los árboles y una reducción del 21% del incremento anual (Elek & Baker, 2017). Esto sugiere que la rotación debiera extenderse entre 3 y 4 años más de lo normal para alcanzar los rendimientos esperados sin defoliación (Elek & Baker, 2017).

Por otra parte, la inefectividad de la estrategia implementada con el controlador biológico está probablemente relacionada con la incapacidad del parasitoide *Anaphes nitens* de adaptarse a las regiones más frías de Chile (Valente *et al*., 2018). Adicionalmente, existe una limitación para el uso de

plaguicidas en Chile porque el 37% de las plantaciones de *Eucalyptus* está

bajo certificación con restricciones para la aplicación de productos químicos

para el control de plagas (Beéche Cisternas *et al.*, 1999).
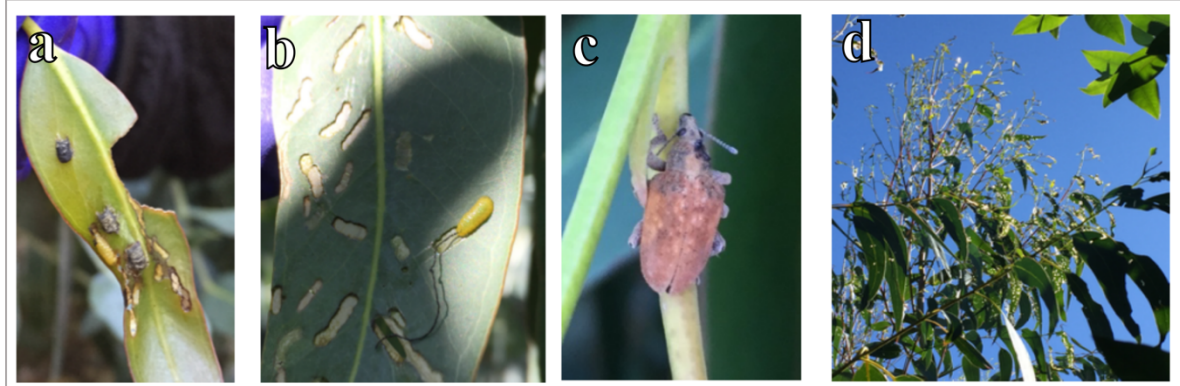
Figura **1**.**1.** *Gonipterus* *platensis* en plantaciones de *Eucalyptus*
ubicadas en las cercanías a la cuidad de Yumbel, Región del Biobío, Chile,
2019. (a) Capsulas llamadas ootecas que contienen entre 8 y 10 huevos. (b)
Larva alimentándose de la hoja. (c) Gorgojo adulto. (d) Daños causados por
larvas y adultos en la copa de un árbol de *E. globulus*.

Finalmente, las especies de *Eucalyptus* plantadas en Chile presentan

distinta susceptibilidad a la herbivoría por *G. platensis*. Estudios previos de

Huerta-Fuentes y colaboradores indican que las especies con mayor
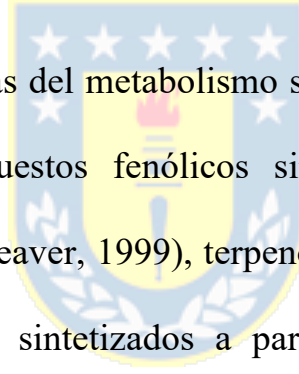
susceptibilidad son *E. globulus globulus* Labill., *E. camaldulensis* Dehnh. y *E. robusta* Smith (Huerta-Fuentes *et al.*, 2008)

Por el contrario, mostraron ser especies resistentes *E. saligna*, *E. citriodora* y la segunda especie más extensamente plantada en Chile, *E. nitens* (Lanfranco & Dungey, 2001). Se ha mencionado que esta resistencia por parte de ciertas especies de *Eucalyptus* a plagas puede deberse en la composición química de las hojas (Matsuki *et al.*, 2011). Hasta hace algunos años las plantaciones se habían realizado en su mayor parte en zonas de cultivo óptimas y, a medida que la industria establece plantaciones en zonas más marginales, se infiere que aumenten los problemas de plagas ya que la susceptibilidad puede verse acrecentada por factores ambientales (Lanfranco & Dungey, 2001; Gessler *et al.*, 2017).

1.5. Estudios sobre el metabolismo especializado en *Eucalyptus spp.*

Los compuestos producidos por plantas son categorizados en metabolitos primarios y metabolitos especializados. Los metabolitos primarios, como carbohidratos, lípidos, y proteínas, están directamente

involucrados en procesos de desarrollo y crecimiento (Neilson *et al.*, 2013). En contraste, los metabolitos secundarios son multifuncionales, ya que generalmente están involucrados en la defensa de la planta como respuesta frente a algún estrés (Jan *et al.*, 2021). Estos participan de la mitigación del estrés abiótico, como la temperatura, estrés hídrico, la salinidad y la luz ultravioleta (Külheim *et al.*, 2011; Machado *et al.*, 2017), pero también están involucrados en el combate de patógenos (Neilson *et al.,* 2013; Jan *et al.,* 2021).

Las rutas biosintéticas del metabolismo secundario se dividen en tres grupos principales: compuestos fenólicos sintetizados por la ruta del shikimato (Herrmann & Weaver, 1999), terpenos sintetizados por la vía del mevalonato y compuestos sintetizados a partir del ciclo de los ácidos tricarboxílicos. La ruta del shikimato es la ruta biosintética inicial para la biosíntesis de aminoácidos aromáticos, que es activada en condiciones de estrés para producir triptófano, tirosina, y fenilalanina (Herrmann & Weaver, 1999). La fenilalanina es el precursor común de flavonoides, lignanos, ligninas, taninos condensados, y fenilpropanoides, compuestos ampliamente distribuidos en el reino vegetal (Jan *et al*., 2021).

La limitación de agua es uno de los factores abióticos más problemáticos, ya que provoca cambios morfológicos, fisiológicos y bioquímicos en la planta con el fin de tolerar o resistir el estrés provocado. En particular, son escasos los estudios que aborden las respuestas metabólicas de las especies de *Eucalyptus* (Myrtaceae) frente a la restricción hídrica. Algunos estudios han abordado el efecto del estrés hídrico a nivel bioquímico. McKiernan y colaboradores investigaron la influencia de la disponibilidad de agua en un amplio rango de metabolitos secundarios foliares en plantas juveniles de *E. globulus* y *E. viminalis* a través de análisis por GC-MS. La disponibilidad moderada y baja de agua en el tratamiento redujo las concentraciones de compuestos fenólicos en ambas especies, pero no se encontró diferencia significativa en las concentraciones de terpenos y derivados de floroglucinoles. Sí bien este estudio abordó los cambios en el metabolismo secundario, no entregó información acerca de rutas metabólicas o mecanismos de acción (Mckiernan *et al.*, 2014). Por su parte, Correia y col., evaluaron la respuesta metabólica al déficit hídrico de clones de *E. globulus* mediante un análisis que integró proteómica y metabolómica mediante GC-MS. En este trabajo se demostró que el efecto del estrés hídrico afectaba enzimas clave para la biosíntesis de isoflavonoides (isoflavona reductasa) y

terpenoides (linalool sintasa) que se vieron reducidas en abundancia en la planta. También se vieron reducidas las concentraciones de precursores biosintéticos como ácido shikimico (Shikimato), el ácido 3-*trans*-cafeoilquínico, el flavonol quercetina y el estilbeno piceatanol (Correia *et al.*, 2016). Pero estos estudios generalmente fueron enfocados solo a la especie *E. globulus* y no aportaron información acerca de otras especies que se están propagando en la actualidad, incluido el híbrido *E. nitens × E. globulus*.

Por otra parte, Valdés y colaboradores evaluaron individuos de *E. globulus* de distinto origen con tolerancia contrastada a la sequía y encontraron diferencias en la morfología y acumulación de contenidos de ácido abscísico (ABA) (Valdés *et al.*, 2013). Similarmente, Correia y colaboradores estudiaron genotipos tolerantes a sequía y calor de la misma especie, donde encontraron un aumento del contenido de ABA y una disminución de la también fitohormona ácido jasmónico (JA). Nuevamente se trata de estudios dirigidos a metabolitos específicos de ciertas rutas biosintéticas y no a la variación global del metabolismo (Correia *et al.*, 2018).

Estos estudios ponen de manifiesto la necesidad de incorporar técnicas multidisciplinarias que incluyan un enfoque holístico más integrador, y sean

capaces de desvelar las vías metabólicas implicadas en la respuesta de las plantas a tales factores, así como biomarcadores que permitan la selección de genotipos resistentes. De igual forma, se hace necesario la inclusión en estos estudios de especies diferentes de interés para el sector productivo forestal nacional.

1.6. Metabolómica en plantas

Las plantas son capaces de utilizar rápidamente su complemento enzimático para ensamblar un gran número de sustancias químicas con diversas estructuras y funciones (Jan *et al.*, 2021). Se estima que hay más de 200.000 metabolitos en el reino vegetal que pueden dividirse en metabolitos primarios y metabolitos secundarios. Los metabolitos primarios son tipos de metabolitos que participan principalmente en el crecimiento, desarrollo y la reproducción de las plantas y que se acumulan constitutivamente en las células vegetales (Fiehn, 2002; Sumner *et al.*, 2003). La abundancia de metabolitos secundarios determina en gran medida la diversidad de metabolitos en las plantas, que se acumulan en tejidos específicos o en etapas de desarrollo específicas, y desempeñan un papel importante en la defensa de las plantas frente a estrés biótico y/o abiótico (Fiehn, 2002).

La metabolómica es una estrategia analítica que busca la identificación sistemática y cuantificación de todos los metabolitos en un determinado organismo o muestra biológica. Permite el estudio del perfil metabólico o metaboloma de las células, tejidos u organismos en relación con la variación genética frente a estímulos externos (fenotipo) (Fernie & Keurentjes, 2011). El metaboloma se define como el conjunto de metabolitos de bajo peso molecular presentes en una célula u organismo en determinadas de condiciones fisiológicas (Kell *et al.*, 2005).

La metabolómica se divide en dos enfoques complementarios; metabolómica no dirigida (*untarget metabolomics*) y metabolómica dirigida (*target metabolomics*). El enfoque de "*untarget metabolomics*" consiste en determinar todos los posibles metabolitos expresados diferencialmente en las condiciones que se comparan en el estudio, con el propósito de detectar e identificar potenciales biomarcadores implicados en una condición específica (Sumner *et al.*, 2003; Naz *et al.*, 2014). Además de ofrecer un enfoque holístico en el ámbito de la investigación es un generador de hipótesis (Hendriks *et al.*, 2011; Naz *et al.*, 2014). Por otra parte, "*target metabolomics*" mide una lista específica de metabolitos, que generalmente está condicionada a una pregunta bioquímica concreta, o hipótesis, que

motiva la investigación. Los estudios dirigidos, en cambio, suelen proporcionar conocimientos más profundos porque se miden concentraciones absolutas de las moléculas (cuantificación absoluta) para obtener tasas o flujos de conversión de una molécula a otra (Liu & Locasale, 2017). Por tanto, un análisis metabolómico dirigido requiere un conocimiento previo sustancial y su éxito depende de la fuerza de la hipótesis que se esté probando (Liu & Locasale, 2017).

La plataforma analítica más utilizada en estudios metabolómicos para identificar metabolitos es la espectrometría de masas (MS), y en menor medida la Resonancia Magnética Nuclear (RMN) (Sumner *et al.*, 2003; Spina *et al.*, 2021). La espectrometría de masas es una técnica que posee una alta resolución y una alta precisión de masa (Dudzik *et al.*, 2018). La precisión de masas permite el cálculo de la composición elemental para ayudar a la diferenciación y caracterización estructural (Sumner *et al.*, 2003). Generalmente se utiliza acoplada a técnicas cromatográficas como cromatografía de líquidos (LC-MS) o cromatografía de gases (GC-MS) (Shen *et al.*, 2023). La combinación de la técnica de separación con la espectrometría de masas tiene como ventaja una alta selectividad y sensibilidad (Shen *et al.*, 2023) que facilita la interpretación de espectros al

disminuir su complejidad y reducir la supresión de iones causadas por compuestos coeluyentes, las interferencias isobáricas y separación de compuestos isómeros o isobáricos (Naz *et al.*, 2014). Además, incorpora información adicional sobre las propiedades químicas de los metabolitos como su tamaño molecular y polaridad (Sumner *et al.*, 2003).

En los estudios "*omicos*" se utilizan métodos estadísticos multivariados para visualizar y reducir la dimensión del conjunto de datos obtenidos de los análisis LC-MS y/o GC-MS. Los enfoques más utilizados incluyen métodos no supervisados como el Análisis de Componentes Principales (PCA) para visualizar el agrupamiento inherente de muestras y la detección de muestras anómalas (*outliers*) (Yamamoto *et al.*, 2009; Worley & Powers, 2016), además de métodos supervisados como Análisis Discriminante de Mínimos Cuadrados Parciales Ortogonales (OPLS-DA) para la selección de metabolitos significativamente diferenciadores entre dos grupos de estudio (Boccard & Rutledge, 2013). Los métodos multivariados son óptimos para conjunto de datos de gran dimensión por sobre métodos univariados como ANOVA, ya que estos consideran la correlación presente entre variables y las correlaciones entre muestras (Chong *et al.*, 2019). Por otra parte, hay que considerar que los métodos supervisados, como el OPLS-DA, deben contar

con una validación del set de calibración para evitar el sobre ajuste u *overfitting* de la data. Esta validación puede ser una prueba de permutación de las clases con validación interna *cross validation* o incluyendo un set externo de validación (Chong *et al.*, 2019).

El análisis e identificación en metabolómica no dirigida incluye un flujo de trabajo definido que considera el filtrado de ruido espectral, la detección de picos, la deconvolución de picos, alineación de los tiempos de retención, y finalmente la anotación de *features* (Schrimpe-Rutledge *et al.*, 2016).

Los *features* (relación *m/z*, tiempo de retención e intensidad) pueden ser asignados a un vasto número de estructuras que no siempre son metabolitos, pueden tratarse de isótopos, pérdidas neutras y aductos de un solo metabolito que pueden estar presentes con diferentes valores de *m/z*. La identificación de metabolitos es necesaria para extraer conclusiones biológicas de los datos, para lo que se utilizan bases datos experimentales de carácter público de espectros de fragmentación MS/MS con el objetivo de alcanzar una calidad de la anotación más alta. Estas bases de datos son PubChem (https://pubchem.ncbi.nlm.nih.gov), MassBank, ChemSpider (http://www.chemspider.com), METLIN (https://metlin.scripp.edu), mzCloud (https://www.mzcloud.org), GNPS (http://gnps.ucsd.edu/).

La anotación de *features* se realiza comparando una medición de masa (m/z) experimental con una base de datos dentro de una ventana de tolerancia de masa; tolerancia de error < 5 ppm, para generar posibles estructuras candidatas (Schrimpe-rutledge *et al.*, 2016). Sin embargo, la validación de tiempos de retención y de la data de fragmentación MS/MS con un estándar de referencia siempre es recomendable para la confirmación definitiva del compuesto en cuestión (Schrimpe-Rutledge *et al.*, 2016). Finalmente, la interpretación biológica de la data metabolómica depende de la capacidad de poder relacionar los metabolitos identificados con redes y rutas metabólicas a fin de trazar un contexto bioquímico de la respuesta de la planta al estímulo externo que fue sometida (Schrimpe-Rutledge *et al.*, 2016). En resumen, del flujo de trabajo de los estudios metabolómicos se muestra en la Figura 1.2.
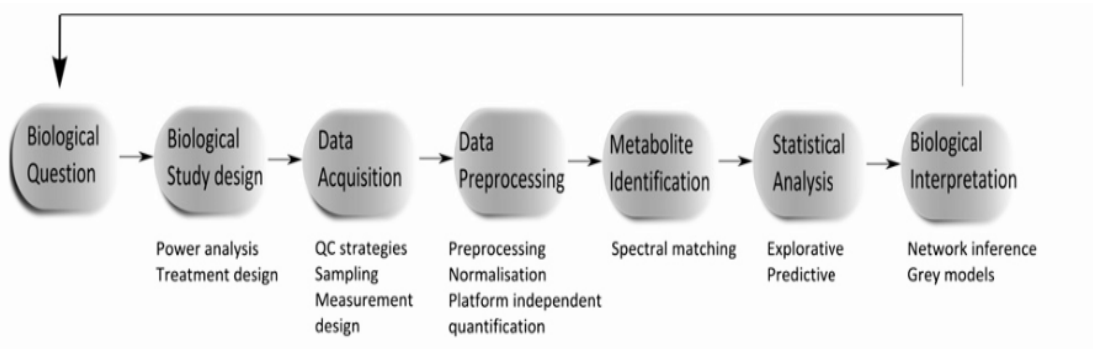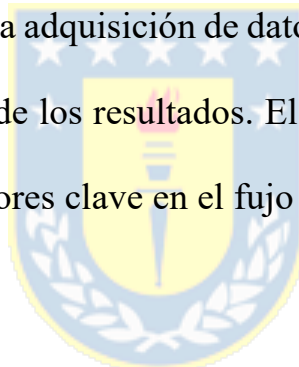
Figura 1.2. Representación gráfica del "flujo de trabajo de la metabolómica" (Hendriks *et al*., 2011). Comienza con una pregunta biológica, pasando por el diseño de experimentos, la adquisición de datos y análisis, y terminado con la interpretación biológica de los resultados. El procesamiento de datos y el análisis estadístico son factores clave en el fujo de trabajo.

CAPITULO 2: HIPÓTESIS Y OBJETIVOS

2.1. Hipótesis

El estrés hídrico en especies de *Eucalyptus* influye directamente en la biosíntesis de metabolitos secundarios no volátiles de las hojas y predispone a la planta al ataque del insecto herbívoro *Gonipterus platensis*.

2.2. Objetivo General

Identificar los cambios metabólicos a nivel de metabolismo especializado en hojas de especies de *Eucalyptus* y la predisposición al ataque de *Gonipterus platensis* causados por el estrés hídrico.

2.3. Objetivos específicos

1- Determinar mediante análisis metabolómico los efectos más significativos del estrés hídrico sobre el metabolismo secundario de plantas jóvenes en especies *Eucalyptus* a escala de laboratorio.

2- Determinar mediante análisis metabolómico los efectos más significativos del estrés hídrico sobre el metaboloma de plantas de un año en las especies *Eucalyptus globulus*, *Eucalyptus nitens* y el híbrido *Eucalyptus nitens x Eucalyptus globulus* en experimento a escala de campo.

3- Evaluar mediante ensayo biológico la predisposición de especies de *Eucalyptus* en estrés hídrico a la defoliación por *Gonipterus platensis*.

CAPITULO 3: ESTRATEGIA ANALÍTICA

Durante la realización de este trabajo de investigación se abordó el estudio de factores ambientales que afectan las plantaciones de *Eucalyptus*, estos factores afectan la composición del metabolismo secundario foliar de la planta y estimulan respuestas bioquímicas específicas. En esta tesis doctoral se estudió la incidencia del estrés hídrico sobre la biosíntesis de metabolitos secundarios y la predisposición a la defoliación por *G. platensis*, a través de un análisis metabolómico en especies de *Eucalyptus* de importancia comercial para la industria forestal chilena. Para abordar dicha problemática se dispuso de distintas estrategias analíticas, de forma tal de incluir la respuesta de las plantas a ambos factores, abiótico y biótico, y discernir la correlación entre estas.

I. Como primera estrategia, se estudiaron los cambios ocurridos en el metabolismo especializado de especies de *Eucalyptus* en respuesta a la defoliación por el insecto *Gonipterus platensis*. Para ello se realizó un muestreo en plantaciones reales de clones de las especies *E. globulus* Labill. ssp *globulus* y *E. nitens* (Deane &Maiden) Maiden ubicadas en

al sureste de la ciudad de Nacimiento en la Región del Biobío, Chile. Para el muestreo, se tuvieron las siguientes consideraciones: 1) La disponibilidad de plantaciones de dos años de ambas especies, edad a la cual suele comenzar el ataque por parte de *G. platensis*; 2) Ubicación de las plantaciones dentro de la zona de infestación del gorgojo (Memoria anual Consorcio Protección Fitosanitaria Forestal S.A., 2018). Una vez establecido el sitio de muestreo la colecta se realizó considerando tres grupos de estudio compuesto por árboles sanos de *E. globulus* (HT-EG), árboles infestados de *E. globulus* (IT-EG), y árboles sanos de *E. nitens* (EN). En cada caso se colectaron hojas maduras (pecioladas) completamente extendidas desde la parte superior de la copa de los árboles, del segundo tercio, y del tercer tercio. Las muestras vegetales se sumergieron en nitrógeno líquido inmediatamente y se almacenaron a -80 °C hasta su posterior análisis.
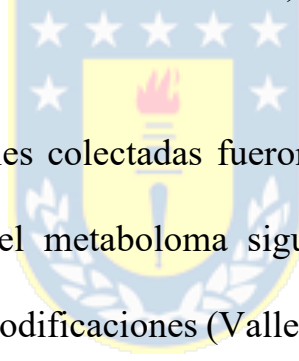
II. En segunda instancia se estudió los rasgos metabólicos de resistencia a la herbívora por *G. platensis* heredados por la especie híbrida *E. nitens* × *E. globulus*, obteniéndose el material vegetal desde un campo de experimentación ubicado en el vivero Carlos Douglas cerca de la

localidad de Yumbel en la Región de Biobío. Esta especie híbrida fue escogida debido a su gran masificación forestal en la actualidad (Coopman *et al.*, 2008; Rubilar *et al.*, 2020). Para este objetivo se consideraron siete genotipos de este híbrido los cuales hemos nombrado desde *En×Egg*1 hasta *En×Egg*7. Las especies progenitoras puras utilizadas para cruces también fueron muestreadas en el mismo sitio. Se contó con un genotipo de *E. nitens* (*En1*) y siete de *E. glolulus* (*Eg1-Eg7*). Al momento del muestreo, todas las plantas tenían dos años. Se realizaron en total dos muestreos denominados T0 y T1, con un tiempo de distanciamiento de 30 días entre ellos. El muestreo T0 se consideró como el control y se llevó a cabo con todos los árboles sin signos de defoliación por *G. platensis*. Sin embargo, al encontrarse el campo de experimentación dentro de una zona de alta incidencia de este insecto y debido a que los árboles habían cambiado sus hojas a maduras que son las preferidas por el gorgojo, en apenas un mes se observaron signos de ataque severo en muchos casos. Convenientemente, el segundo muestreo, T1, fue realizado en este momento con el fin de poder registrar la respuesta más inmediata

posible de los árboles a este ataque. La colecta y tratamiento de muestras se realizó en forma idéntica al muestreo anterior.

III. Finalmente, se desarrolló un experimento controlado de restricción hídrica en un vivero experimental de la Universidad de Concepción con fin de revelar en esta instancia la respuesta a este factor abiótico en plántulas. Para ello se consideraron las especies de *Eucalyptus* anteriormente estudiadas (*E. globulus*, *E. nitens*, y *E. nitens* × *E. globulus*), para las que ya conocíamos la respuesta específica a la defoliación por *G. platensis*. Se consideraron además otras tres especies también de interés para la industria forestal nacional con el fin de contrastar y comparar los resultados. Estas fueron *E. smithii*, *E. badjensi*s, y el híbrido *E. camaldulensis* × *E. globulus*. Luego de un periodo de aclimatación, las plántulas se dividieron en dos grupos, uno control que disponía de irrigación diaria a capacidad de campo y otro grupo tratamiento de sequía al cual se le suspendió el riego una vez comenzado el estudio. Ambos grupos, control y sequía, fueron muestreados en dos instancias, al inicio del tratamiento (T0) y luego de 22 días de iniciado el tratamiento (T1). Se colectaron tres hojas

totalmente expandidas de cada plántula y fueron inmediatamente sumergidas en nitrógeno líquido y conservadas a -80 °C hasta su posterior procesamiento. Para asegurar la condición de estrés hídrico, se midió el contenido de humedad del suelo de todas las plántulas utilizando el instrumento TDR (Time Domain Reflectometry), y el potencial hídrico foliar de prealba ($\psi_{prealba}$; 4:00 a.m. a 6:00 a.m.) se monitorió utilizando una bomba de presión Schollander (1505D Model, PMS Instruments Co., OR, USA).

Todas las muestras vegetales colectadas fueron procesadas y sometidas al protocolo de extracción del metaboloma siguiendo el procedimiento de Valledor y col., con leves modificaciones (Valledor *et al*., 2014). Finalmente, se llevaron a cabo los análisis metabolómicos para evaluar el grupo control con el grupo tratamiento en cada uno de experimentos de muestreo mencionados anteriormente (I, II y III). Los extractos de cada estudio fueron analizados mediante cromatografía líquida acoplada a espectrometría de masas, UHPLC-QTOF-MS/MS.

El procesamiento de la data fue realizado en el software Bruker Compass MetaboScape v.3.0 (Bruker Daltonik GmbH, Bremen, Alemania), el cual

permitió realizar la extracción de los *features* (tiempo de retención, *m/z*, intensidad) y confeccionar la matriz de datos (*bucket table*). Las matrices generadas fueron exportadas a MetaboAnalyst 5.0 (Chong *et al.*, 2019) para un proceso de filtrado de la data, normalización de las muestras y posterior escalado. Estas técnicas de transformación y pre-procesamiento son aplicables según las características de la data y el juicio del investigador. Posteriormente los datos fueron examinados mediante un modelo estadístico exploratorio, Análisis de Componentes Principales (PCA) el cual es utilizado para la reducción de la data y el reconocimiento de patrones (Yamamoto *et al.*, 2009). A continuación, se aplicó al conjunto de datos un análisis discriminante por mínimos cuadrados parciales ortogonales (OPLS-DA) para la identificación de las variables o *features* significativos que aportan a la diferenciación entre los dos grupos, control y tratamiento, o sano e infectado (Chong *et al.*, 2019). La identificación se realizó mediante la comparación del patrón de fragmentación MS/MS de los metabolitos con datos de fragmentación de libre acceso en forma de librerías espectrales (http://www.chemspider.com, https://pubchem.ncbi.nlm.nih.gov). De forma complementaria se utilizó el software Sirius 5.6.3, disponible de forma gratuita para el análisis de data de LC-MS/MS. Este programa integra el

análisis de patrones isotópicos de alta resolución y árboles de fragmentación para la elucidación estructural de compuestos (Dührkop *et al.*, 2019). Finalmente, los metabolitos identificados fueron ubicados en sus correspondientes rutas biosintéticas a fin de darles una significancia biológica relacionada con la respuesta de las plantas a los factores externos estudiados. A continuación, se muestra el esquema de trabajo para la estrategia analítica planteada en las Figuras 3.1 y 3.2.
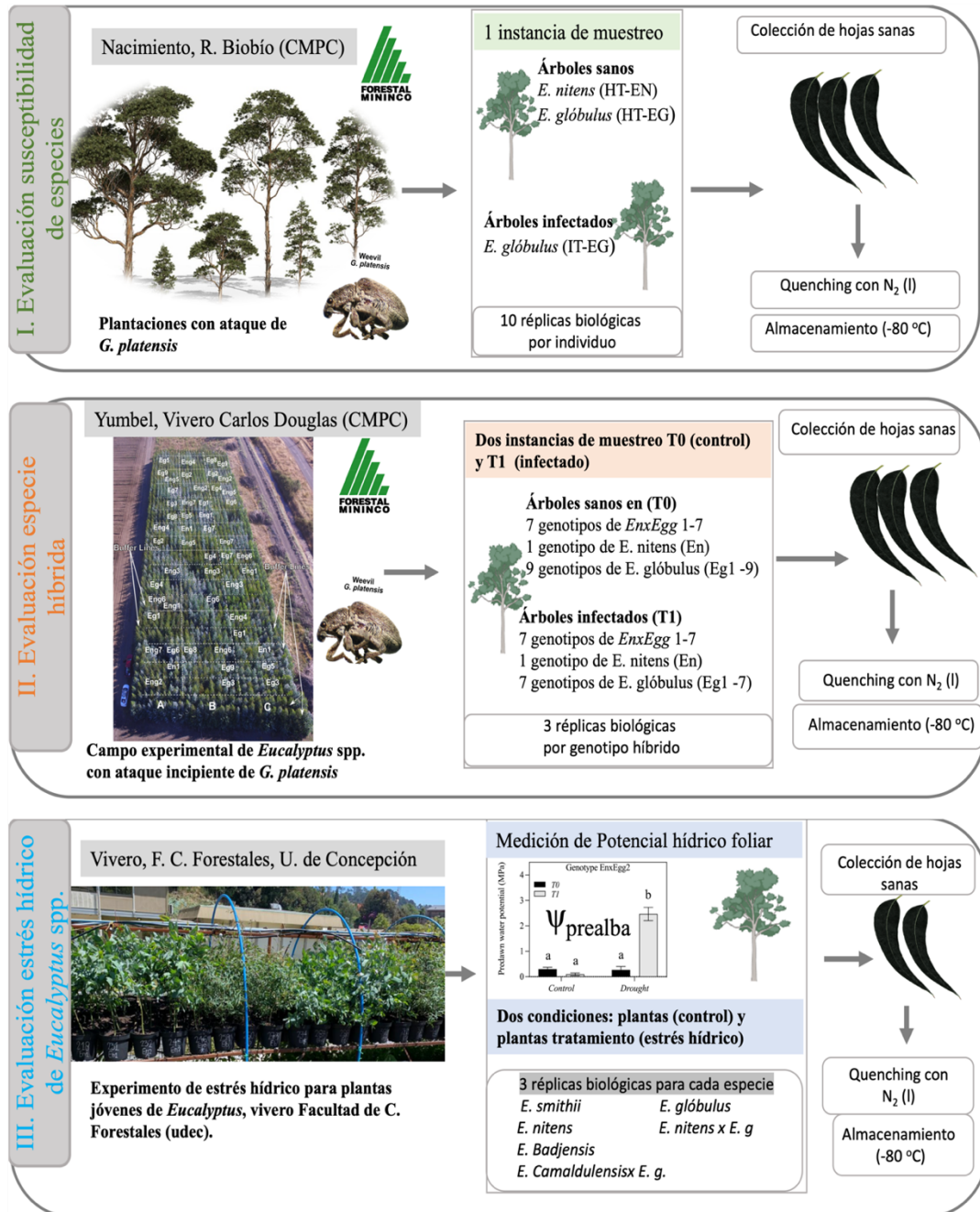
Figura 3.1. Esquema de diseño experimental de muestreo para los enfoques de estudio abordados en este trabajo para evaluar el factor de estrés por herbivoría (biótico) y por restricción hídrica (abiótico).
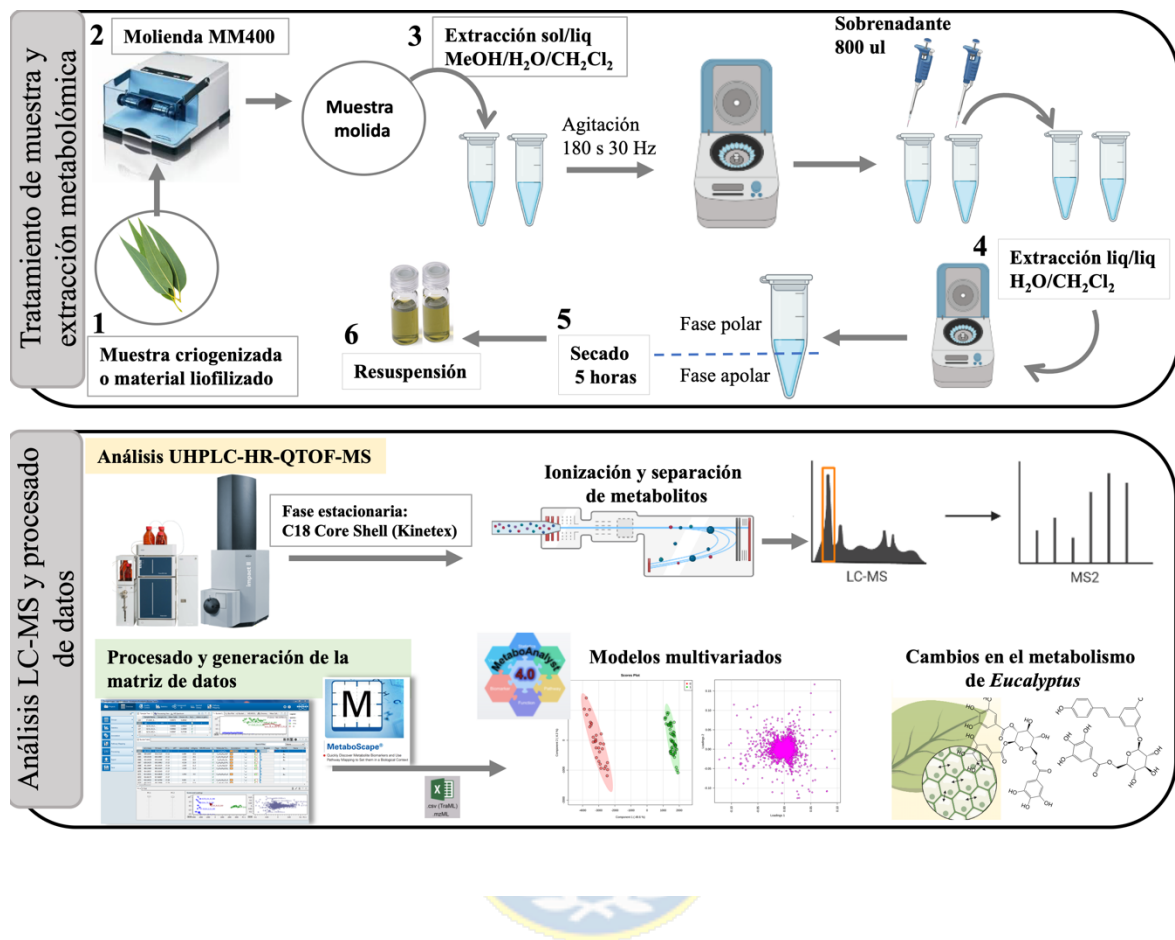
Figura 3.2. Protocolo general de tratamiento de muestras vegetales, análisis por LC-MS y posterior tratamiento de datos.

Referencias

Adame P, Alberdi I, Cañellas I, Hernández L, Aguirre A, Ruano A, Moreno-Fernández D, Isabel González A, Torres MB, Montes F. **2022**. Drivers and spread of non-native pests in forests: The case of Gonipterus platensis in Spanish *Eucalyptus* plantations. *Forest Ecology and Management* **510**.

Aguirre DS, Gysling Caselli J, Kahler González C, Poblete Hernandez P, Álvarez González V, Pardo Velasquez E, Bañados JC, Baeza Rocha D. **2021**. *Chilean statistical yearbook of forestry. Statistical bulletin N°180*. Instituto Forestal, INFOR. Ministerio de Agricultura.

Álvarez V, Poblete Hernandez P, Aguirre Soto D, Gysling Caselli J, González Kahler C, Velásquez Pardo E, Bañados Munita JC, Baeza Rocha D. **2022**. *Chilean statistical yearbook of forestry. Statistical bulletin N°187*.

Anderegg WRL, Hicke JA, Fisher RA, Tague C, Aukema J, Lichstein JW, Stephenson NL, Bentz B, Sala A, Shaw JD, *et al.* 2015. Tree mortality from drought, insects, and their interactions in a changing climate. *New Phytologist* **208**: 674–683.

Beéche Cisternas MA, Sandoval Clavería A, Rothmann Toro S, Ravanales Villalobos J, Cereceda Leinz C, Muñoz Godoy R, Olivera Alvarez G, Corvalán Latapia L, Galarce Marambio G, San Martín López A. **1999**. Detección y control del Gorgojo del eucalipto Gonipterus scutellatus Gyllenhal en Chile (Coleoptera: Curculionidae). : 43.

Berenguer HDP, Alves A, Amaral J, Leal L, Monteiro P, de Jesus C, Pinto G. **2018**. Differential physiological performance of two *Eucalyptus* species and one hybrid under different imposed water availability scenarios. *Trees - Structure and Function* **32**: 415–427.

Boccard J, Rutledge DN. **2013**. A consensus orthogonal partial least squares discriminant analysis (OPLS-DA) strategy for multiblock Omics data fusion. *Analytica Chimica Acta* **769**: 30–39.

Bouwer MC, Slippers B, Wingfield MJ, Rohwer ER. **2014**. Chemical signatures affecting host choice in the *Eucalyptus* herbivore, Gonipterus sp. (Curculionidae: Coleoptera). *Arthropod-Plant Interactions* **8**: 439–451.

Chaves MM, Flexas J, Pinheiro C. **2009**. Photosynthesis under drought and salt stress: Regulation mechanisms from whole plant to cell. *Annals of Botany* **103**: 551–560.

Chong J, Wishart DS, Xia J. **2019**. Using MetaboAnalyst 4.0 for Comprehensive and Integrative Metabolomics Data Analysis Jasmine. *Current Protocols in Bioinformatics* **68**: 1–128.

Clarke AR, Paterson S, Pennington P. **1998**. Gonipterus scutellatus Gyllenhal (Coleoptera: Curculionidae) oviposition on seven naturally co-occurring *Eucalyptus* species. *Forest Ecology and Management* **110**: 89–99.

Coopman RE, Jara JC, Bravo LA, Sáez KL, Mella GR, Escobar R. **2008**. Changes in morpho-physiological attributes of *Eucalyptus globulus* plants in response to different drought hardening treatments. *Electronic Journal of Biotechnology* **11**.

Correia B, Hancock RD, Amaral J, Gomez-Cadenas A, Valledor L, Pinto G. **2018**. Combined Drought and Heat Activates Protective Responses in *Eucalyptus globulus* That Are Not Activated When Subjected to Drought or Heat Stress Alone. *Frontiers in Plant Science* **9**: 1–14.

Correia B, Pintó-Marijuan M, Neves L, Brossa R, Dias MC, Costa A, Castro BB, Araújo C, Santos C, Chaves MM, *et al.* 2014. Water stress and recovery in the performance of two *Eucalyptus globulus* clones: Physiological and biochemical profiles. *Physiologia Plantarum* **150**: 580–592.

Correia B, Valledor L, Hancock RD, Renaut J, Pascual J, Soares AMVM, Pinto G. **2016**. Integrated proteomics and metabolomics to unlock global and clonal responses of *Eucalyptus globulus* recovery from water deficit. *Metabolomics* **12**.

Costa E Silva F, Shvaleva A, Maroco JP, Almeida MH, Chaves MM, Pereira JS. **2004**. Responses to water stress in two *Eucalyptus globulus* clones differing in drought tolerance. *Tree Physiology* **24**: 1165–1172.

Cowles RS, Downer JA. **1995**. *Eucalyptus* snout beetle detected in California. *California Agriculture* **49**: 38–38.

Dudzik D, Barbas-Bernardos C, García A, Barbas C. **2018**. Quality assurance procedures for mass spectrometry untargeted metabolomics. a review. *Journal of Pharmaceutical and Biomedical Analysis* **147**: 149–173.

Dührkop K, Fleischauer M, Ludwig M, Aksenov AA, Melnik A V., Meusel M, Dorrestein PC, Rousu J, Böcker S. **2019**. SIRIUS 4: a rapid tool for turning tandem mass spectra into metabolite structure information. *Nature Methods* **16**: 299–302.

Elek JA, Baker SC. **2017**. Timing and frequency are the critical factors affecting the impact of defoliation on long term growth of plantation eucalypts. *Forest Ecology and Management* **391**: 1–8.

EPPO 2005. Gonipterus gibberus and Gonipterus scutellatus. **2005**. EPPO,2005. Gonipterus gibberus and Gonipterus scutellatus. : 368–370.

Estay S, Araya JE, Guerrero ME. **2002**. Biologia de Gonipterus scutellatus en San Felipe, Chile. *Boletin de Sanidad Vegetal Plagas* **28**: 391–397.

Fernie AR, Keurentjes JJB. **2011**. *GENETICS, GENOMICS AND METABOLOMICS*.

Fiehn O. **2002**. Metabolomics - The link between genotypes and phenotypes. *Plant Molecular Biology* **48**: 155–171.

Garcia L, Rubilar R, Bascuñan L, Bozo D, Valverde JC. **2022**. Effect of Water Stress on Physiology and Carbon Balance in Seedlings of Different Eucalyptus Genotypes †. : 1–2.

Gaylord ML, Kolb TE, Pockman WT, Plaut JA, Yepez EA, Macalady AK, Pangle RE, Mcdowell NG. **2013**. Drought predisposes piñon-juniper woodlands to insect attacks and mortality. *New Phytologist* **198**: 567–578.

Gessler A, Schaub M, McDowell NG. **2017**. The role of nutrients in drought-induced tree mortality and recovery. *New Phytologist* **214**: 513–520.

Gonçalves CI, Vilas-Boas L, Branco M, Rezende GD, Valente C. **2019**. Host susceptibility to Gonipterus platensis (Coleoptera: Curculionidae) of Eucalyptus species. *Annals of Forest Science* **76**.

González P, Sossa K, Rodríguez F, Sanfuentes E. **2018**. Rhizobacteria strains as promoters of rooting in hybrids of eucalyptus nitens × eucalyptus globulus. *Chilean Journal of Agricultural Research* **78**: 3–12.

Hamann E, Blevins C, Franks SJ, Jameel MI, Anderson JT. **2021**. Climate change alters plant–herbivore interactions. *New Phytologist* **229**: 1894–1910.

Harfouche A, Meilan R, Altman A. **2018**. Invited review Molecular and physiological responses to abiotic stress in forest trees and their relevance to tree improvement. *Tree Physiology*: 1181–1198.

Hendriks MMWB, Eeuwijk FA van, Jellema RH, Westerhuis JA, Reijmers TH, Hoefsloot HCJ, Smilde AK. **2011**. Data-processing strategies for metabolomics studies. *TrAC - Trends in Analytical Chemistry* **30**: 1685–1698.

Herrmann KM, Weaver LM. **1999**. The shikimate pathway. *Annual Review of Plant Biology* **50**: 473–503.

Huerta-Fuentes A, Chiffelle-Gomez I, Serrano-Garzon M, Vazquez-Silva T, Araya-Clericus J. **2008**. Susceptibility of *eucalyptus s*pecies to Gonipterus scutellatus and electrophoretic profiles of adult marker proteins. *Agrociencia* **42**: 327–334.

Jan R, Asaf S, Numan M, Lubna, Kim KM. **2021**. Plant secondary metabolite biosynthesis and transcriptional regulation in response to biotic and abiotic stress conditions. *Agronomy* **11**: 1–31.

Jofré Filgueira, Paola AuroraBahamóndez V. C, Barros Asenjo S, Büchner C, Cabrera Perramón J, García P, Ipinza Carmona R. **2013**. *Estado del arte. Las plantaciones forestales y el agua*.

Kell DB, Brown M, Davey HM, Dunn WB, Spasic I, Oliver SG, Building MS. **2005**. METABOLIC FOOTPRINTING AND SYSTEMS BIOLOGY : THE MEDIUM IS THE MESSAGE. **3**.

Kröner A, Marnet N, Andrivon D, Val F. **2012**. Nicotiflorin, rutin and chlorogenic acid: Phenylpropanoids involved differently in quantitative resistance of potato tubers to biotrophic and necrotrophic pathogens. *Plant Physiology and Biochemistry* **57**: 23–31.

Külheim C, Moran GF, Laffan S, Yeoh SH, Wallis IR, Foley WJ. **2011**. The molecular basis of quantitative variation in foliar secondary metabolites in *Eucalyptus globulus*. *New Phytologist* **191**: 1041–1053.

Lanfranco D, Dungey HS. **2001**. Insect damage in Eucalyptus: A review of plantations in Chile. *Austral Ecology* **26**: 477–481.

Lim CW, Baek W, Jung J, Kim JH, Lee SC. **2015**. Function of ABA in stomatal defense against biotic and drought stresses. *International Journal of Molecular Sciences* **16**: 15251–15270.

Lincoln TIMM. **2019**. *Plant Physiology and Development*.

Liu X, Locasale JW. **2017**. Metabolomics : A Primer. *Trends in Biochemical Sciences* **42**: 274–284.

Loch AD, Matsuki M. **2010**. Effects of defoliation by *Eucalyptus* weevil, *Gonipterus scutellatus*, and *chrysomelid* beetles on growth of *Eucalyptus globulus* in southwestern Australia. *Forest Ecology and Management* **260**: 1324–1332.

Machado F, Dias MC, Pinho PG de, Araújo AM, Pinto D, Silva A, Correia C, Moutinho-Pereira J, Santos C. **2017**. Photosynthetic

performance and volatile organic compounds profile in *Eucalyptus globulus* after UVB radiation. *Environmental and Experimental Botany* **140**: 141–149.

Madhibha T, Murepa R, Musokonyi C, Gapare W. **2013**. Genetic parameter estimates for interspecific *Eucalyptus* hybrids and implications for hybrid breeding strategy. *New Forests* **44**: 63–84.

Mapondera TS, Burgess T, Matsuki M, Oberprieler RG. **2012**. Identification and molecular phylogenetics of the cryptic species of the Gonipterus scutellatus complex (Coleoptera: Curculionidae: Gonipterini). *Australian Journal of Entomology* **51**: 175–188.

Matsuki M, Foley WJ, Floyd RB. **2011**. Role of Volatile and Non-Volatile Plant Secondary Metabolites in Host Tree Selection by Christmas Beetles. : 286–300.

McDowell N, Pockman WT, Allen CD, Breshears DD, Cobb N, Kolb T, Plaut J, Sperry J, West A, Williams DG, *et al.* **2008**. Mechanisms of plant survival and mortality during drought: Why do some plants survive while others succumb to drought? *New Phytologist* **178**: 719–739.

Mckiernan AB, Hovenden MJ, Brodribb TJ, Potts BM, Davies NW, Reilly-wapstra JMO. **2014**. Effect of limited water availability on foliar plant secondary metabolites of two *Eucalyptus* species. *Environmental and Experimental Botany* **105**: 55–64.

Nardini A, Pitt F. **1999**. Drought resistance of Quercus pubescens as a function of root hydraulic conductance, xylem embolism and hydraulic architecture. *New Phytologist* **143**: 485–493.

Navarrete-Campos D, Bravo LA, Rubilar RA, Emhart V, Sanhueza R. **2013**. Drought effects on water use efficiency, freezing

tolerance and survival of *Eucalyptus globulus* and *Eucalyptus globulus ×
nitens* cuttings. *New Forests* **44**: 119–134.

Naz S, Vallejo M, García A, Barbas C. **2014**. Method validation
strategies involved in non-targeted metabolomics. *Journal of
Chromatography A*.

Neilson EH, Goodger JQD, Woodrow IE, Møller BL. **2013**. Plant
chemical defense: At what cost? *Trends in Plant Science* **18**: 250–258.

**de Oliveira TWG, Rubilar R, Sanquetta CR, Corte APD, Medina
A, Mardones O, Emhart V, Quiroga JJ, Valenzuela H, Bozo D**. **2022**.
Differences in early seasonal growth efficiency and productivity of
eucalyptus genotypes. *New Forests* **53**: 811–829.

Pinet C. **1984**. Patasson nitens. **287**: 285–287.

Reis AR, Ferreira L, Tomé M, Araujo C, Branco M. **2012b**.
Efficiency of biological control of Gonipterus platensis (Coleoptera:
Curculionidae) by *Anaphes nitens* (Hymenoptera: Mymaridae) in cold areas
of the Iberian Peninsula: Implications for defoliation and wood production in
Eucalyptus globulus. *Forest Ecology and Management* **270**: 216–222.

Rivera AC, Carbone SS, Andrés JA. **1999**. Life cycle and biological
control of the *Eucalyptus* snout beetle (Coleoptera, Curculionidae) by
Anaphes nitens (Hymenoptera, Mymaridae) in north-west Spain.
Agricultural and Forest Entomology **1**: 103–109.

**Romão K de CS, Nunes ACP, Santos AP dos, Santos OP dos,
Valente BM dos RT**. **2023**. Multi-site comparison of clonal arrangements

for tropical and subtropical hybrids of *Eucalyptus*. *Industrial Crops and Products* **197**.

Rubilar R, Hubbard R, Emhart V, Mardones O, Quiroga JJ, Medina A, Valenzuela H, Espinoza J, Burgos Y, Bozo D. **2020**. Climate and water availability impacts on early growth and growth efficiency of *Eucalyptus* genotypes: The importance of GxE interactions. *Forest Ecology and Management* **458**: 117763.

Santolamazza S, Fernández A. **2004**. Efectos de dos insecticidas de síntesis y de dos bio-insecticidas sobre el defoliador del eucalipto *Gonipterus scutellatus Gyllenhal* y su agente de control biológico *Anaphes nitens* Girault. *Boletín de sanidad vegetal. Plagas* **30**: 265–277.

Schrimpe-Rutledge AC, Codreanu SG, Sherrod SD, McLean JA. **2016**. Untargeted Metabolomics Strategies—Challenges and Emerging Directions. *Journal of the American Society for Mass Spectrometry* **27**: 1897–1905.

Shen S, Zhan C, Yang C, Fernie AR, Luo J. **2023**. Metabolomics-centered mining of plant metabolic diversity and function: Past decade and future perspectives. *Molecular Plant*: 1–21.

Sperry JS, Hacke UG. **2002**. Desert shrub water relations with respect to soil characteristics and plant functional type. *Functional Ecology* **16**: 367–378.

Spina R, Saliba S, Dupire F, Ptak A, Hehn A, Piutti S, Poinsignon S, Leclerc S, Bouguet-Bonnet S, Laurain-Mattar D. **2021**. Molecular identification of endophytic bacteria in leucojum aestivum in vitro culture, nmr-based metabolomics study and lc-ms analysis leading to potential

amaryllidaceae alkaloid production. *International Journal of Molecular Sciences* **22**: 1–21.

Spokevicius A V., Tibbits J, Rigault P, Nolin MA, Müller C, Merchant A. **2017**. Medium term water deficit elicits distinct transcriptome responses in Eucalyptus species of contrasting environmental origin. *BMC Genomics* **18**: 1–17.

Sumner LW, Mendes P, Dixon RA. **2003**. Plant metabolomics: Large-scale phytochemistry in the functional genomics era. *Phytochemistry* **62**: 817–836.

Valdés AE, Irar S, Majada JP, Rodríguez A, Fernández B, Pagès M. **2013**. Drought tolerance acquisition in *Eucalyptus globulus* (Labill.): A research on plant morphology, physiology and proteomics. *Journal of Proteomics* **79**: 263–276.

Valente C, Gonçalves CI, Monteiro F, Gaspar J, Silva M, Sottomayor M, Paiva MR, Branco M. **2018**. Economic Outcome of Classical Biological Control: A Case Study on the *Eucalyptus* Snout Beetle, *Gonipterus platensis*, and the Parasitoid Anaphes nitens. *Ecological Economics* **149**: 40–47.

Valledor L, Escandón M, Meijón M. **2014**. A universal protocol for the combined isolation of metabolites, DNA, long RNAs, small RNAs, and proteins from plants and microorganisms.: 173–180.
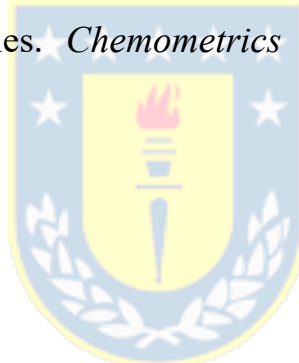
Volker PW, Potts BM, Borralho NMG. **2008**. Genetic parameters of intra- and inter-specific hybrids of *Eucalyptus globulus* and *E. nitens*. *Tree Genetics and Genomes* **4**: 445–460.

Wasternack C, Song S. **2017**. Jasmonates: Biosynthesis, metabolism, and signaling by proteins activating and repressing transcription. *Journal of Experimental Botany* **68**: 1303–1321.

White D a, Beadle CL, Worledge D. **1996**. Seasonal, Drought and Species Effects. *Tree Physiology* **16**: 469–476.

Worley B, Powers R. **2016**. PCA as a predictor of OPLS-DA model reliability. *Current Metabolomics* **4**: 97–103.

Yamamoto H, Yamaji H, Abe Y, Harada K, Waluyo D, Fukusaki E, Kondo A, Ohno H, Fukuda H. **2009**. Dimensionality reduction for metabolome data using PCA, PLS, OPLS, and RFDA with differential penalties to latent variables. *Chemometrics and Intelligent Laboratory Systems* **98**: 136–142.

CAPITULO 4: RESULTADOS

4.1. Constitutive and inducible defense in Eucalyptus determines the feeding host of Gonipterus platensis, denoting specific plant-insect coevolution and a strategy for resistance improvement.

Constitutive and inducible defense in *Eucalyptus* determines the feeding host of *Gonipterus platensis*, denoting specific plant-insect coevolution and a strategy for resistance improvement.

Jasna V. Campos [a], Sebastián Riquelme [a], Łukas Pecio [b], Lubia Guedes [c], Claudia Mardones [a], Rosa Alzamora [d, g], Luis E. Arteaga-Pérez [e], Rafael Rubilar [f, g], Oliver Fiehn [h], Andy J. Pérez [a, *]

[a] Departamento de Análisis Instrumental, Facultad de Farmacia, Universidad de Concepción, Concepción, Chile.

[b] Department of Biochemistry and Crop Quality, Institute of Soil Science and Plant Cultivation, State Research Institute, ul. Czartoryskich 8, 24-100 Puławy, Poland.

[c] Laboratorio de Semioquímica Aplicada, Facultad de Ciencias Forestales, Universdiad de Concepción, Concepción, Chile.

[d] Departamento Manejo de Bosques y Medio Ambiente, Facultad de Ciencias Forestales, Universidad de Concepción, Concepción, Chile.

[e] Laboratory of Thermal and Catalytic Processes (LPTC), Department of Wood Engineering, University of Bío-Bío, Chile.

[f] Cooperativa de Productividad Forestal, Departamento de Silvicultura, Facultad de Ciencias Forestales, Universidad de Concepción, Concepción, Chile.

[g] Centro Nacional de Excelencia para la Industria de la Madera (CENAMAD), Pontificia Universidad Católica de Chile, Santiago, Chile.

[h] NIH West Coast Metabolomics Center, UC Davis Genome Center, University of California, Davis, CA 95616, USA.

[*] Corresponding author E-mail: aperezd@udec.cl Phone: + 56 41 220 3027

Abstract

Defoliation caused by *Gonipterus platensis* on *Eucalyptus* seriously impacts tree growth rate and forest production. The weevil's feeding preference has sometimes limited which species of *Eucalyptus* to plant, although the plant's metabolic features that govern such choice still need to be uncovered. We used metabolomics to reveal the chemical traits mediating this interaction, focusing on a model formed by two *Eucalyptus* species with

markedly different susceptibility, *E. globulus (susceptible),* and *E. nitens (resistant)*. Our results suggest that the insect's feeding preference strongly depends on the *Eucalyptus* species' constitutive metabolome, especially on the stilbenes and hydrolysable tannins accumulation. The susceptible *E. globulus* could not produce such classes of metabolite either constitutively or after herbivory, which indicated an apparent lack of critical enzymes for biosynthesis of these substances, such as stilbene synthase (STS) and gallate 1-β-glucosyltransferase. On the other hand, it seems that no matter how toxic the systemic defense induced in *E. globulus* after herbivory could be to an insect, counteradaptations, apparently evolved by the weevil, may efficiently detoxify them. This may result from plant-insect coevolution, given their common geographical origin. Inter-specific hybridizations between *E. nitens* and *E. globulus* have adapted hybrid species better to low temperatures and frost conditions, consequently being propagated for plantations in temperate regions. Thus, this research lays the groundwork for selecting the best parent genotypes and obtained hybrids, aiming to warrant the transfer of key resistance traits to progenies as an attractive strategy for future breeding programs.

4.1.1. Introduction

The *Eucalyptus* (Myrtaceae) species, appreciated for their adaptation and fast growth, are among the most widely planted pulpwood in temperate regions worldwide (Cerasoli *et al.*, 2016). In Chile, eucalypt plantations cover over 800 thousand ha, around 37% of total forest planted, surpassed only by *Pinus radiata*, which covers about 56% of the whole forest surface (Gysling Caselli *et al.*, 2018). *Eucalyptus globulus* Labill. (Tasmanian blue gum) and *E. nitens* (Deane & Maiden) Maiden (shining gum) are the two most planted species in Chile, accounting for 24.5% and 11.1% of the total area, respectively (Gysling Caselli *et al.*, 2017).

Together with the success of eucalypts adoption, harmful exotic pathogens and specialist insects have been accidentally spread worldwide. One of these is the eucalyptus weevil, *Gonipterus platensis* Marelli (Coleoptera: Curculionidae), a specialist insect native to Eastern Australia that feeds on eucalypts' new foliage causing severe defoliation in the tree crown (EPPO 2005; Mapondera et al., 2012). It has economically impacted plantations within Europe (France, Italy, Portugal, and Spain) (Cordero-Rivera & Santolamazza-Carbone, 2000; EPPO 2005; Reis et al., 2012; Valente et al.,

2018), North America (California) (Paine & Millar, 2002), South America (Argentina, Brazil, Chile, and Uruguay) (Lanfranco & Dungey, 2001b; Huerta-Fuentes *et al.*, 2008b), and Oceania (New Zealand and Southwestern Australia) (Loch & Floyd, 2001; Withers, 2001; Loch & Matsuki, 2010b). Based on the damage it usually causes, its quarantine and obliged control have been implemented in some of the countries mentioned above (Beéche Cisternas et al., 1999; EPPO 2018). However, given the difficulties in implementing large-scale phytosanitary control programs, selecting which species to plant has been used as an alternative solution to avoid productivity losses (Coppen, 2002). This species selection has been based on the weevil's marked preference for some *Eucalyptus* species, being *E. globulus* the most affected one as it is the natural host of *G. platensis* (Mapondera *et al.*, 2012b).

In the case of Chile, the weevil was first detected in 1998 by the Agricultural and Livestock Service (SAG, Spanish acronym) of the Chilean Agriculture Ministry, which declared its mandatory control (Beéche Cisternas *et al.*, 1999b). It was initially classified as *G. scutelatus*, but more than a decade later, it was redefined as *G. platensis* Marelli (Mapondera et al., 2012; Informativo fitosanitario forestal N°8, SAG, 2012). Despite efforts made for its biological control with the egg-parasites *Anaphes nitens* and *A.*

tasmaniae (Hymenoptera: Mymaridae), spreading and damage persist, and the insect has become a severe concern to SAG and Chilean forest companies (Gysling Caselli *et al.*, 2019). According to the Forestry Institute of the Chilean Agriculture Ministry, recent projections for future wood availability from *E. globulus* plantations alert about a deficit of 1.6 million m^3, pointing to the weevil among factors that have affected the growth rate (Aguirre *et al.*, 2021).

In Chile, like in the rest of the world, plantations of *E. globulus* are by far the most affected by the weevil, although the second most planted species, *E. nitens*, appears to evade herbivory (Lanfranco & Dungey, 2001b; Huerta-Fuentes *et al.*, 2008b; Gonçalves *et al.*, 2019b). Such preference has been attributed to a coevolutionary process associated with the plant-insect common geographical origin, Tasmania, and where the insect has developed counteradaptations for overcoming the plant's chemical defenses (Mapondera et al., 2012; Pentzold et al., 2014). However, the implication of plant constitutive or induced metabolism in this interaction has yet to be uncovered and understood.

Analytical measurement of the plant metabolome expression is always challenging, given its vast diversity in metabolite classes and chemical

structures. Metabolomics has strongly emerged as an appropriate tool for functional analysis of specialized plant metabolites that facilitates a simultaneous quantitative comparison of hundreds to thousands of metabolites, describing the physiological state and comprehensively understanding of response to abiotic and biotic stresses (Fiehn *et al.*, 2000; Fiehn, 2001; Li & Gaquerel, 2021). Since metabolites are downstream products of cellular biochemical processes, their identification and quantitative analysis represent a sensitive measure of upstream molecular function. The usefulness of metabolomics for revealing the fundamental role of plant chemical defense and cryptic chemical traits determining the host range for herbivores and pathogens has been noted, especially for plant-specialist insect interactions (Sedio, 2017).

Despite the previously described dose-dependent deterrent effect of *Eucalyptus*'s foliar 1,8-cineole monoterpene against other pathogens such as Christmas beetles (Coleoptera: Scarabaeidae) (Matsuki *et al.*, 2011b), insufficient knowledge exists about the role of non-volatile specialized metabolites in the insect host selection or concerning the leaf's metabolome changes in response to herbivory. Therefore, in the present research, we used a multiple approach study, including LC-MS-based untargeted

metabolomics, histochemical analysis, and antifeedant assays, to identify the non-volatile metabolites constitutively present in *Eucalyptus* leaves influencing the weevil feeding choice. At the same time, we revealed the metabolic response induced in *E. globulus* leaves upon weevil herbivory, discussing its functional relevance for defending.

4.1.2. Material and methods

4.1.2.1. Origin of plant material and collection

Clonal plantations of *E. globulus* Labill. ssp. *globulus* (37°34′21.9″S 72°45′18.1″W) and *E. nitens* (Deane & Maiden) Maiden (37°32′43.6″S 72°43′58.0″W), located Southwest of Nacimiento city in the Biobio Region of Chile, were selected for this study. The stands, two years of age, and 3.5 km distant from each other, belonged to Forestal Mininco S.A. and were planted for commercial purposes. On August 10th, 2018, the foliage was sampled between 10:00 a.m. and 12:00 am. Weather conditions during August 2018 are detailed in Method S1.

The sampling site was selected based on 1) availability of two-year-old stands with both species, which is the age from which bulk incidences of *G. platensis* usually begin regardless of the year season, and 2) location within

a wide area of intense infestation by the weevil (Memoria Anual Consorcio Protección Fitosanitaria Forestal S.A., 2018). At the time of sampling, an early infestation was observed within the *E. globulus* stand, evidenced by 1) partial defoliation of buds in the tree crown and scalloped edges in the canopy leaves caused by adults feeding, 2) photosynthetic tissues loss in expanded leaves due to larvae feeding following a characteristic pattern, 3) oviposition of greyish capsules (ootheca) in the leaves surface, and 4) adults and larvae sighting. Both infested and healthy (without sign of damage) *E. globulus* trees were sampled. Meanwhile, *E. nitens* stand sampled simultaneously had no symptoms of infestation by the weevil.

Sampling considered three groups of ten trees, each coded HT-EG (healthy trees of *E. globulus*), IT-EG (infested trees of *E. globulus*), and EN (healthy trees of *E. nitens*), that were randomly selected within an area of 4 ha within stands. A total of 15 fully expanded mature leaves (petiolate) without signs of herbivory were collected from each selected tree, considering five leaves from the top of the canopy, five at mid-canopy height, and five at the bottom of the canopy. Samples were immediately submerged in liquid nitrogen in the field, transported to the laboratory, and stored at -80°C until grinding, homogenization, and metabolome extraction.

4.1.2.2. Samples handling and metabolome extraction

Frozen fresh samples (FFSs) were ground into a fine powder and homogenized using an MM-400 mixer mill (Retsch GmbH, Haan, Germany) under cryogenic conditions. The moisture content of each sample was determined by a thermogravimetric method to normalize the weighing before extraction. All samples were processed in triplicate within a complete randomized block for metabolome extraction and analysis. The extraction was performed following the procedure suggested by Valledor et al. (2014) with slight modifications. Briefly, 1000 µl of cold (4°C) MeOH/H_2O/CH_2Cl_2 (2.5:0.5:1.0) were added to 100 mg (dried weight basis) of each powdered FFS contained in a 2 ml microcentrifuge tube and shaken for 60 s at 30 Hz in MM-400 mixer mill. Simultaneously, blanks containing only extraction solvent were also processed in triplicate and included in the randomized block. Then, samples were centrifuged at 13300 g for 10 min at 4°C, and 600 µl supernatants were transferred to new 2 ml microcentrifuge tubes. These extracts were subjected to liquid-liquid extraction by adding CH_2Cl_2 and water, 400 µl each, and shaken for 30 s at 20 Hz. After centrifuging at 13300 g for 5 min at 4°C, two phases were clearly defined with a sharp interface.

600 µl of the hydrophilic (top layer) fractions were transferred to new tubes, dried in a vacuum centrifuge (Eppendorf, Concentrator plus), and stored at - 80°C until needed. The bottom lipophilic fractions containing pigments and other non-polar substances were discarded.

4.1.2.3. LC-MS analysis

Immediately before analysis, dried extracts and blanks were resuspended in 600 µl of 80% methanol (in water, v/v) at 4°C, shaken for 30 s at 30 Hz, and centrifuged for 10 min at 13300 g. A pooled quality control (QC) sample was conformed with 60 µl aliquots taken from each sample. Blank, QC, and plant extract samples were then transferred to 200 µl inserts contained in 1.5 ml amber vials and placed in a liquid chromatography autosampler maintained at 4°C according to the predetermined random sequence. This started with three blank samples, six consecutive QCs, and other QC after every ten plant extracts.

Metabolomics analysis was carried out by LC-MS/MS on an ultrahigh performance liquid chromatography system (Elute UHPLC, Bruker Daltonik GmbH, Bremen, Germany) equipped with a diode array detector (Elute DAD) and coupled in tandem with a quadrupole-time-of-flight mass

spectrometer equipped with an atmospheric pressure electrospray ion source (Compact ESI-QTOF, Bruker Daltonik GmbH, Bremen, Germany). Chromatographic separation was performed on a Kinetex C18 UHPLC column (100 × 3.0 mm, 1.7 μm; Phenomenex) using a SecurityGuard Ultra Cartridge UHPLC C18 3.0 mm pre-column and maintained at 30°C. The mobile phase consisted of solvent A (0.1% formic acid in Milli-Q water, v/v) and solvent B (0.1% formic acid in acetonitrile hypergrade, v/v) at a flow rate of 400 μl min⁻¹. Gradient elution began with 2.0 min equilibration time at 5% B and continued as follow: 0.0 – 24.0 min, 5 – 57.6% B in concave 2 shape; 24.0 – 25.0 min, 57.6 – 100% B linear; 25.0 – 28.0 min, 100% B; 28.0 – 29.0 min, 100 – 5% B linear. The injection volume was 2.0 μl. DAD was operated in the wavelength range from 194 nm to 600 nm at a data acquisition rate of 10.0 Hz.

The mass spectrometer was operated in negative and positive ESI modes in data-dependent auto-MS/MS acquisition. MS parameters were set as follow: mass range, 50 – 1500 m/z; scan cycle time, 0.2 s; dry temperature, 200°C; capillary voltage, 3.5 kV (–ESI) and 4.5 kV (+ESI); endplate offset, 0.5 kV (both ESI modes); desolvation gas flow, 9.0 l min⁻¹ (N_2); nebulizer pressure, 4.0 Bar. MS/MS spectra were acquired from each scan by

subjecting ions (maximum 2) to collision-induced dissociation (CID) if their absolute intensities exceeded 1000 counts per 0.2 s cycle, with variable collision energy in the range of $20 - 50$ eV. Active exclusion of precursor ion was applied after one spectrum, and fragmentation was reconsidered if its intensity was at least equal to the previously measured one. For internal reference, sodium formate solution (10 mM in iso-PrOH/H_2O, 1:1, v/v) was pumped continuously at a rate of 1 µl min^{-1} through a six-port-valve so that 20 µl of it was delivered to the mass spectrometer just before each analysis.
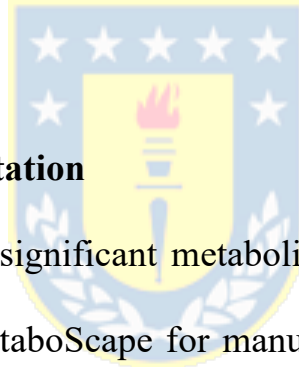
4.1.2.4. Data processing and statistics

The raw LC-MS data acquired in both ESI modes were processed in MetaboScape 3.0 (Compass, Bruker Daltonik GmbH, Germany) by selecting the algorithm Time aligned Region complete eXtraction (T-ReX 3D). It integrates all processing steps, including mass re-calibration, retention time (Rt) alignment, feature extraction (m/z – Rt pairs), adduct and neutral losses handling, whole region feature extraction, import of MS/MS spectra, and generates Bucket Tables where features are assigned to Buckets (m/z – Rt pairs with respective ion intensity) across samples with recursive extraction of missed peaks for improved statistics. The parameters used for bucket table

generation through the T-ReX 3D algorithm were set as follows: intensity threshold, 1000 counts; minimum spectra peak length, 5; minimum recursive peak length, 4; minimum number of recursive features to be extracted, if present in 1/3 of a group; features in a minimum number of analysis, present in 1/3 of a group; mass range, 100 – 1500 *m/z*; retention time range, 0.5 – 25.0 min; MS/MS import, average.

Generated bucket tables were first manually curated using exploratory statistics in MetaboScape and then exported to MetaboAnalyst 5.0 for a high-throughput analytical pipeline for metabolomics (Chong et al., 2019; Pang et al. 2021). After uploading, data were normalized by sum, Pareto-scaled, and examined by applying principal component analysis (PCA) for reducing data dimensionality and uncovering the inherent clusters pattern (Worley & Powers, 2013a). Then, Orthogonal Projections to Latent Structures Discriminant Analysis (OPLS-DA) was applied to the dataset. This is a supervised modeling method, which allowed for discovering features that best discriminated between the metabolome of these two species (EN and HT-EG) or features correlated with the systemic response in *E. globulus* upon *G. platensis* herbivory. In this case, HT-EG and IT-EG labels were used for healthy and infested trees, respectively. However, the OPLS-DA model

aggressively enforces the separation of these two classes, thus causing a risk of over-fitting the model to the data. Therefore, validation was performed to avoid such bias and ensure model reliability by using a combined random permutation test of class labels with internal leave-*n*-out cross-validation. The parameters of a measure of internal consistency between the original and cross-validated predicted data (Q^2) and the measure of model fit to the original data (R^2Y) were used to assess statistical quality (Worley & Powers, 2013a, 2016b).

4.1.2.5.   Metabolite annotation

The chemical nature of significant metabolite was determined using an integrated workflow in MetaboScape for manual annotation. The first step included the SmartFormula task to determine molecular formulas based on accurate-mass and isotopic pattern information for a given extracted feature. Elements such as C, H, N, O, P, and S, were considered in the calculations, with a tolerance of 5 ppm. SmartFormula 3D calculation was also applied in this step for all features with available MS/MS spectra, improving the quality of the calculated molecular formula. This is an intelligent interface for annotating all monoisotopic peaks in the MS/MS spectrum. Thus, for each

possible explanation of the *m/z* of a feature's precursor and isotopic pattern, SmartFormula 3D determined which ion formulas best explained the monoisotopic peak and isotopic pattern of the MS/MS fragment spectrum and ranked them according to MS/MS fragment explained and intensity coverage. In the next step, the Compound Crawler tool searches possible structures that fit the first ranked formula, sending queries for a given molecular formula to databases such as ChEBI, ChemSpider, and PubChem and returns results that can be used to annotate compounds. The selection of the correct structure was then performed using the MetFrag algorithm, as multiple structure candidates were typically found in Compound Crawler for a given elemental composition. Using the MS/MS fragment spectrum, MetFrag searches for ions matching with *in-silico* fragmentation of possible candidates provided by Compound Crawler and ranks them according to explained fragment peaks and intensity coverage (Ruttkies *et al.*, 2016a). Finally, the selection of the best candidate for a given feature was refined by the MS/MS Library Search tool, which compared the MS/MS spectrum of the features with those of known compounds contained in Spectral Libraries previously imported in MetaboScape such as Bruker MetaboBASE Plant Library and Vaniya/Fiehn Natural Products Library of the MassBank of

North America (MoNA). SIRIUS 4.0, a freely available web service integrating high-resolution isotopic pattern analysis and fragmentation trees for structural elucidation, was also used to improve annotation (Dührkop *et al.*, 2019b). Retention times coincidence, as well as MS and MS/MS spectral matching with pure chemical standards, where available, were also examined for final structure confirmation and higher annotation (A). Pure standards of *trans*-Piceid (*trans*-Polydatin), Astringin, Ellagic acid, Rutin, Quinic acid, Isocitrate, and Isoquercitrin were purchased from Sigma-Aldrich/Merck-Chile (Phyproof® Reference Subtance, PhytoLab GmbH., Germany).

4.1.2.6. Feeding inhibition test

To explore the potential antifeedant role of *E. nitens* differential metabolites (**1-12**), a feeding test was performed with adults of *G. platensis*. For this purpose, an extract mainly containing these metabolites was obtained from *E. nitens* leaves and purified to exclude polar and lipophilic undesirable interferences. Extraction and fractionation methodology and composition confirmation are described in Method S2.

Adults of *G. platensis* were collected in the field within an *E. globulus* plantation and reared under laboratory conditions in a transparent and well-

ventilated cage (60×60×50 cm; length/width/height). They were fed with fresh *E. globulus* branches and supplied with water daily. After two weeks of conditioning, insects were transferred to a smaller plastic box with ventilation and immediately subjected to starvation with a water supply for two days. Insect conditioning and experiments were carried out in a plant growth chamber (FH-1200 Series LED Z190 L4, HiPoint, Taiwan) at 20°C/17°C (day/night), 70% RH, and 355 µmol s^{-1} m^{-2} PPFD in the range of active photosynthetic radiation (λ_{max} = 575 nm), with constant photoperiod of 16 h of light and eighth of darkness.

The feeding inhibitory capacity of the *E. nitens* purified fraction against the adults of *G. platensis* was assayed in a choice test, considering three independent replicates. Fresh branches with petiolate leaves collected from the upper third of *E. globulus* trees were used for testing. Twenty-four leaves in their branches were selected according to their similar size, morphology, ontology, and without signs of herbivory. Half of them were sprayed on both sides with an aqueous solution of the *E. nitens* fraction at 20 g l^{-1}, a similar dose as the average of the biological concentration found in *E. nitens* leaves. The other half was sprayed only with distilled water and used as a control. After treatment, leaves were left to dry in a fuming hood at room temperature.

Two flasks containing branches with the sprayed leaves and other with the control leaves were placed in a transparent cage (45×60×45 cm) in front of each other, and 180 weevils were released from a small box equidistant from both flasks (Fig. S2). The exposure was prolonged for 24 h in the plant growth chamber. At the end of the experiment, weevils settled in branches of each condition were counted and removed to stop consumption. Leaves were cut from the stems and photographed to register the foliar area consumed by weevils using the LeafByte software, an open-source mobile application that allows for an accurate measure of herbivory (Getman-Pickering et al., 2020). Statistics treatment of results was performed in GraphPad Prism software (v. 8.4.3), where data were first tested for normality and then subjected to a non-parametric Mann-Whitney test to determine how much was the leaf consumption in control concerning treatment, considering a statistical significance for $p < 0.05$. The antifeedant index (AFI), defined as $AFI = C - T/C + T$ (MaSchlyter et al., 2004), was also determined to quantify the feeding inhibitory capacity, where C and T refer to the consumption in control and treatment, respectively. Accordingly, AFI=1 indicates maximum antifeedant effect, AFI=0 no effect, and AFI= -1 perfect feeding stimulant.

4.1.2.7. Histochemical analysis

Given the case that *E. nitens* differential metabolites were all annotated as polyphenols (Table 1), a histochemical analysis was performed to detect the accumulation tissues of phenolic metabolites within the leaf tissues of both *E. nitens* and *E. globulus*. Fully expanded mature leaves (petiolate) of six trees were used in this study (three leaves per tree and species). After collection, leaves were fixed for 48 hours in formalin-ferrous sulfate (2 ml of 37% formaldehyde and 5 g of iron (II) sulfate heptahydrate in 50 ml of water) (Johansen, 1940). In this reaction, formalin fixes, while iron both fixes and stains phenol-containing cells by forming black precipitate (Johansen, 1940). After the reaction, leaves were washed in distilled water and hand-sectioned (Ferreira *et al.*, 2017). Sections were observed and photographed under a light microscope (Leica DM500, Wetzlar, Germany, equipped with a Leica ICC50 HD camera) and compared to their respective blank section (without staining).

4.1.3. Results

4.1.3.1. Constitutive metabolome differentiation between the resistant and susceptible species

The LC-MS raw data obtained from the leaf sample extracts of healthy *E. globulus* (HT-EG) and *E. nitens* (EN) trees were processed in MetaboScape software to generate bucket tables as the main matrixes for statistical treatments. 3233 and 8418 features (*m/z* – Rt pairs) were detected in –ESI and +ESI acquisition modes.

To distinguish the differential metabolome composition constitutively expressed in the leaves of these two species, we first examined the inherent clusters pattern in the dataset by using principal component analysis (PCA). The scores plot of this model showed distributions of HT-EG and EN samples along PC1 with 56.7% of explained variance in the dataset, forming clearly defined species-specific separated clusters (Fig. 4.1.1a, b and S4a,b). It was not that surprising because, despite belonging to the same genus (*Eucalyptus*), subgenus (*Symphyomyrtus*), section (Maidenaria), and series (Globulares), *E. globulus* and *E. nitens* are still different species (Brooker, 2000; Gonçalves *et al.*, 2019b). Therefore, such separation suggested an extremely different composition between their leaf's metabolome before herbivory.

OPLS-DA model was then used to identify the features (metabolites) differentially expressed in the leaves of these two species. The score plots

showed perfect separation of samples labeled as EN from that of HT-EG along the predictive component (T score [1]) with 52.9% of the data variance correlated to classes separation (Fig. 4.1.1c and S4c). In the loading S-plots, each data point represents a specific feature (Fig. 4.1.1d and S4d). Those features at the end of both sides of the "S" contribute most to the class distinction. Thus, features on the left end were correlated with *E. nitens*, and the metabolites that they represent were constitutively present in the leaves of this species while absent or at a significantly lower level in the leaves of *E. globulus*. Their accumulation in the leaves occurs naturally as phytoanticipins, without an exogenous stimulus like herbivory. The first twelve most significant metabolites (**1-12**) comprised eight stilbenes derived from resveratrol and piceatannol (**1-5**, **7**, **11**, and **12**), three hydrolysable tannins (**6**, **8**, and **10**), and a flavonol glycoside (**9**) (Fig. 4.4.1d and S4d). In contrast, features at the right end represent metabolites expressed in *E. globulus* leaves while absent or at a significantly lower level in the leaves of *E. nitens*. Seven metabolites were identified (**1′-7′**), comprising a flavonol hexuronide (**1′**), a cyclitol (**2′**), two chromone-*C*-glycosyl derivatives (**3′** and **4′**), and three monoterpene glycosyl derivatives (**5′-7′**) (Fig. 4.1.1d and S4d). Complete chemical data for each of these metabolites are given in Table 1.

Results of the OPLS-DA model validation by random permutation of class labels with internal leave-n-out cross-validation indicated an excellent assessment of the statistical quality of the model, proving consistency between predicted and original data ($Q^2 > 0.990$), a good degree of model fit to data ($R^2Y > 0.990$), and complete separation between original model statistics (black arrow) and distribution statistics for all permutations (Fig. 4.1.1e and S4e).

Hierarchical cluster analysis in a heatmap is also shown to easily visualize the differential concentration of the top 25 most significant metabolites expressed constitutively in the leaves of *E. nitens* and *E. globulus* (Fig. 4.1.1f and S4f). A sharp contrast of metabolites accumulation was observed, where compounds **1-12** and **1′-7′** can be found in the rows enclosed by red rectangles. At the same time, samples are perfectly clustered by their species origin in columns.
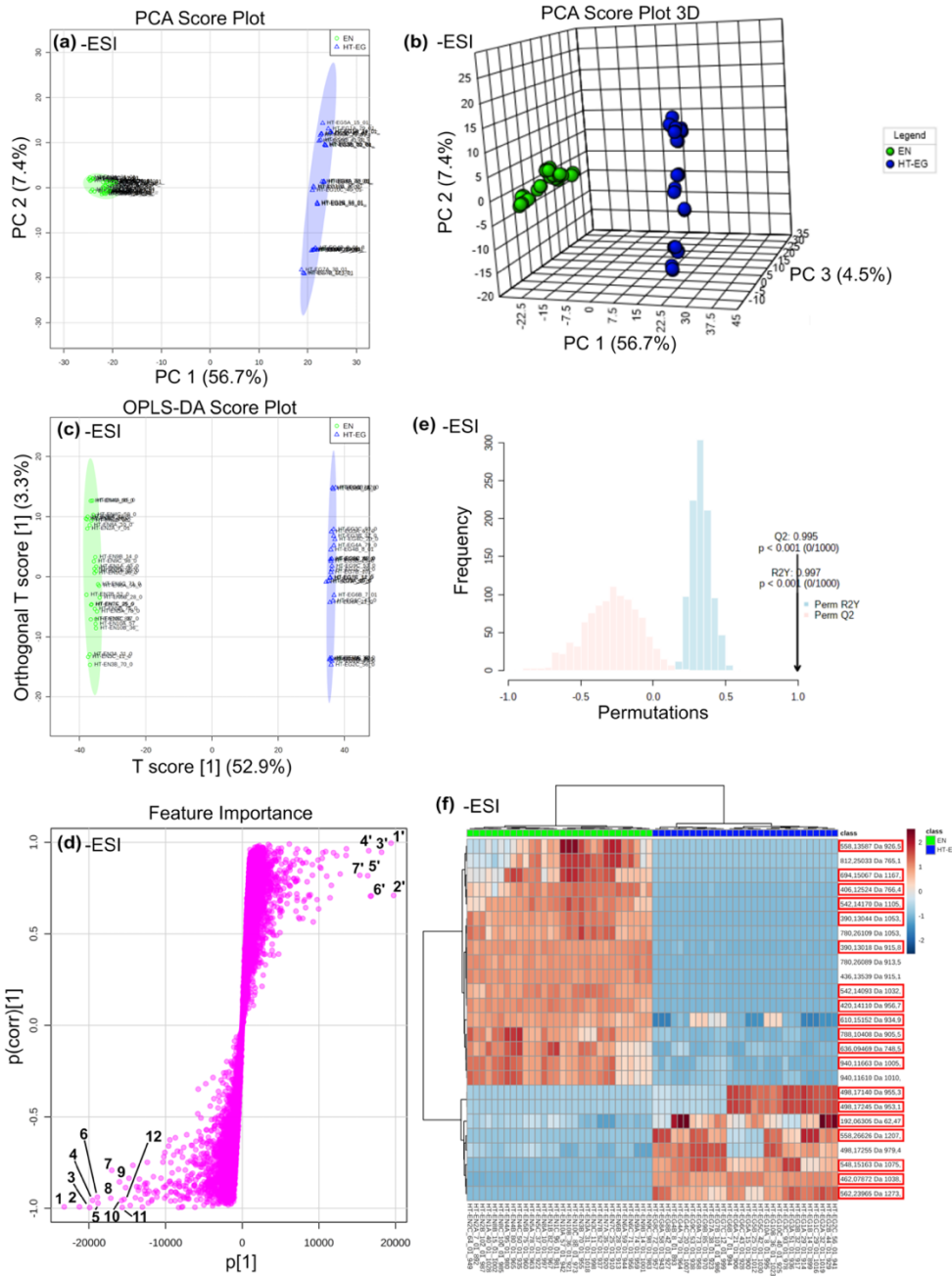
Figure 4.1.1. Statistical treatment results of the LC-MS dataset acquired in – ESI mode for distinguishing differential leaves metabolome constitutively expressed in *E. nitens* (EN) concerning *E. globulus* (HT-EG). **(a)** PCA score

plot showing species-specific cluster pattern between the first two principal components (PC1 and PC2), where green circles and blue triangles represent samples from EN and HT-EG, respectively, with their 95% confidence intervals (shadowed regions). (**b**) The same PCA score plot but incorporating the third PC for a 3D projection of sample distributions. (**c**) Score plot of the OPLS-DA model showing separation of samples labeled as EN from that of HT-EG with their 95% confidence intervals (shadowed regions). The regression method used LC-MS data as the X, and the binary vector Y formed with a value of 0 for EN class and 1 for HT-EG class. The Y-predictive component (T score [1]) shown on the x-axis represents the variation in the dataset correlated to class separation, while the orthogonal component shown on the y-axis refers to the uncorrelated variation for class distinction. (**d**) S-plot of the OPLS-DA model for visualizing the feature influence in the predictive component, combining covariance (p[1]) and correlation (p(corr)[1]) loading profiles. Covariance plotted on the x-axis visualizes the contribution to the predictive component, while correlation on the y-axis spans between ±1 as the reliability has a theoretical minimum of -1 and a maximum of +1 to predict class 1 (HT-EG). Thus, features visualized on the left-hand side contribute to class separation by high correlation with label EN

($Y = 0$) and the opposite. In this way, significant features were selected by combining high covariance ($> |15000|$) and high correlation ($> |0.5|$), and their numbers were assigned according to Table 1. (**e**) Validation of the OPLS-DA model by a random permutation test of class membership with 1000 permutations and internal cross-validation, showing the observed original model statistics (black arrow), cross-validated R^2Y and Q^2 coefficients, and distribution statistics for all permutations. (**f**) Hierarchical cluster analysis presented as a heatmap for the 25 top features according to PLS-DA variable important in projection (VIP) using Euclidean distance for similarity measure and Ward's linkage algorithm for clustering. Colors of cells indicate relative concentration values as high (dark brown) and low (dark blue), with samples in columns and features (exact mass in Da and Rt in seconds) in rows. Features identified from S-plots of the OPLS-DA models are enclosed in red rectangles.

4.1.3.2. Tissues accumulation for *E. nitens* differential constitutive metabolites

The accumulation site of metabolites differentially expressed in the leaves of *E. nitens* (**1-12**) was visualized using the formalin-ferrous sulfate reaction,

a routine method by which all polyphenols give a positive reaction forming black precipitates (Fig. 4.1.2) (Johansen, 1940). Worth noting that, unlike *E. globulus*, considerable amounts of polyphenols accumulate in the vacuoles of the pavement epidermal cells, forming a continuous layer of the one-row cell across *E. nitens* leaf (Fig. 4.1.2b, c). It may have a direct ecological implication, representing the first defense barrier in the leaf that may lead to the host's rejection by the weevil. However, the most likely function could be the well-known photoprotection against UVB radiation, especially for the stilbenes **1-3** and **12** (Table 1), which also explains their accumulation in the palisade parenchyma cells (Fig. 4.1.2b, d). In contrast, black precipitates in the *E. globulus* leaf were almost exclusively located at the spongy parenchyma and midrib (Fig. 4.1.2h-i).
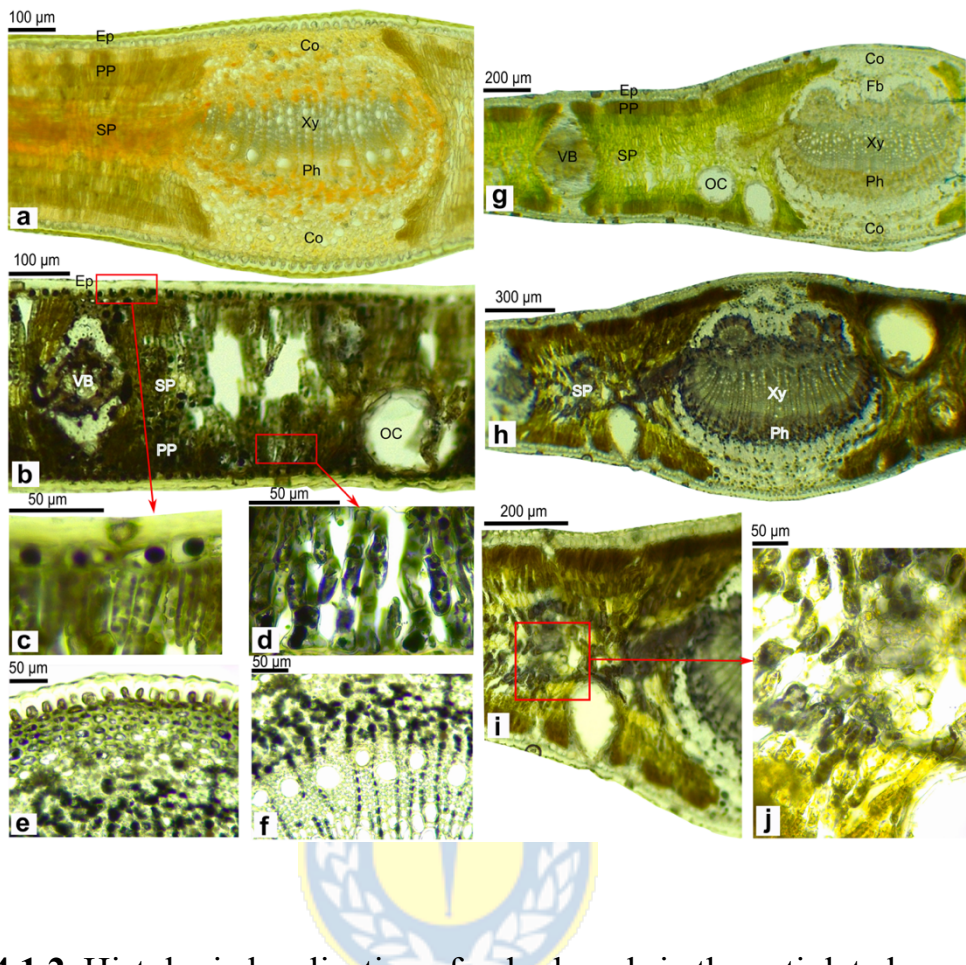
Figure 4.1.2. Histologic localization of polyphenols in the petiolate leaves of *E. nitens* (a-f) and *E. globulus* (g-j) by the black coloration formed after their reaction with ferrous sulfate and formalin. (**a** and **g**) Control leaves without staining. (**b**) Polyphenols in epidermis, palisade, spongy parenchyma, and vascular bundles of an *E. nitens* leaf. (**h**) In the spongy parenchyma, collenchyma, and phloem of an *E. globulus* leaf. (**c**) Magnified epidermal cells showing big central vacuoles containing polyphenols. (**d**) Magnification on palisade parenchyma cells, (**e-f**) in collenchyma, phloem, and

parenchymal rays of the midrib. (**i-j**) Polyphenols accumulated in the cytoplasm of spongy parenchyma cells of an *E. globulus* leaf. Co: collenchyma; Ep: epidermis; OC: oil bodies; Ph: phloem; PP: palisade parenchyma; SP: spongy parenchyma; Xy: xylem; VB: vascular bundles; Fb: fibers.

4.1.3.3. Inhibition of *G. platensis* feeding by Combination of *E. nitens* differential metabolites

The inhibitory effect exerted against the *G. platensis* feeding by a natural combination of *E. nitens* differential metabolites (**1-12**) was evaluated using a choice test. Weevils, 180 total, were subjected to choose between two groups of *E. globulus* branches for feeding. One of them contained leaves treated with the purified fraction solution at nearly the biological concentration of major metabolites (20 g l⁻¹), and the other group contained only leaves sprayed with distilled water for control (Fig. S2). Weevils showed a marked feeding preference for the control leaves, although all used leaves had similar size, morphology, and ontology. After 24 hours of each replicate, more than 50% of the total weevils were found settled in control leaves, while less than 30% were in sprayed leaves (Fig. S2b, c). The foliar area consumed by weevils was quantified and presented as the mean of the

76

three independent replicates (Fig. S3). Herbivory in treated leaves was significantly lower than in control leaves, denoted by an antifeedant index of 0.36, indicating that feeding was inhibited by 36% (Fig. S3). These results may suggest the ecological implication, at least in this case, of the *E. nitens* differential metabolites for the host plant selection by the weevil *G. platensis*.

4.1.3.4. *E. globulus* response to the *G. platensis* herbivory

To reveal the systemic metabolic response induced in *E. globulus* leaves by the *G. platensis* herbivory, an exhaustive comparison of the leaf's metabolome was performed between healthy (HT-EG) and infested (IT-EG) trees. The PCA scores plots for data acquired in -ESI and +ESI modes showed this time partially overlapped clusters for both conditions along PC1, with 23.3% and 20.0% of explained variance, respectively (Fig. 4.1.3a, e). The 3D projection of these plots by adding the variance explained by the third PC allowed for better visualization of separation (Fig. 4.1.3b, f), which suggested a clear differentiation due to infested trees' response to herbivory. The score plots of the OPLS-DA regression models perfectly separated both clusters, with 13.9% and 13.0% of the data variance correlated to group distinction as shown in the predictive component (T score [1]) for -ESI and

+ESI modes, respectively (Fig. 4.1.3c, g). The S-plots of the OPLS-DA models showed this time features up or down-regulated in infested trees during herbivory (Fig. 4.1.3d, h). Those features on the left end were correlated with HT-EG, and the metabolites they represent were significantly down-regulated in the leaves of IT-EG. At the same time, features on the right end correlated with IT-EG, and the metabolites they represent were significantly up-regulated upon herbivory. The first nine up-regulated metabolites comprised six flavonol derivatives (**9**, **9′**, **10′**, **13′-15′**), a hydroxycinnamate ester (**8′**), a cyanogenic glycoside gallate *de-novo* synthesized (**11′**), and the ellagic acid (**12′**) (Fig. 4.1.3d, h and Table 1). Interestingly, no stilbenes or their derivatives were expressed. From the other side, the first eleven down-regulated metabolites included a flavonol hexuronide (**1′**), quinic acid (**2′**), isocitric acid (**16′**), the potential phytohormone precursor vomifoliol glycoside (**17′**), four monoterpene esters (**18′**, **19′**, **21′**, **23′**), a vitamer of vitamin B6 (**24′**), and two unknown substances (**20′**, **22′**) (Fig. 4.1.3d, h and Table 1). These supervised models were validated using random permutation of class labels with internal leave-*n*-out cross-validation, indicating an excellent statistic quality assessment with Q^2=0.98 and R^2Y=0.99 for -ESI, and Q^2=0.978 and R^2Y=0.992 for +ESI

(Fig. S5). Altogether, it represented the systemic metabolic response in *E. globulus* to the defoliation caused by *G. platensis* feeding.
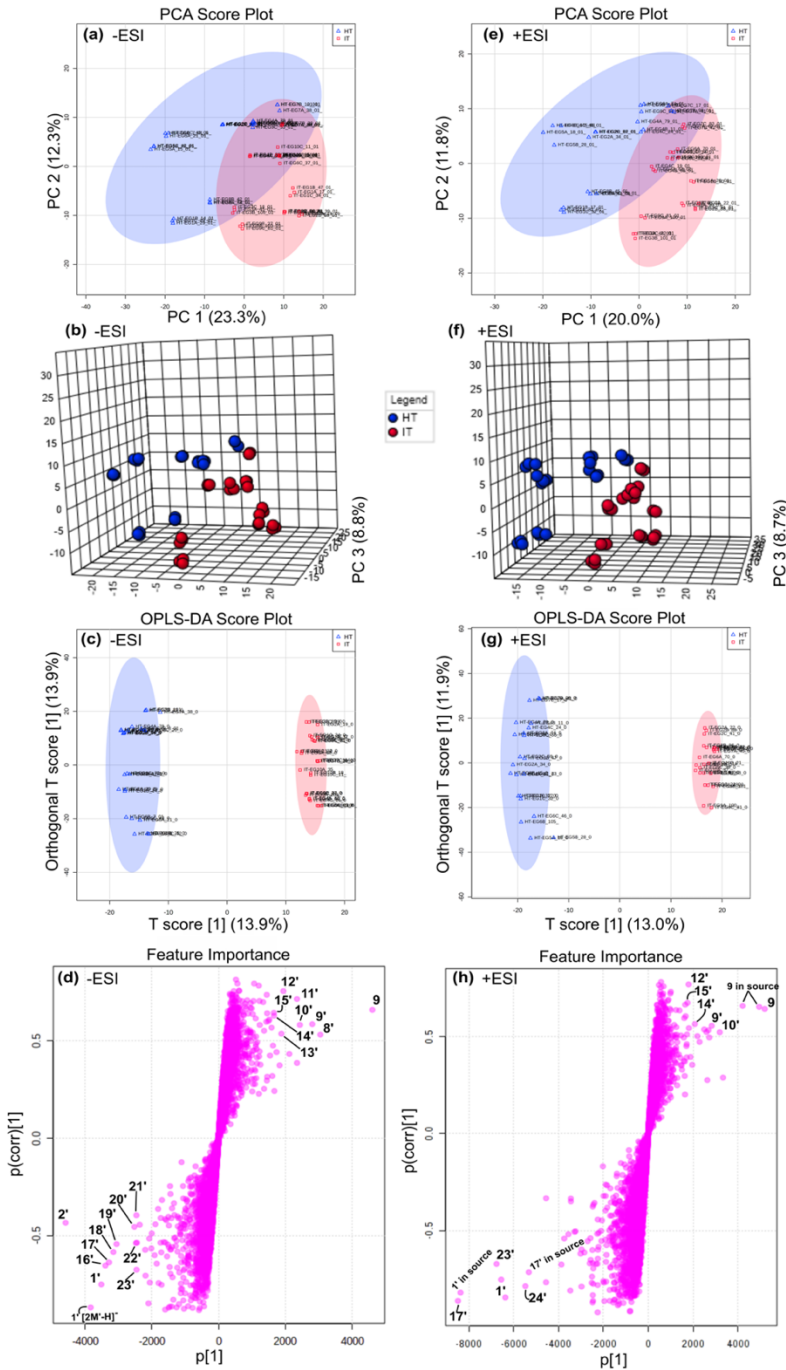
Figure 4.1.3. Statistical treatment results of the LC-MS dataset acquired in –

ESI and +ESI modes for the leaf's metabolome comparison between infested

(IT-EG) and healthy (HT-EG) *E. globulus* trees. (**a** and **e**) PCA score plots showing clustering pattern between the first two principal components (PC1 and PC2), where blue triangles and red squares represent samples from HT-EG and IT-EG, respectively, with their 95% confidence intervals (shadowed regions). (**b** and **f**) The same PCA score plots but incorporating the third PC for a 3D projection of sample distributions. (**c** and **g**) Score plots of the OPLS-DA models showing separation of samples labeled as HT-EG from that of IT-EG with their 95% confidence intervals (shadowed regions). The regression method used LC-MS data as the X, and the binary vector Y formed with a value of 0 for HT-EG class and 1 for IT-EG class. The Y-predictive component (T score [1]) shown on the x-axis represents the variation in the dataset correlated to class separation, while the orthogonal component shown on the y-axis refers to the uncorrelated variation for class distinction. (**d**) S-plots of the OPLS-DA models for visualizing the feature influence in the predictive component, combining covariance (p[1]) and correlation (p(corr)[1]) loading profiles. Covariance plotted on the x-axis visualizes the contribution to the predictive component, while correlation on the y-axis spans between ±1 as the reliability has a theoretical minimum of -1 and a maximum of +1 to predict class 1 (IT-EG). Thus, features visualized on the

right-hand side contribute to class separation by high correlation with label IT-EG (Y = 1) and the opposite. Significant features were selected by combining high covariance (> |1500|) and high correlation (> |0.5|), and their numbers were assigned according to Table 1.

4.1.4. Discussion

4.1.4.1. Differential constitutive metabolism driving host preference

The metabolomics analysis performed between *E. nitens* (resistant) and *E. globulus* (susceptible) healthy trees covered a wide array of leaf's specialized and primary metabolisms before herbivory, revealing the most probable chemical basis for the *G. platensis* feeding preference. An integral view of the most significant differential expression in the metabolomes of these two species is presented in Fig. 4.

Eight out of the twelve constitutive differential metabolites expressed in the leaves of *E. nitens* were stilbenes derivatives (**1-5**, **7**, **11**, **12**) (Fig. 4.1.1d and S4d). The occurrence of stilbenes in the leaves of *Eucalyptus* species, including *E. nitens*, was reported for the first time more than five decades ago (Hillis, 1966; Pederick & Lennox, 1979; Close *et al.*, 2007). However, apart from describing their presence, the specific ecological function these

82

metabolites play on *Eucalyptus* has not been suggested until today. Interestingly, *E. camaldulensis*, a species that has proved to be especially palatable to *G. platensis* (Huerta-Fuentes *et al.*, 2008b), also lacks constitutive stilbenes in the leaves (Hillis, 1966).

The first approach for understanding the metabolic pathway's activity differentially expressed in the resistant species (*E. nitens*) was conducted using a pathway enrichment functional analysis applied to the MS data (*m/z* peaks ranked by *p*-value) and bypassing the metabolite annotations step (Fig. 4.1.4a, b) (Li *et al.*, 2013; Chong *et al.*, 2019b). The flavones and flavonols biosynthesis (FFB) had the highest significance and enrichment factor for the MS-data acquired in -ESI mode, followed by the biosyntheses of stilbenes (SB) and phenylpropanoids (PB) (Fig. 4a). The SB pathway was not the most enriched because this is not exclusive to stilbenes but includes diarylheptanoids and gingerols. Indeed, this pathway comprises only two stilbenes, resveratrol (C03582) and pterostilbene (C10287) (Fig. S6), from which only resveratrol forms the core part of at least five identified stilbene derivatives (**1**-**3**, **5**, **12**). The same analysis using the +ESI MS-data yielded similar results, but PB was the most active (Fig. 4.1.4b). It makes sense as it

provides precursors for SB and FFB pathways such as *p*-Coumaric acid (C00811) (Fig. 4.1.4c).

As shown in Fig. 4.1.4c, SB and FFB are divergent pathways sharing the same precursors. After the actions of the phenylalanine ammonia-lyase (PAL, K10775), the *trans*-cinnamate 4-monooxygenase (K00487), and the 4-coumarate-CoA ligase (4CL, K01904), phenylalanine is converted into 4-coumaroyl-CoA that is one of the common substrates for these two pathways (Austin & Noel, 2003; Chong *et al.*, 2009a). They both begin with the reaction of three molecules of malonyl-CoA with one of 4-coumaroyl-CoA, producing the same linear tetraketide intermediate. This conversion can be catalyzed by two divergent enzymes members of the type-III polyketide synthases superfamily, the chalcone synthase (CHS, K00660) and the stilbene synthase (STS, K13232) (Austin & Noel, 2003). However, CHS cyclizes the linear tetraketide intermediate by an intramolecular Claisen condensation to produce the primary backbone for the flavonoid biosynthesis, Naringenin chalcone. In contrast, STS does it by an aldol condensation with decarboxylation to yield Resveratrol (Austin & Noel, 2003).

Despite STS and CHS may share 60-90% of the same amino-acids sequence, the former occurs in a limited number of plant species. In contrast, CHS is ubiquitous within the plant kingdom (Austin & Noel, 2003; Chong *et al.*, 2009a). It happens because STS has evolved from CHS several times in its evolution, which has taken place *via* gene duplication and neofunctionalization. This also explains why both enzymes compete for the same substrates (Tropf *et al.*, 1994; Hammerbacher *et al.*, 2011). However, it is known that such gene duplication provides CHS activity with functional redundancy, allowing the *chs* gene to mutate without endangering the biosynthesis of flavonoids (Austin & Noel, 2003). It was evidenced in this study since both flavonoids and stilbenes levels were significantly higher in *E. nitens* than in the leaves of *E. globulus* (Fig. 4.1.4c). That is the case for the flavonol Rutin (**9**) and all stilbenes (**1-5**, **7**, **11**, **12**). The former was present in *E. nitens* at a rate of 3-fold ($\log_2 FC = 1.60$) higher than in the leaves of *E. globulus*. At the same time, stilbenes were found in a range between 30 and 204-fold ($\log_2 FC = 4.9\ to\ 7.7$) higher in *E. nitens* (Fig. 4.1.4c and Table S1), suggesting that the absence of STS in *E. globulus* limits its capability to biosynthesize these substances constitutively. Although the antifeedant role of stilbenes against herbivores in plants has not been

documented, the feeding choice test presented in this research suggested a potential ecological role of these metabolites in *Eucalyptus* species against the weevil *G. platensis* (Fig. S2 and S3).

The other three metabolites differentially expressed in *E. nitens* were hydrolysable tannins (**6**, **8**, **10**). They are formed by glucose with hydroxyl groups partially or totally esterified with Gallic acid units (gallotannins). The biosynthesis of these tannins has a critical first step in the formation of β-Glucogallin from Gallic acid by the enzyme gallate 1-β-glucosyltransferase (K23279) (Fig. 4.1.4c) (Muir *et al.*, 2011). Subsequent linkages of galloyl units to the glucose require β-Glucogallin as the galloyl donor group, the limiting substance for the biosynthesis of **6**, **8**, and **10**. β-Glucogallin was present in the leaves of *E. nitens* at a rate of 30-fold higher ($\log_2 FC = 4.9$) than in the leaves of *E. globulus*, suggesting that *E. globulus* also lacks this critical enzyme. The feeding deterrent role of hydrolysable tannins is well known against invertebrates and vertebrates and may influence the tree surrounding ecosystem. For instance, the variable constitutive levels of tannins in *Populus angustifolia* genotypes determine the composition of communities living around them (Whitham *et al.*, 2008).
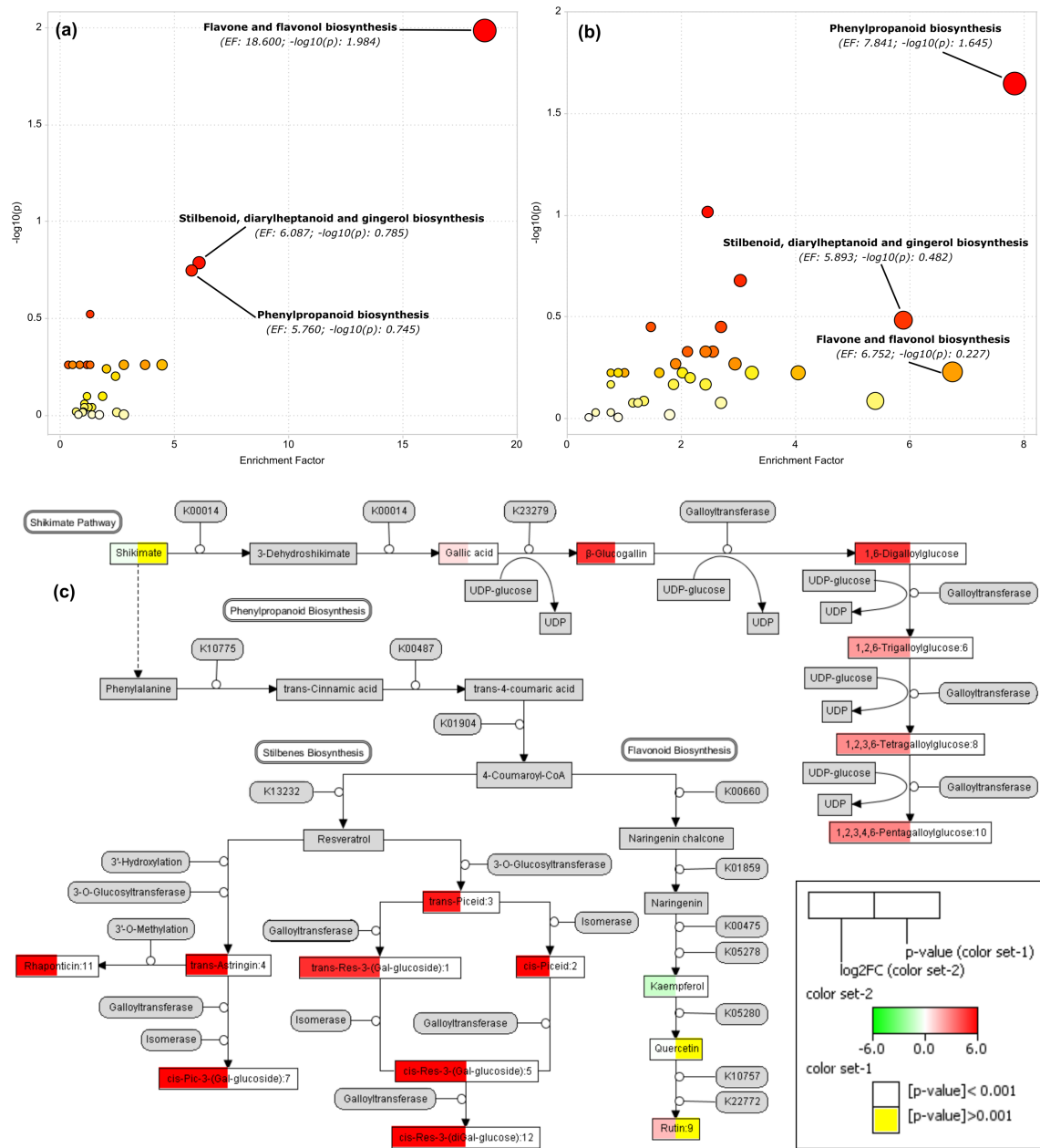
Figure 4.1.4. Pathway analysis for the constitutive leaf's metabolism differentially expressed in *E. nitens* concerning *E. globulus*. Enrichment analysis for an untargeted visual exploration of the matched pathways

according to the MS-peak-to-pathway calculation based on the *mummichog* algorithm for (**a**) –ESI MS data and (**b**) +ESI MS data. Increasing size and color intensity of circles indicate higher significance (*p*-value) of given pathway and enrichment factor, respectively, using 10^{-5} of *p*-value cutoff and *osa-kegg* library. The most active pathways are shown with their enrichment factor value, *EF*, and statistical significance as $-\log_{10} p$. The *EF* is the ratio between the number of significant *m/z* hits found in the data and the expected number of hits according to metabolites mapped in the pathway of a given model organism. (**c**) Scheme for the pathways analysis showing the significant differential expression of constitutive metabolites in the leaves of *E. nitens* concerning that in the leaves of *E. globulus*. Metabolites are presented as nodes rectangles with their annotated names and assigned numbers. Color set-1 shows the statistical significance in a t-test, where white indicates significant ($p < 0.001$) and yellow not significant ($p > 0.001$). Color set-2 refers to the expression data according to the $\log_2 FC$, where FC is the fold-change ($FC = EN/HTEG$), $EN/HTEG$ is the ration between the average intensities of the metabolite between *E. nitens* and *E. globulus* trees. The scale was adjusted between -6 and 6 for ease of interpretation. Metabolites filled in grey were not detected. Enzymes involved in specific

transformations are shown as rounded rectangles, labeled, if possible, with their KEGG Ortholog number (KO). Dashed line indicates several conversion steps.

4.1.4.2. Induced response in *E. globulus* upon herbivory and functional implications

The most significant metabolome changes systemically induced in the leaves of *E. globulus* by the *G. platensis* herbivory are presented in Fig. 4.1.5. It represents the chemical basis for the plant's systemic acquired resistance (SAR), showing the main active biosynthetic pathways and metabolites significantly up or down-regulated.

The FFB pathway was significantly activated during herbivory (Fig. 4.1.5a, b). Consistently, six flavonol glycosides (**9**, **9′**, **10′**, **13′-15′**) were up-regulated (Fig. 4.1.3d, h and Fig. 5c). Among them, Rutin (**9**), Kaempferol-rutinoside (**9′**), and Quercetin-feruloyl-glucoside (**15′**) increased their levels by more than 2-fold (Table S2). The glycosylation of flavonols usually occurs in plants to sequester them into vacuoles of epidermal cells to filter the UV-B radiation, avoiding damage to the photosensitive tissues (Schulze *et al.*, 2019a). However, it is evident that, in our case, trees under herbivory are not

subjected to a different UV exposure. Thus, these metabolites' up-regulation should be directly or indirectly related to a protection role against either wound or herbivory. In contrast, the glucuronide flavonol **1′** was down-regulated by 1.3-fold (Fig. 4.1.5c and Table S2). The conjugation of potentially toxic endogenous substances with glucuronic acid is a well-known detoxification mechanism used by herbivorous mammals to make them more soluble and facilitate excretion (Adiji *et al.*, 2021). Thus, down-regulation of **1′** during herbivory may prevent its natural detoxification after herbivores consumption. It could be a learned nonspecific response of *E. globulus* to defoliation that is not only caused by insects like *G. platensis* in its natural habitat but also by marsupials.

Metabolites **10′** and **14′** were also glycosyl-flavonols derivatives of quercetin and kaempferol but esterified in the glucose unit with the monoterpene Oleuropeic acid. Both compounds were up-regulated in leaves during herbivory by almost equal rates, 1.6-fold, and 1.7-fold, respectively (Table S2). They have been previously localized in the exterior of *Eucalyptus* leaves' secretory cells, which can be favored by their amphipathic property (Heskes *et al.*, 2012). Consequently, a protective role in the secretory cells by forming a barrier of non-volatile substances that avoid diffusion of auto-

toxic volatile terpenes in the oil cavities' lumen across the lipid bilayer was suggested (Goodger & Woodrow, 2011). Interestingly, metabolites **18′/19′** (Eucaglobulin) and **23′** (Cypellocarpin C) have also been reported to be localized at the exterior of secretory cells in *Eucalyptus* leaves, playing the same protection role (Goodger & Woodrow, 2011; Heskes et al., 2012). However, their levels dropped in the leaves of *E. globulus* trees under herbivory by 1.7-fold and 1.8-fold, respectively (Fig. 4.1.5c and Table S2). Coincidently, these were similar rates by which **10′** and **14′** overexpressed simultaneously. Thus, we can suggest that such a protective barrier in secretory cells is being reinforced during herbivory by the cleavage of oleuropeyl-glucoside from **18′/19′** and **23′** to be then transferred to flavonols such as Quercetin/Quercetin-glucoside (**13′**) and Kaempferol/Astragalin, giving rise the compounds **10′** and **14′**, respectively (dashed lines Fig. 4.1.5c).

Together with oleuropeyl-glucoside in the above-proposed cleavage for compounds **18′/19′**, a gallic acid unit is also released. It contributed, or at least in part, to an increase in 2.3-fold of gallic acid content in the leaves of trees under herbivory (Fig. 4.1.5c and Table S2), which serves as a precursor for increasing the ellagic acid (**12′**) accumulation by 1.3-fold. The ellagic

acid is a dilactone gallic acid dimer formed after an intramolecular dehydrogenation, reported inhibiting insects' feeding and development in other plant species (Maas *et al.*, 1991; Sánchez-Gómez *et al.*, 2017). In our case, however, ellagic acid was detected in the leaves of *E. globulus* before herbivory at higher content than in the leaves of *E. nitens* (Fig. S7), suggesting a possible insect counteradaptation for its efficient detoxification. On the other hand, no hydrolysable tannins were synthesized, highlighting the lack of the critical enzyme K23279 in *E. globulus* again (Fig. 4.1.4c).

It is worth noting that there were no stilbenes among up-regulated metabolites in the *E. globulus* leaves under herbivory of *G. platensis*. Therefore, stilbenes biosynthesis was not triggered *de-novo* either, confirming the lack of STS in this species and its probable relevance for plant resistance in *E. nitens*.

The pathway for the metabolism of cyanoamino acids also appeared active upon herbivory (Fig. 4.1.5b). Cyanogenic glucosides are synthesized in this pathway, which the plant can use to release hydrogen cyanide (HCN) to defend against biotic stressors. As hydrogen cyanide can also be a non-specific auto-toxic substance for plants, affecting mitochondrial respiration by inhibiting oxygen binding to cytochrome c oxidase, the plant must store it

in a conjugated form. In our case, they were stored as prunasin and its gallate derivative **11′** (Fig. 4.1.5c). Several species within the genus *Eucalyptus* are cyanogenic, producing prunasin as the major cyanogen (Gleadow *et al.*, 2008; Hansen *et al.*, 2018). Upon wounding, prunasin hydrolase becomes active, breaking the glycosidic bond to yield a glucose unit and the hydroxynitrile mandelonitrile. Finally, hydroxynitrilases release hydrogen cyanide from mandelonitrile (Schulze *et al.*, 2019b). Since the leaves collected from *E. globulus* trees under herbivory had no visual damage caused by *G. platensis* consumption or mechanically, the *de-novo* biosynthesis of compound **11′** and prunasin represents a direct resistant trait systemically signalized against herbivory (Table S2). This should allow *E. globulus* to reduce the intensity of continuous defoliation by *G. platensis*. However, one can see in the field that it does not happen, which may be explained by evolved counteradaptations in *G. platensis* that allow for HCN detoxification, becoming a perfect specialist insect (Gleadow & Woodrow, 2002).

Other active pathways were significantly down-regulated during herbivory. Vitamin B6 metabolism was one of them. Vitamin B6 is a term commonly given to six interconvertible metabolites, including pyridoxine,

pyridoxal, pyridoxamine, and their phosphorylated derivatives (Fitzpatrick, 2011). Among them, pyridoxine glucoside (**24′**) was strongly down-regulated by a rate of 2.3-fold (Fig. 4.1.5c and Table S2). Pyridoxine and pyridoxal were also down-regulated but to a lesser extent. Pyridoxine glucoside (**24′**) commonly constitutes 5–70% of the total vitamin B6 pool in plants (Fitzpatrick, 2011), and such significant dropping levels could have severe implications for the plant. Apart from being an essential co-factor for crucial metabolic reactions, its deficit may increase sensitivity to high light and photooxidative stress (Havaux *et al.*, 2009). On the other hand, it may also be interpreted as an attempt of the plant to increase photosynthetic activity, diverting carbon fixation towards specialized metabolite synthesis. It has been typically described as a response of tolerant plants to herbivory (Kerchev *et al.*, 2012). In this case, reactive oxygen species (ROS) production increases as a photosynthesis byproduct, serving as potentially systemic signalers for defense induction (Kerchev *et al.*, 2012). After that, plants need to quench ROS with vitamin B6, especially singlet-oxygen ($^1O_2$), to avoid photooxidative damages (Havaux et al., 2009; Denslow et al., 2005), and this may be the cause why its levels dropped.

Finally, the up-regulation of a potential phytohormone was detected in the leaves of *E. globulus* trees under herbivory. Stomatal regulation or slowing plant growth in preparation for winter are some of the functional attributes of abscisic acid (ABA) in plants (Finkelstein, 2013; Wang *et al.*, 2016). Regulation of ABA levels usually involves its 'inactivation' by hydroxylation and glycosylation catabolic reactions (Nambara & Marion-Poll, 2005). Vomifoliol is an ABA structural relative suggested as a metabolite of ABA in plants (Hasegawa *et al.*, 1984). Nevertheless, down-regulation of the vomifoliol glycoside 17′ upon herbivory may indicate the action of a glucosidase to release the needed free aglycone. Indeed, Vomifoliol was up-regulated by 1.7-fold in trees under herbivory, although it was less significant ($p = 0.003$) (Fig. 4.1.5c and Table S2). The capacity of Vomifoliol to regulate stomatal closure has been reported to be as similar as that of ABA (Stuart & Coke, 1975). We believe, however, that Vomifoliol may cause different signal transduction in *E. globulus* under herbivory, although further research is needed for an accurate elucidation of its function.

The induced response mentioned above in *E. globulus* after *G. platensis* herbivory may suggest plant-insect coevolution (Zunjarrao et al., 2020). It is reasonable considering that both *G. platensis* and the species *E. globulus* spp.

globulus are endemic to Tasmania (Coppen, 2002; Dutkowski and Potts, 1999; Mapondera et al., 2012). This common origin may explain why *E. globulus* spp. *globulus* is the weevil's natural host and, therefore, the most affected species in plantations worldwide. Thus, the insect has probably evolved adaptations to overcome the plant's defense, and the plant has had to learn tolerance mechanisms to survive despite continuous defoliations. In other words, the plant-insect relationship is a bidirectional process where plants elicit specific defenses upon insect feeding (Zunjarrao et al., 2020). To trigger such defense, plants need to differentiate between physical injury and insect feeding, for instance, by insect's oral secretion (Zunjarrao et al., 2020). It presumably begins in ours case through the cleavage of Vomifoliol glycoside (**17′**) by the action of a glycoside, releasing Vomifoliol aglycone. This compound is a potential phytohormone that we presume could be directly correlated with transducing the above-described defensive response. However, further investigation is needed to prove such a hypothesis.
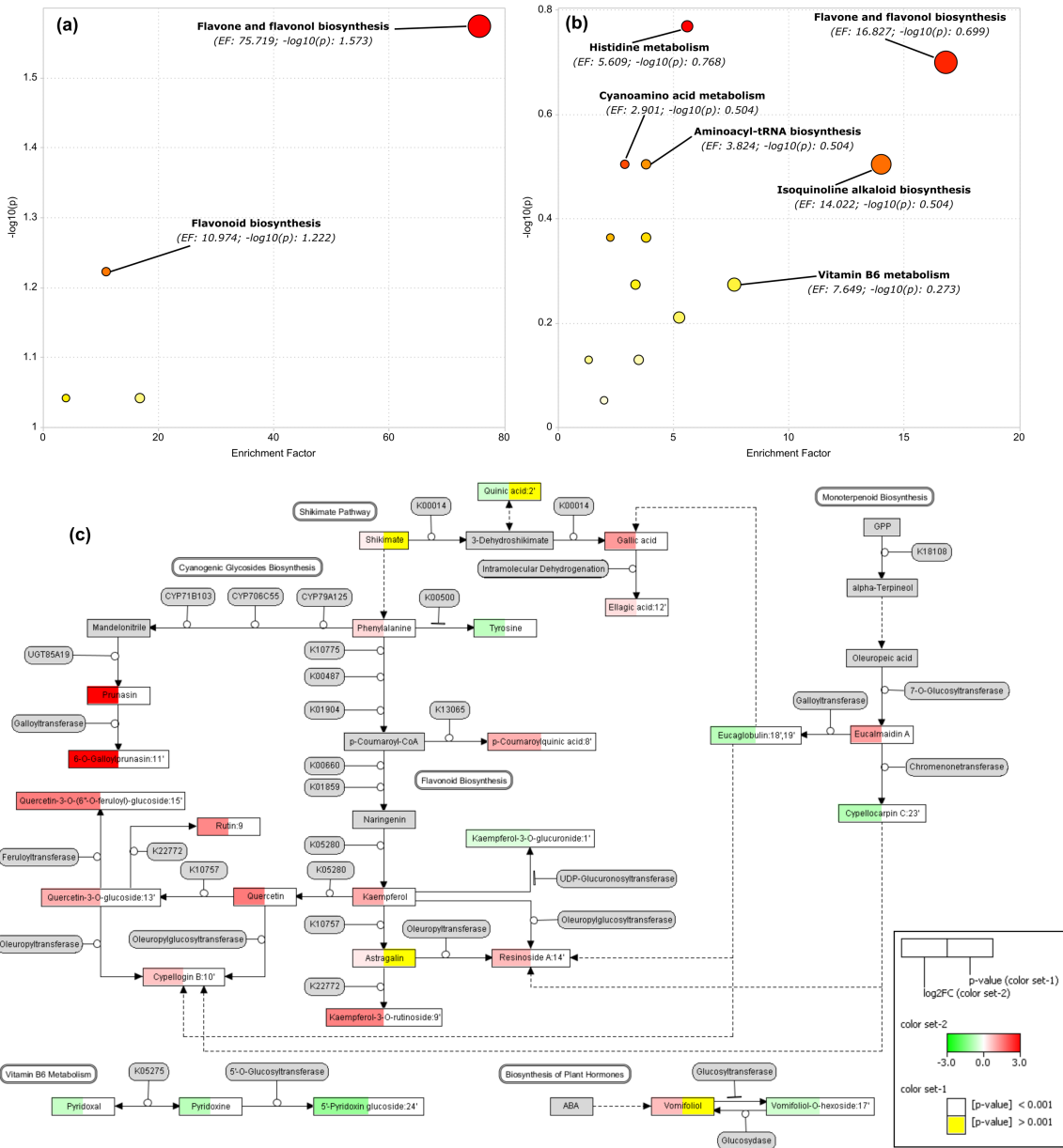
Figure 4.1.5. Pathway analysis for the systemically induced response in *E. globulus* leaves upon herbivory of *G. platensis*. Pathway enrichment analysis using the MS-peak-to-pathway calculation based on the *mummichog* algorithm for (**a**) –ESI MS-data and for (**b**) +ESI MS data. Increasing size
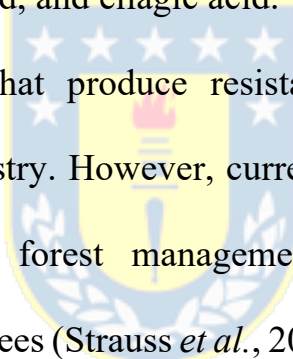
and color intensity of circles indicate higher significance (p-value) of given pathway and enrichment factor, respectively, using 10^{-3} of p-value cutoff and *ath-kegg* library. The most active pathways are shown with their enrichment factor value, *EF*, and statistical significance as $-\log_{10} p$. (**c**) Scheme for the pathways analysis showing the expression of significant metabolites in the leaves of *E. globulus* during herbivory. Metabolite nodes are presented as rectangles with their annotated names and assigned numbers. Color set-1 shows the statistical significance in a t-test, where white indicates significant ($p < 0.001$) and yellow not significant ($p > 0.001$). Color set-2 refers to the expression data according to the $\log_2 FC$, where FC is the fold-change ($FC = IT/HT$), IT/HT is the ratio between the average intensities of the metabolite between infested (under herbivory) and healthy (without herbivory) trees. The scale was adjusted between -3 (down-regulation) and 3 (up-regulation) for ease of interpretation. Metabolites filled in grey were not detected. Enzymes involved in specific transformations are shown as rounded rectangles, labeled, if possible, with their KEGG Ortholog number (KO). Dashed lines indicate several reaction steps or proposed conversions. For prunasin and **11′**, small arbitrary intensity values were given to HT-EG as they were "*de novo*" synthesized and consequently not detected before

herbivory. The enzymes that catalyze the biosynthesis of cyanogenic compounds are presented by their exact cytochromes P450s (CYPs) identified and functionally characterized in *Eucalyptus cladocalyx* (Hansen *et al.*, 2018).

4.1.5. Conclusions

In this research, non-volatile metabolites constitutively present in the leaves of *Eucalyptus* spp., especially stilbenes and hydrolysable tannins, were suggested to potentially govern the feeding preferences of the eucalyptus weevil *G. platensis*. The metabolome constitutively expressed in the leaves of *E. nitens* and *E. globulus*, two species with clearly different susceptibilities to the herbivory of *G. platensis*, were compared. We found that the susceptible species (*E. globulus*) was unable to accumulate stilbenes and hydrolysable tannins constitutively. In consequence, the lack of key enzymes like stilbene synthase (STS) and gallate 1-β-glucosyltransferase was suggested. Upon herbivory, none of the pathways for the biosynthesis of these metabolites were activated. Interestingly, an antifeedant test evidenced that *G. platensis* would not choose leaves containing these metabolites for feeding, which denoted its marked specialization. It is worth noting that *G.*

platensis and *E. globulus* belong from the same geographical location in the southeast of Australia in Tasmania, while *E. nitens* is native from continental Australia (Mapondera *et al.*, 2012b). These results suggest that plant and insect had to coevolve in developing adaptations for minimizing the plant chemical defense in the case of the insect. Such defense includes toxic substances like cyanogenic glucosides that may release hydrogen cyanide upon herbivory, flavonols which can be glycosylated and conjugated with the monoterpene oleuropeic acid, and ellagic acid.

Genetic modifications that produce resistant trees seem a plausible solution for the forest industry. However, current international certification programs for sustainable forest management exclude all genetically engineered or gene-edited trees (Strauss *et al.*, 2019), and companies certified under such systems may not consider genetic engineering as an option. Nevertheless, breeding programs developing inter-specific hybridizations between *E. nitens* (resistant) and *E. globulus* (susceptible), such as *E. nitens* × *globulus,* besides being better adapted to low temperatures and frost in southern Chile (Ipinza *et al.*, 2014) may provide an opportunity to increase plantations resistance to *G. platensis*. However, constitutive metabolome expression of such hybrids or induced systemic response upon herbivory is

so far unexplored. Therefore, this research lays the groundwork for a fascinating alternative approach to managing this pest by selecting specific crosses and monitoring the transfer of resistant traits from parents to progenies in future breeding programs.

Credit authorship contribution statement

AJP: Conceptualization; JVC: Data curation; JVC, SR, ŁP, and LG: Formal analysis; AJP: Funding acquisition; JVC: Investigation; JVC, SR, and RA: Methodology; OF: Supervision; AJP and JVC: Writing original draft; LEAP, CM; and RR: reviews & editing.

Acknowledgments

Data availability statement

Data associated with this paper, including LC-MS raw data (.d/.mzXML files) and processed bucket tables will be freely available upon request or after acceptance for publication.

Table 1. Chemical data of significant metabolites for species distinction and for the response to the *G. platensis* herbivory.

No	Rt (min)	Metabolite name	Metabolite class	Mol. formula	ESI (-) Theor m/z	ESI (-) Meas. m/z	ESI (+) Theor m/z	ESI (+) Meas m/z	m/z error (ppm)[a]	MS/MS ESI (-) fragments m/z (int. %)	MS/MS ESI (+) fragments m/z] (int. %)	UV/Vis (nm)	InChI-Key	Ident. level (A-D)
						Metabolites constitutively expressed in the leaves of *E. nitens* trees that best explained its metabolome differentiation from that of *E. globulus*.								
1	17.21	*trans*-Resveratrol-*O*-(galloyl)-hexoside*	Stilbene-gallate glycoside	$C_{27}H_{26}O_{12}$	541.1351	541.1340 [M-H]-	543.1497	543.1475 [M+H]+	2.06, 4.10	541.1 (100), 313.0 (15), 227.1 (50), 169.0 (52), 151.0 (8), 125.0 (22)	315.1 (11), 297.1 (26), 229.1 (100), 153.0 (11), 107.1 (32)	292	YGKDMUYXJBMRBO-XMPPFBFMSA-N	B
2	17.56	*cis*-Resveratrol-*O*-hexoside (*cis*-Piceid)	Stilbene glycoside	$C_{20}H_{22}O_8$	389.1242	389.1237 [M-H]-	391.1387	391.1375 [M+H]+	1.28, 3.26	227.1 (100), 185.1 (21), 143.0 (15)	229.1 (100), 107.1 (42), 91.1 (11)	284	HSTZMXCBWJGKHG-BUFXCDORSA-N	A
3	15.26	*trans*-Resveratrol-*O*-hexoside (*trans*-Piceid)	Stilbene glycoside	$C_{20}H_{22}O_8$	389.1242	389.1231 [M-H]-	391.1387	391.1369 [M+H]+	2.85, 4.84	227.1 (100), 185.1 (19), 143.0 (8)	229.1 (100), 107.1 (28), 91.1 (13)	305	HSTZMXCBWJGKHG-CUYWLFDKSA-N	A
4	12.77	*trans*-Piceatannol-*O*-hexoside (*trans*-Astringin)	Stilbene glycoside	$C_{20}H_{22}O_9$	405.1191	405.1178 [M-H]-	407.1337	407.1326 [M+H]+	3.26, 2.52	405.1 (8), 243.1 (100), 201.1 (11), 159.0 (13)	245.1 (100), 107.1 (20)	325	PERPNFLGJXUDDW-CUYWLFDKSA-N	A
5	18.43	*cis*-Resveratrol-*O*-(galloyl)-hexoside*	Stilbene-gallate glycoside	$C_{27}H_{26}O_{12}$	541.1351	541.1341 [M-H]-	543.1497	543.1476 [M+H]+	1.99, 3.81	541.1 (100), 313.1 (17), 227.1 (63), 169.0 (54), 151.0 (10), 125.0 (21)	315.1 (22), 297.1 (46), 229.1 (33), 153.0 (100), 107.1 (28), 97.0 (33)	278	YGKDMUYXJBMRBO-XMPPFBFMSA-N	B
6	12.48	1,2,6-Trigalloyl-glucose	Gallate glycoside	$C_{27}H_{24}O_{18}$	635.0889	635.0874 [M-H]-	619.0930	619.0916 [M-H2O+H]+	2.34, 2.15	635.1 (60), 465.1 (100), 313.1 (69), 169.0 (80), 125.0 (15)	277.0 (15), 153.0 (100), 125.0 (17), 107.0 (16)	277	LLENXGNWVNSBQG-VFTFQOQOSA-N	B
7	15.44	*cis*-Piceatannol-*O*-(galloyl)-hexoside*	Stilbene-gallate glycoside	$C_{27}H_{26}O_{13}$	557.1301	557.1286 [M-H]-	559.1446	559.1421 [M+H]+	2.63, 4.57	557.1 (100), 313.1 (17), 243.1 (96), 169.0 (43), 125.0 (14)	315.1 (10), 297.1 (33), 245.1 (100), 153.0 (73), 107.1 (18), 97.0 (16)	274	HZCOWROLPVDVCR-XMPPFBFMSA-N	B
8	15.09	1,2,3,6-Tetragalloyl-glucose	Gallate glycoside	$C_{34}H_{28}O_{22}$	787.0999	787.0966 [M-H]-	771.1039	771.1034 [M-H2O+H]+	4.21, 0.70	787.1 (100), 635.1 (14), 465.1 (26), 295.1 (31), 169.0 (93), 125.0 (7)	303.0 (19), 277.0 (23), 153.0 (100), 125.0 (13), 97.0 (19)	273	RATQVALKDAUZBW-XPMKZLBQSA-N	B
9	15.58	Rutin	Flavonol glycoside	$C_{27}H_{30}O_{16}$	609.1461	609.1442 [M-H]-	611.1607	611.1587 [M+H]+	3.15, 3.20	609.1 (54), 300.0 (100), 271.0 (9), 255.0 (5)	303.1 (100), 229.1 (4)	257, 351	IKGXIBQEEMLURG-NVPNHPEKSA-N	A
10	16.77	1,2,3,4,6-Pentagalloyl-glucose	Gallate glycoside	$C_{41}H_{32}O_{26}$	939.1109	939.1098 [M-H]-	n.d.	n.d.	1.22	939.1 (100), 769.1 (35), 617.1 (19), 447.1 (17), 431.1 (15), 295.1 (7), 169.0 (25)	n.d.	279	QJYNZEYHSMRWBK-NIKIMHBISA-N	B

#	RT	Name	Class	Formula	[M-H]⁻ calc	[M-H]⁻ exp	[M+H]⁺ calc	[M+H]⁺ exp	Δppm	MS/MS (−)	MS/MS (+)	UV	InChIKey	Lvl
11	15.95	*trans*-Methoxypiceatannol-*O*-hexoside*	Stilbene glycoside	$C_{21}H_{24}O_9$	419.1348	419.1338 [M-H]⁻	421.1493	421.1487 [M+H]⁺	2.24, 1.46	257.1 (100), 241.1 (91)	259.1 (100), 227.1 (18), 199.1 (23)	325	GKAJCVFOJ GXVIA-DXKBKAGU SA-N	B
12	19.46	*cis*-Resveratrol-*O*-(digalloyl)-hexoside**	Stilbene-gallate glycoside	$C_{34}H_{30}O_{16}$	693.1461	693.1436 [M-H]⁻	695.1607	695.1600 [M+H]⁺	3.64, 0.97	693.1 (100), 541.1 (34), 465.1 (9), 313.1 (34), 227 (17), 169.0 (76), 125.0 (9)	297.1 (13), 229.1 (30), 153.0 (100), 107.0 (15)	281	-	B

Metabolites constitutively expressed in the leaves of healthy *E. globulus* trees that best explained its metabolome differentiation from that of *E. nitens*.

#	RT	Name	Class	Formula	[M-H]⁻ calc	[M-H]⁻ exp	[M+H]⁺ calc	[M+H]⁺ exp	Δppm	MS/MS (−)	MS/MS (+)	UV	InChIKey	Lvl
1'	17.31	Kaempferol-*O*-hexuronide	Flavonol glycoside	$C_{21}H_{18}O_{12}$	461.0725	461.0714 [M-H]⁻	463.0871	463.0859 [M+H]⁺	2.54, 2.70	461.1 (14), 285.0 (100), 257.0 (8), 229.0 (18)	287.1 (100)	265, 344	FNTJVYCFN VUBOL-UHFFFAOYS A-N	B
2'	1.04	Quinic acid	Cyclitol carboxylic acid	$C_7H_{12}O_6$	191.0561	191.0558 [M-H]⁻	193.0707	193.0702 [M+H]⁺	1.62, 2.28	191.1 (100), 173.0 (3), 127.0 (5), 93.0 (9)	111.1 (100), 95.0 (82)	-	AAWZDTNX LSGCEK-LNVDRNJUS A-N	A
3'	17.93	5,7-dihydroxy-2-prenylchromone 6-*C*-(Galloyl hexoside)**	Chromone *C*-glycoside	$C_{26}H_{28}O_{13}$	547.1457	547.1441 [M-H]⁻	549.1603	549.1578 [M+H]⁺	3.03, 4.41	547.1 (19), 395.1 (52), 305.1 (3), 275.1 (73), 247.1 (20), 169.0 (100), 125.0 (41)	549.2 (14), 429.1 (25), 397.2 (6), 379.1 (37), 361.1 (20), 277.1 (100), 259.1 (15), 247.1 (20), 206.1 (24), 153.0 (11)	257, 278	-	B
4'	21.22	5,7-dihydroxy-2-prenylchromone 8-*C*-(Oleuropyl hexoside)**	Chromone monoterpene *C*-glycoside	$C_{29}H_{38}O_{11}$	561.2341	561.2324 [M-H]⁻	563.2487	563.2479 [M+H]⁺	3.07, 1.40	561.2 (5), 377.1 (19), 257.1 (100), 183.1 (99), 125.1 (8)	545.2 (52), 425.2 (44), 379.1 (35), 277.1 (100), 259.1 (35), 247.1 (23), 148.1 (26), 93.1 (24)	256, 284	-	B
5'	20.13	Cuniloside B	Monoterpene glycoside	$C_{26}H_{40}O_{10}$	557.2604	557.2584 [M+HCO₂H-H]⁻	329.1595ᵇ	329.1565ᵇ [M+H-OleuA]⁺	3.47, -	557.3 (65), 511.3 (15), 451.2 (5), 373.2 (10), 327.1 (8), 225.1 (28), 183.1 (100), 167.1 (6), 139.1 (8), 125.1 (4)	149.1 (63), 121.1 (96), 93.1 (100)	278	JOLLIDAUJS AZHE-SKNUFNKIS A-N	B
6'	15.89	Cypellocarpin A (I)	Monoterpene-gallate glycoside	$C_{23}H_{30}O_{12}$	497.1664	497.1652 [M-H]⁻	499.1810	499.1803 [M+H]⁺	2.53, 1.46	497.2 (100), 331.1 (4), 169.0 (79), 125.0 (40)	329.2 (14), 311.1 (70), 293.1 (100), 167.1 (17), 149.1 (89), 121.1 (29), 93.1 (57)	267	QIYRQEHCC PTEPY-VJOHEAABS A-N	B
7'	16.32	Cypellocarpin A (II)	Monoterpene-gallate glycoside	$C_{23}H_{30}O_{12}$	497.1664	497.1652 [M-H]⁻	499.1810	499.1804 [M+H]⁺	2.48, 1.20	497.2 (100), 183.1 (8), 169.0 (22), 151.0 (10), 139.0 (6), 125.0 (11)	n.d.	279	QIYRQEHCC PTEPY-VJOHEAABS A-N	B

Up-regulated metabolites in the leaves of *E. globulus* trees upon *G. platensis* herbivory.

#	RT	Name	Class	Formula	[M-H]⁻ calc	[M-H]⁻ exp	[M+H]⁺ calc	[M+H]⁺ exp	Δppm	MS/MS (−)	MS/MS (+)	UV	InChIKey	Lvl
8'	11.72	p-coumaroylquinic acid	Hydroxycinnamate ester and cyclitol carboxylic acid	$C_{16}H_{18}O_8$	337.0929	337.0920 [M-H]⁻	361.0893	361.0885 [M+Na]⁺	2.71, 2.35	337.1 (100), 191.1 (98), 119.0 (23)	147.0 (100), 119.0 (70), 91.1 (63)	272	ANUSKTCU RGICPQ-JTNJOIGYSA -N	B
9'	16.81	Kaempferol-*O*-rutinoside	Flavonol glycoside	$C_{27}H_{30}O_{15}$	593.1512	593.1496 [M-H]⁻	595.1657	595.1636 [M+H]⁺	2.71, 3.66	593.1 (82), 284.0 (100), 255.0 (16), 227.0 (7)	287.1 (100)	265, 347	RTATXGUC ZHCSNG-QHWHWDP RSA-N	B
10'	19.79	Cypellogin B	Flavonol	$C_{31}H_{34}O_{14}$	629.1876	629.1861	631.2021	631.2012	2.36, 1.41	629.2 (49), 463.1 (4), 300.0	303.1 (100)	250,	GUDLVBZW	B

No.	RT	Compound	Class	Formula	[M-H]⁻ meas	[M-H]⁻ theor	[M+H]⁺ meas	[M+H]⁺ theor	RT	MS/MS (−)	MS/MS (+)	UV	InChIKey	
		glycoside monoterpene				[M-H]⁻		[M+H]⁺		(100), 271.0 (10)		350	VXAHOX-ZWQPYCCR SA-N	
11′	16.71	6-O-Galloylsambunigrin	Cyanogenic glycoside gallate	$C_{21}H_{21}NO_{10}$	446.1093	446.1078 [M-H]⁻	315.0711[b]	315.0686[b] [M+H-Man]⁺	3.37, -	446.1 (100), 313.1 (4), 169.0 (23), 125.0 (17)	153.0 (100), 125.0 (30)	271	BYILEHCAH ZEAIX-IHGRRFEYS A-N	B
12′	15.42	Ellagic acid	Gallate	$C_{14}H_6O_8$	300.9989	300.9985 [M-H]⁻	303.0135	303.0121 [M+H]⁺	1.69, 4.84	301.0 (100)	303.0 (50), 285.0 (47), 275.0 (82), 257.0 (100), 247.0 (43), 229.0 (54)	253, 367	AFSDNFLW KVMVRB-UHFFFAOYS A-N	A
13′	16.05	Quercetin-O-hexoside	Flavonol glycoside	$C_{21}H_{20}O_{12}$	463.0882	463.0871 [M-H]⁻	303.0499[b]	303.0469[b] [M+H-Hex]⁺	2.36, -	463.0 (100), 300.0 (92), 271.0 (92), 255.0 (38), 243.0 (22)	303.0 (100), 285.0 (15), 274.0 (23), 257.0 (75)	258, 353	OVSQVDMC BVZWGM-QSOFNFLRS A-N	A
14′	20.75	Resinoside A	Flavonol glycoside monoterpene	$C_{31}H_{34}O_{13}$	613.1927	613.1905 [M-H]⁻	615.2072	615.2062 [M+H]⁺	3.60, 1.68	613.2 (64), 284.0 (100), 255.0 (26), 227.2 (17)	287.1 (100)	250, 350	XJYKKSWB SUUWAV-MJFDLWPTS A-N	B
15′	19.73	Quercetin-O-feruloyl-hexoside	Flavonol glycoside hydroxycinnamate ester	$C_{31}H_{28}O_{15}$	639.1355	639.1342 [M-H]⁻	641.1501	641.1497 [M+H]⁺	2.15, 0.68	639.1 (63), 463.1 (7), 300.0 (100), 271.0 (11)	303.0 (53), 177.1 (100), 117.0 (46)	n.d.	PSBFVXDM NYDZMV-SMTCTBLTS A-N	B
Down-regulated metabolites in the leaves of *E. globulus* trees upon *G. platensis* herbivory.[c]														
16′	1.21	Isocitric acid	Tricarboxylic acid	$C_6H_8O_7$	191.0197	191.0198 [M-H]⁻	193.0343	193.0346 [M+H]⁺	0.19, 1.71	191.0 (5), 129.0 (7), 111.0 (100)	n.d.	n.d	ODBLHEXU DAPZAU-UHFFFAOYS A-N	A
17′	10.82	Vomifoliol hexoside	Cyclohexanone monoterpene glycoside	$C_{19}H_{30}O_8$	431.1923	431.1912 [M+HCO₂H-H]⁻	387.2013	387.1999 [M+H]⁺	2.49, 3.79	431.2 (21), 385.2 (100), 223.1 (31), 205.1 (15), 179.1 (10), 161.0 (24), 153.1 (24)	207.1 (46), 189.1 (14), 123.1 (34), 95.1 (100)	250	SWYRVCGN MNAFEK-PUVRWCM WSA-N	B
18′	17.10	Eucaglobulin (I)	Monoterpene-gallate glycoside	$C_{23}H_{30}O_{12}$	497.1664	497.1651 [M-H]⁻	n.d	n.d.	2.80, -	497.2 (66), 169.0 (100), 125.0 (54)	n.d.	267, 297	GMBUWWL CKJYTTG-UHFFFAOYS A-N	B
19′	17.02	Eucaglobulin (II)	Monoterpene-gallate glycoside	$C_{23}H_{30}O_{12}$	497.1664	497.1646 [M-H]⁻	n.d	n.d	3.74, -	497.2 (26), 169.0 (100), 125.0 (48)	n.d	267, 292	GMBUWWL CKJYTTG-UHFFFAOYS A-N	B
20′	21.89	Unknown	Unknown	$C_{19}H_{28}O_{10}$	415.1609	415.1594 [M-H]⁻	n.d	n.d	3.75, -	415.2 (28), 397.2 (100), 235.1 (62), 207 (58), 191.0 (20)	n.d	285	-	-
21′	15.26	Dihydro-Eucaglobulin	Monoterpene-gallate glycoside	$C_{23}H_{32}O_{12}$	499.1821	499.1806 [M-H]⁻	n.d	n.d	3.05, -	499.2 (100), 169.0 (95), 125.0 (45)	n.d	275	RZSYEJWK QPWMQI-PTLWZDEX SA-N	B
22′	22.22	Unknown	Unknown	$C_{19}H_{26}O_9$	397.1504	397.1488	n.d	n.d	4.02, -	397.1 (100), 235.1 (84), 207.1	n.d	294	-	-

#	RT	Name	Class	Formula	Calc. mass	Neg. ion	Calc. (pos)	Pos. ion	Error[a]	Neg. MS/MS	Pos. MS/MS	UV/Vis	InChI-Key	Level
23′	20.83	Cypellocarpin C	Chromene monoterpene glycoside	$C_{26}H_{32}O_{11}$	565.1927	[M-H]⁻ 565.1912 [M+HCO₂H -H]⁻	503.1912	503.1889 [M-H₂O+H]⁺	2.54, -	(48), 191.0 (44), 163.0 (18) 519.2 (7), 191.0 (100)	193.1 (100)	282	OUBDJJFZU QGQLU- ZHFYLPRNS A-N	B
24′	1.21	Pyridoxine hexoside	Hydroxymeth ylpyridine glycoside	$C_{14}H_{21}NO_8$	n.d.	n.d.	332.1339	332.1324 [M+H]⁺	- , 4.74	n.d.	314.1 (6), 152.1 (33), 134.1 (14), 124.1 (30), 108.1 (100)	277	MDLTWTOQ CHCLSZ- RGCYKPLRS A-N	B

[a]: Mean accurate mass error for negative and positive ESI acquisition modes; [b]: in-source fragmented; [c]: including metabolites **1′** and **2′**; UV/Vis: maximum absorbance; InChI-Key: IUPAC international identifier for chemicals according to PubChem; Identification level (A-D): A–standard or NMR, B–MS/MS, C–MS[E], D–MS only; *geometric configuration inferred from UV-spectrum; **potentially new compound; I, II: isobaric compounds with similar MS/MS spectrum; Man: mandelonitrile; OleuA: oleuropeic acid; n.d.: not detected.

References

Adiji, O.A., Docampo-Palacios, M.L., Alvarez-Hernandez, A., Pasinetti, G.M., Wang, X., Dixon, R.A., 2021. UGT84F9 is the major flavonoid UDP-glucuronosyltransferase in *Medicago truncatula*. Plant Physiology 1–21. https://doi.org/10.1093/plphys/kiab016

Austin, M.B., Noel, J.P., 2003. The chalcone synthase superfamily of type III polyketide synthases. Natural Product Reports 20, 79–110. https://doi.org/10.1039/b100917f

Beéche Cisternas, M.A., Sandoval Clavería, A., Rothmann Toro, S., Ravanales Villalobos, J., Cereceda Leinz, C., Muñoz Godoy, R., Olivera Alvarez, G., Corvalán Latapia, L., Galarce Marambio, G., San Martín López, A., 1999. Detección y control del gorgojo del eucalipto *Gonipterus scutellatus* Gyllenhal en Chile (Coleoptera: Curculionidae). Santiago de Chile.

Brooker, M.I.H., 2000. A new classification of the genus *Eucalyptus* L'Her. (Myrtaceae). Australian Systematic Botany 13, 79–148. https://doi.org/10.1071/SB98008

Cerasoli, S., Caldeira, M.C., Pereira, J.S., Caudullo, G., de Rigo, D., 2016. *Eucalyptus globulus* and other eucalypts in Europe: distribution, habitat, usage and threats, in: San-Miguel-Ayanz, J., de Rodrigo, D., Caudullo, G., Houston Durrant, T., Mauri, A. (Eds.), European Atlas of Forest Tree Species. Publ. Off. EU, Luxembourg, pp. 90–91.

Chong, J., Poutaraud, A., Hugueney, P., 2009. Metabolism and roles of stilbenes in plants. Plant Science 177, 143–155. https://doi.org/10.1016/j.plantsci.2009.05.012

Chong, J., Wishart, D.S., Xia, J., 2019. Using MetaboAnalyst 4.0 for comprehensive and integrative metabolomics data analysis. Current Protocols in Bioinformatics 68, 1–128.

Close, D.C., McArthur, C., Hagerman, A.E., Davies, N.W., Beadle, C.L., 2007. Phenolic acclimation to ultraviolet-A irradiation in *Eucalyptus nitens* seedlings raised across a nutrient environment gradient. Photosynthetica 45, 36–42. https://doi.org/10.1007/s11099-007-0006-4

Coppen, J.J.W., 2002. *Eucalyptus*: the genus *Eucalyptus*. Taylor & Francis, London, New York.

Cordero-Rivera, A., Santolamazza-Carbone, S., 2000. The effect of three species of *Eucalyptus* on growth and fecundity of the *Eucalyptus* snout beetle (*Gonipterus scutellatus*). Forestry 73, 21–29.

Denslow, S.A., Walls, A.A., Daub, M.E., 2005. Regulation of biosynthetic genes and antioxidant properties of vitamin B6 vitamers during plant defense responses. Physiological and Molecular Plant Pathology 66, 244–255. https://doi.org/10.1016/j.pmpp.2005.09.004

Dührkop, K., Fleischauer, M., Ludwig, M., Aksenov, A.A., Melnik, A. V., Meusel, M., Dorrestein, P.C., Rousu, J., Böcker, S., 2019. SIRIUS 4: a rapid tool for turning tandem mass spectra into metabolite structure information. Nature Methods 16, 299–302.

Dutkowski, G. W., & Potts, B. M., 1999. Geographic patterns of genetic variation in *Eucalyptus globulus* ssp. globulus and a revised racial classification. Australian Journal of Botany, 47, 237-263.

EPPO, 2018. EPPO A1 and A2 list of pests recommended for regulation as quarantine pests - PM1/2(27), EPPO Standards. Paris. https://doi.org/10.1353/cpp.2011.0032

EPPO, 2005. *Gonipterus gibberus* and *Gonipterus scutellatus*. EPPO Bulletin 35, 368–370. https://doi.org/10.1111/j.1365-2338.2005.00855.x

Ferreira, B.G., Falcioni, R., Guedes, L.M., Avritzer, S.C., Antunes, W.C., Souza, L.A., Isaias, R.M.S., 2017. Preventing False Negatives for Histochemical Detection of Phenolics and Lignins in PEG-Embedded Plant Tissues. Journal of Histochemistry and Cytochemistry 65, 105–116. https://doi.org/10.1369/0022155416677035

Fiehn, O., 2001. Combining genomics, metabolome analysis, and biochemical modelling to understand metabolic networks. Comparative and Functional Genomics 2, 155–168. https://doi.org/10.1002/cfg.82

Fiehn, O., Kopka, J., Dörmann, P., Altmann, T., Trethewey, R.N., Willmitzer, L., 2000. Metabolite profiling for plant functional genomics. Nature Biotechnology 18, 1157–1161. https://doi.org/10.1038/81137

Finkelstein, R., 2013. Abscisic Acid Synthesis and Response. The Arabidopsis Book 11, e0166. https://doi.org/10.1199/tab.0166

Fitzpatrick, T.B., 2011. Vitamin B6 in plants: More than meets the eye, in: Rébeillé, F., Douce, R. (Eds.), Advances in Botanical Research. Elsevier Ltd, pp. 1–38. https://doi.org/10.1016/B978-0-12-385853-5.00006-4

Getman-Pickering, Z.L., Campbell, A., Aflitto, N., Grele, A., Davis, J.K., Ugine, T.A., 2020. LeafByte: A mobile application that measures leaf area and herbivory quickly and accurately. Methods in Ecology and Evolution 11, 215–221. https://doi.org/10.1111/2041-210X.13340

Gleadow, R.M., Haburjak, J., Dunn, J.E., Conn, M.E., Conn, E.E., 2008. Frequency and distribution of cyanogenic glycosides in *Eucalyptus* L'Hérit. Phytochemistry 69, 1870–1874. https://doi.org/10.1016/j.phytochem.2008.03.018

Gleadow, R.M., Woodrow, I.E., 2002. Constraints on effectiveness of cyanogenic glycosides in herbivore defense. Journal of Chemical Ecology 28, 1301–1313. https://doi.org/10.1023/A

Gonçalves, C.I., Vilas-Boas, L., Branco, M., Rezende, G.D., Valente, C., 2019. Host susceptibility to *Gonipterus platensis* (Coleoptera: Curculionidae) of *Eucalyptus* species. Annals of Forest Science 76. https://doi.org/10.1007/s13595-019-0850-y

Goodger, J.Q.D., Woodrow, I.E., 2011. α,β-Unsaturated monoterpene acid glucose esters: Structural diversity, bioactivities and functional roles. Phytochemistry 72, 2259–2266. https://doi.org/10.1016/j.phytochem.2011.08.026

Gysling Caselli, A.J., Alvarez Gonzalez, V. del C., Soto Aguirre, D.A., Pardo Velasquez, E.J., Poblete Hernandez, P.A., 2018. Chilean Statistical Yerabook of Forestry, N°163. ed. Forestry Institute (INFOR), Santiago.

Gysling Caselli, A.J., Álvarez González, V.D.C., Soto Aguirre, D.A., Pardo Velasquez, E.J., Poblete Hernandez, P.A., Bañados Munita, J.C., 2017. Chilean Statistical Yearbook of Forestry, N°159. ed. Forestry Institute (INFOR), Santiago.

Gysling Caselli, A.J., Álvarez González, V.D.C., Soto Aguirre, D.A., Pardo Velasquez, E.J., Poblete Hernandez, P.A., Kahler González, C., 2019. Chilean statistical yearbook of forestry, N° 168. ed, Anuario Forestal INFOR.

Forestry Institute (INFOR), Santiago. https://doi.org/ISBN: 978-956-318-098-5

Hammerbacher, A., Ralph, S.G., Bohlmann, J., Fenning, T.M., Gershenzon, J., Schmidt, A., 2011. Biosynthesis of the major tetrahydroxystilbenes in spruce, astringin and isorhapontin, proceeds via resveratrol and is enhanced by fungal infection. Plant Physiology 157, 876–890. https://doi.org/10.1104/pp.111.181420

Hansen, C.C., Sørensen, M., Veiga, T.A.M., Zibrandtsen, J.F.S., Heskes, A.M., Olsen, C.E., Boughton, B.A., Møller, B.L., Neilson, E.H.J., 2018. Reconfigured cyanogenic glucoside biosynthesis in *Eucalyptus cladocalyx* involves a cytochrome P450 CYP706C55. Plant Physiology 178, 1081–1095. https://doi.org/10.1104/pp.18.00998

Hasegawa, S., Poling, S.M., Maier, V.P., Bennett, R.D., 1984. Metabolism of abscisic acid: Bacterial conversion to dehydrovomifoliol and vomifoliol dehydrogenase activity. Phytochemistry 23, 2769–2771. https://doi.org/10.1016/0031-9422(84)83012-5

Havaux, M., Ksas, B., Szewczyk, A., Rumeau, D., Franck, F., Caffarri, S., Triantaphylidès, C., 2009. Vitamin B6 deficient plants display increased sensitivity to high light and photo-oxidative stress. BMC Plant Biology 9, 130. https://doi.org/10.1186/1471-2229-9-130

Heskes, A.M., Goodger, J.Q.D., Tsegay, S., Quach, T., Williams, S.J., Woodrow, I.E., 2012. Localization of oleuropeyl glucose esters and a flavanone to secretory cavities of myrtaceae. PLoS ONE 7, e40856. https://doi.org/10.1371/journal.pone.0040856

Hillis, W.E., 1966. Variation in polyphenol composition within species of *Eucalyptus* l'herit. Phytochemistry 5, 541–556. https://doi.org/10.1016/S0031-9422(00)83632-8

Huerta-Fuentes, A., Chiffelle-Gomez, I., Serrano-Garzon, M., Vazquez-Silva, T., Araya-Clericus, J., 2008. Susceptibility of *Eucalyptus* species to *Gonipterus scutellatus* and electrophoretic profiles of adult marker proteins. Agrociencia 42, 327–334.

Informativo fitosanitario forestal N°8, Servicio Agrícola y Ganadero (SAG), 2012. , Servicio Agrícola y Ganadero (SAG). Santiago de Chile.

Ipinza, R., Barros, S., Gutiérrez, B., Borralho, N., 2014. Mejoramiento genético de eucaliptos en Chile. Instituto Forestal, INFOR, Santiago de Chile.

Johansen, D.A., 1940. Plant microtechnique, First Edit. ed. McGraw-Hill Bokk Company, Inc., New York and London.

Kerchev, P.I., Fenton, B., Foyer, C.H., Hancock, R.D., 2012. Plant responses to insect herbivory: Interactions between photosynthesis, reactive oxygen species and hormonal signalling pathways. Plant, Cell and Environment 35, 441–453. https://doi.org/10.1111/j.1365-3040.2011.02399.x

Lanfranco, D., Dungey, H.S., 2001. Insect damage in *Eucalyptus*: a review of plantations in Chile. Austral Ecology 26, 477–481. https://doi.org/10.1046/j.1442-9993.2001.01131.x

Li, S., Park, Y., Duraisingham, S., Strobel, F.H., Khan, N., Soltow, Q.A., Jones, D.P., Pulendran, B., 2013. Predicting Network Activity from High Throughput Metabolomics. PLoS Computational Biology 9. https://doi.org/10.1371/journal.pcbi.1003123

Loch, A.D., Floyd, R.B., 2001. Insect pests of Tasmanien blue gum, *Eucalyptus globulus globulus*, in south-western Australia: History, current perspectives and future prospects. Austral Ecology 26, 458–466. https://doi.org/10.1046/j.1442-9993.2001.01145.x

Loch, A.D., Matsuki, M., 2010. Effects of defoliation by *Eucalyptus* weevil, *Gonipterus scutellatus*, and chrysomelid beetles on growth of *Eucalyptus globulus* in southwestern Australia. Forest Ecology and Management 260, 1324–1332. https://doi.org/10.1016/j.foreco.2010.07.025

Maas, J.L., Galletta, G.J., Stoner, G.D., 1991. Ellagic Acid, an Anticarcinogen in Fruits, Especially in Strawberries: A Review. HortScience 26, 10–14. https://doi.org/10.21273/hortsci.26.1.10

Mapondera, T.S., Burgess, T., Matsuki, M., Oberprieler, R.G., 2012. Identification and molecular phylogenetics of the cryptic species of the *Gonipterus scutellatus* complex (Coleoptera: Curculionidae: Gonipterini). Australian Journal of Entomology 51, 175–188. https://doi.org/10.1111/j.1440-6055.2011.00853.x

MaSchlyter, F., Marling, E., Löfqvist, J., 2004. A new microassay for antifeedants in Hylobius pine weevils (Coleoptera). Journal of Pest Science 77, 191–195. https://doi.org/10.1007/s10340-004-0050-9

Matsuki, M., Foley, W.J., Floyd, R.B., 2011. Role of volatile and non-volatile plant secondary metabolites in host tree selection by christmas beetles. Journal of Chemical Ecology 37, 286–300. https://doi.org/10.1007/s10886-011-9916-5

Memoria anual Consorcio Protección Fitosanitaria Forestal S.A., 2018, 2018.

Muir, R.M., Ibáñez, A.M., Uratsu, S.L., Ingham, E.S., Leslie, C.A., McGranahan, G.H., Batra, N., Goyal, S., Joseph, J., Jemmis, E.D., Dandekar, A.M., 2011. Mechanism of gallic acid biosynthesis in bacteria (*Escherichia coli*) and walnut (*Juglans regia*). Plant Molecular Biology 75, 555–565. https://doi.org/10.1007/s11103-011-9739-3

Nambara, E., Marion-Poll, A., 2005. ABSCISIC ACID BIOSYNTHESIS AND CATABOLISM. Annual Review of Plant Biology 56, 165–185. https://doi.org/10.1146/annurev.arplant.56.032604.144046

Paine, T.D., Millar, J.G., 2002. Insect pests of eucalypts in California: implications of managing invasive species. Bulletin of Entomological Research 92, 147–151. https://doi.org/10.1079/ber2002151

Pederick, L.A., Lennox, F.G., 1979. Variation in polyphenolic constituents of *Eucalyptus nitens* Maiden. Australian Journal of Botany 27, 217–226. https://doi.org/10.1071/BT9790217

Pentzold, S., Zagrobelny, M., Rook, F., Bak, S., 2014. How insects overcome two-component plant chemical defence: Plant β-glucosidases as the main target for herbivore adaptation. Biological Reviews 89, 531–551. https://doi.org/10.1111/brv.12066

Reis, A.R., Ferreira, L., Tomé, M., Araujo, C., Branco, M., 2012. Efficiency of biological control of *Gonipterus platensis* (Coleoptera: Curculionidae) by *Anaphes nitens* (Hymenoptera: Mymaridae) in cold areas of the Iberian Peninsula: Implications for defoliation and wood production in *Eucalyptus globulus*. Forest Ecology and Management 270, 216–222. https://doi.org/10.1016/j.foreco.2012.01.038

Ruttkies, C., Schymanski, E.L., Wolf, S., Hollender, J., Neumann, S., 2016. MetFrag relaunched: Incorporating strategies beyond in silico fragmentation. Journal of Cheminformatics 8, 1–16. https://doi.org/10.1186/s13321-016-0115-9

Sánchez-Gómez, R., Sánchez-Vioque, R., Santana-Méridas, O., Martín-Bejerano, M., Alonso, G.L., Salinas, M.R., Zalacain, A., 2017. A potential use of vine-shoot wastes: The antioxidant, antifeedant and phytotoxic activities of their aqueous extracts. Industrial Crops and Products 97, 120–127. https://doi.org/10.1016/j.indcrop.2016.12.009

Schulze, E.-D., Beck, E., Buchmann, N., Clemens, S., Müller-Hohenstein, K., Scherer-Lorenzen, M., 2019a. Part I. Molecular stress physiology: Light, in: Plant Ecology. Springer, Berlin, pp. 80–83.

Schulze, E.-D., Beck, E., Buchmann, N., Clemens, S., Müller-Hohenstein, K., Scherer-Lorenzen, M., 2019b. Part I Molecular stress physiology: Biotic stress, in: 2nd (Ed.), Plant Ecology. Springer, Berlin, pp. 276–290.

Sedio, B.E., 2017. Recent breakthroughs in metabolomics promise to reveal the cryptic chemical traits that mediate plant community composition, character evolution and lineage diversification. New Phytologist 214, 952–958. https://doi.org/10.1111/nph.14438

Strauss, S.H., Boerjan, W., Chiang, V., Costanza, A., Coleman, H., Davis, J.M., Lu, M.-Z., Mansfield, S.D., Merkel, S., Myburg, A., Nilsson, O., Pilate, G., Powel, W., Seguin, A., Valenzuela, S., 2019. Certification for gene-edited forest. Science 365, 767–768.

Stuart, K.L., Coke, L.B., 1975. The effect of vomifoliol on stomatal aperture. Planta 122, 307–310. https://doi.org/10.1007/BF00385281

Tropf, S., Lanz, T., Rensing, S.A., Schröder, J., Schröder, G., 1994. Evidence that stilbene synthases have developed from chalcone synthases several times in the course of evolution. Journal of Molecular Evolution 38, 610–618. https://doi.org/10.1038/269464b0

Valente, C., Gonçalves, C.I., Monteiro, F., Gaspar, J., Silva, M., Sottomayor, M., Paiva, M.R., Branco, M., 2018. Economic Outcome of Classical Biological Control: A Case Study on the *Eucalyptus* Snout Beetle, *Gonipterus platensis*, and the Parasitoid *Anaphes nitens*. Ecological Economics 149, 40–47. https://doi.org/10.1016/j.ecolecon.2018.03.001

Valledor, L., Escandón, M., Meijón, M., Nukarinen, E., Cañal, M.J., Weckwerth, W., 2014. A universal protocol for the combined isolation of metabolites, DNA, long RNAs, small RNAs, and proteins from plants and microorganisms. Plant Journal 79, 173–180. https://doi.org/10.1111/tpj.12546

Wang, D., Gao, Z., Du, P., Xiao, W., Tan, Q., Chen, X., Li, L., Gao, D., 2016. Expression of ABA metabolism-related genes suggests similarities and differences between seed dormancy and bud dormancy of peach (Prunus persica). Frontiers in Plant Science 6, 1248. https://doi.org/10.3389/fpls.2015.01248

Whitham, T.G., DiFazio, S.P., Schweitzer, J., Shuster, S., Allan, G., Bailey, J., Woolbright, S., 2008. Extending genomics to natural communities and ecosystems. Science 320, 492–495.

Withers, T.M., 2001. Colonization of eucalypts in New Zealand by Australian insects. Austral Ecology 26, 467–476. https://doi.org/10.1046/j.1442-9993.2001.01140.x

Worley, B., Powers, R., 2016. PCA as a predictor of OPLS-DA model reliability. Curr. Metabolomics 4, 97–103.

Worley, B., Powers, R., 2013. Multivariate Analysis in Metabolomics. Curr. Metabolomics 1, 92–107.

Zunjarrao, S. S., Tellis, M. B., Joshi, S. N., Joshi, R. S., et al., 2020. Plant-insect interaction: the saga of molecular coevolution. Reference Series in Phytochemistry. Springer Nature Switzerland AG, pp. 19-45.

4.2. Exploring inherited defensive traits in *Eucalyptus* inter-specific hybrids to combat herbivory by *Gonipterus platensis* and enable genotype selection for building resistance.

Manuscrito enviado a la revista Plant, Cell & Environment el 23 de mayo 2023.

Exploring inherited defensive traits in *Eucalyptus* inter-specific hybrids to combat herbivory by *Gonipterus platensis* and enable genotype selection for building resistance.

Jasna V. Campos [a], Rafael Rubilar [b], Rosa Alzamora [c], Luis E. Arteaga-Pérez [d], Claudia Mardones [a], Oliver Fiehn [e], Andy J. Pérez [a, *].

[a] Departamento de Análisis Instrumental, Facultad de Farmacia, Universidad de Concepción, Concepción, Chile.

[b] Cooperativa de Productividad Forestal, Departamento de Silvicultura, Facultad de Ciencias Forestales, Universidad de Concepción, Concepción, Chile.

[c] Departamento Manejo de Bosques y Medio Ambiente, Facultad de Ciencias Forestales, Universidad de Concepción, Concepción, Chile.

[d] Laboratory of Thermal and Catalytic Processes (LPTC), Department of Wood Engineering, University of Bío-Bío, Chile.

[e] NIH West Coast Metabolomics Center, UC Davis Genome Center, University of California, Davis, CA 95616, USA.

* Corresponding author E-mail: aperezd@udec.cl (A.J. Pérez). Phone: +56 41 220 3027

Abstract

Eucalyptus plantations in temperate regions often face productivity challenges due to frost damage. One potential solution is to create interspecific hybrid by crossing the frost-sensitive *E. globulus* (*Eg*) with cold-hardy species like *E. nitens* (*En*), which can produce the *E. nitens × globulus* (*En×Egg*) hybrid. Besides, hybrids should also inherit the parents' resistance to main pests, such as the specialist insect *Gonipterus platensis* (weevil). However, there is a need to identify measurable biomarkers that can distinguish differential resistance among hybrid genotypes. Therefore, this study explored the inherited defensive traits of seven hybrid genotypes crucial to deterring weevil herbivory. Our findings revealed that, unlike the susceptible *Eg*, the hybrids had the necessary enzymes to synthesize stilbenes constitutively, which provide resistance to *En*. However, the level of both constitutive and inducible stilbenes in the hybrids were significantly lower than in *En*. Therefore, the hybrids exhibited better resistance than *Eg* but not as good as *En*. However, we also revealed that resistance imputation among *En×Egg* genotypes is not possible based solely on stilbenes since there were

no consistency found between the fold-change by which they were upregulated upon herbivory and the severity of defoliation suffered in each case. Interestingly, it was found that among all the up- or down-regulated metabolites described in hybrids, an unprecedented correlation existed with the monoterpene Roseoside (Vomifoliol glucoside). This metabolite was down-regulated at a rate higher than 2.0-fold in the *En×Egg* genotypes that were only moderately defoliated, suggesting a cleavage of this molecule to release free Vomifoliol. Accordingly, the resistance parent, *En*, downregulated this substance by 3.34-fold, being consequently highly protected. Since Vomifoliol is lipophilic, it is probably sequestered in the leaves' oil bodies after the cleavage. Then, through the weevil feeding, oil bodies may disrupt, releasing essential oil containing Vomifoliol, which could exert a direct deterrent effect. While these finding are a crucial first step toward developing resistance in *En×Egg* genotypes, further research is necessary to get a better understanding of the underlying mechanism of deterrence.

Key words:

Plant metabolomics; *Eucalyptus* spp.; Inter-specific hybrids; Herbivory; Defensive response; *Gonipterus platensis* (eucalyptus weevil).

4.2.1. Introduction

Most of the pulpwood supply to paper pulp production worldwide is provided by *Eucalyptus* genus (Myrtaceae) trees, which partly respond to their fast-growing aptitudes and adaptability to temperate regions. Within this genus, the species *E. globulus* (Tasmanian blue gum) is planted to a greater extent because of its high wood density and pulp yield (Volker et al., 2008). Currently, *E. globulus* Labill. ssp. *globulus* and *E. nitens* (Deane & Maiden) Maiden comprise 25% and 11.8% of the total forest planted area in Chile (2.3 million ha), respectively (Aguirre et al., 2021). A significant portion of these forest resources goes to bleached pulp production, which only in 2020 was more than 2.7 million tons, 61% of the total output (Aguirre et al., 2021).

In Chile, as in the rest of the world, plantations of *E. globulus* have been confined to relative frost climates that usually challenge its adaptability, affecting growth and productivity (Geldres and Schlatter, 2004). While attention has been paid to the acquired tolerance mechanisms that enhance cold acclimation in this species (Aguayo et al., 2019; Fernández et al., 2015;

Navarrete-Campos et al., 2017), *E. nitens* is often used for replacement, given its higher cold hardiness (Close, 2012; Tibbits and Hodge, 2003). At the same time, breading programs for developing inter-specific hybrids between these two species, *E. nitens × globulus* (*En×Egg*), have been gaining interest in Chile to improve the growth and productivity of eucalypts plantations under sites of frequent frost events (Ipinza et al., 2014; Volker et al., 2008). The annual new plantations of eucalypts in Chile have been dominated by *E. nitens* since 2019, with more than 20 thousand ha. In contrast, new plantations of *E. globulus* have significantly decreased from more than 16 thousand ha in 2019 to only 8.5 thousand ha in 2020 (Aguirre et al., 2021). Simultaneously, other eucalypts species, including hybrids, increased from 1.5 thousand ha in 2015 to 5.5 thousand ha in 2020 (Aguirre et al., 2021).

Regardless of the frost tolerance achieved with *En×Egg* hybrids, susceptibility or resistance to main pests stressing eucalypts plantations may also be inherited from parents. One of the most significant pests worldwide is the eucalyptus weevil *Gonipterus platensis* Marelli (Coleoptera: Curculionidae), a specialist insect that feeds on eucalypts' new foliage causing severe defoliation in the tree crown (Lanfranco and Dungey, 2001; Loch and Matsuki, 2010; Mapondera et al., 2012; Reis et al., 2012).

According to the Forestry Institute of the Chilean Agriculture Ministry, projections for future wood availability from *E. globulus* plantations alert about a deficit of 1.6 million m^3, pointing to the weevil among factors that have affected their growth rate (Aguirre et al., 2021). It is because this species is one of the preferred hosts of the weevil (Gonçalves et al., 2019; Lanfranco and Dungey, 2001). In contrast, *E. nitens* has shown a particular resistance within the section Maidenaria to avoiding the herbivory (Gonçalves et al., 2019). In a recent work by our research group, we used metabolomics to reveal the plant chemical traits that govern such different susceptibility (Campos et al., 2022). We reported the chemical evidence based on *Eucalyptus* non-volatile constitutive and inducible defense that may drive the *G. platensis* host range for the first time. After a differential metabolome comparison between *E. nitens* and *E. globulus*, we suggested an apparent lack of stilbene synthase (STS) and gallate 1-β-glucosyltransferase (G1βGluT) in the last, restricting both constitutive and upon-herbivory accumulation of stilbenes and hydrolysable tannins, respectively. We demonstrated that these classes of specialized metabolites may significantly inhibit the feeding of *G. platensis* adults by more than 30% (Campos et al., 2022). In such context, biosynthetic capacity belonging to *E. nitens* must be inherited, to some

extent, by their progeny *En×Egg*. Then, different protection levels could be achieved in hybrids depending on the crossing type, generations, and parents.

Given the challenge that plant metabolome diversity represents in terms of analytical measurements, metabolomics has strongly emerged as an appropriate tool for functional analysis of specialized plant metabolites focusing on their ecological implications (Li and Gaquerel, 2021). Metabolomics uses high-throughput analytical means to allow for simultaneous quantitative comparison of hundreds to thousands of metabolites within a living system, distinguishing a reduced number of them that best describes the pathophysiological state in response to a given stress (Alseekh and Fernie, 2018; Fiehn, 2001; Fiehn et al., 2000). In addition, the critical upstream molecular expression, including genes, transcripts, or enzymes, can be inferred since metabolites are downstream products of the cellular biochemical processes. This is particularly advantageous when metabolomics needs to be applied as an independent technique to non-model plant species for which genome and transcriptome data are unavailable (Li and Gaquerel, 2021).

Breeding programs in Chile use several quantifiable variables such as wood density, rhizogenesis, growth rate, seed quality, and fiber productivity

to develop successful *Eucalyptus* hybrids (Ipinza et al., 2014). However, pest resistance is usually attributed to a specific genotype only after observing its performance under pest attack. Therefore, it is recommended to identify measurable biomarkers that can be used in a systematic selection method of resistant genotypes. Even though complex hybridizations such as retro-crosses are attractive to producers and are incorporated into breeding programs (Ipinza et al., 2014), it is crucial to identify measurable entities that aid in selecting resistant genotypes.

In this study, we used LC-MS-based untargeted metabolomics to identify the metabolic resistance traits transferred to *E. nitens × globulus* hybrids by their parents. We focused on constitutive and inducible defenses against *G. platensis* herbivory based on non-volatile specialized metabolites. Our findings provide unprecedented chemical evidence related to the tree response that may lay the groundwork for resistance imputation in *Eucalyptus* species or hybrid genotypes.

4.2.2. Material and methods

4.2.2.1. Origin of plant material and sampling

The plant material used in this study was obtained from an experimental field planted in 2017 in the nursery garden "Carlos Douglas" owned by Forestal Mininco S.A., located near Yumbel town in the Biobio Region of Chile (37º07'59.6''S 72º27'34.5''W). For sampling, we considered seven F1 hybrids created by an interspecific hybridization using *E. nitens* as the mother species and *E. globulus* as the pollen donor. They were named from *En×Egg*1 to *En×Egg*7, each belonging to different parents. A genotype of pure *E. nitens* (*En*1) and seven of pure *E. globulus* (*Eg*1-*Eg*7) were simultaneously sampled to be used for metabolome comparison purposes. At sampling time, plants aged two years and all genotypes presented petiolate mature leaves in the canopy, the type of leaves that the weevil usually prefers for feeding. In the experimental field, 16 clones of each genotype were planted in 4.5 m square plots at a 1.5 m distance from each other and with three replicates within the field area to avoid gradients in soil conditions (Fig. S1).

Sampling was carried out at two points in time, T0 and T1. The first one, T0, took place on February 22nd, 2019, between 07:00 a.m. and 09:00 a.m., without signs of defoliation by *G. platensis* in any genotype. However, as the

experimental field was located within a wider area of weevil incidence, an intense attack appeared just one month later. At this point (March 22nd, 2019, between 08:00 a.m. and 10:00 a.m.), the second sampling, T1, was conveniently implemented to register the metabolome changes induced in genotypes of interest in response to the herbivory. The weevil attack was evidenced by 1) defoliation of buds in the tree crown and scalloped edges in the canopy leaves caused by adults feeding; 2) photosynthetic tissues loss in expanded leaves due to larvae feeding following a characteristic pattern; 3) oviposition of greyish capsules (ootheca) in the leaves surface; 4) adults and larvae sighting (Fig. S2). The severity of infestation was qualitatively determined by visual evaluation of the defoliation caused by *G. platensis* in the apex of the four central trees per genotype plot, assigning values on a scale from 0G (absence of defoliation) to 4G (severe defoliation) (Table S1 and Method S2).

Five fully expanded mature leaves (petiolate) without signs of herbivory were collected from the canopy of the four central trees per genotype plot and mixed as only one sample. Immediately after harvest, samples were submerged in liquid nitrogen, transported to the laboratory, and stored at -80°C until further processing.

4.2.2.2. Sample preparation and metabolome extraction

Frozen fresh samples were freeze-dried and then ground into a fine powder and homogenized using an MM-400 mixer mill (Retsch GmbH, Haan, Germany). Each ground and homogenized sample (GHS) was processed in triplicate within a complete randomized block for metabolome extraction and analysis. The extraction was performed using a protocol previously implemented in our laboratory with slight modifications (Campos et al., 2022). Briefly, 1000 µL of cold (4°C) MeOH/H_2O/CH_2Cl_2 (2.5:0.5:1.0) were added to 100 mg of GHSs contained in 2.0 ml Eppendorf tubes and shaken for 2 min at 30 Hz in MM-400 mixer mill. Simultaneously, blanks containing only extraction solvent were also processed in triplicate and included in the randomized block. Then, samples and blanks were centrifuged at 13300 *rpm* for 10 min at 4°C, and 700 µl supernatants were transferred to new 2.0 ml Eppendorf tubes. Subsequently, liquid-liquid extraction was performed by adding CH_2Cl_2 and water, 400 µl each, and shaken for 30 s at 20 Hz. Two phases were sharply defined after centrifuging at 13300 *rpm* for 5 min at 4°C. 700 µl of top aqueous fractions were transferred to new tubes and evaporated to dryness in a vacuum centrifuge (Eppendorf, Concentrator plus). The bottom lipophilic fractions containing photosynthetic pigments and other

129

non-polar substances were discarded. Dried extracts were stored at -80°C until needed.

4.2.2.3. LC-MS analysis

Immediately before analysis, dried extracts and blanks were resuspended in 1000 µl of cold (4°C) 80% methanol (in water, v/v), shaken for 3 min at 30 Hz, and centrifuged for 15 min at 13300 *rpm* and 4°C. A pooled quality control (QC) sample, constituted by mixing 200 µl aliquots taken from each resuspended extract, was used to monitor the instrument performance during analysis. Blanks, QCs, and resuspended plant extracts were then transferred to 200 µl inserts contained in 1.5 ml amber vials with pre-slit caps and placed in a liquid chromatography autosampler maintained at 4°C following the predetermined random sequence. The sequence started with three blank samples, followed by six QCs, and another QC sample after every ten plant extracts.

The metabolomics analysis was carried out by LC-MS/MS on an ultra-high performance liquid chromatography system (Elute UHPLC, Bruker Daltonik GmbH, Bremen, Germany) equipped with a diode array detector (Elute DAD) and coupled in tandem with a quadrupole-time-of-flight mass

spectrometer equipped with an atmospheric pressure electrospray ionization source (Compact ESI-QTOF, Bruker Daltonik GmbH, Bremen, Germany). Chromatography separation and mass spectrometer operation were performed under the same conditions previously described by our research group (Campos et al., 2022). Finally, 135 resuspended extracts (figteen genotypes × three biological replicates × three technical replicates), 20 QCs (six at sequence beginning + fourteen inserted between each ten plant-extracts), and 3 blanks were analyzed both in –ESI and +ESI acquisition modes.

4.2.2.4. Data processing and statistics

Raw LC-MS data acquired in both ESI modes were first processed in MetaboScape 3.0 (Compass, Bruker Daltonik GmbH, Germany) using the algorithm "*Time aligned Region complete eXtraction*" (T-ReX 3D). It integrates the mass re-calibration, retention time (Rt) alignment, feature extraction (*m/z* – Rt pairs), adduct and neutral losses handling, whole region feature extraction, MS/MS import for identification, and generates bucket tables where features are assigned to buckets (*m/z* – Rt pairs with respective ion intensity) across samples with recursive extraction of missed peaks for

improving statistics. The parameter used for bucket table generation were set as follows: intensity threshold, 1000 counts; minimum spectra peak length, 5; minimum recursive peak length, 4; minimum number of recursive features to be extracted, if present in 1/3 of a group; features in a minimum number of analysis, present in 1/3 of a group; mass range, 50 – 2000 *m/z*; retention time range, 0.5 – 25.0 min; MS/MS import, as average.

The generated bucket tables were first manually curated using exploratory statistics in MetaboScape and then exported to MetaboAnalyst 5.0 for high-throughput metabolomics analytical pipeline (Pang *et al.*, 2021). After uploading, data were normalized by sum, Pareto-scaled, and examined by applying principal component analysis (PCA) for reducing data dimensionality and uncovering the inherent cluster pattern (Worley & Powers, 2013b). Then, Orthogonal Projection to Latent Structure Discriminant Analysis (OPLS-DA) was applied to the dataset. This is a supervised modeling method that allowed for discovering features that best discriminate between the leaves metabolome of two species under study, for instance, between *E. nitens* (*En*) and *E. nitens × globulus* (*En×Egg*) or between *E. globulus* (*Eg*) and *En×Egg*. At the same time, OPLS-DA models were used to reveal the features correlated with the systemic response in each

hybrid *En×Egg* genotype after *G. platensis* herbivory. In this case, T0 and T1 labels were used for trees before and after defoliation, respectively. As the OPLS-DA model aggressively enforces the separation of the two classes considered, it causes the risk of overfitting the model to the data. Therefore, model validation is mandatory. It was performed by using a combined random permutation test of class labels with internal leaves-*n*-out cross-validation. The parameters of a measure of internal consistency between the original and cross-validated predicted data (Q^2) and the measure of model fit to the original data (R^2Y) were used to assess the statistical quality of the validation (Worley & Powers, 2013c, 2016c).

Additional statistical treatment and visualization of the quantitative data for the metabolites of interest were performed in GraphPad Prism (v. 8.4.3) software. Statistical tests used for mean comparison are declared in each case.

4.2.2.5. Metabolite Annotation

The chemical nature of significant metabolites was first determined using an integrated workflow in MetaboScape for manual annotation. The first step consisted of molecular formula calculation, where C, H, N, O, P, and S elements were considered with a tolerance of 5 ppm. SmartFormula 3D

calculation was also applied in this step for all features with available MS/MS spectra, which improved the quality of the calculated molecular formula. This is an intelligent interface for annotating all monoisotopic peaks in the MS/MS spectrum. Thus, for each possible explanation of the *m/z* of a feature's precursor and isotopic pattern, SmartFormula 3D determines which ion formulas best explain the monoisotopic peak and isotopic pattern of the MS/MS fragment spectrum and ranked them according to MS/MS fragment explained and intensity coverage. In the workflow's next step, the tool Compound Crawler searches for possible structures that fit the first ranked formula, sending queries for a given molecular formula to databases such as ChEBI, ChemSpider, and PubChem and returns results that can be used to annotate compounds. The MetFrag algorithm is then applied for selecting the correct structure, as multiple structure candidates were typically found in Compound Crawler for a given elemental composition. Based on the measured MS/MS fragment spectrum, MetFrag searches for ions matching with *in-silico* fragmentation of possible candidates provided by Compound Crawler and ranks them according to explained fragment peaks and intensity coverage (Ruttkies *et al.*, 2016b). Selection of best candidate for a given feature was refined by the MS/MS Library Search tool, which compared the

MS/MS registered spectrum of the features with those of known compounds contained in Spectral Libraries previously imported in MetaboScape such as Bruker MetaboBASE Plant Library and Vaniya/Fiehn Natural Products Library of the MassBank of North America (MoNA).

To improve metabolites annotation, SIRIUS 5.6.3, a freely available web service integrating high-resolution isotopic pattern analysis and fragmentation trees for structural elucidation, was also used (Dührkop et al., 2019). Finally, retention times coincidence, as well as MS and MS/MS spectral matching with pure chemical standards, where available, were also examined for final structure confirmation and higher annotation level (A). All the pure standards used for maximum level annotation (A) were purchased from Sigma-Aldrich/Merck-Chile (Phyproof® Reference Substance, PhytoLab GmbH & Co., Germany).

4.2.3. Results

4.2.3.1 Differential constitutive metabolome between hybrids and parent species

The LC-MS raw data obtained from the analysis of leaves sample extracts collected before herbivory from seven genotypes of *E. nitens × globulus*

(*En×Egg*), nine of *E. globulus* (*Eg*) genotypes, and one of *E. nitens* (*En*) were processed in MetaboScape software to generate bucket tables as the main matrixes for statistical treatment. Such tables consisted of a total of 10314 and 4126 features (*m/z* – Rt pairs) with their respective intensities per sample detected in –ESI and +ESI acquisition modes, respectively.

Inherent clustering patterns in the dataset were examined using the unsupervised multivariate Principal Component Analysis (PCA) (Fig. 4.2.1a, b and Fig. S3a, b). The scores plot of this model showed the distribution of leaves samples between the first two Principal Components (PCs), where clear separation of species-specific clusters was observed along PC1, with 31.4% of the total explained variance of the data in –ESI (Fig. 4.2.1a), and 29.1% in +ESI (Fig. S3a). Such separation was even more evident when a third PC was added to the plot (Fig. 4.2.1b and Fig. S3b), suggesting a sharply defined leaf's metabolome differentiation between hybrid genotypes and parent species.

For distinguishing the differential metabolome composition in the leaves of *En×Egg* genotypes concerning parent species, supervised OPLS-DA models were applied to the dataset. We used it first to compare the metabolome of hybrids with that of the susceptible parent, *E globulus*. The

scores plot showed a perfect separation between hybrids (samples labeled with the *En×Egg* class) and the parent (samples labeled with the *Eg* class) along the predictive component (T score [1]), indicating that a 31.9% of data variance directly correlates to the class differentiation in –ESI data, and a 26.7% in the +ESI data (Fig. 4.2.1c and Fig. S3c). Significant features for class distinction were visualized in the S-plot (Fig. 4.2.1d and Fig. S3d), where data points represent features, with those displayed toward the end of both sides of the "S" contributing most to the class distinction. In this way, features on the right end correlate with the *En×Egg* class, and the metabolites they represent were constitutively accumulated in the leaves of hybrid genotypes while absent or at significantly lower levels in *Eg* parent genotypes. Significant features selected according to their high contribution to the predictive component (covariance >40) and high reliability in predicting *En×Egg* class (correlation >0.5) were identified to be two stilbenes (**1** and **6**), a hydrolysable tannin (**6′**), and Shikimate (**7′**) (Fig. 4.2.1d, Fig. S3d and Table 2). In contrast, features at the left end of the "S" represent metabolites accumulated in the leaves of *Eg* parent genotypes while absent or at significantly lower levels in hybrids. They were also selected according to high contribution to the predictive component (covariance >|40|) but with

the lowest reliability in predicting *En×Egg* class (correlation < –0.5). These features were identified as being two flavonol glucuronides (**5′** and **3″**), two chromone-*C*-glycoside monoterpene esters (**1″** and **2″**), a di-monoterpene glucoside ester (**4″**), and glucose (Fig. 4.2.1d, Fig. S3d and Table 2). Validation of OPLS-DA models by random permutation of class labels with internal leave-*n*-out cross-validation indicated a perfect statistical quality assessment. It was judged by the consistency between predicted and original data (Q^2 > 0.98), the good degree of model fit to data (R^2Y > 0.99), and the complete separation between original model statistics (black arrows) and statistic distributions for all permutations (Fig. S4a, b).

The scores plot of the OPLS-DA models used to compare the leaves metabolome of hybrid genotypes with that of the resistant parent, *E. nitens*, also showed a complete separation between classes along the predictive component (Fig. 4.2.1e and Fig. S3e). A 20.3% and 18.3% of the total data variance were correlated to the class discrimination in –ESI and +ESI data, respectively. Significant features differentially accumulated in the leaves of *En×Egg* genotypes (right end of the "S") were selected in this case by covariance and reliability higher than 30 and 0.5, respectively. They were identified to be three monoterpene gallate glucoside esters (**1′**, **3′**, and **4′**), a

flavonol rutinoside (**2′**), and a flavonol glucuronide (**5′**) (Fig. 4.2.1f, Fig. S3f, and Table 2). In contrast, metabolites differentially accumulated in the leaves of *En* (left end of the "S", covariance $> |-40|$, and reliability < -0.5 for predicting *En×Egg* class) were three stilbenes (**1**, **5**, and **6**), a hydroxycinnamic alcohol glycoside (**2**), a hydroxycinnamate ester (**3**), and a flavonol glucoside (**4**) (Fig. 4.2.1f, Fig. S3f, and Table 2). These models successfully passed the validation assessment, with $Q^2 > 0.95$ and $R^2Y > 0.99$ (Fig. S4c, d).
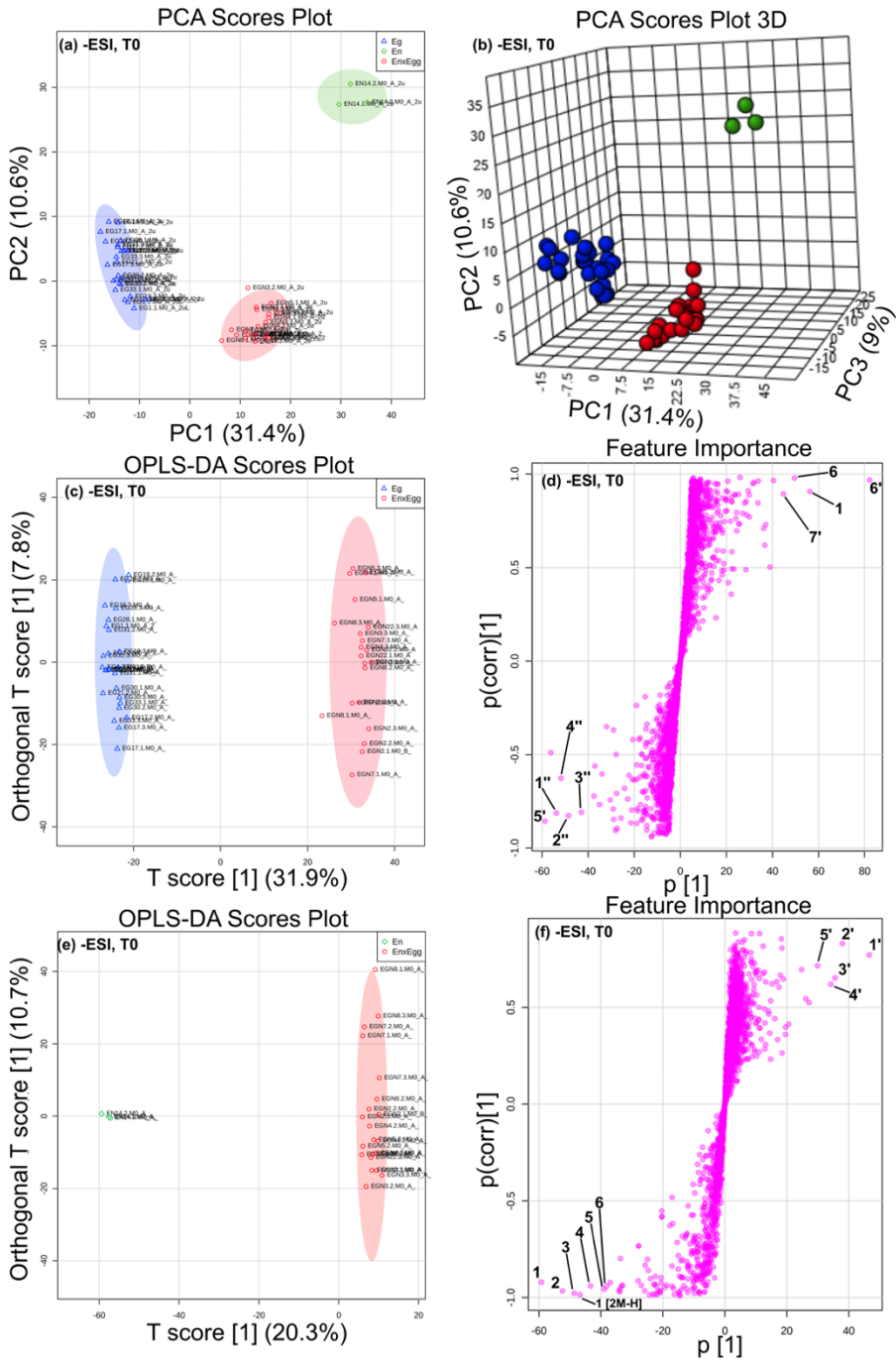
Figure 4.2.1. Results of the multivariate statistical models based on the LC-

MS dataset acquired in –ESI mode for distinguishing differential constitutive

metabolome in the leaves of *En×Egg* genotypes regarding the parent species *Eg* and *En*. (**a**) Scores plot of the PCA model showing species-specific clustering pattern between the first two principal components (PC1 and PC2), where blue triangles, green diamonds, and red circles represent *Eg*, *En*, and *En×Egg* samples with their 95% confidence intervals (shadowed regions), respectively. (**b**) Scores plot of the same PCA model incorporating the third PC for a 3D projection of sample distribution. (**c** and **e**) Scores plot of the OPLS-DA models showing separation of samples labeled as *En×Egg* (red circles) from that of *Eg* (blue triangles) and *En* (green diamonds), with their 95% confidence intervals (shadowed regions). In the OPLS-DA regression method, LC-MS data was used as the *X*, and the binary vector *Y* was formed with the value of 0 for *Eg* or *En* class and 1 for *En×Egg*. The *Y*-predictive component (T score [1]) plotted on the *x*-axis represents the variance in the dataset correlated to class separation, while the orthogonal component plotted on the *y*-axis refers to the uncorrelated variance for class distinction. (**d** and **f**) S-plot of the OPLS-DA models for visualizing the feature influence in the predictive component, combining covariance (p[1]) and correlation (p (corr)[1]) loading profiles. Covariance plotted on the *x*-axis indicates the contribution of features to the predictive component, while correlation on the

141

y-axis spans between ±1 as the reliability has a theoretical minimum of -1 and a maximum of +1 to predict class 1 (*En×Egg*). Features displayed on the right-hand side contribute to class separation by high correlation with label *En×Egg* ($Y = 1$), and those shown on the left-hand side contribute to separation by high correlation with label *Eg* or *En* ($Y = 0$). Thus, significant features were selected by combining the highest possible covariance with correlation >|0.5|. Their numbers were assigned according to Table 2.

4.2.3.2. Constitutive metabolome differentiation among hybrid genotypes

In the scores plots of the PCA models obtained from the dataset acquired in both –ESI and +ESI modes, genotype-specific clusters separated from each other were observed (Fig. 4.2.2a, b). Despite *En×Egg*5 and *En×Egg*6 clusters dispersion, groups for *En×Egg*1, *En×Egg*2, *En×Egg*4, and *En×Egg*7, were separated from the model center and the rest of the genotypes. These separations indicated a differential leaf metabolome composition of hybrids at T0. In Fig. 4.2.3, the quantitative data for the metabolites discriminating hybrids from *E. globulus* (**1**, **6**, **6′**, and **7′**) are shown in a comparative way to distinguish statistically significant differences among genotypes. The

142

stilbene glycoside *trans*-Piceid (**1**) accumulates at significantly higher levels in the leaves of genotypes *En×Egg*2 and *En×Egg*7, while *En×Egg*4 and *En×Egg*6 presented the lowest levels. For the *cis* isomer of **1** (compound **6**), there were no significant differences among genotypes except for *En×Egg*4 and *En×Egg*6, which had the lowest levels again. At the same time, β-Glucogallin (**6′**), a galloyl donor in the biosynthesis of gallotannins such as **17′**, **21′**, and **23′** (Table 2), accumulated at significantly higher rates in the leaves of *En×Egg*7. However, as discussed below, it does not mean that such a high constitutive level of compound **6′** in *En×Egg*7 contributes to the Galloyl unit transfer to glucose in forming of gallotannins. On the other hand, metabolites differentiating hybrids from *E. nitens* (**1′ - 5′**) also showed variations among genotypes. Worth to note the monoterpene gallate-glycosides Cyperllocarpin A (**1′**) and Eucaglobulin (**3′** and **4′**) were present at significantly lower levels in *En×Egg*4. In comparison, the accumulation of the glucuronic acid derivative of Kaempferol (**5′**) was substantially lower in the leaves of *En×Egg*2 and *En×Egg*7, while *En×Egg*4 presented one of the higher records.
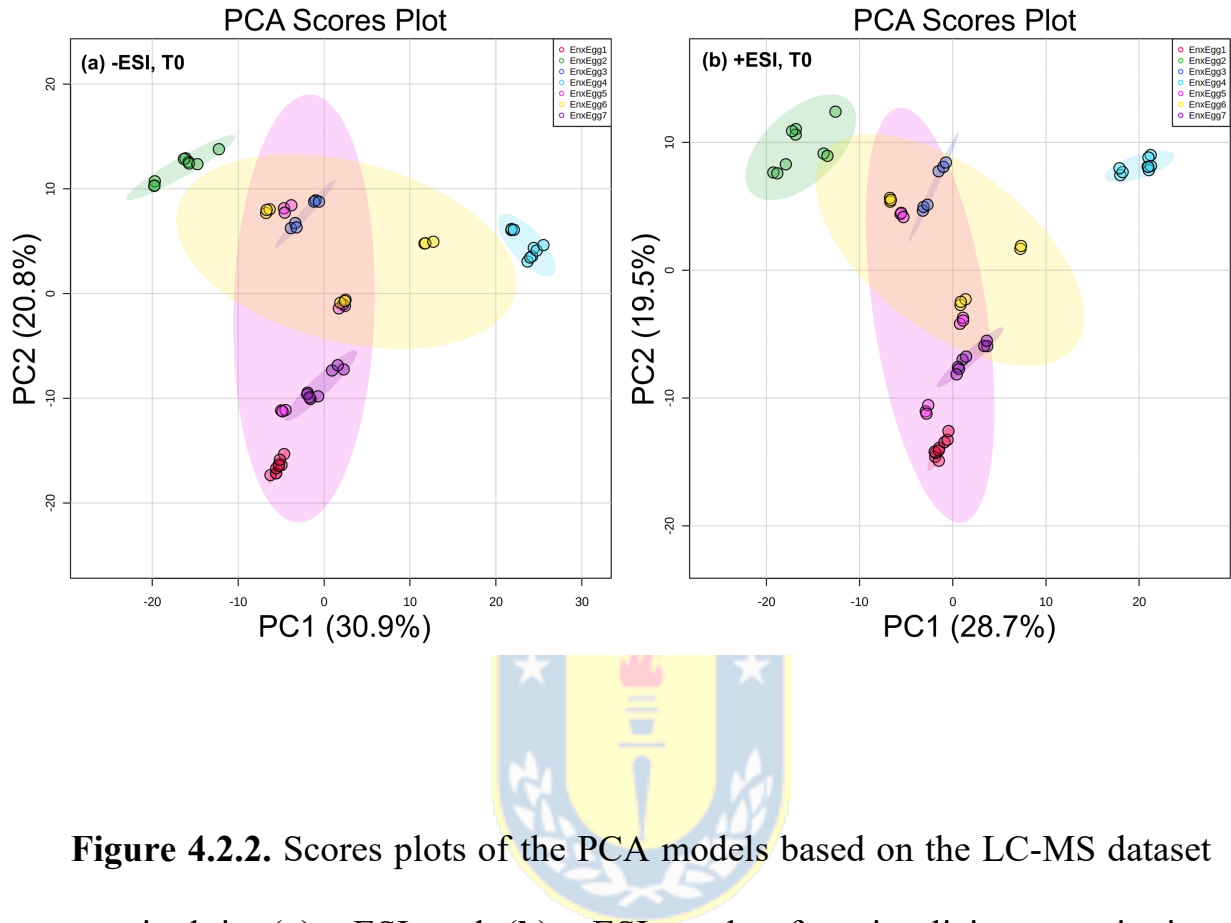
Figure 4.2.2. Scores plots of the PCA models based on the LC-MS dataset acquired in (**a**) –ESI and (**b**) +ESI modes for visualizing constitutive differences in the leaf metabolome among *En×Egg* genotypes at T0. Samples from each genotype are represented as circles with unique colors and shadowed regions for the 95% confidence intervals.
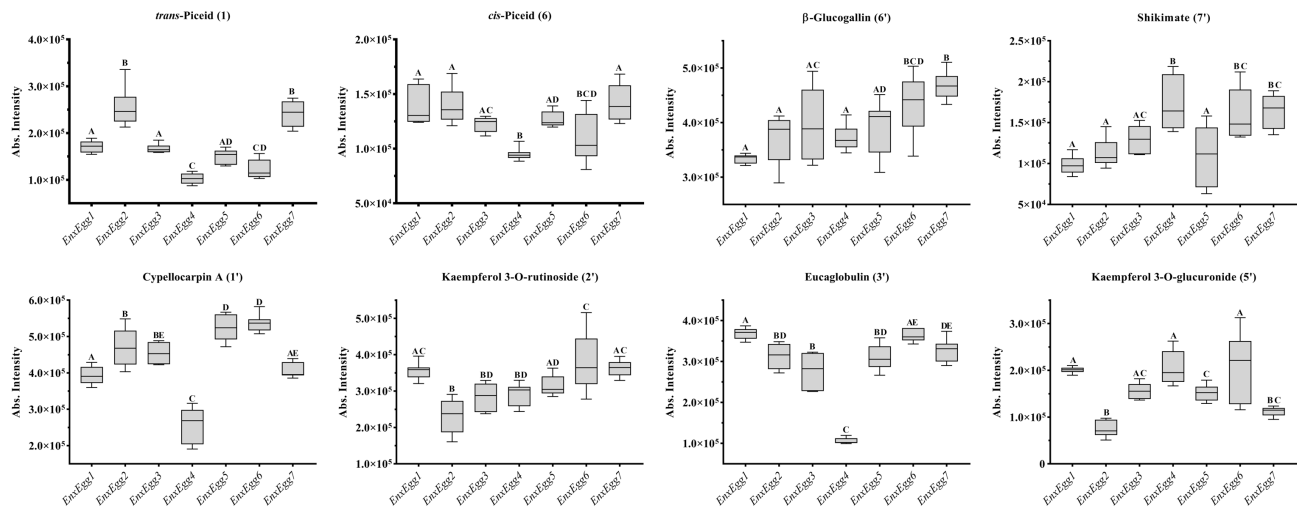
Figure 4.2.3. Constitutive differential levels of metabolites distinguishing hybrids from parents among *En×Egg* genotypes. Quantitative data are presented as box-and-whisker diagrams, showing the median of values distribution (horizontal line in the box), the 25% (lower horizontal line of the box) and 75% (upper horizontal line of the box) quartiles, and grey whiskers indicating the extremes lower and upper values. Metabolites **1**, **6**, **6′**, and **7′** discriminate hybrid genotypes from the susceptible parent (*Eg*), while **1′**-**3′**, and **5′** from the resistant (*En*) (Fig. 4.2.1d, f). Individual metabolite data were first tested for normal Gaussian distribution and then subjected to an ordinary one-way ANOVA to compare the mean level in each genotype with the mean

145

level of every other genotype. Tukey's test was used for multiple comparisons of the mean levels of each metabolite among the seven genotypes, where statistical significance was set at $p < 0.05$. The same letter over the boxes of a graphic indicates a no-significant difference. The y-axis represents the absolute intensity values detected in the mass spectrometer for monoisotopic ion peaks.

4.2.3.3. Systemic induced response in hybrid genotypes upon *G. platensis* herbivory

Comparison of leaves' metabolome before and after *G. platensis* herbivory per each *En×Egg* hybrid revealed specific inducible defenses and their differences among genotypes. As only healthy leaves (without signs of weevil feeding) were used in this study, the results presented below are considered the systemic response of trees to herbivory. We first applied PCA models to the dataset as an initial exploratory approach to visualize the magnitude of metabolome changes in hybrids' leaves due to herbivory. The PCA scores plots for the distribution of leaves samples between the first two principal components (PC1 and PC2) are presented in Fig. 4.2.4. Samples collected before herbivory (T0) are represented by blue circles, while those

harvested just a month later (T1) during the weevil attack are red triangles. The more separated the clusters are along PC1, the most extensive metabolome differentiation in the leaves of a genotype before and after herbivory. Accordingly, plots are presented in descending order of clusters separation magnitude, given by the complete separation of their 95% confidence regions (colored shadows) and the explained variance by PC1. Thus, the genotypes that most dramatically changed their leaves' metabolome composition due to herbivory were *En×Egg*1, *En×Egg*7, and *En×Egg*4 (Fig. 4.2.4a-c). In contrast, genotypes *En×Egg*2, *En×Egg*3, *En×Egg*6, and *En×Egg*5 overlaid their shaded regions and sample distributions (Fig. 4.2.4e-g), suggesting that their leaves' metabolome changes were moderate.
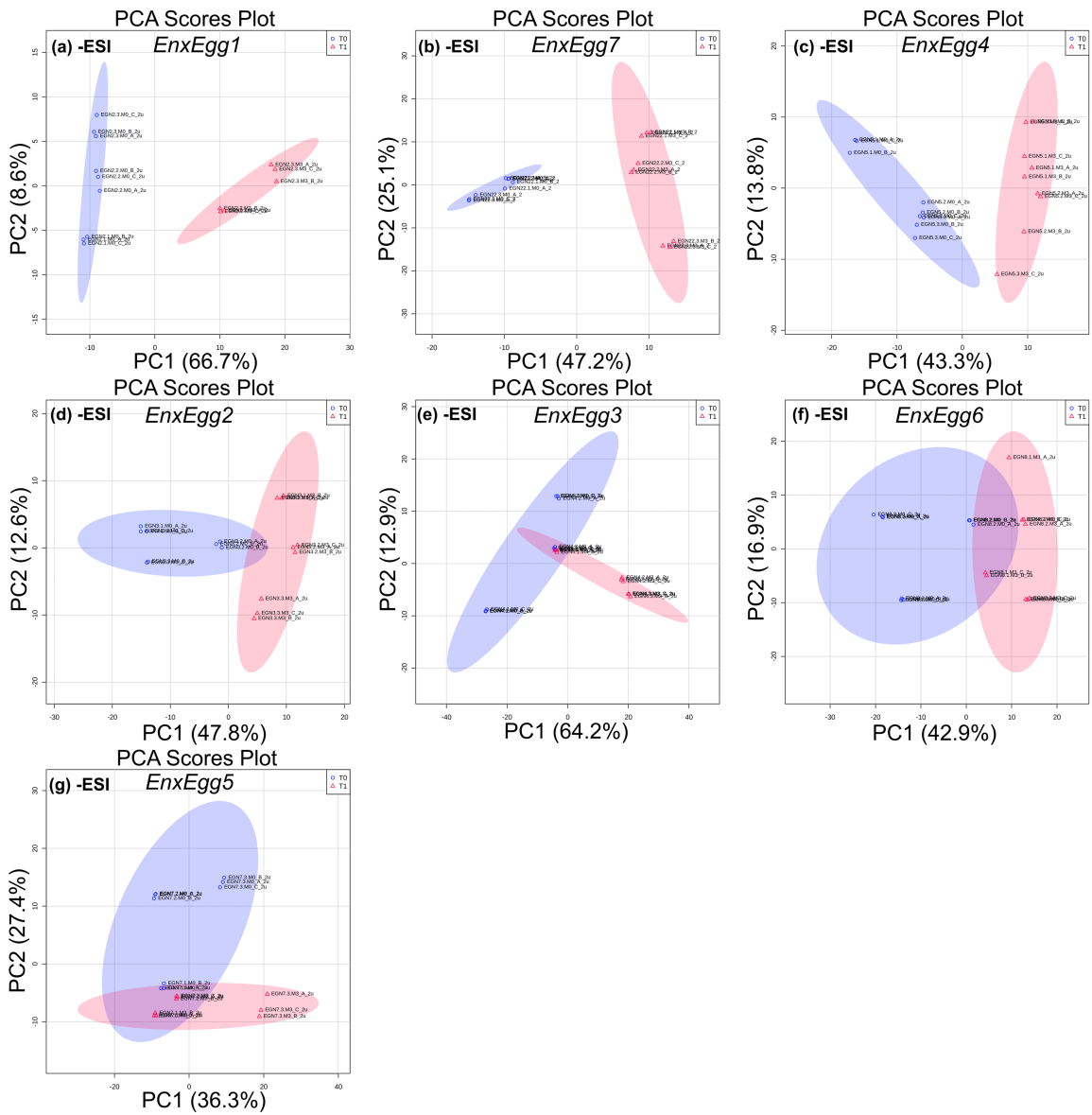
Figure 4.2.4. Overview of the metabolome changes caused by *G. platensis* herbivory in each hybrid genotype. The scores plot of the PCA models per *En×Egg* genotype between the first two principal components (PC1 and PC2) show clustering patterns and distribution of samples collected before

(T0, blue circles) and after (T1, red triangles) *G. platensis* attack, with their 95% confidence intervals (shadowed regions). Plots are presented in descending order of groups separation degree along PC1 from (**a**) to (**g**).

To reveal the specific composition changes in leaves' metabolome induced in individual hybrid genotypes by the weevil defoliation, we applied OPLS-DA models to the dataset. Detailed individual results of these models are shown in Fig. 4.2.5a-n, using the same order as that of Fig. 4.2.4. The scores plots presented first per genotype showed perfect separations along the predictive component (T score [1]) between T0 and T1 (Fig. 4.2.5a, c, e, g, i, k, m) in all cases. For genotypes *En×Egg*1 and *En×Egg*7, the percentage of data variance directly correlated to the class distinction was the highest, with 48.1% and 36.1%, respectively (Fig. 4.2.5a, c). In contrast, for genotypes *En×Egg*5 and *En×Egg*2, that variance was the lowest, with 21.4% and 32%, respectively (Fig. 4.2.5g, m). Although data variance unrelated to class differentiation (orthogonal component) was found between 11% and 15%, the genotypes *En×Egg*3 and *En×Egg*6 presented relatively high values with 32.1% and 17.8%, respectively (Fig. 4.2.5i, k).
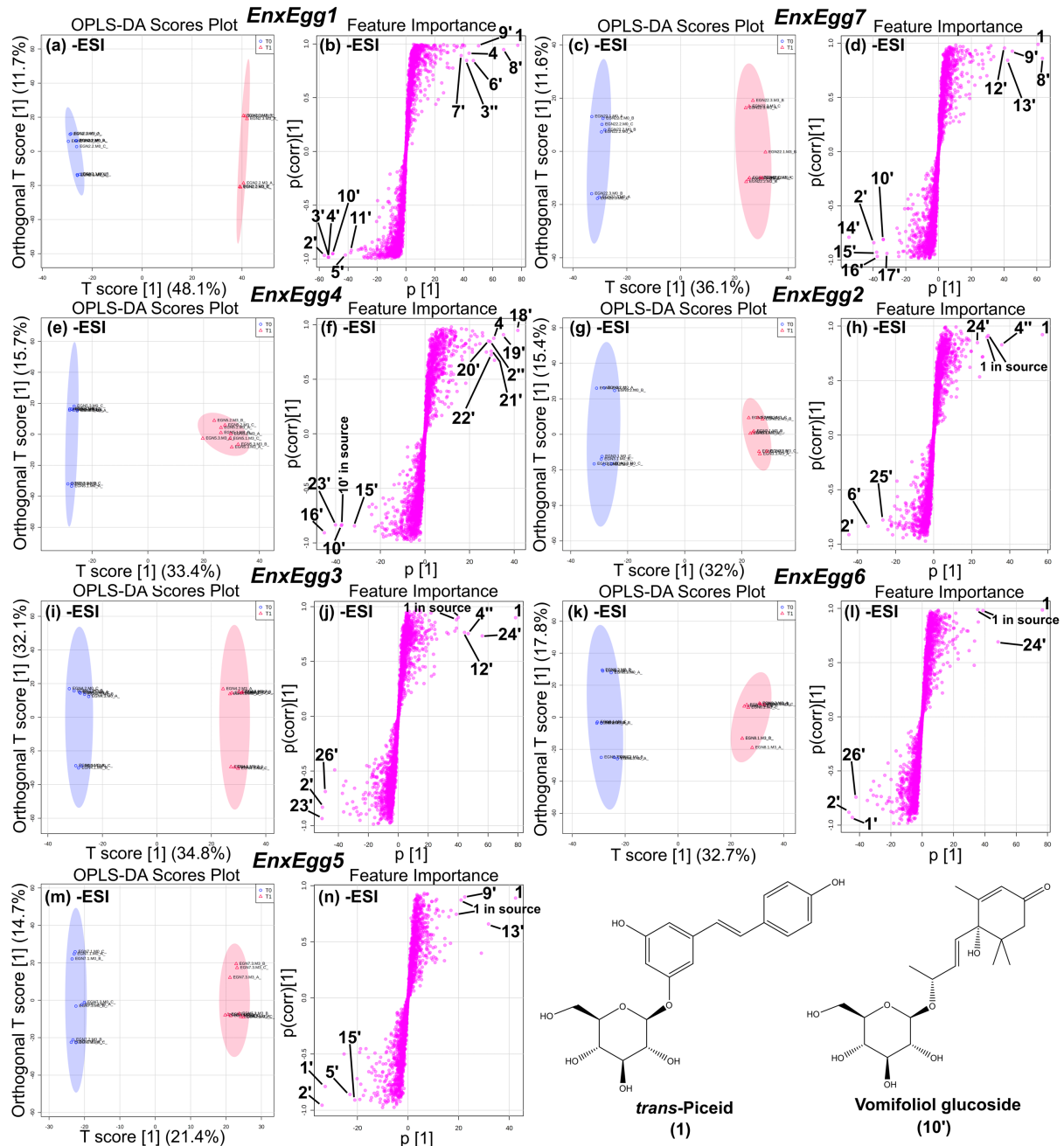
Figure 4.2.5. Results of the OPLS-DA statistical models applied to the LC-MS dataset acquired in –ESI mode for the leaves' metabolome comparison

in each *En×Egg* genotype before and after herbivory caused by *G. platensis*. Per each genotype, the scores plot is presented on the left, showing the separation of samples labeled as T0 (blue circles) from that of T1 (red triangle) with their 95% confidence intervals (shadowed colored regions). The regression method of this model used LC-MS data as the X and the binary vector Y formed by the values of 0 and 1 assigned to the labels T0 and T1, respectively. The Y-predictive component (T score [1]) plotted on the x-axis represents the variance in the dataset correlated to class separation, while the orthogonal component plotted on the y-axis refers to the uncorrelated variance for class distinction. The S-plot of each genotype is presented on the right. It allows visualizing the features' influence in the predictive component, combining covariance (p[1]) and correlation (p(corr)[1]) loading profiles. Covariance plotted on the x-axis indicates the contribution of features to the predictive component, while correlation on the y-axis spans between ±1 as the reliability has a theoretical minimum of −1 and a maximum of +1 to predict class 1 (T1). Thus, features displayed on the right-hand side contribute to class separation by high correlation with label T1 ($Y = 1$), and those shown on the left-hand side contribute to separation by high correlation with label T0 ($Y = 0$). Selection of significant features combined the highest

possible covariance with correlation >|0.5|. Features' numbers were assigned according to Table 2. Genotypes' models appear in the same order as established in Fig. 4.2.4. Given the relevance for discussion, the chemical structures of metabolites *trans*-Piceid (**1**) and Vomifoliol glucoside (**10′**) are shown down-right.

Before identifying metabolites that significantly changed their levels due to defoliation, random permutation tests with internal cross-validation were applied to each OPLS-DA model to assess the statistical quality (Fig. S5). Regardless of the excellent validation for the seven models that confirm a significant difference between the leaves' metabolome before and after herbivory in every genotype, the consistency between predicted and original data for *En×Egg*2, given by the Q^2 value, was the worst with 0.944. Nevertheless, this is still a reasonable degree of validation. Thus, all the models were successfully validated, which warrants the reliability for identifying significant metabolites using the S-plots.

Herbivory induced significant alterations in the concentration levels of certain metabolites in the hybrids' leaves as the response. Some of them overexpressed, while others downregulated. Together are responsible for

152

class separations shown in the OPLS-DA scores plots. The S-plot of OPLS-DA models allowed for identifying the features representing the significantly upregulated metabolites through data points with high contribution to the predictive component (covariance >40, >30, or >20 depending on genotype) and high reliability in predicting the T1 class (correlation >0.5). Each case displays these features toward the right end of the S (Fig. 4.2.5b, d, f, h, j, l, n). At the same time, metabolites significantly downregulated are also represented by the features with high contribution to the predictive component (covariance >|40|, >|30|, or >|20|) but with the lowest reliability in predicting the T1 class (correlation < –0.5). In this case, these features are shown toward the left end of the S (Fig. 4.2.5b, d, f, h, j, l, n).

For the genotype *En×Egg*1, the metabolites significantly upregulated were the following ones: the stilbene glycoside *trans*-Piceid (**1**), a disaccharide (**8′**), the flavonol glycoside monoterpene Cypellogin A (**9′**), the hydrolysable tannin β-Glucogallin (**6′**), two flavonol glycosides, Isoquercitrin (**4**) and Quercetin 3-O-glucuronide (**3″**), and Shikimate (**7′**) (Fig. 4.2.5b). Genotype *En×Egg*7 also overexpressed *trans*-Piceid (**1**), the disaccharide **8′**, and Cypellogin A (**9′**) together with its isomer **12′** (Fig. 4.2.5d). Genotype *En×Egg*4 did not overexpress *trans*-Piceid (**1**) as the other genotypes (Fig.

4.2.5f). However, as in the previous genotypes, the flavonol glycoside Isoquercitrin (**4**) and the analog Astragalin (**19′**), together with two similar hydrolysable tannins (**21′** and **22′**), were found to upregulate. In addition, two similar chromone-C-glycosides (**18′** and **2″**) were also overexpressed (Fig. 4.2.5f). In the leaves of *En×Egg*2, *trans*-Piceid (**1**) was upregulated together with the monoterpene glycoside Cuniloside B (**4″**) and the cinnamate ester *p*-Coumaroylquinic acid (**24′**) (Fig. 4.2.5h). Identical compounds upregulate in *En×Egg*3, also including the isomer of Cypellogin A, **12′** (Fig. 4.2.5j). Genotype *En×Egg*6 upregulates *trans*-Piceid (**1**) and *p*-Coumaroylquinic acid (**24′**) (Fig. 4.2.5h), while *En×Egg*5 does it with **1** and **9′** (Fig. 4.2.5n). Quantitative level changes of these metabolites upon herbivory are shown in Fig. 4.2.6 across the seven genotypes for a better understanding of hybrids' differential chemical response. Apart from statistical significance, the fold change values (FC), defined as the ratio of the mean intensities of metabolites in trees under herbivory (i_{T1}) between that in the same trees before herbivory (i_{T0}), are also shown in each case ($FC = i_{T1}/i_{T0}$). Complete spectral data used for metabolite annotation is reported in Table 1.

On the other hand, in the leaves of *En×Egg*1, two flavonol glycosides, Kaempferol 3-O-rutinoside (**2′**) and Kaempferol 3-O-glucuronide (**5′**), three

monoterpene gallate-glycosides, Eucaglobulin I (**3′**) and II (**4′**) and dihydro-Eucaglobulin (**11′**), and the cyclohexanone monoterpene glycoside Roseoside (**10′**) were found to be significantly downregulated due to the herbivory of *G. platensis* (Fig. 4.2.5b). The last one, also known as Vomifoliol-glucoside, was previously reported by our research group to presumably be a phytohormone precursor able to release the active aglycone Vomifoliol upon herbivory (Campos et al., 2022). Such function of Roseoside (**10′**) is discussed below in section 4.2 based on the new evidence. The genotype *En×Egg*7 also downregulates metabolites **2′** and **10′**, together with Quinic acid (**14′**), Isocitric acid (**15′**), a chromone digalloyl-C-glycoside (**16′**), and the hydrolysable tannin 1,2,6-Trigalloyl-glucose (**17′**) (Fig. 4.2.5d). In common with previous genotypes, *En×Egg*4 also downregulates metabolites **10′**, **15′**, and **16′**. In addition, the hydrolysable tannin Tetragalloyl-glucose (**23′**) also significantly dropped (Fig. 4.2.5f). In the case of *En×Egg*2, the levels of the flavonol glycosides **2′** and Rutin (**25′**), together with that of β-Glucogallin (**6′**), significantly decreased (Fig. 4.2.5h and Fig. 4.2.6). Genotype *En×Egg*3 also downregulates **2′** and **23′**, as well as a chromone galloyl-C-glycoside (**26′**) (Fig. 4.2.5j). For *En×Egg*6, the level of **2′** and **26′** dropped together with that of the monoterpene galloyl-glucoside

Cypellocarpin A (**1′**) (Fig. 4.2.5l). Finally, the genotype *En×Egg*5, downregulates the metabolites **1′**, **2′**, **5′**, and **15′** (Fig. 4.2.5n). The quantitative changes of all above-mentioned metabolites in the leaves of each of the seven hybrid genotypes are shown in Fig. 4.2.7.
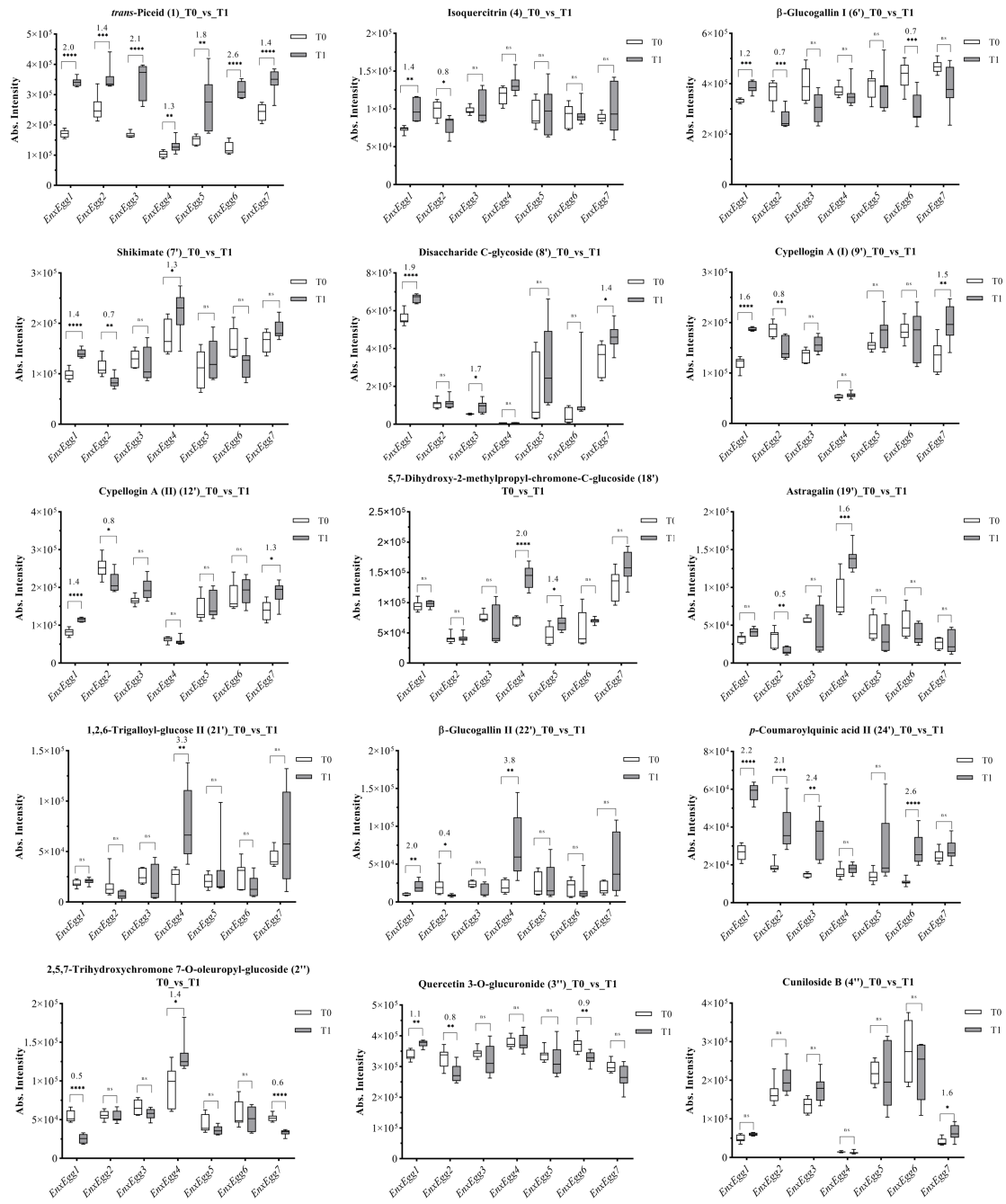
Figure 4.2.6. Systemic quantitative level changes of the overexpressed metabolites in the leaves of each *En×Egg* genotype as the response to the *G.*

platensis herbivory. Presented metabolites (**1**, **4**, **6′-9′**, **12′**, **18′**, **19′**, **21′**, **22′**, **24′**, **2″-4″**) were significantly upregulated in at least one hybrid genotype during herbivory (Fig. 4.2.5). Quantitative data is presented as box-and-whisker plots, showing the median of values distribution (horizontal line in the box), the 25% (lower horizontal line of the box) and 75% (upper horizontal line of the box) quartiles, and whiskers indicating the extremes lower and upper values. Individual metabolite data were subjected to multiple t-tests for comparing the mean levels in each genotype before (T0) and after (T1) herbivory, where statistical significance was defined at $p < 0.05$ (adjusted p value). The brackets between boxes on a genotype indicate the significance of the quantitative level changes as significant (*, $0.01 > p < 0.05$), very significant (**, $0.001 > p < 0.01$), extremely significant (***, $0.0001 > p < 0.001$), extremely significant (****, $p < 0.0001$), and not significant (ns, $p \geq 0.05$). The fold-change, defined as the ratio of the mean intensities in trees under herbivory between that in the same trees before herbivory ($FC = i_{T1}/i_{T0}$), is also shown above the brackets in those cases where the level changes were statistically significant. The *y*-axis represents

the absolute intensity values detected in the mass spectrometer for monoisotopic ion peaks.

Figure 4.2.7. Systemic quantitative level changes of the downregulated metabolites in the leaves of each *En×Egg* genotype as the response to the *G. platensis* herbivory. Presented metabolites (**1′-5′, 10′, 11′, 14′-17′, 23′, 25′, 26′**) were significantly lowered by at least one hybrid genotype during herbivory (Fig. 4.2.5). Quantitative data is presented as box-and-whisker plots, showing the median of values distribution (horizontal line in the box), the 25% (lower horizontal line of the box) and 75% (upper horizontal line of the box) quartiles, and whiskers indicating the extremes lower and upper values. Individual metabolite data were subjected to multiple t-tests for comparing the mean levels in each genotype before (T0) and after (T1) herbivory, where statistical significance was defined at $p < 0.05$ (adjusted p value). The brackets between boxes on a genotype indicate the significance of the quantitative level changes as significant (*, $0.01 > p < 0.05$), very significant (**, $0.001 > p < 0.01$), extremely significant (***, $0.0001 > p < 0.001$), extremely significant (****, $p < 0.0001$), and not significant (ns, $p \geq 0.05$). The fold-change, defined as the ratio of the mean intensities in trees under herbivory between that in the same trees before herbivory ($FC = i_{T1}/i_{T0}$), is also shown above the brackets in those cases where the level changes were statistically significant. The *y*-axis represents the absolute

160

intensity values detected in the mass spectrometer for monoisotopic ion peaks.

4.2.4. Discussion

4.2.4.1. Constitutive defense transferred to hybrids by parents

Before considering the *E. nitens × globulus* inducible defenses upon herbivory, we'll discuss the constitutive defensive traits transferred by parents based on leaves' non-volatile specialized metabolites that may provide resistance against *G. platensis*. The molecules of constitutive chemical defense are synthesized and stored in plant tissues always before any herbivorous attack. These are the first defensive barriers that deter feeding or toxins affecting insect growth and fitness, usually known as phytoanticipins. As expected, the results shown in Fig. 4.2.1 evidenced that hybrids inherited constitutive metabolome traits from both parents. When the metabolome of *En×Egg* was compared with that of *E. globulus*, the stilbene glycosides *trans*- and *cis*-Piceid (**1** and **6**) and the hydrolysable tannin β-Glucogallin (**6′**) arose as specific metabolites for the former (Fig. 4.2.1c, d). Coincidently, these substances were previously found among *E. nitens* significant leaves' metabolites that best explain its metabolome

161

differentiation from *E. globulus* (Campos et al., 2022). That similitude represents a critical finding suggesting that, unlike the susceptible parent *E. globulus*, hybrids posse the suitable enzyme for the biosynthesis of stilbenes inherited from *E. nitens*. The stilbene synthase (STS, K13232), a type-III polyketide synthases superfamily member, cyclizes the linear tetraketide intermediate of the reaction between three molecules of malonyl-CoA with *p*-coumaroyl-CoA by an aldol condensation with decarboxylation to yield Resveratrol as the first stilbene (Austin and Noel, 2003; Campos et al., 2022). Then, glucosyltransferases transfer glucose to Resveratrol, giving rise to the constitutive accumulation of Piceid in leaves.

We previously confirmed that this metabolic trait inhibits significantly the *G. plantensis* feeding, being one of the most probable cause of resistance in *E. nitens* (Campos et al., 2022). In other words, the accumulation of *trans*- and *cis*-Piceid (**1** and **6**) in the leaves of hybrids *En×Egg* before the weevil attack could provide resistance, avoiding the herbivory to some extent in the first instance. However, constitutive levels of these stilbenes in the leaves of *En×Egg* are still significantly lower than in *E. nitens* (Fig. 4.2.8a, b). Consequently, hybrids should be more resistant than *E. globulus* but less than *E. nitens*. Indeed, according to the field observation, the damage produced by

G. platensis in four of the seven *E. globulus* genotypes at T1 was from intense to severe, which means that the weevil reduced the crown foliage of those trees in 20-70% or >70%, respectively (Table S1). Oppositely, the *E. nitens* genotype suffered just minimum damage, with 5% of its crown defoliated (Table S1). In between, five of the seven hybrid genotypes were moderately defoliated by the weevil, losing 10-20% of their crown foliage (Table S1).

Similarly, the hybrids *En×Egg* may conserve some *E. globulus* metabolic characteristics, which may be detrimental to resistant aptitude. As shown in results obtained from the constitutive metabolome comparison between hybrids and *E. nitens* (Fig. 4.2.1e,f), metabolites differentially accumulated in the former are similar or the same as those previously reported for *E. globulus* (Campos et al., 2022). Such are the cases of monoterpene gallate-glycoside **1′**, **3′**, and **4′**, and the flavonol glycoside Kaempferol 3-O-glucuronide (**5′**). Regardless the constitutive defensive role these substances may have to protect the plant against other organisms, it seems clear that the weevil *G. platensis* has well adapted to detoxify them. It is known that *E. globulus* is the natural host of *G. platensis*. They both are native to Tasmania (Mapondera et al., 2012), where they have had to coevolve in developing counteradaptations to minimize irreversible damage due to their mutual

163

interaction (Campos et al., 2022). We believe these metabolites could not inhibit the weevil feeding but improve the leaves' palatability reducing the resistance.
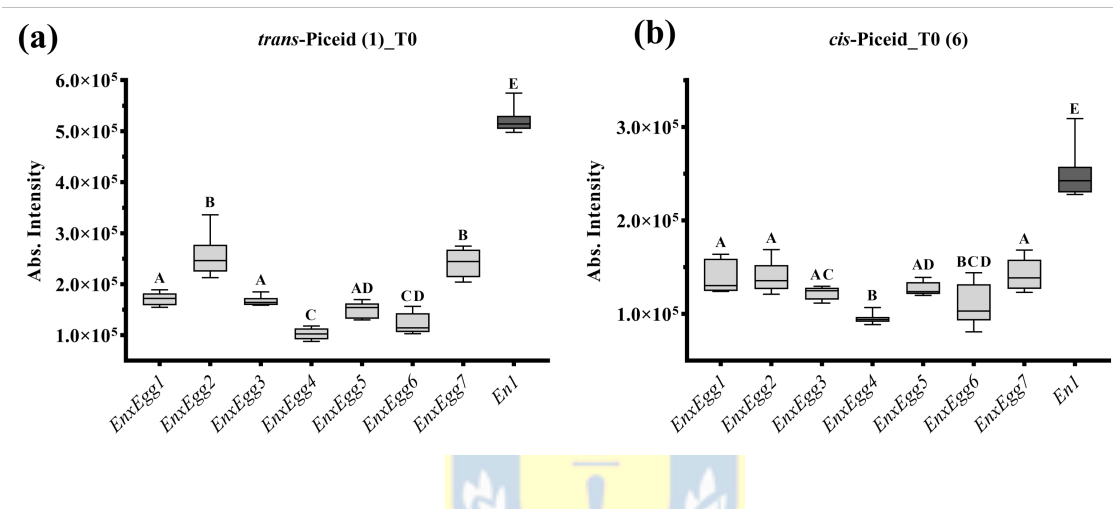
Figure 4.2.8. Comparative levels for the stilbenes *trans*- and *cis*-Piceid (**1** and **6**) in the leaves of *En×Egg* genotypes with that in *E. nitens* at T0 (constitutive). Quantitative data are presented as box-and-whisker diagrams, showing the median of values distribution (horizontal line in the box), the 25% (lower horizontal line of the box) and 75% (upper horizontal line of the box) quartiles, and grey whiskers indicating the extremes lower and upper values. Individual metabolite data were first tested for normal Gaussian distribution and then subjected to an ordinary one-way ANOVA to compare the mean level in each genotype with the mean level of every other genotype

including *En*1. Tukey's test was used for multiple comparisons of the mean levels, where statistical significance was set at $p < 0.05$. The same letter over the boxes of a graphic indicates a no-significant difference.

4.2.4.2. Constitutive metabolome variation among hybrid genotypes may be an unprecise approach for resistance imputation

The remarkable variations in the constitutive leaf metabolome found among hybrid genotypes (Fig. 4.2.2 and Fig. 4.2.3) may be a first-instance approach for resistance imputation to the *G. platensis* herbivory. Following a simplistic interpretation and knowing that *trans*-Piceid (**1**) inhibits weevil feeding (Campos et al., 2022), the genotypes *En×Egg*2 and *En×Egg*7 may be attributed with the best resistance capacity due to their higher contents of this specialized metabolite compared to the rest of genotypes (Fig. 4.2.3). For the same reason, genotypes *En×Egg*4 and *En×Egg*6 could be the most susceptible (Fig. 4.2.3). Unfortunately, the resistance imputation is more complex than it seems. According to the field observation, genotype *En×Egg*2 suffered a severe attack, while *En×Egg*7 behaved as expected. Similarly, genotypes *En×Egg*4 and *En×Egg*6 were only moderately defoliated (Table S1). Therefore, the constitutive level of stilbenes in the

leaves of an *E. nitens × globulus* hybrid is not enough to predict its capability for herbivory avoidance unless concentrations could reach a comparable value to that in *E. nitens* (Fig. 4.2.8). In addition, the systemic induced resistance to herbivory discussed below must be considered.

4.2.4.3. Induced defenses in hybrids may differentially modulate resistance to herbivory

Upon herbivory, plants quickly respond by the damage-associated molecular pattern (DAMP) recognition, inducing a plethora of chemical defenses (Schulze et al., 2019). Such response can be locally where the insect has fed, through metabolism reprogramming in the cells surrounding the damage site to up-regulate the synthesis of defense molecules. However, we here report the evidence of systemically induced defense upon herbivory by the up- or down-regulated metabolites occurring in tissues distant from the site of the attack that turn them into a more hostile environment for the weevil *G platensis*. We found two specialized metabolites that were considered essential in such interaction. They were the stilbene *trans*-Piceid (**1**) and the isoprenoid Roseoside (**10′**). Therefore, the following discussion is mainly focused on the implication of these two metabolites in plant resistance.

The biosynthesis of *trans*-Piceid (**1**) is drastically induced upon herbivory (T1), leading to a significant systemic increment of its level in the leaves of all *E. nitens* × *globulus* genotypes (Fig. 4.2.9a). All the hybrids now exhibit similar concentrations of this metabolite, being not significantly different among them except for *En*×*Egg*4, which remains low (Fig. S6). Regardless of such increment, none of the genotypes could reach a comparable level of **1** as that constitutively present in the leaves of *E. nitens* (Fig. 4.2.9a). Perhaps, it may explain the higher predisposition to herbivory shown by hybrids. Furthermore, inducing stilbene pathway biosynthesis seems to be a unique characteristic for *En*×*Egg* hybrids since any of the parents, neither *Eg* nor *En*, respond to the weevil herbivory by upregulating stilbenes. Despite *En* can immediately respond to minimum defoliation by reprograming its metabolism (Fig. S6), the stilbene levels remain invariable (Fig. 4.2.9a). On the other side, as was previously reported by our research group, *E. globulus* does not have the enzymatic ability to synthesize stilbenes (Campos et al., 2022). Consistently, *trans*-Piceid was almost undetectable, confusing with spectral noise, and with no level changes in any *Eg* genotypes during herbivory (Fig. 4.2.9b, d).

However, the upregulation of *trans*-Piceid (**1**) by hybrids appears not entirely coherent with the degree of defoliation that some of them suffered; for instance, *En×Egg*2 overexpressed this metabolite by 1.4-fold, the same as *En×Egg*7 (Fig. 4.2.9a). The former was severely attacked by the weevil, losing more than 70% of its crown foliage. In comparison, less than 20% was damaged in the last (Fig. 4.2.9a, Table S1). In the same way, *En×Egg*5 upregulated **1** by the rate of 1.8-fold. Still, anyway, it was intensively defoliated by the weevil (20-70% foliage lost) (Fig. 4.2.9a). Most notably, genotype *En×Egg*4, which only overexpressed **1** by 1.3-fold, was only moderately attacked (Fig. 4.2.9a). In Fig. 4.2.9c, the seven hybrid genotypes, as well as *En*1, were rearranged in descending order of fold-change expressed of **1**. Genotypes *En×Egg*6 > *En×Egg*3 > *En×Egg*1 upregulated this metabolite by the rate of 2-fold or higher. In this case, all of them were as resistant to defoliation as expected (Fig. 4.2.9a, Table S1). Nevertheless, it is worth noting that at T1 all the hybrid genotypes maintain a concentration of **1** in leaves which is not significantly different among them, except for *En×Egg*4. These inconsistencies suggest that resistance in hybrids could not only lay on stilbenes but most likely depend on other types of metabolites or their combination.
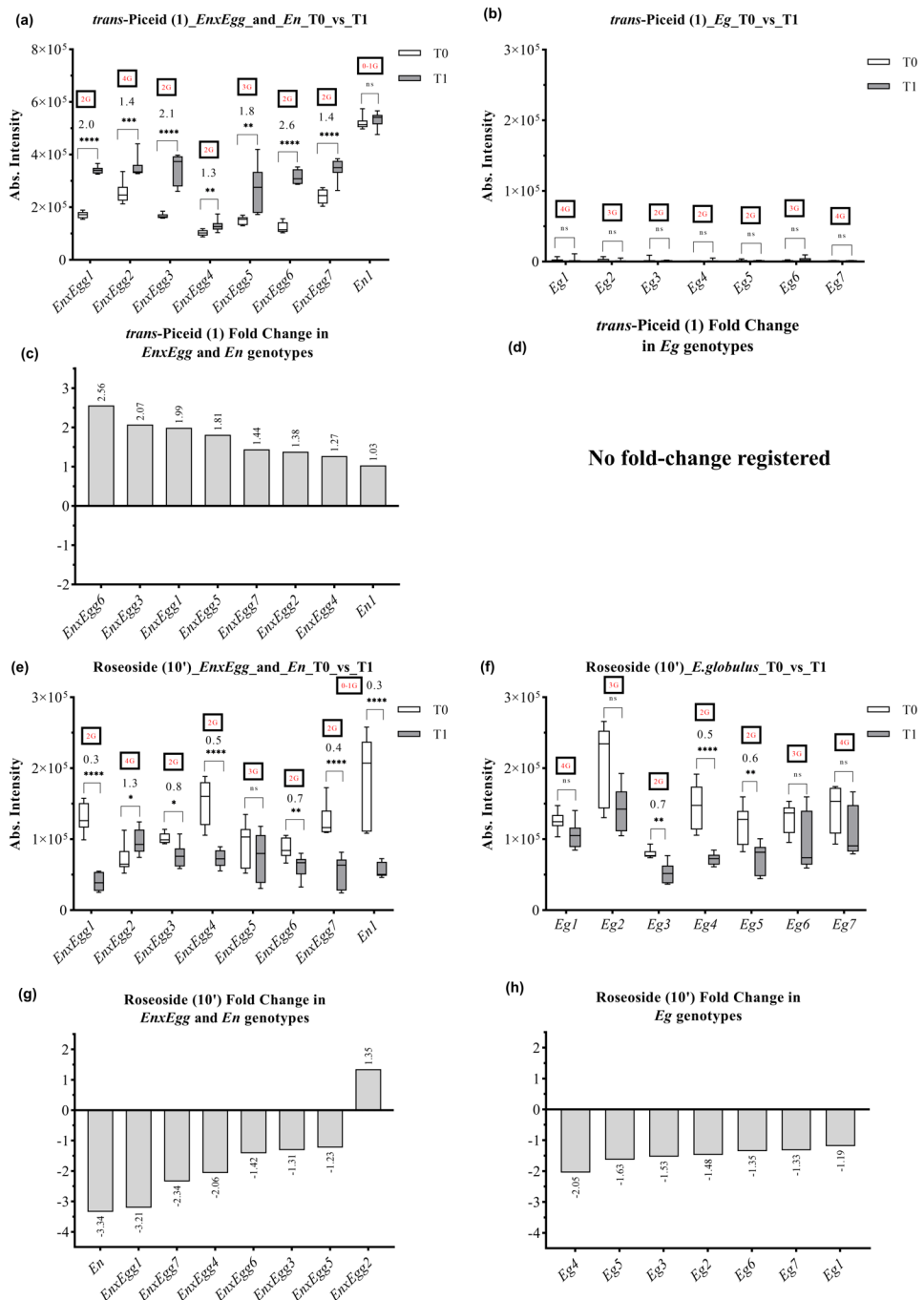
Figure 4.2.9. Comparative graphics for level changes of trans-Piceid (1) and Roseoside (10′) systemically induced in leaves by *G. platensis* herbivory

169

among En×Egg genotypes and with parent species, En1 (*E. nitens*), and Eg1-Eg7 (*E. globulus*). Quantitative data are presented as box-and-whisker plots, showing the median of values distribution (horizontal line in the box), the 25% (lower horizontal line of the box) and 75% (upper horizontal line of the box) quartiles, and whiskers indicating the extremes lower and upper values. Individual data were subjected to multiple t-tests for comparing the mean levels in each genotype before (T0) and after (T1) herbivory, where statistical significance was defined at $p < 0.05$ (adjusted p value). The brackets between boxes on a genotype indicate the significance of the quantitative level changes as significant (, $0.01 > p < 0.05$), very significant (, $0.001 > p < 0.01$), extremely significant (*, $0.0001 > p < 0.001$), extremely significant (*, $p < 0.0001$), and not significant (ns, $p \geq 0.05$). The fold-change, defined as the ratio of the mean intensities in trees under herbivory between that in the same trees before herbivory (FC=i_T1/i_T0), is shown above the brackets in the cases where the level changes were statistically significant. The severity of defoliation suffered per genotype according to Table S1 is also shown in red above brackets. The y-axis represents the absolute intensity values detected in the mass spectrometer for monoisotopic ion peaks.

A more coherent relationship existed between Roseoside (**10′**) level changes and herbivory severity. This compound is, in fact, the glucoside of Vomifoliol (PubChem CID: 5280462), a monoterpene derived from abscisic acid (ABA) metabolism with a similar chemical structure (Hasegawa et al., 1984). In most hybrid genotypes, the expression of Roseoside tended to significantly decrease when herbivory started, except for *En×Egg*2 and *En×Egg*5 (Fig. 4.2.9e). In the former, an overexpression of Roseoside was registered instead. At the same time, in the last, no significant level changes were experimented on before and during herbivory.

The same as ABA is inactivated in plants by glycosylation (Nambara and Marion-Poll, 2005), we believe that Roseoside is an inactive substance that, upon the stimulus of herbivory, a glycosidase hydrolyses the glycosidic bond releasing free Vomifoliol as the active molecule. Vomifoliol may also be transformed into Dehydrovomifoliol (Colom et al., 2007; Hasegawa et al., 1984), although none were detected because of their lipophilicity and volatility. Nevertheless, we can estimate the amount of liberated Vomifoliol by the magnitude of the Roseoside concentration decrease given by the calculated fold-change (Fig. 4.2.9g, h). We found an interesting correlation between Roseoside decreasing fold change, or what is presumably the same,

the amount of liberated Vomifoliol, and the severity of defoliation by *G. platensis*. The higher the absolute value of fold-change, the lesser the defoliation severity (Fig. 4.2.9e-h). For instance, in hybrids *En×Egg*1, *En×Egg*7, and *En×Egg*4, Roseoside decreased by 3.21, 2.34, and 2.06-fold upon herbivory, respectively. Accordingly, they suffered moderate defoliation, with only 10% to 20% of crown foliage lost (Table S1, Method S2). Herbivory seems to even turn into moderate with not so pronounced decrease of Roseoside, as in *En×Egg*6 (1.42-fold) and *En×Egg*3 (1.31-fold). In contrast, genotype *En×Egg*5 did not change the Roseoside level significantly during herbivory (Fig. 4.2.9e), consequently being intensively defoliated with the loss of 20% to 70% of its crown foliage. To finally confirm the relevance of Vomiliol in herbivory resistance, the severity of defoliation suffered by *En×Egg*2 with more than 70% of its crown foliage lost was crucial (Fig. 4.2.9e, Table S1). Coincidently, this genotype was the unique one that upregulated Roseoside significantly (by 1.35-fold) (Fig. 4.2.9e, g), which means that instead of releasing Vomifoliol, it is being inactivated by glycosylation. This response reinforces the hypothesis mentioned above that *trans*-Piceid (**1**) alone cannot deter the herbivory of *G. platensis* in hybrids since the genotype *En×Egg*2, as well as *En×Egg*7,

172

accumulate the highest constitutive contents of this metabolite in leaves (Fig. 4.2.8a).

In the case of the parent species *En*, the higher absolute fold-change value for Roseoside decreasing levels due to herbivory was registered, with 3.34-fold (Fig. 4.2.9e, g). This response, together with the highest constitutive content of *trans*-Piceid (**1**) among all under study *Eucalyptus* species, may explain its better resistance to the defoliation by *G. platensis*. On the other hand, the observed changes in Roseoside levels among *Eg* genotypes also support all the above discussed. As our research group recently described, *E. globulus* responds to herbivory by down-regulating Roseoside, among others (Campos et al., 2022). The same trend was observed in the present study (Fig. 4.2.9f). However, that tendency was not significant for *E. globulus* genotypes included in this study *Eg*1, *Eg*2, *Eg*6, and *Eg*7, which, coincidently, were intensive to severity defoliated by the weevil (Fig. 4.2.9f). Oppositely, *E. globulus* genotypes *Eg*3, *Eg*4, and *Eg*5 were only moderately defoliated because they significantly downregulate Roseoside in between 1.5-fold and 2.0-fold (Fig. 4.2.9h), like in the cases of *En×Egg*4 and *En×Egg*6 (Fig. 4.2.9e, g).

A critical question that arises now is: how does Vomifoliol act in *Eucalyptus* to defend against *G. platensis* herbivory?

We can formulate at least two hypotheses about the function of Vomifoliol in *Eucalyptus*. The first one, and the most likely, is that after herbivory signaling, Roseoside (**10′**) is hydrolyzed by a glycosidase systemically in healthy foliage distant from the weevil feeding site to yield the free Vomifoliol. Then, as this molecule is lipophilic, it is sequestered in the numerous oil bodies present within the *Eucalyptus* leaves. These oil bodies can be mechanically disrupted upon weevil feeding, releasing the essential oil containing Vomifoliol, which may exert a direct defensive function as a deterrent or antifeedant against *G. platensis*. However, scarce and contradictory evidence regarding Vomifoliol's defensive role in plants against insects has been described. For instance, an ethanolic extract obtained from the leaves and twigs of the tree *Rollinia emarginata* (Annonaceae), which contained Vomifoliol together with Dehydrovomifoliol, Blumeol C, Vanillin, among many others, exerted an antifeedant and toxic effect against the moth *Spodoptera frugiperda* at a dose of 200 mg/l (Colom et al., 2007). However, the authors did not attribute such an effect to any particular metabolite. On the other hand, synthetic Vomifoliol and its relative

174

Dehydrovomifoliol were found to have a phagostimulant activity in favor of the solanaceous fruit fly *Bactrocera latifrons* (Yoshida et al., 2021). At the same time, low attractant activity was described to these compounds when used as a male lure trap. Therefore, additional scientific evidence is required to determine the actual location or specific tissues where Vomifoliol accumulates in *Eucalyptus* plants under *G. platensis* herbivory and assess this substance's effect on adult behavior through biological tests.

The second potential role of Vomifoliol in *Eucalyptus* could be related to certain physiological or signaling functions, like those of a phytohormone. It is known that Vomifoliol has the capacity to cause the stomata closure similar to its relative, ABA (Stuart and Coke, 1975). Such a physiological function of ABA occurs when plants are under water deficiency to reduce the stomatal conductance avoiding excessive water loss (Schulze et al., 2019). However, as the plants used in this study were not subjected to a water restriction that justifies drought stress, this cannot be the signal elicited by Vomifoliol. Interestingly, in a relatively recent investigation where hop plants (*Humulus lupuls* L.) were exposed to severe drought stress, Roseoside and ABA were detected among the significantly upregulated metabolistes in leaves (Morcol et al., 2020). Although the authors suggested that Roseoside could participate

in stomata closure, it is unlikely since that activity was proved for Vomifoliol and not for its glycosylated derivative. In addition, as ABA was also upregulated in the hop leaves, it is most probable that stomata closure is being regulated by this known phytohormone and not by Roseoside. Nevertheless, it is intriguing why Roseoside accumulation increases under water stress in hop plants. It may occur to prevent the attack of opportunistic organisms or insects due to the plant weakness caused by drought stress. Therefore, if Vomifoliol can transduce a signal in response to herbivory in *Eucalyptus*, it should likely be the induction of the systemic chemical defense. As shown in Fig. 4.2.4, the PCA scores plots indicate that *En×Egg*1, *En×Egg*7, and *En×Egg*4 were the three genotypes that exhibited the most significant changes in their leaves' metabolome in response to herbivory (Fig. 4.2.4a-c). These genotypes downregulated Roseoside in a more substantial manner in the same order, as shown in Fig. 4.2.9g. Interestingly, genotype *En×Egg*2 also responded to weevil herbivory by altering its metabolome, but in contrast, it upregulates Roseoside instead (Fig. 4.2.9g). Therefore, further investigation is required to determine if Vomifoliol would have or not the capacity to elicit the chemical defense in *Eucalyptus* species.

Among the rest of the metabolites that exhibited significant changes in levels in response to herbivory in hybrids, flavonol glycosides are major. However, their regulations per individual genotype did not follow a coherent trend that may suggest a particular function. Perhaps the most consistent changes were for the levels of Kaempferol 3-O-glucuronide (**5′**) and Kaempferol 3-O-rutinoside (**2′**). The former was significantly down-regulated in all hybrid genotypes except for *En×Egg*4 where a significant up-regulation was detected (Fig. 4.2.7). Our research group recently reported such a response in *E. globulus* under *G. platensis* herbivory (Campos et al., 2022). We think this could be a learned nonspecific response to prevent herbivores' rapid detoxification of potential toxic flavonols. However, the functions of flavonoids glucuronidation in plants are still unclear (Adiji et al., 2021). In the case of compound **2′**, all genotypes downregulated it in a rate between 1.4-fold and 2.0-fold, except in *En×Egg*4 where it did not suffer any significant changes (Fig. 4.2.7). Interestingly, this is the opposite of what we reported previously from the parent species *E. globulus* (Campos et al., 2022). Although the downregulation of flavonol glycosides should be directly or indirectly related to a plant protection role, it has yet to be fully understood and requires further investigation.

4.2.5. Conclusions

Following a metabolomics approach, the present research revealed the constitutive and inducible defensive traits based on non-volatile specialized metabolites against *G. platensis* herbivory in seven genotypes of the inter-specific hybrids *E. nitens × globulus*. We evidenced that hybrid genotypes inherited the enzymatic capability to produce stilbenes constitutively from the resistance parent, *E. nitens*, an essential metabolic attribute lacking in the susceptible parent *E. globulus*. Even hybrids can deploy their stilbene biosynthesis capability to enhance metabolites such as *trans*-Piceid in response to herbivory significantly. However, neither constitutive nor inducible stilbenes levels in hybrids could not reach that constitutively present in *E. nitens*, being always considerably lower. Consequently, hybrids must show better resistance to *G. platensis* herbivory than *E. globulus* but worse than *E. nitens*, which was verified in the field. Regardless of such metabolic trait, we evidenced that resistance imputation in hybrid genotypes cannot be based on stilbenes constitutive or inducible accumulation unless it could reach similar levels as in *E. nitens*.

The systemically induced defense based on non-volatile metabolites upon herbivory of *G. platensis* was also described per each hybrid genotype. Unlike the differential constitutive level of *trans*-Piceid found among hybrid genotypes, upon herbivory, it was significantly augmented unanimously, reaching similar concentrations except for *En×Egg*4. This response, however, did not show a clear correlation with the intensity of defoliation observed within genotypes. The most remarkable case was *En×Egg*4, which despite the upregulation of this metabolite, its final level was significantly lower than in the rest of the genotypes. Anyway, *En×Egg*4 was just moderately defoliated by the weevil in contrast to other genotypes, such as *En×Egg*2, which suffered a severe defoliation with the loss of more than 70% of its crown foliage despite having *trans*-Piceid accumulated in one of the higher rates before and after herbivory. Therefore, resistance in *En×Egg* hybrids cannot be attributed based on stilbenes.

In contrast, only the monoterpene Roseoside (Vomifoliol glucoside) among all registered up- or down-regulated metabolites showed an evident relationship between its level changes and the defoliation severity caused by the weevil in each case. In most of the genotypes, Roseoside was significantly downregulated in response to herbivory, suggesting that it is being

179

hydrolyzed to release the active substance, Vomifoliol. Thus, the higher the absolute value of its fold-change, the better protection against weevil defoliation. The genotype *En×Egg*4 exhibited one of the most pronounced Roseoside levels decreases, while *En×Egg*2 increased its level instead, and *En×Egg*5 did not significantly change it. Accordingly, *En×Egg*2 and *En×Egg*5 suffered from intense to severe defoliation. As Vomifoliol is a lipophilic metabolite, it is highly probable that after released, it is sequestered in the oil bodies of *Eucalyptus* leaves that can be mechanically disrupted when a weevil feeds from new healthy leaves, exerting its direct deterrent or antifeedant effect.

The results presented here, especially the above-mentioned close correlation between the severity of defoliation caused by the weevil and the absolute value of the fold-change by which Roseoside is being downregulated in response, unprecedentedly lays the foundations for resistance imputation in *E. nitens × globulus* genotypes or other *Eucalyptus* species. In addition, it is a valuable insight into the ununderstood Vomifoliol's actual function in plants, particularly in *Eucalyptus*. However, additional scientific evidence is required to precisely determine the tissues' location of Vomifoliol accumulation in *Eucalyptus* plants under *G. platensis*

herbivory and assess this substance's effect on adults' behavior. Furthermore, artificial elicitation of the plant defense in this kind of hybrid could be an outstanding research line to finally increase the constitutive Vomifoliol levels to prevent severe defoliation by *G. platensis*.

Funding

CRediT authorship contribution statement

AJP: Conceptualization; JVC: Data curation; JVC: Formal analysis; AJP: Funding acquisition; JVC: Investigation; JVC: Methodology; OF: Supervision; JVC and AJP: Writing original draft; LEAP, CM; RA; and RR: reviews & editing.

Data Availability

Data associated with this paper, including LC-MS raw data (.d/.mzXML files) and processed bucket tables are available on request.

Acknowledgment

Table 2. Chemical data of significant metabolites for species distinction and response upon *G. platensis* herbivory.

No	Rt (min)	Metabolite name	Metabolite class	Mol. formula	-ESI Theor m/z	-ESI Meas m/z	+ESI Theor m/z	+ESI Meas m/z	m/z error (ppm)[a]	MS/MS -ESI fragments m/z (int. %)	MS/MS +ESI fragments m/z (int. %)	UV/Vis (nm)	InChI-Key	Ident. level (A-D)	Traits from
							Differential metabolites constitutively present in E. nitens concerning E. nitens × globulus at T0								
1	15.52	trans-Piceid	Stilbene glycoside	$C_{20}H_{22}O_8$	389.1242	389.1234 [M-H]⁻	391.1387	391.1373 [M-H]⁺	2.09, 3.83	227 (100), 185 (10), 143 (6)	229 (100), 135 (22), 119 (14), 107 (53), 91 (17)	300	HSTZMXC BWJGKH G-CUYWLF DKSA-N	A	-
2	10.01	Caffeyl glucoside	Hydroxycinnamic alcohol glycoside	$C_{15}H_{20}O_8$	327.1085	327.1082 [M-H]⁻	n.d.	n.d.	1.04, -	327 (56), 165 (17), 147 (100)	n.d.	278	WPUZPU NIENJVIU -WNEYBD SHSA-N	B	-
3	7.85	p-Coumaroylquinic acid I	Hydroxycinnamate ester	$C_{16}H_{18}O_8$	337.0929	337.0926 [M-H]⁻	361.0893	361.0873 [M+Na]⁺	0.73, 5.90	337 (2), 191 (13), 163 (100), 119 (20)	361 (100), 215 (60), 147 (48), 91 (35)	310	XWRHBG VVCOSN KO-OPGYGNE ESA-N	A	-
4	16.26	Isoquercitrin	Flavonol glycoside	$C_{21}H_{20}O_{12}$	463.0882	463.0873 [M-H]⁻	465.1027	465.1013 [M+H]⁺	1.85, 3.17	463 (100), 419 (12), 300 (63), 271 (55), 257 (35), 241 (18)	303 (100), 285 (1.2), 257 (2), 229 (3)	256, 343	OVSQVD MCBVZW GM-QSOFNFL RSA-N	A	-
5	17.29	trans-Piceatannol-O-(galloyl)-glucoside	Stilbene gallate-glycoside	$C_{27}H_{26}O_{13}$	557.1301	557.1290 [M-H]⁻	n.d.	n.d.	1.84, -	557 (28), 405 (33), 243 (100)	n.d.	286	HZCOWR OLPVDVC R-XMPPFBF MSA-N	B	-
6	17.77	cis-Piceid	Stilbene glycoside	$C_{20}H_{22}O_8$	389.1242	389.1238 [M-H]⁻	229.0859	229.0852 [M-Hex+H]⁺	0.95, 3.08	227 (100), 185 (10), 143 (5)	241 (59), 229 (100), 135 (35), 119 (27), 107 (73), 91(15)	282	HSTZMXC BWJGKH G-BUFXCDO RSA-N	A	-
							Differential metabolites constitutively present in E. nitens × globulus concerning E. nitens at T0								
1′	16.51	Cypellocarpin A	Monoterpene gallate-glycoside	$C_{23}H_{30}O_{12}$	497.1664	497.1656 [M-H]⁻	499.1810	499.1793 [M+H]⁺	1.72, 3.44	497 (100), 169 (13), 123 (7)	311 (47), 293 (40), 167 (25), 149 (100), 121 (33), 93 (22)	278	QIYRQEH CCPTEPY-VJOHEAA BSA-N	B	Eg
2′	16.99	Kaempferol 3-O-rutinoside	Flavonol glycoside	$C_{27}H_{30}O_{15}$	593.1512	593.1502 [M-H]⁻	595.1657	595.1629 [M+H]⁺	1.73, 4.80	593 (100), 284 (91), 255 (16), 227 (8)	449 (7), 287 (100), 129 (4)	266, 349	RTATXGU CZHCSNG -QHWHWD PRSA-N	A	Eg
3′	17.27	Eucaglobulin I	Monoterpene gallate-glycoside	$C_{23}H_{30}O_{12}$	497.1664	497.1657 [M-H]⁻	n.d.	n.d.	1.58, -	497 (32), 169 (100), 125 (42)	n.d.	267	GMBUW WLCKJYT TG-UHFFFAO YSA-N	B	Eg

No.	RT	Name	Class	Formula	Theor. [M−H]−	Exp. [M−H]−	Theor. [M+H]+	Exp. [M+H]+		MS/MS (−)	MS/MS (+)	UV	InChIKey		
4′	17.20	Eucaglobulin II	Monoterpene gallate-glycoside	$C_{23}H_{30}O_{12}$	497.1664	497.1651 [M−H]−	n.d.	n.d.	2.81,	497 (29), 169 (100), 125 (29)	n.d.	267	GMBUWWLCKJYTTG-UHFFFAOYSA-N	B	Eg
5′	17.53	Kaempferol 3-O-glucuronide	Flavonol glycoside	$C_{21}H_{18}O_{12}$	461.0725	461.0718 [M−H]−	463.0871	463.0856 [M+H]+	1.54, 3.29	461 (15), 285 (100), 257 (5), 229 (12)	287 (100), 113 (5)	266, 349	FNTJVYCFNVUBOL-ZUGPOPFOSA-N	B	Eg

<p align="center">Differential metabolites constitutively present in E. globulus concerning E. nitens × globulus at T0</p>

No.	RT	Name	Class	Formula	Theor. [M−H]−	Exp. [M−H]−	Theor. [M+H]+	Exp. [M+H]+		MS/MS (−)	MS/MS (+)	UV	InChIKey		
1″	21.38	5,7-dihydroxy-2-methylpropyl-chromone 8-C-oleuropyl-glucoside	Chromone-C-glycoside monoterpene ester	$C_{29}H_{38}O_{11}$	561.2341	561.2331 [M−H]−	563.2486	563.2457 [M+H]+	1.88, 5.35	561 (4), 377 (10), 257 (100), 183 (93), 125 (6)	563 (2), 545 (100), 277 (83), 149 (35), 121 (20), 93 (26)	282	RCOKBEQNXSUVDZ-UHFFFAOYSA-N	B	-
2″	20.09	2,5,7-trihydroxychromone 7-O-oleuropyl-glucoside	Chromone-C-glycoside monoterpene ester	$C_{26}H_{34}O_{12}$	537.1978	537.1969 [M−H]−	521.2017	521.1986 [M+H−H₂O]+	1.59, 6.0	537 (100), 453 (8), 209 (19), 167 (14), 125 (75)	503 (100), 235 (50), 205 (17), 149 (23)	283	BNOXWGIIFHBMQJ-HNHMJIFOSA-N	B	-
3″	16.21	Quercetin 3-O-glucuronide	Flavonol glycoside	$C_{21}H_{18}O_{13}$	477.0675	477.0665 [M−H]−	479.0820	479.0803 [M+H]+	1.98, 3.53	477 (32), 301 (100), 178 (7), 151 (15)	303 (100), 257 (2), 229 (2), 153 (1.2), 113 (5), 85 (3)	256, 354	DUBCCGAQYVUYEU-ZUGPOPFOSA-N	B	-
4″	20.26	Cuniloside B	Di-monoterpene glycoside ester	$C_{26}H_{40}O_{10}$	557.2604	557.2595 [M+HCO₂H−H]−	329.1594	329.1584 [M+H−OleuA]+	1.50, 4.95	557 (56), 511 (14), 373 (8), 327 (5), 225 (21), 183 (100)	293 (20), 149 (100), 121 (49), 93 (67)	273	JOLLIDAUJSAZHE-KWNAMUSHSA-N	B	-

Compound 5′ is also included

<p align="center">Differential metabolites constitutively present in E. nitens × globulus concerning E. globulus at T0</p>

No.	RT	Name	Class	Formula	Theor. [M−H]−	Exp. [M−H]−	Theor. [M+H]+	Exp. [M+H]+		MS/MS (−)	MS/MS (+)	UV	InChIKey		
6′	3.38	β-Glucogallin I	Galloyl glucose (hydrolysable tannin)	$C_{13}H_{16}O_{10}$	331.0671	331.0666 [M−H]−	333.0816	333.0801 [M+H]+	1.48, 4.53	331 (2), 169 (100), 125 (31)	171 (72), 127 (100),	255, 298	GDVRUDXLQBVIKP-HQHREHCSSA-N	B	En
7′	1.15	Shikimate	Cyclohexenecarboxylic acid	$C_{7}H_{10}O_{5}$	173.0455	173.0452 [M−H]−	n.d.	n.d.	1.73, -	173 (6), 137 (50), 111 (26), 93 (100)	n.d.	n.d.	JXOHGGNKMLTUBP-HSUXUTPPSA-N	A	-

Compounds 1 and 6 are also included | | | | | | | | | | | | | | | En |

<p align="center">Up-regulated metabolites in En×Egg1 upon herbivory</p>

No.	RT	Name	Class	Formula	Theor. [M−H]−	Exp. [M−H]−	Theor. [M+Na]+	Exp. [M+Na]+		MS/MS (−)	MS/MS (+)	UV	InChIKey		
8′	9.46	Disaccharide-C-glycoside	Carbohydrate	$C_{14}H_{26}O_{9}$	337.1504	337.1499 [M−H]−	361.1469	361.1452 [M+Na]+	1.57, 4.63	337 (100), 179 (5), 161 (2), 149 (3), 119 (28), 113 (11), 101 (11)	361 (100), 315 (18), 299 (8), 199 (9)	254	HQJFKKNIMVMXTD-GCEXTZRISA-N	B	-
9′	20.10	Cypellogin A (I)	Flavonol glycoside monoterpene	$C_{31}H_{34}O_{14}$	629.1876	629.1874 [M−H]−	631.2021	631.1990 [M+H]+	0.33, 4.92	629 (50), 463 (3), 300 (100), 271 (10)	631 (2.9), 329 (20), 303 (100), 167 (24), 149 (64)	248, 352	GUDLVBZWVXAHOX-	B	Eg

															En
Compounds 1 and 6′ are also included															
Compounds 4, 3″, and 7′ are also included															Eg
Down-regulated metabolites in En×Egg1 upon herbivory															
10′	11.19	Roseoside (Vomifoliol glucoside)	Cyclohexanone monoterpene glycoside	$C_{19}H_{30}O_8$	431.1923	431.1922 [M+HCO₂H-H]⁻	387.2013	387.1995 [M+H]⁺	0.23, 4.85	431 (30), 385 (100), 223 (38), 205 (21), 179 (8), 161 (32), 153 (30)	207 (32), 189 (16), 149 (17), 123 (35), 113 (23), 95 (100)	248	SWYRVC GNMNAF EK-MHXFFU GFSA-N	B	Eg, En
11′	17.58	Dihydro-Eucaglobulin	Monoterpene-gallate glycoside	$C_{23}H_{32}O_{12}$	499.1821	499.1813 [M-H]⁻	n.d.	n.d.	1.59, -	499 (29), 169 (100), 125 (27)	n.d.	268	RZSYEJW KQPWMQ I-PTLWZDE XSA-N	B	Eg
Compounds 2′, 4′, 3′, and 5′ are also included															Eg
Up-regulated metabolites in En×Egg7 upon herbivory															
12′	19.94	Cypellogin A (II)	Flavonol glycoside monoterpene	$C_{31}H_{34}O_{14}$	629.1876	629.1870 [M-H]⁻	631.2021	631.1991 [M+H]⁺	0.90, 4.79	629 (60), 463 (3), 300 (100), 271 (12)	631 (2), 329 (20), 303 (100), 167 (24), 149 (60)	248, 355	GUDLVBZ WVXAHO X-SCCIGHL QSA-N	B	Eg
13′	19.86	Unknown	Unknown	$C_{24}H_{40}O_{11}$	503.2498	503.2490 [M-H]⁻	527.2462	527.2440 [M+Na]⁺	1.56, 4.28	503 (100), 225 (11), 197 (10), 183 (19), 167 (6), 139 (11)	527 (100), 481 (15)	276	-	-	-
Compounds 1, and 9′ are also included															En
Compound 8′ is also included															-
Down-regulated metabolites in En×Egg7 upon herbivory															
14′	1.10	Quinic acid	Cyclitol carboxylic acid	$C_7H_{12}O_6$	191.0561	191.0556 [M-H]⁻	n.d.	n.d.	2.64, -	191 (100), 173 (3), 127 (6), 93 (4)	n.d.	n.d.	AAWZDT NXLSGCE K-LNVDRNJ USA-N	A	Eg
15′	1.43	Isocitric acid	Tricarboxylic acid	$C_6H_8O_7$	191.0197	191.0195 [M-H]⁻	193.0342	193.0345 [M+H]⁺	0.95, 0.97	191 (15), 129 (7), 111 (100)	99 (100)	n.d.	ODBLHEX UDAPZAU -UHFFFAO YSA-N	A	Eg
16′	19.57	5,7-dihydroxy-2-methylpropyl-chromone-C-(digalloyl)glucoside*	Chromone gallate-C-glycoside*	$C_{33}H_{32}O_{17}$	699.1567	699.1558 [M-H]⁻	701.2070	701.1687 [M+H]⁺	1.21, 4.31	699 (100), 547 (15), 529 (13), 395 (93), 275 (58), 169 (49), 125 (8)	701 (57), 379 (100), 277 (88), 153 (48)	279	-	B	Eg
17′	12.99	1,2,6-Trigalloyl-glucose I	Hydrolysable tannin	$C_{27}H_{24}O_{18}$	635.0890	635.0884 [M-H]⁻	619.0929	629.0894 [M-H₂O+H]⁺	0.94, 5.76	635 (99), 465 (43), 313 (44), 169 (100), 125 (15)	619 (19), 153 (100)	277	LLENXGN WVNSBQ G-VFTFQOQ OSA-N	B	En
Compounds 2′ and 10′ are also included															Eg
Up-regulated metabolites in En×Egg4 upon herbivory															
18′	16.59	5,7-dihydroxy-2-methylpropyl-	Chromone-C-glycoside	$C_{19}H_{24}O_9$	395.1348	395.1342 [M-H]⁻	397.1493	397.1478 [M+H]⁺	1.49, 3.92	395 (93), 275 (100), 247 (38), 204 (65)	397 (86), 379 (53), 361 (40), 277 (100), 247 (46), 206 (61)	278	NZMMUL PLBZWYS X-	B	Eg

185

No	RT	Name	Class	Formula	Calc. [M-H]⁻	[M-H]⁻	Calc. [M+H]⁺	[M+H]⁺	Error	MS/MS (−)	MS/MS (+)	UV	InChIKey	Level	Source
19′	17.47	chromone-C-glucoside Astragalin	Flavonol glycoside	C₂₁H₂₀O₁₁	447.0933	447.0926 [M-H]⁻	449.1078	449.1059 [M+H]⁺	1.52, 4.27	447 (100), 284 (35), 255 (63), 227 (64)	287 (100)	266, 348	ZIIYPAMZSA-N JPUKWEQWGBDDQB-QSOFNFLRSA-N	B	Eg
20′	22.00	Unknown	Unknown	C₂₆H₂₈O₁₅	579.1355	579.1342 [M-H]⁻	n.d.	n.d.	2.27, -	579 (63), 331 (16), 247 (100), 181 (10), 169 (11)	n.d.	276	-	-	-
21′	12.78	1,2,6-Trigalloyl-glucose II	Hydrolysable tannin	C₂₇H₂₄O₁₈	635.0890	635.0884 [M-H]⁻	619.0929	619.0894 [M-H₂O+H]⁺	1.00, 5.76	635 (58), 465 (100), 313 (56), 169 (67), 125 (11)	449 (2.9), 153 (100)	276	LLENXGNWVNSBQG-VFTFQOQOSA-N	B	En
22′	1.70	β-Glucogallin II	Galloyl glucose (hydrolysable tannin)	C₁₃H₁₆O₁₀	331.0671	331.0665 [M-H]⁻	n.d.	n.d.	1.70, -	331 (100), 271 (23), 211 (17), 169 (48), 125 (21)	n.d.	278	GDVRUDXLQBVIKP-HQHREHCSSA-N	B	En

Compound 7′ is also included — -
Compounds 4 and 2″ are also included — Eg

						Down-regulated metabolites in En×Egg4 upon herbivory									
23′	15.46	1,2,3,6-Tetragalloyl-glucose	Hydrolysable tannin	C₃₄H₂₈O₂₂	787.0999	787.0980 [M-H]⁻	789.1144	789.1115 [M+H]⁺	2.49, 3.81	787 (100), 635 (18), 465 (27), 295 (32), 169 (96), 125 (6)	449 (3.6), 279 (9), 153 (100), 125 (4)	276	RATQVALKDAUZBW-UHFFFAOYSA-N	B	En

Compounds 10′, 15′, and 16′ are also included — Eg

						Up-regulated metabolites in En×Egg2 upon herbivory									
24′	12.12	p-Coumaroylquinic acid II	Cinnamate ester	C₁₆H₁₈O₈	337.0929	337.0927 [M-H]⁻	n.d.	n.d.	0.70, -	191 (100), 173 (9), 163 (5), 119 (4), 93 (6)	n.d.	289	XWRHBGVVCOSNKO-OPGYGNEESA-N	B	Eg

Compound 1 is also included — En
Compound 4″ is also included — Eg

						Down-regulated metabolites in En×Egg2 upon herbivory									
25′	15.78	Rutin	Flavonol glycoside	C₂₇H₃₀O₁₆	609.1461	609.1451 [M-H]⁻	611.1606	611.1581 [M+H]⁺	1.73, 4.17	609 (75), 300 (100), 271 (12), 255 (6)	465 (35), 303 (100), 129 (4), 85 (6)	256, 354	IKGXIBQEEMLURG-NVPNHPEKSA-N	A	En

Compound 2′ is also included — Eg
Compound 6′ is also included — En

						Up-regulated metabolites in En×Egg3 upon herbivory									

Compound 1 — En
Compounds 12′, 24′, and 4″ — Eg
Compound 8′ — -

						Down-regulated metabolites in En×Egg3 upon herbivory									
26′	18.12	5,7-dihydroxy-2-methylpropyl-chromone-C-	Chromone gallate-C-glycoside	C₂₆H₂₈O₁₃	547.1457	547.1448 [M-H]⁻	549.1575	549.1602 [M+H]⁺	1.62, 4.99	547 (15), 395 (42), 275 (37), 247 (10), 169 (100), 125 (23)	549 (82), 379 (11), 361 (7), 277(100), 247 (28), 153 (18)	278	DKDRHLHPRDJJRT-	B	Eg

	(galloyl)glucoside			UHFFFAO YSA-N	
Compound 23′ is also included					En
Compound 2′ is also included					Eg
		Up-regulated metabolites in En×Egg6 upon herbivory			
Compound 1					En
Compound 24′					Eg
		Down-regulated metabolites in En×Egg6 upon herbivory			
Compounds 1′, 2′, and 26′					Eg
		Up-regulated metabolites in En×Egg5 upon herbivory			
Compound 1					En
Compound 13′					-
Compound 9′					Eg
		Down-regulated metabolites in En×Egg5 upon herbivory			
Compounds 1′, 2′, 5′, and 15′					Eg

[a]: Mean accurate mass error for -ESI and +ESI; [1-7]: Metabolite expressed in any of the genotypes from *En×Egg1* to *En×Egg7*; UV/Vis: Absorbance maxima; InChI-Key: IUPAC international identifier for chemical according to PubChem; Identification level (A-D): A-standard or NMR, B-MS/MS, C-MS[E], D-MS only; *En* or *Eg*: traits from *E. nitens* or *E. globulus* transferred to hybrids; + Overexpressed in *E. globulus* upon herbivory; - downregulated in *E. globulus* upon herbivory; (I), (II): isobaric compounds with similar MS/MS spectrum; *potentially new compound; n.d.: not detected.

References

Adiji, O.A., Docampo-Palacios, M.L., Alvarez-Hernandez, A., Pasinetti, G.M., Wang, X., Dixon, R.A., 2021. UGT84F9 is the major flavonoid UDP-glucuronosyltransferase in Medicago truncatula. Plant Physiol. 1–21. https://doi.org/10.1093/plphys/kiab016

Aguayo, P., Lagos, C., Conejera, D., Medina, D., Fernández, M., Valenzuela, S., 2019. Transcriptome-wide identification of WRKY family genes and their expression under cold acclimation in Eucalyptus globulus. Trees - Struct. Funct. 33, 1313–1327. https://doi.org/10.1007/s00468-019-01860-3

Aguirre, D.S., Gysling Caselli, J., Kahler González, C., Poblete Hernandez, P., Álvarez González, V., Pardo Velasquez, E., Bañados, J.C., Baeza Rocha, D., 2021. Chilean statistical yearbook of forestry. Statistical bulletin N°180. Instituto Forestal, INFOR. Ministerio de Agricultura.

Alseekh, S., Fernie, A.R., 2018. Metabolomics 20 years on: what have we learned and what hurdles remain? Plant J. 94, 933–942. https://doi.org/10.1111/tpj.13950

Austin, M.B., Noel, J.P., 2003. The chalcone synthase superfamily of type III polyketide synthases. Nat. Prod. Rep. 20, 79–110. https://doi.org/10.1039/b100917f

Campos, J. V., Riquelme, S., Pecio, Ł., Guedes, L., Mardones, C., Alzamora, R., Arteaga-Pérez, L.E., Rubilar, R., Fiehn, O., Pérez, A.J., 2022. Constitutive and inducible defense in Eucalyptus determines the feeding host of Gonipterus platensis, denoting specific plant-insect coevolution

and a strategy for resistance improvement. Ind. Crops Prod. 189, 115811. https://doi.org/10.1016/j.indcrop.2022.115811

Close, D.C., 2012. A review of ecophysiologically-based seedling specifications for temperate Australian eucalypt plantations. New For. 43, 739–753. https://doi.org/10.1007/s11056-012-9321-0

Colom, O.A., Popich, S., Bardon, A., 2007. Bioactive constituents from Rollinia emarginata (Annonaceae). Nat. Prod. Res. 21, 254–259. https://doi.org/10.1080/14786410500462819

Dührkop, K., Fleischauer, M., Ludwig, M., Aksenov, A.A., Melnik, A. V., Meusel, M., Dorrestein, P.C., Rousu, J., Böcker, S., 2019. SIRIUS 4: a rapid tool for turning tandem mass spectra into metabolite structure information. Nat. Methods 16, 299–302. https://doi.org/10.1038/s41592-019-0344-8

Fernández, M., Troncoso, V., Valenzuela, S., 2015. Transcriptome profile in response to frost tolerance in Eucalyptus globulus. Plant Mol. Biol. Report. 33, 1472–1485. https://doi.org/10.1007/s11105-014-0845-7

Fiehn, O., 2001. Combining genomics, metabolome analysis, and biochemical modelling to understand metabolic networks. Comp. Funct. Genomics 2, 155–168. https://doi.org/10.1002/cfg.82

Fiehn, O., Kopka, J., Dörmann, P., Altmann, T., Trethewey, R.N., Willmitzer, L., 2000. Metabolite profiling for plant functional genomics. Nat. Biotechnol. 18, 1157–1161. https://doi.org/10.1038/81137

Geldres, E., Schlatter, J.E., 2004. Crecimiento de las plantaciones de Eucalyptus globulus sobre suelos rojo arcillosos de la provincia de Osorno, Décima Región. Bosque (Valdivia) 25, 95–101.

189

https://doi.org/10.4067/s0717-92002004000100008

Gonçalves, C.I., Vilas-Boas, L., Branco, M., Rezende, G.D., Valente, C., 2019. Host susceptibility to Gonipterus platensis (Coleoptera: Curculionidae) of Eucalyptus species. Ann. For. Sci. 76. https://doi.org/10.1007/s13595-019-0850-y

Hasegawa, S., Poling, S.M., Maier, V.P., Bennett, R.D., 1984. Metabolism of abscisic acid: Bacterial conversion to dehydrovomifoliol and vomifoliol dehydrogenase activity. Phytochemistry 23, 2769–2771. https://doi.org/10.1016/0031-9422(84)83012-5

Ipinza, R., Barros, S., Gutiérrez, B., Borralho, N., 2014. Mejoramiento genético de eucaliptos en Chile. Instituto Forestal, INFOR, Santiago de Chile.

Lanfranco, D., Dungey, H.S., 2001. Insect damage in *Eucalyptus*: a review of plantations in Chile. Austral Ecol. 26, 477–481. https://doi.org/10.1046/j.1442-9993.2001.01131.x

Li, D., Gaquerel, E., 2021. Next-generation mass spectrometry metabolomics revives the functional analysis of plant metabolic diversity. Annu. Rev. Plant Biol. 72, 867–891. https://doi.org/10.1146/annurev-arplant-071720-114836

Loch, A.D., Matsuki, M., 2010. Effects of defoliation by Eucalyptus weevil, Gonipterus scutellatus, and chrysomelid beetles on growth of Eucalyptus globulus in southwestern Australia. For. Ecol. Manage. 260, 1324–1332. https://doi.org/10.1016/j.foreco.2010.07.025

Mapondera, T.S., Burgess, T., Matsuki, M., Oberprieler, R.G., 2012. Identification and molecular phylogenetics of the cryptic species of the

Gonipterus scutellatus complex (Coleoptera: Curculionidae: Gonipterini). Aust. J. Entomol. 51, 175–188. https://doi.org/10.1111/j.1440-6055.2011.00853.x

Morcol, T.B., Wysocki, K., Sankaran, R.P., Matthews, P.D., Kennelly, E.J., 2020. UPLC-QTof-MSE metabolomics reveals changes in leaf primary and secondary metabolism of hop (Humulus lupulus L.) plants under drought stress. J. Agric. Food Chem. 68, 14698–14708. https://doi.org/10.1021/acs.jafc.0c05987

Nambara, E., Marion-Poll, A., 2005. Abscisic acid biosynthesis and catabolism. Annu. Rev. Plant Biol. 56, 165–185. https://doi.org/10.1146/annurev.arplant.56.032604.144046

Navarrete-Campos, D., Le Feuvre, R., Balocchi, C., Valenzuela, S., 2017. Overexpression of three novel CBF transcription factors from Eucalyptus globulus improves cold tolerance on transgenic Arabidopsis thaliana. Trees - Struct. Funct. 31, 1041–1055. https://doi.org/10.1007/s00468-017-1529-3

Pang, Z., Chong, J., Zhou, G., De Lima Morais, D.A., Chang, L., Barrette, M., Gauthier, C., Jacques, P.É., Li, S., Xia, J., 2021. MetaboAnalyst 5.0: narrowing the gap between raw spectra and functional insights. Nucleic Acids Res. 49, W388–W396. https://doi.org/10.1093/nar/gkab382

Reis, A.R., Ferreira, L., Tomé, M., Araujo, C., Branco, M., 2012. Efficiency of biological control of Gonipterus platensis (Coleoptera: Curculionidae) by Anaphes nitens (Hymenoptera: Mymaridae) in cold areas of the Iberian Peninsula: Implications for defoliation and wood production in Eucalyptus globulus. For. Ecol. Manage. 270, 216–222.
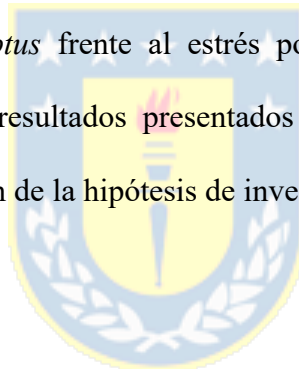
https://doi.org/10.1016/j.foreco.2012.01.038

Ruttkies, C., Schymanski, E.L., Wolf, S., Hollender, J., Neumann, S., 2016. MetFrag relaunched: Incorporating strategies beyond in silico fragmentation. J. Cheminform. 8, 1–16. https://doi.org/10.1186/s13321-016-0115-9

Schulze, E.D., Beck, E., Buchmann, N., Clemens, S., Müller-Hohenstein, K., Scherer-Lorenzen, M., 2019. Plant Ecology, 2nd ed. Springer-Verlag GmbH Germany. https://doi.org/10.1007/978-3-662-56233-8

Stuart, K.L., Coke, L.B., 1975. The effect of vomifoliol on stomatal aperture. Planta 122, 307–310. https://doi.org/10.1007/BF00385281

Tibbits, W.N., Hodge, G.R., 2003. Genetic parameters for cold hardiness in Eucalyptus nitens (Deane & Maiden) Maiden. Silvae Genet. 52, 89–97.

Volker, P.W., Potts, B.M., Borralho, N.M.G., 2008. Genetic parameters of intra- and inter-specific hybrids of Eucalyptus globulus and E. nitens. Tree Genet. Genomes 4, 445–460. https://doi.org/10.1007/s11295-007-0122-0

Worley, B., Powers, R., 2016. PCA as a predictor of OPLS-DA model reliability. Curr. Metabolomics 4, 97–103. https://doi.org/10.2174/2213235X04666160613122429.PCA

Worley, B., Powers, R., 2013. Multivariate Analysis in Metabolomics. Curr. Metabolomics 1, 92–107. https://doi.org/10.2174/2213235x130108

Yoshida, Y., Haraguchi, D., Ukuda-Hosokawa, R., Andou, T., Matsuyama, T., Kohama, T., Eguchi, T., Ohno, S., Ono, H., Nishida, R., 2021. Synthesis and activity of 3-oxo-α-ionone analogs as male attractants for the solanaceous fruit fly, Bactrocera latifrons (Diptera: Tephritidae).

Biosci. Biotechnol. Biochem. 85, 2360–2367. https://doi.org/10.1093/bbb/zbab166

4.3. La metabolómica no-dirigida revela la regulación de fitoanticipinas inducida por el estrés hídrico en *Eucalyptus*, sugiriendo la preparación para el ataque de plagas

Con el objetivo de complementar los estudios previos realizados en especies de *Eucalyptus* y considerando el conocimiento generado en estos, a continuación, se explora la correlación entre la respuesta metabólica a estímulos de tipo biótico con lo de carácter abiótico. Este estudio contempla los cambios en el metabolismo especializado de diferentes especies de *Eucalyptus* frente al estrés por sequía utilizando un enfoque metabolómico. Por tanto, los resultados presentados en este capítulo constituyen la culminación de la comprobación de la hipótesis de investigación planteada.

4.3.1. Introducción

Una de las especies exóticas más extensamente plantadas en climas templados no tropicales y mediterráneos es la especie *Eucalyptu*s (familia Mirtácea) (Lanfranco & Dungey, 2001a; Costa E Silva *et al.*, 2004). Esta especie es bien conocida por su rápido crecimiento y alta adaptabilidad, y es
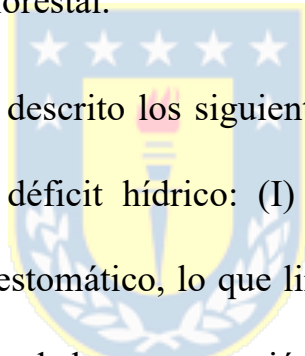
una de las especies exóticas más plantadas en el mundo (Elisa *et al.*, 2013; Gysling, 2017). Los cambios actuales en los patrones de precipitaciones y temperaturas suponen una amenaza significativa para la producción y sostenibilidad de las plantaciones forestales (Berenguer *et al.*, 2018; Singh *et al.*, 2021). La sequía es un factor determinante que afecta el crecimiento y la supervivencia de las plantas entre una variedad de factores climáticos (Singh *et al.*, 2021). En este escenario, la productividad de las plantaciones de *Eucalyptus* solo puede sustentarse a través de la selección de especies con mayor capacidad de tolerar las condiciones de baja disponibilidad de agua.

Actualmente, las plantaciones de *Eucalyptus* ocupan más de 20 millones de hectáreas en todo el mundo y, además es una de las especies forestales más intensamente plantadas (Rubilar *et al.*, 2020). Estas plantaciones se componen principalmente de plántulas mejoradas genéticamente y su propagación vegetativa por medio de esquejes enraizados de genotipos seleccionados en base a su crecimiento, calidad de la pulpa y propiedades de la fibra (Madhibha *et al.*, 2013). La sustentabilidad y productividad de estas plantaciones son principalmente desafiadas por la escasez de agua (Berenguer *et al.*, 2018). Los rasgos fisiológicos implícitos en las respuestas a la sequía difieren entre especies, *Eucalyptus* glóbulus Labill. se selecciona

195

para sitios con una moderada limitación hídrica estacional, y algunos estudios han sugerido que tiene una mejor tolerancia a la sequía (White *et al.*, 1996) en comparación con *Eucalyptu*s nitens H. Deane et Maiden, especie que se considera tiene mayor tolerancia a sitios propensos a heladas y frío (Tibbits & Hodge, 2003; White *et al.*, 2009; Navarrete-Campos *et al.*, 2017).

Las especies híbridas son importantes en silvicultura, particularmente en regiones subtropicales y tropicales, donde la propagación clonal efectiva es la clave para su uso y la oportunidad de mejorar la adaptabilidad de la especie (Potts & Dungey, 2004). Los híbridos de eucalipto presentan con frecuencia una mayor plasticidad ambiental a los factores abióticos y una buena supervivencia (Potts & Dungey, 2004; Volker *et al.*, 2008). Si la complementariedad genética es la clave de la superioridad de las especies híbridas, definir el entorno ambiental es crucial (Rubilar *et al.*, 2020). Existen pruebas de que algunas familias de híbridos de *Eucalyptus* pueden superar a la mayoría de las especies puras en los lugares de baja pluviosidad (Madhibha *et al.*, 2013). Algunas especies híbridas como *E. grandis* × *E. urophylla* cultivadas en Brasil son un ejemplo de éxito (Bison et al., 2006). Por otra parte, los clones de especies híbridas F1 entre *E. glóbulus* y *E. nitens*, que también se han desarrollado y comercializado en Chile, han tenido éxito

similar (Griffin *et al.*, 2000). La hibridación inter-especie en *Eucalyptus* ha demostrado ser un método efectivo y de bajo costo para los programas de mejoramiento genético forestal (Rezende *et al.*, 2014). En Chile, el uso del híbrido *E. nitens* × *globulus* ha cobrado relevancia debido a los mayores niveles de producción en comparación con sus especies parentales, presentando características intermedias en sus propiedades tecnológicas de la madera (Madhibha *et al.*, 2013; González *et al.*, 2018), aspecto altamente valorizado por la industria forestal.

Para los eucaliptos, se han descrito los siguientes mecanismos fisiológicos generales en respuesta al déficit hídrico: (I) Se produce inhibición del crecimiento foliar y cierre estomático, lo que limita el intercambio gaseoso provocando una disminución de la concentración de CO_2 y, en consecuencia, de la actividad fotosintética (Villar *et al.*, 2011; Correia *et al.*, 2016) . (II) Se produce un ajuste del potencial osmótico (Spokevicius *et al.*, 2017) para mantener una turgencia celular positiva a través de la acumulación activa de solutos (Warren *et al.*, 2011). En los últimos años, los estudios de respuesta a la sequía de *Eucalyptus* han documentado diferencias en la estructura del xilema, cambios en los niveles de proteínas (Valdés *et al.*, 2013), metabolitos y minerales. Además de cambios en los parámetros fisiológicos relacionados

con la dinámica del agua y la transpiración (Warren *et al.*, 2011). A pesar de investigaciones previas centradas en metabolitos específicos asociados al estrés hídrico, como la prolina y el ácido abscísico (ABA) (Zeevaart & Creelman, 1988), se carece de una comprensión global que describa la modificación de metabolismo especializado en eucalipto bajo estrés por sequía.

Debido a que la respuesta a nivel de metabolismo secundario al estrés por sequía en plantas a menudo es específica de cada especie, es interesante estudiar las respuestas específicas del *Eucalyptus* al estrés por restricción hídrica (Külheim *et al.*, 2011; Morcol *et al.*, 2020). En este trabajo realizamos un estudio de la variación del metabolismo especializado en plantas de seis especies de *Eucalyptus* sometidas a estrés por sequía utilizando como herramienta analítica la metabolómica. En este estudio se incluyeron las especies *E. globulus* y *E. nitens*, dos especies que han sido extensamente plantadas en Chile desde la década del 80. Además, se incluye la especie híbrida *E. nitens × globulus* que en los últimos 7 años se ha plantado cada vez más, ya que combina características deseables de fibra y pulpa, además de plasticidad al medio ambiente y menor susceptibilidad a plagas (González *et al.*, 2018; Rubilar *et al.*, 2020). Igualmente se incluyeron especies que

pudieran ser prometedoras para la industria de pulpa y papel como, *E. smithii*, *E. badjensis* y, el híbrido *E. camaldulensis × globulus*. Nuestro objetivo es comprender como afecta la sequía al metabolismo especializado de estas especies, e identificar marcadores químicos específicos del estrés por sequía para una posible aplicación y complementariedad con la selección genética que se realiza en los programas de mejoramiento forestal.

4.3.2. Materiales y métodos

4.3.2.1. Evaluación de parámetros fisiológicos

El experimento desarrollado consideró las siguientes especies del género *Eucalyptus*: *E. globulus*, *E. smithii*, *E. badjensis*, *E. camaldulensis × globulu*s, *Eucalyptus nitens* con sus 2 genotipos (En1, En2) y los 4 genotipos de la especie híbrida *E. nitens × globulus* (En×Egg1, En×Egg2, En×Egg3, y En×Egg4). Las plántulas seleccionadas, se establecieron en macetas plásticas de 7,5L con sustrato de compost de corteza de pino homogenizado y se dejaron en periodo de aclimatación al medio de crecimiento durante un mes y medio, tiempo en que se realizaron los riegos necesarios para mantener el potencial hídrico del suelo cerca de capacidad de campo, monitoreado por

sensores de potencial matricial del suelo (229-L SMP sensor Campbell Scientific, USA) para evitar limitaciones de agua. Además, durante el periodo de aclimatación se aplicó fertilizante a nivel del sustrato cada 15 días con una solución de Phostrogen ® (NPK 13-10-27, S, Mg, Ca y microelementos como Fe, B, Mn, Cu y Mo, Bayer Garden, Cambridge, UK) a una concentración de 1 g por cada litro de agua. Después del periodo de aclimatación, dos grupos (tratamientos) de 21 plantas cada uno fueron mantenidas bajo riego diario cerca de la capacidad de campo (Tratamiento Control) y 21 plantas fueron mantenidas sin riego (Tratamiento de sequía) para evaluar la respuesta fisiológica de las plantas al estrés hídrico.

Durante el experimento de estrés hídrico se registró el potencial hídrico foliar de prealba (ψ_predawn; 4:00 a 6:00 a.m.) como parámetro fisiológico para evaluar el grado de estrés experimentado por las plantas en distintas instancias de muestreo. El potencial hídrico foliar de prealba se considera la mejor representación del estado hídrico de una planta, ya que en prealba no hay transpiración, y por tanto puede considerarse como el equivalente al potencial hídrico del suelo prospectado por las raíces (Ameglio *et al.*, 1997). Las mediciones de potencial hídrico de la planta fueron realizadas por medio de una bomba Schollander (1505D Model, PMS Instruments Co., OR, USA),

instrumento que cuenta con una cámara que aplica presión a una hoja o un brote pequeño, lo cual permite cuantificar la presión necesaria para que el agua fluya a través del xilema hasta salir por el peciolo. Un valor alto de presión significa un alto grado de estrés hídrico y las unidades de presión más utilizadas son el bar o MPa.

El contenido de humedad del suelo de todas las plántulas en cada tratamiento se registró diariamente utilizando un TDR calibrado (Time Domain Reflectometry, Campbell Scientific CS650), el cual mide el contenido de humedad con sensores que se introducen en el sustrato. Para establecer las instancias de muestreo se consideró el nivel del potencial mátrico del sustrato de las plantas, donde la instancia T0 corresponde a un potencial cercano a 0 MPa y la instancia T1 corresponde a un potencial cercano a 2.5 MPa. El tiempo transcurrido en el que el sustrato alcanzó la instancia de estrés severo (T1) para todos los genotipos fue de 22 días. Para cada instancia de potencial mátrico crítico predefinido, se midió el potencial hídrico foliar de pre-alba en tres plantas representativas de cada tratamiento, pero sólo considerando hojas del primer tercio de la planta y que estuviesen completamente expandidas.

En el tratamiento de datos se utilizó la prueba de Shapiro-Wilk para comprobar normalidad. Para determinar diferencias significativas entre las medias del control y el tratamiento se realizó un análisis estadístico ANOVA de dos vías ($p > 0.05$) seguido de una prueba post hoc de comparaciones múltiples, test de Tukey. Este tratamiento estadístico se llevó a cabo en el software GraphPad Prism versión 9.2.0.

4.3.2.2. Origen y muestreo del material vegetal

El estudio fue establecido en febrero de 2021 en un invernadero experimental de Facultad de Ciencias Forestales de la Universidad de Concepción (36°50'05.2"S 73°01'56.9"W). Para el experimento de déficit hídrico se acondicionaron plantas de las siguientes especies del género *Eucalyptus* las cuales se utilizarán con el siguiente código: *E. globulus* (Eg), *E. smithii* (Es), *E. badjensis* (Eb), *E. camaldulensis × globulu*s (Ec×Egg), *Eucalyptus nitens* con sus 2 genotipos (En1, En2) y los 4 genotipos de la especie híbrida *E. nitens × globulus* (En×Egg1, En×Egg2, En×Egg3, y En×Egg4). En total 10 genotipos fueron incluidos en el estudio, cada uno con 6 réplicas biológicas. El material vegetal fue proporcionado por la unidad de

mejora genética forestal de la empresa Forestal Mininco localizada en la comuna de Yumbel, Región del Biobío, Chile. Las plántulas fueron producidas según los estándares del vivero de la empresa. Las plántulas fueron acondicionadas durante un mes y medio en el cual se mantuvo el potencial hídrico del suelo cercano a la capacidad de campo mediante constante riego y fertilización con Phostrogen ®.

Luego del período de acondicionamiento, las plántulas se dividieron en dos grupos tratamiento, un grupo control que disponía de irrigación de agua diaria y un grupo tratamiento de sequía o restricción hídrica al cual se le suspendió el riego una vez comenzado el experimento.

Se realizaron dos muestreos en el transcurso del experimento de estrés hídrico, T0 y T1. El primero, T0, se realizó el día 4 de febrero de 2021 a las 11:00 a.m., y fueron muestreadas plantas control y sequía. En esta instancia todas las plantas se encontraban con riego y libres de estrés, ya que se consideró este punto como línea base del experimento. El segundo muestreo, T1, se realizó el día 23 de febrero a las 10:30 a.m., se muestrearon ambos grupos nuevamente, control y sequía, pero en esta ocasión las plantas del tratamiento sequía contaban con casi 20 días de restricción hídrica, mientras

las plantas control se mantuvieron con irrigación constante durante todo el experimento (Figura S1).

Por instancia de muestreo (T0 y T1) se consideraron los 10 genotipos descritos anteriormente, cada uno con 3 réplicas biológicas para plantas control y 3 réplicas biológicas para plantas sometidas a estrés por sequía. Las muestras vegetales se colectaron aleatoriamente de cada plántula, tres hojas en promedio (1.5 g aprox.) por individuo, las que fueron etiquetadas y sumergidas inmediatamente en nitrógeno líquido para detener todo proceso metabólico.

4.3.2.3. Extracción de metabolitos

Las hojas de las muestras de *Eucalyptu*s se liofilizaron durante 5 días y después se molieron y homogeneizaron con el molino Restch MM 400 (Retsch GmbH, Haan, Alemania) y se almacenaron a -80 ºC. Para la extracción sólido-líquido se añadieron 800 µl de disolvente de extracción metanol/diclorometano/agua (2,5:1,0:0,5) a 4 ºC a 50 mg del material vegetal en tubos de microcentrífuga de 2 ml (Eppendorf Safe-Lock) y a continuación se agitaron vigorosamente durante tres minutos a 30 Hz de frecuencia de vibración en el molino mezclador Retsch MM 400 Mixer Mill.

Posteriormente, las muestras se centrifugaron a 13.300 rpm durante 10 minutos a 4 °C (centrífuga refrigerante, Nanbei). Se transfirieron 700 µl de sobrenadante por muestra a otro tubo de microcentrífuga de 2 ml y se añadió 500 µl de diclorometano y 500 µl de agua para realizar una extracción líquido-líquido durante 30 segundos a 20 Hz. Posteriormente, las muestras se centrifugaron a 13.300 rpm durante 5 minutos a 4 °C y se separaron las porciones polar y no polar. 700 µl de la porción polar se utilizó en el análisis por cromatografía en fase reversa. De esta fracción se tomaron 450 µl y se secaron a 30 °C durante 5 horas utilizando un concentrador centrífugo Eppendorf Concentrator Plus en modo V-HV (*vapor-high vapor*). Antes del análisis por cromatografía líquida acoplada con espectrometría de masas (LC-MS), el conjunto de extractos secos aleatorizados y tres blancos se resuspendieron en 500 µl con 80% MetOH (en agua, v/v) a 4 °C y luego se agitaron durante 1 minuto a 30 Hz. Posteriormente se centrifugaron durante 15 minutos a 13.000 rpm a 4 °C, y los extractos se transfirieron directamente a insertos de vidrio de 200 µl contenidos en viales ámbar de 2 ml con tapones pre-ranurados de teflón para HPLC.

4.3.2.4. Análisis LC-MS

El análisis se realizó en un sistema de cromatografía líquida de ultra-alta eficiencia (UHPLC) acoplado mediante interfaz de ionización a presión atmosférica (API) con un espectrómetro de masas de alta resolución de analizador híbrido cuadrupolo - tiempo de vuelo (HR/Q-TOF/MS, Compact, Bruker Daltonik GmbH, Bremen, Alemania). La separación cromatográfica del metaboloma del eucalipto se realizó en una columna UHPLC Kinetex C18 (100 × 3,0 mm, 1,7 μm; Phenomenex) utilizando una precolumna Security Guard Ultra Cartridge UHPLC C18 de 3,0 mm y se mantuvo a 30°C. La fase móvil consistió en disolvente A (ácido fórmico al 0,1% en agua Milli-Q, v/v) y disolvente B (ácido fórmico al 0,1% en acetonitrilo hipergrado, v/v) a un flujo de 0,4 ml/min. El gradiente de elución fue el siguiente: 0.0 – 24.0 minutos, 5-57.6% B en forma cóncava, 24.0 - 25.0 minutos, 57.6 – 100 % B lineal, 25.0 – 28.0 minutos, 100% B, 28.0 – 29.9 minutos, 100 – 5% B lineal. La columna se eluyó con esta concentración de disolvente B durante 5 min más y después se reequilibró con 5% B durante 1,5 min. Las muestras se mantuvieron a 4 °C en el automuestreador. El volumen de inyección fue de 2,0 μl. El espectrómetro de masas fue operado en modo de ionización por electrospray negativa y positiva, utilizando los siguientes parámetros: el

voltaje capilar se fijó en 3,5 kV; nebulizador 4,0 bar; gas seco 9,0 L/min; temperatura de secado, 200 °C. El intervalo de barrido de masas se fijó en 50 - 2000 m/z. Los espectros MS/MS se adquirieron en función de los datos, por lo que los iones (máximo 2) de cada barrido se sometieron a fragmentación inducida por colisión (CID) si su intensidad absoluta superaba los 1800 recuentos. En función de la relación m/z del ion, se utilizó una energía de colisión variable en el intervalo de 20 a 50 eV. La calibración interna se realizó con una solución de formiato de sodio 10 mM introducida en la fuente de iones a través de un bucle de 20 µl al principio de cada análisis utilizando una válvula de 6 puertos. La calibración se realizó utilizando el modo de calibración de alta precisión (HPC). Después de cada análisis, los datos adquiridos se procesaron automáticamente con un método Script en el software DataAnalysis 4.4 (Bruker Daltonik GmbH, Alemania), que incluía la recalibración y la creación de un archivo de datos del tipo mzXML.

4.3.2.5. Procesamiento de datos LC-MS, análisis estadístico y anotación de biomarcadores

Los datos LC-MS se procesaron con MetaboScape 3.0 (Compass, Bruker Daltonik GmbH, Alemania) seleccionando el flujo de trabajo Time aligned Region complete eXtraction (T-ReX 3D). Este algoritmo integra todos los pasos de procesamiento, incluida la recalibración de masas, la alineación del tiempo de retención (Rt), la extracción de características o "*features*" (pares m/z - Rt con la intensidad del ion), la detección de aductos y pérdidas neutras, la extracción de *features*, la importación de espectros MS/MS y la generación de la matriz de datos donde los *features* son asignados a través de las muestras. Los parámetros de MetaboScape T-ReX 3D se establecieron de la siguiente forma: umbral de intensidad, 500 counts; longitud mínima de pico de espectro, 5; longitud mínima de peak recursiva, 4; número mínimo de *features* para la extracción, 2; *features* en un número mínimo de análisis, 2; rango de masa, 50 - 2000 m/z; rango de tiempo de retención, 0.5 - 25.0 min; importación MS/MS, promedio. Las tablas de datos se sometieron primero a curación manual y estadísticas exploratorias en MetaboScape y luego se exportaron a MetaboAnalyst 5.0 para un procesado analítico de alto rendimiento para metabolómica (Chong *et al.*, 2019a). Para

los datos las variables se escalaron con el algoritmo Pareto, mientras las muestras se normalizaron por la suma. Posteriormente, se realizó un análisis de componentes principales (PCA) para descubrir patrones de agrupamiento inherentes en los datos y realizar la detección de valores atípicos. Además, se aplicó al conjunto de datos un análisis discriminante por mínimos cuadrados parciales ortogonales (OPLS-DA) para la identificación de las variables o *features* significativos que aportan a la diferenciación entre los grupos control y estrés por restricción hídrica. La validación de los modelos multivariados se realizó para evitar el sobreajuste de la data y evaluar su capacidad de predicción. Se implemento pruebas de permutación (n=100) con validación cruzada con los parámetros de validación, R^2Y para evaluar el ajuste del modelo a los datos y Q^2 para evaluar la capacidad de predicción del modelo.

La anotación de biomarcadores significativos se basó en su masa exacta, fórmula molecular, coincidencia de iones de fragmentos MS/MS con fragmentación *in silico* realizada con el algoritmo MetFrag integrado en MetaboScape 3.0. Los posibles candidatos para estructura química de los metabolitos identificados se verificaron en bases de datos en línea como ChemSpider, KEGG, ChEBI, Analyte DB o PubChem (Ruttkies et al., 2016).

Para mejorar la anotación de metabolitos se utilizó el software SIRIUS 4.9.2, que incluye "árboles" de fragmentación y CSI: FingerID (Böcker *et al.*, 2009; Dührkop *et al.*, 2019a; Hoffmann *et al.*, 2021). Además, para algunos de los metabolitos más importantes, utilizamos estándares analíticos para su confirmación de identidad como, por ejemplo, *trans*-piceid (*trans*-polidatina), astringina, rutina, ácido quínico, ácido isocítrico, e isoquercitina fueron adquiridos de Sigma-Aldrich/Merck Millipore Chile (Phyproof® Reference Substance, PhytoLab GmbH & Co., Alemania). Los metabolitos identificados en este estudio se reportan en la Tabla 3.

4.3.3. Resultados

4.3.3.1. Evaluación del estrés por sequía en especies de *Eucalyptus*

Durante el experimento de sequía se evaluó el parámetro de potencial hídrico foliar en prealba ($\psi_{predawn}$) en las instancias de muestreo como una forma de cuantificación del estrés hídrico. En la Figura 4.3.1a. se pueden apreciar los resultados del tratamiento estadístico de ANOVA de dos vías y test de post hoc a los datos de potencial foliar para los genotipos Es, Ec×Egg, En1, En2, Eg, Eb y los híbridos En×Egg (Figura 4.3.1.a). Durante el

experimento se registró una disminución del potencial hídrico foliar en respuesta a una disminución del potencial hídrico del sustrato de las plantas, que varió desde 0 MPa (T0) hasta 2.5 MPa (T1).

Como se observa en la Figura 4.3.1a. no hubo diferencias significativas ($p > 0.05$) entre las medias de las muestras control entre las instancias de muestreo T0 y T1, con valores promedio de 0.25 ± 0.08 MPa y 0.21 ± 0.07 MPa respectivamente, lo que da cuenta de que no hubo una variación significativa en el potencial y que las plantas control se mantuvieron en rangos basales sin estrés. Por el contrario, en las plantas tratamiento sequía sí hubo diferencia significancia ($p < 0.05$) en las medias entre T0 y T1, con valores promedio de 0.15 ± 0.1 MPa y 2.61 ± 0.7 MPa, respectivamente. En este caso sí hubo una disminución significativa del potencial hídrico foliar ocasionada por el estrés hídrico (Ameglio *et al.*, 1997) en plantas estresadas y se puede apreciar en el gráfico para cada genotipo (Figura 4.3.1a.), en el cual distintas letras indican diferencias significativas.

Adicionalmente se realizó la comparación de valores medios de potencial hídrico foliar para los cuatro genotipos del híbrido En×Egg en la instancia T1 (2.5 MPa), para evaluar el efecto de la variabilidad de los genotipos con el

tratamiento estrés, a través de un análisis ANOVA de dos vías y test de Tukey (Figura 4.3.1b). De este modo se puede observar que no hay diferencia significativa entre controles ($p > 0.05$), pero sí hay diferencia significativa entre control y tratamiento sequía ($p < 0.05$) para cada genotipo de esta especie híbrida en la instancia T1. Además, se observa que no hay diferencia significativa entre los valores de potencial en sequía para los genotipos En×Egg1 y En×Egg3, ambos con valores de potencial hídrico foliar sobre 3.0 MPa. Del mismo modo, tampoco hubo diferencia significativa entre los valores de potenciales para En×Egg2 y En×Egg4 ($p > 0.05$), ambos genotipos con valores medios de potenciales de 2.47 MPa y 2.42 MPa, lo que se interpretaría como una mayor tolerancia al estrés hídrico por parte de estos genotipos.

Finalmente, en el Figura 5S se dispone de los datos de contenido volumétrico de agua para el sustrato de plantas tratamiento sequía durante el experimento, como prueba de la disminución gradual del agua para las plantas.
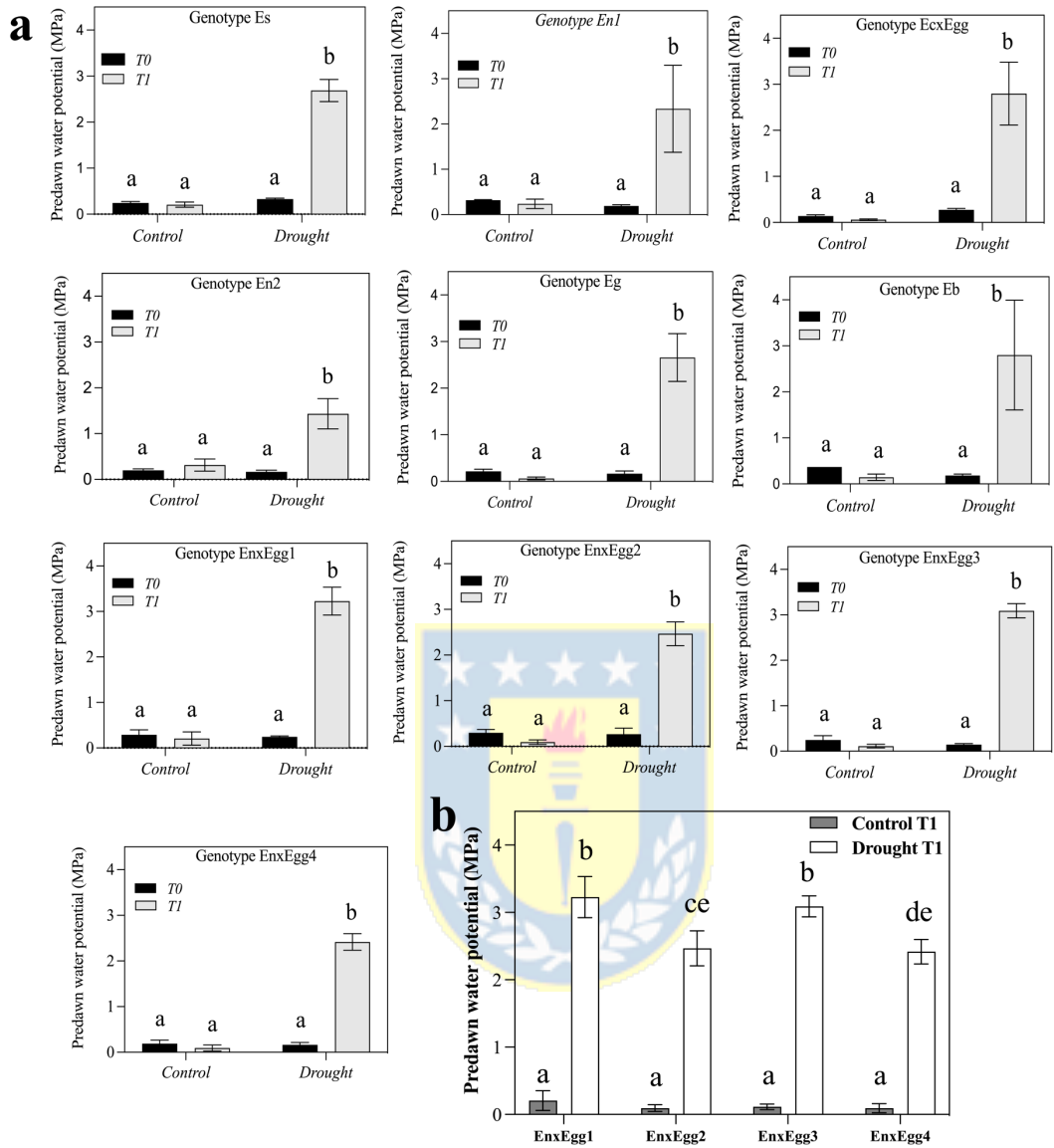
Figura 4.3.1. (**a**) Media y error estándar para los potenciales hídricos de pre-alba ($\psi_{predawn}$) para genotipos Es, Ec×Egg, En1, En2, Eg, Eb y genotipos En×Egg en plantas control y tratamiento en dos instancias de muestreo T0 (0 MPa) y T1 (2.5MPa). Distintas letras indican diferencias significativas entre tratamientos para un mismo genotipo. Se consideró una prueba ANOVA de

dos vías ($p < 0.05$) seguido de una prueba post hoc de comparaciones múltiples test de Tukey para la comparación de medias (n=3). (**b**) Comparación de las medias y error estándar de plantas control y tratamiento sequía para los cuatro genotipos de la especie híbrida En×Egg en T1 (instancia de sequía) para observar la respuesta diferenciada de cada genotipo. Distintas letras entre medias indican diferencias significativas.

4.3.3.2. Diferenciación en los perfiles metabólicos de especies de *Eucalyptus*

Para elucidar las diferencias en el metaboloma constitutivo entre las especies de *Eucalyptus*, los datos crudos obtenidos de los análisis LC-MS de extractos de hojas fueron procesados en el software MetaboScape 3.0 para generar la matriz de datos principal para los tratamientos estadísticos. Se detectaron 4917 y 984 *features* (par m/z y Rt) en los modos de adquisición -ESI y +ESI, respectivamente.

Para evaluar las tendencias en la diferenciación química de las especies se realizó un Análisis de Componentes Principales (PCA). En la Figura 4.3.2a. se observa el gráfico de score de todas las especies para las plantas control

en la instancia T1, evidenciando una marcada cohesión en los agrupamientos por especies, dando cuenta de la composición química distinta entre ellas en el modo de adquisición negativo (-ESI), la misma tendencia fue observada para los gráficos de score en modo de adquisición positivo (+ESI) (Figura suplementaria S2a). A lo largo del primer componente (PC1) se distribuyen las muestras con el 27.6% de la varianza explicada, en donde la especie En se aparta del resto de las especies. Por otra parte, las agrupaciones de En×Egg, Ec×Egg y Eg aparecen en el mismo cuadrante, lo que daría cuenta de una similitud entre ellas. Con respecto a Eb y Es, estas especies muestran un ligero solapamiento entre sí en una combinación de PC1 y PC2, dando cuenta de que no hay una diferenciación clara entre ellas. Una situación diferente se observa en el gráfico de score de las especies para las plantas bajo estrés por sequía en la instancia T1 para el modo de adquisición negativo (-ESI) y positivo (+ESI) (Figura 4.3.2b, Figura S2b), donde hay una modificación en las tendencias de distribución de las especies dando cuenta de un cambio a nivel metabólico de las plantas con respecto al control. En este se puede observar que las especies En×Egg, Ec×Egg y Eg que antes estaban separadas, ahora aparecen cercanas y alejadas de la especie En a lo largo del PC1 con un 25.8% de la varianza explicada en el conjunto de datos.

Por otro lado, Eb y Es aparecen completamente solapados, lo que daría cuenta de su similitud bioquímica.
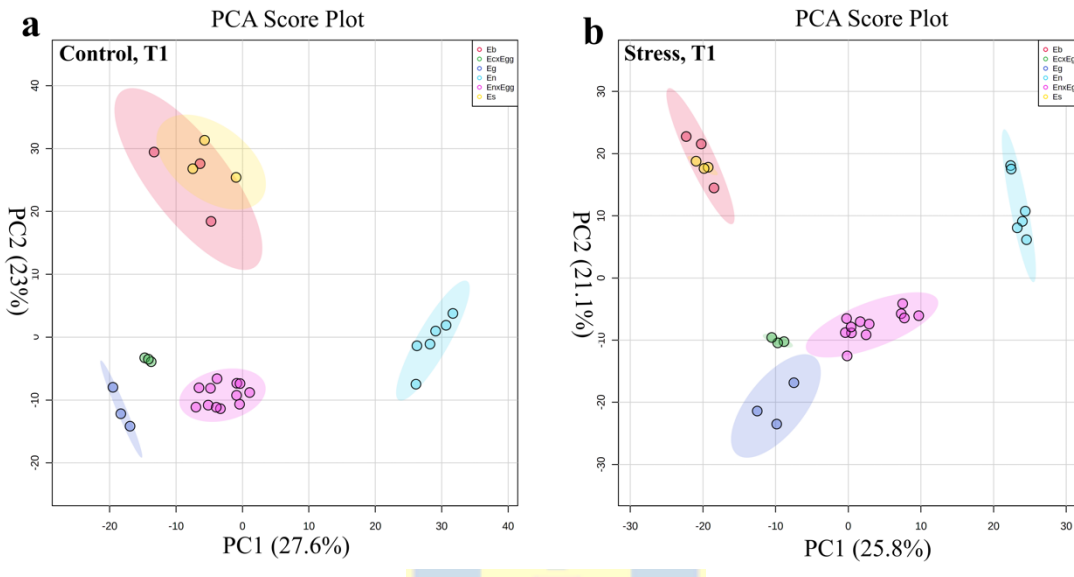
Figura 4.3.2. Modelos de Análisis de Componentes principales (PCA) de las seis especies de *Eucalyptus* en modo de ionización negativa (-ESI) para la distinción de los perfiles metabólicos distintos. (**a**) Grupos control correspondiente a plantas sin estrés por restricción hídrica en la instancia de muestreo T1. (**b**) Grupos tratamiento correspondiente a plantas con estrés severo por restricción hídrica durante 20 días en la instancia de muestreo T1 (2.5MPa). En ambos gráficos distintos colores fueron utilizados por especie, Eb (círculos rojos), el híbrido Ec×Egg (círculos verdes), Eg (círculos azules),

En (círculos celestes), el híbrido En×Egg (círculos morados) y Es (círculos amarillos). Los ejes *x* e *y* representan el primer y segundo componente principal (PC), y la etiqueta de cada eje incluye el porcentaje de la varianza total explicada por el componente correspondiente.

4.3.3.3. Respuesta de especies de *Eucalyptus* al estrés por sequía

Debido a las notables diferencias en el metaboloma constitutivo entre especies de *Eucalyptus* observado en la Figura 4.3.2a, se evaluó la respuesta al estrés por sequía de cada especie por separado en T1, con el fin de revelar las diferencias en las respuestas metabólicas inducidas. En la Figura 4.3.3. se muestran los modelos PCA para las seis especies en modo de adquisición negativo (-ESI) y positivo (+ESI) (Figura S3). Se puede apreciar la distribución de las muestras control y estrés a través del primer componente principal (PC1) en cada uno de los casos con una varianza explicada sobre el 29% en el conjunto de datos, formando agrupaciones separadas por clases; control y estrés; claramente definidas por sus regiones de confianza del 95% (Figura 4.3.3a, b, c, d, e). Excepcionalmente, para la especie híbrida En×Egg (Figura 4.3.3f) se observa solapamiento de ambas clases debido a la

variabilidad de sus 4 genotipos. Estos serán examinados en mayor detalle en el apartado 4.3.3.4. La separación observada en la mayoría de las especies da cuenta de una respuesta clara frente al estimulo de restricción hídrica severa en la instancia T1.

Posteriormente, para identificar los *features* (metabolitos) expresados diferencialmente en las hojas de las plántulas de cada especie en respuesta a la sequía o estrés hídrico se utilizó un modelo de análisis discriminante por mínimos cuadrados parciales ortogonales (OPLS-DA). En la figura 4.3.3. se muestran los gráficos de score (muestras) para los modelos supervisados donde se aprecia una clara separación entre las muestras control y estrés a lo largo del componente predictivo (T score [1]). Los genotipos con la mayor varianza explicada fueron Ec×Egg con el 55.5% (Figura 4.3.3b), y los genotipos Es y Eg con 42.5% y 42.2% (Figura 4.3.3a. y e). Finalmente, el genotipo En1 presentó una varianza explica del 22.9% en el conjunto de datos (Figura 4.3.3c).

 Por otra parte, en los gráficos S-plots (Feature Importance) en los cuales se representan las variables, cada punto representa un *feature* o metabolito específico. Los *features* situados en los extremos de la "S" son los que

contribuyen mayoritariamente a la distinción de clases. De este modo, *features* ubicados en el extremo derecho están correlacionados con las plantas con estrés por sequía, mientras que los *features* ubicados en el extremo izquierdo están correlacionados con plantas control sin signos de estrés.

Un total de 24 metabolitos significativos regulados al alza fueron identificados para los seis genotipos como se muestra en la Figura 4.3.4. que están correlacionados con las plantas estresadas por sequía en la instancia T1 (2.5 MPa). Estos comprendían a taninos hidrolizables como la β-glucogalina (7′) y otros dos taninos con mayor grado de sustitución de ácido gálico sobre la glucosa (22, 23); una variedad de isoprenoides, un monoterpeno (2) identificado como Vomifoliol glucósido y su isómero (5), además monoterpenos glicosilados y esterificados con una unidad de ácido gálico (4, 9, 11, 12, 17), donde 11 y 12 son isómeros al igual que 9 y 17. Dos flavonol glicosilados (25 y 9′), un flavonol glicosilado y esterificado con un ácido monoterpénico (20). Además de derivados de cromonas (15 y 16), glicosiladas con unidades de ácido gálico (18) y ácido monoterpénico (18). Finalmente se encontraron 6 derivados de disacáridos (1, 3, 14, 24, 26 y 27) y junto con el glucósido del ácido salicílico (21) (Tabla 3). En contraste, los *features* ubicados en el extremo izquierdo del S-plot están correlacionados

219

con plantas control, y por tanto están regulados a la baja en hojas de plantas

estresadas en cada uno de los genotipos.
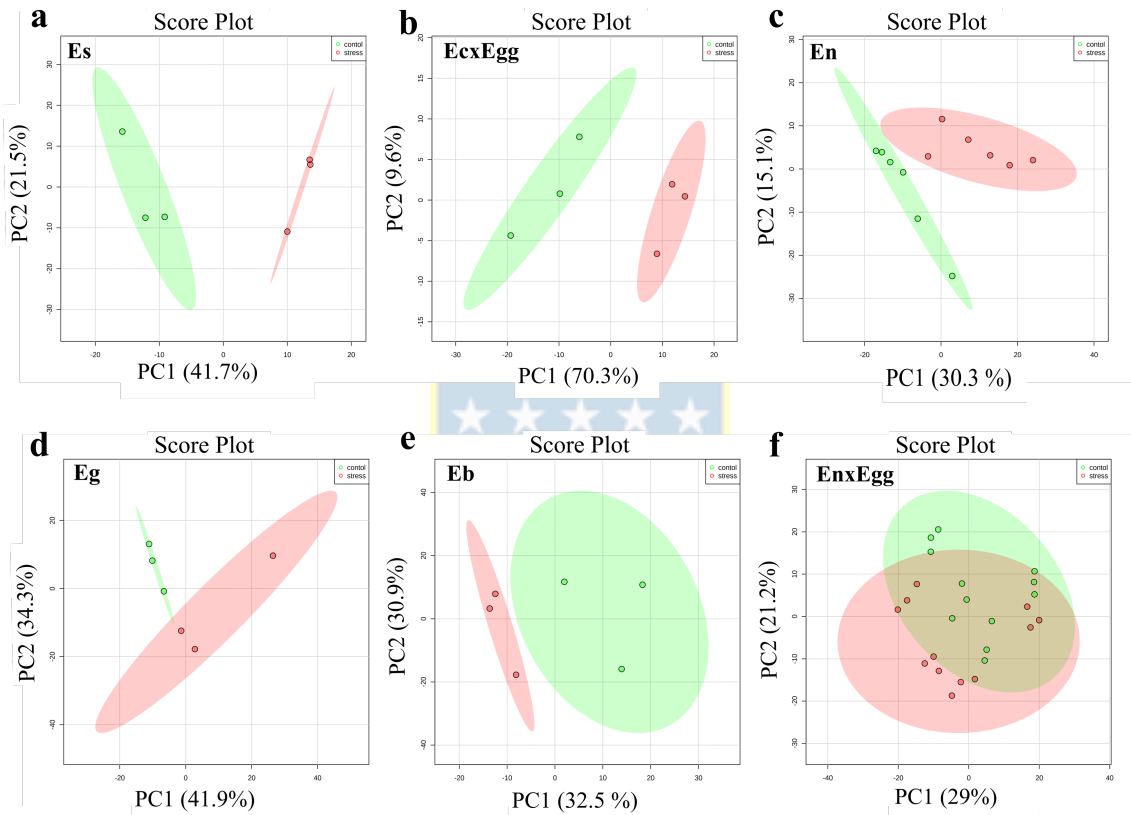
Figure 4.3.3. Modelos de Análisis de Componentes Principales (PCA)

basados en el conjunto de datos LC-MS adquiridos en modo de ionización

negativo (-ESI) para evaluar las tendencias de la composición química de

cada una de las especies de *Eucalyptu*s frente al estrés por sequía en la

instancia T1. Los gráficos se presentan en orden descendente de grado de

separación de los grupos a través de PC1 dispuestos desde la letra (**a**) hasta la (**f**). Plantas con estrés por restricción hídrica son representadas por cirulos rojos mientras plantas control son representadas por círculos verdes, con su respectivo intervalo de confianza del 95% (regiones sombreadas).

Se identificaron 25 metabolitos, que comprenden siete derivados de flavonoles glicosilados (5´, 6´, 8´, 27´, 3´, 9´, 10´ y 11´), de los cuales 5´y 6´son isómeros de posición, además de un flavonoide glicosilado clasificado como un metoxiflavano (21´). Adicionalmente, se regularon a la baja cuatro derivados glicosilados de estilbenos (17´,14´,18´y 15´), además de derivados de ácido gálico como (13´y 7´, 10), donde el compuesto 7´ es la β-Glucogallin I que es regulado al alza por el genotipo En1. El monoterpeno Globulusin B (28´) también es regulado a la baja.

Finalmente, varios ácidos orgánicos fueron regulados a la baja, entre ellos el ácido shikimico (1´), ácido isocítrico (25´), el ácido *trans*-p-cumaroilquínico (16´), un derivado de ácido butanoico (22´) y un derivado de ácido hidroxicinámico (26´). También fueron regulados a la baja un disacárido y carbohidratos, el disacárido **23´**, un alquil-glicósido (20´), el carbohidrato **12´**. Los modelos supervisados para estas seis especies fueron validados

utilizando permutación aleatoria de etiquetas de clase y una validación cruzada interna (*leave-n-out*), mostrando buenos resultados estadísticas para los parámetros con valores de $Q^2 > 0.72$ y $R^2Y > 0.993$ para todos los modelos, a excepción En1 con el valor más bajo de $Q^2 > 0.65$, en el conjunto de datos en modo de adquisición negativo (-ESI) (Figura S4).
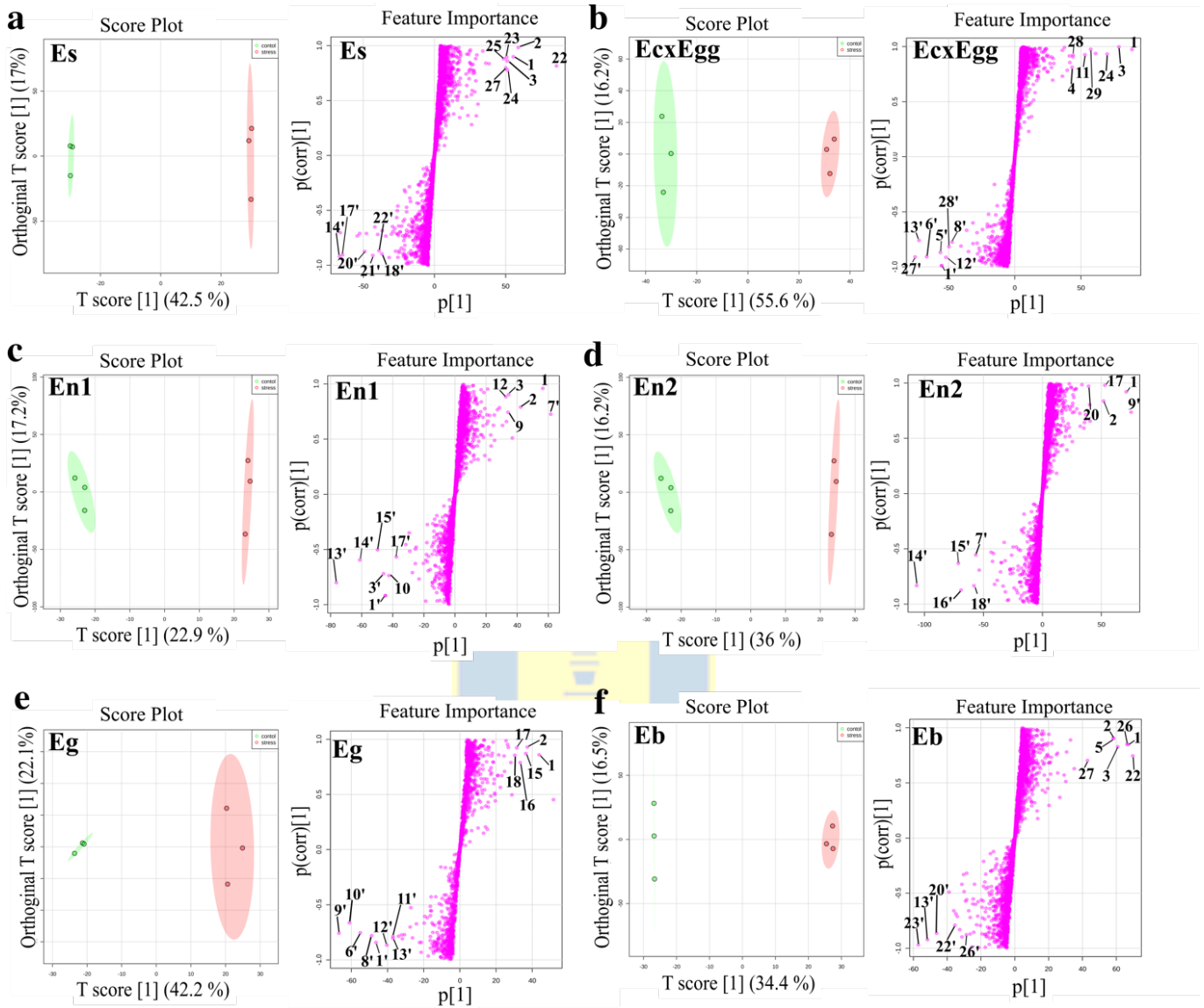
Figura 4.3.4. Resultados de los Modelos supervisados OPLS-DA del conjunto de datos LC-MS adquiridos en modo de ionización negativa (-ESI) para la diferenciación de los metabolitos significativos en plantas de *Eucaly*ptus sometidas a estrés por sequía en la instancia T1 (**a** – **f**). Por cada

especie, se presenta el gráfico de score (muestras), mostrando la separación de las muestras etiquetadas como control (círculos verdes) de las de estrés (círculos rojos) con sus respectivos intervalos de confianza del 95% (regiones sombreadas de color). Los gráficos de variables (S-plot) de los modelos supervisados fueron utilizados para la identificación de metabolitos significativos, los cuales fueron seleccionados por su alta covarianza > 35 en el componente predictivo, y una correlación $\geq$ 0.5 en el componente ortogonal para la predicción de clases (Tabla 3).

Al evaluar la variabilidad química por especie se encontró semejanzas entre los perfiles metabólicos de ciertos genotipos. Se observó un patrón generalizado entre genotipos en su respuesta frente al estrés por sequía, todos los individuos regulaban al alza un compuesto derivado de disacárido (1), el metabolito con mayor significancia en la mayoría de los modelos (Figura 4.3.4). Además, a excepción de la especie *E. camaldulensis* × *globulus*, genotipo Ec×Egg, todas las especies regulan al alza el compuesto Vomifoliol glucósido (2). El glucósido de Vomifoliol es un compuesto derivado del metabolismo del ácido abscísico (ABA) con una estructura similar. Vomifoliol glucósido (2) o Reseoside (PubChem CID: 129316932) al igual que ABA se inactiva en las plantas por glicosilación. Estos dos compuestos

224

aparecen como significativos en todos los modelos (covarianza > 45 en el componente predictivo y una correlación ≥ 0.8 en el componente ortogonal para la predicción de clases) como se observa en la Figura 4.3.4. Otra característica observada fue la similitud de familias de compuestos que fueron reguladas al alza en los genotipos Eg y Ec×Egg, sí bien no se tratan de los mismos compuestos ambos sobre-expresan monoterpenos glicosilados esterificados con unidad de ácido gálico (17 y 11), junto a cromonas glicosiladas y con unidad de ácido gálico (16 y 28). En cambio, Eg además contiene el metabolito Biflorin que es una cromona glicósilada (15) y Cypellocarpin C (18). Está semejanza no es de extrañar considerando que la especie Eg es una de las especies parentales del híbrido Ec×Egg. Por su parte, los genotipos de la especie *E. nitens* presentan una respuesta más bien diferenciada, a excepción de los metabolitos 1 y 2 mencionados anteriormente. En1 sobre-expresa en sus hojas un derivado de ácido gálico (7´) y dos monoterpenos glicósidos con una unidad de ácido gálico (12 y 9), en cambio En2, sólo contiene un monoterpeno glicósido esterificado con ácido gálico (17) e incorpora dos derivados de flavonol glicosilados (20 y 9´), además expresa en su metabolismo el glucósido del ácido salicílico (21) en hojas de plantas estresadas.

En contraste, el patrón metabólico de plantas en la regulación a la baja de metabolitos frente al estrés por sequía fue el siguiente. Se pudo apreciar semejanzas entre los genotipos de la especie *E. nitens*, En1 y En2, con el genotipo Es de la especie *E. smithii*. Estos tres genotipos tienen en común que regulan a la baja en sus hojas una variedad de derivados de estilbenos glicosilados y esterificados con una unidad de ácido gálico (14´, 15, 17´, 18´), compuestos que no se observan en otros genotipos y que hasta ahora eran característicos únicamente de la especie *E. nitens*. Por otra parte, también es posible observar semejanzas entre los genotipos de la especie híbrida *E. camaldulensis × globulus*, *Ec×Egg* con su especie parental *E. globulus*, genotipo *Eg*. Estos genotipos regulan a la baja una variedad de compuestos glicósidos de flavonoles (5´, 6´, 8´, 9´, 10´, 27´) y en especial los derivados de kaempferol (6´) y quercetina (8´). Estos metabolitos se han reportados por ser característicos del metaboloma constitutivo de la especie *E. glóbulus* en estudios previos (Campos *et al.*, 2022). Con respecto al genotipo *Eb* de la especie *E. badjensis*, este no presenta semejanzas significativas en familias de compuestos con otro genotipo.

4.3.3.4. Respuesta metabólica expresada en los híbridos *E. nitens ×E.* g*lobulus* a la sequía
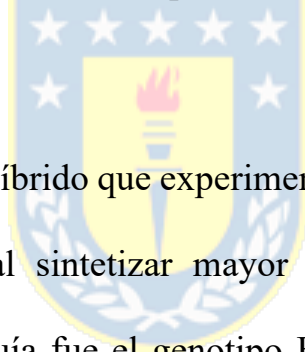
Para entender la respuesta metabólica diferenciada por genotipos de la especie híbrida *E. nitens × E. globulus* (En×Egg) al tratamiento de sequía, se evaluaron sus cuatro genotipos individualmente, En×Egg1, En×Egg2, En×Egg3 y En×Egg4. Para la elucidación de diferencias significativas en el metaboloma constitutivo, la data cruda obtenida de los análisis LC-MS fue procesada en el software MetaboScape 3.0 para generar la matriz principal para cada genotipo utilizada en los análisis estadísticos. Como primera aproximación se aplicó un modelo exploratorio de Análisis de Componentes Principales (PCA) para examinar las tendencias en la composición química de los genotipos híbridos expresados en sus hojas frente al tratamiento sequía. En la Figura 4.3.5a. se presentan los gráficos de score (muestras) para cada uno de estos híbridos, donde la distribución de las muestras control y estresado sucede a través de PC1. Para En×Egg1 las muestras se distribuyen a lo largo de PC1 con 57.4% de la varianza explicada, para En× Egg2 con un 53.7% de la varianza explicada, para En×Egg3 con un 58% de la varianza explicada y finalmente, para En×Egg4 se distribuyen las muestras a través de PC1 con un 49.8% de la varianza explicada en donde se aprecia un leve

solapamiento de las regiones de confianza. El solapamiento observado para el hibrido En×Egg4 puede interpretarse como una respuesta poco diferenciada por parte del híbrido cuando se trata de advertir el estrés producido por sequía en la instancia T1.

 A continuación, se utilizó el modelo supervisado OPLS-DA para identificar los *features* (metabolitos) expresados de forma diferencial entre plantas control y estresadas en T1. Los gráficos de score (muestras) (Figura 3.4.5.) mostraron una separación drástica entre las agrupaciones de muestras etiquetadas como control (círculos verdes) y estresado (círculos rojos) a lo largo del componente predictivo (T score [1]) para cada uno de los modelos (Figura 3.4.5b, c, d, e). En los gráficos de variables S-plot, como se mencionó anteriormente, cada punto de datos representa un *featur*e (metabolito), y los puntos ubicados en los extremos de la "S" del gráfico son los *features* que más contribuyen a la distinción de clases.

De esta forma se identificaron los metabolitos con mayor significancia (covarianza > 35 en el componente predictivo y una correlación > 0.75 en el componente ortogonal para la predicción de clases) para examinar la variabilidad química de la respuesta expresada por los genotipos híbridos. Se

observó que los genotipos En×Egg1, En×Egg2 y En×Egg3 sobre-expresaron, al igual que sus especies parentales, *E. nitens* y *E. globulus*, al disacárido **1** y Vomifoliol glucósido (2) (covarianza > 50 en el componente predictivo y correlación > 0.8 en el componente ortogonal), a excepción del genotipo En×Egg4. Lo que daría cuenta de una respuesta específica de las especies de *Eucalyptu*s consideradas en este estudio asociada a acumulación de este compuesto (**2**), con una potencial función defensiva en plantas contra el ataque de insectos que se ve inducida por el estrés hídrico como se expone en el apartado 4.3.3.2.

Por otra parte, el genotipo híbrido que experimentó un aumento sustancial de la capacidad metabólica al sintetizar mayor número de metabolitos en respuesta al estrés por sequía fue el genotipo En×Egg2, uno de los cuales experimentó mayor tolerancia al estrés según datos de potencial hídrico foliar, ya que a menores valores de potencial menor es la restricción hídrica experimentada por la planta (Ameglio *et al.*, 1997) (Figura 4.3.1b.). Este genotipo sobre-expresó un total 11 metabolitos, que incluyen disacáridos (1, 3 y 5), junto con monoterpenos glicosilados (4) y otros con unidades de ácido gálico (9). Un derivado de ácido gálico (10), además de cromonas (7) y cromonas glicosiladas con una unidad de monoterpeno (18). También reguló

229

al alza dos importantes ácidos orgánicos que están involucrados en importantes rutas metabólicas o procesos de regulación. Como lo es el ácido isocítrico (25´), que participa en el ciclo de los ácidos tricarboxílicos, y el ácido ascórbico, que es un potente reductor de radicales libres en procesos oxidativos (ROS) que enfrentan las plantas (Hasegawa *et al.*, 2008). Una respuesta distinta se identificó para el genotipo En×Egg4, el cual regula al alza derivados de monoterpeno glicósido (4), dos de ellos con unidades de ácido gálico (11 y 12) los cuales corresponden a isómeros. Además de dos disacáridos (6 y 14).

Por otra parte, se observó un patrón generalizado en los genotipos En×Egg1, En×Egg2 y En×Egg4 en los cuales se reguló a la baja cinco derivados de flavonoles glicosilados (3´, 4´, 5´, 6´y 8´), de los cuales 5´y 6´son isómeros del compuesto Kaempferol glucósido, mientras **8´** corresponde a la isoquercitina. Estos metabolitos también están regulados a la baja por el genotipo Ec×Egg, híbrido de la especie *E. globulus* que también regula a la baja la misma familia de compuestos. Por su parte, genotipos En×Egg1, En×Egg2 y En×Egg3 regulan a la baja ácido shíkimico (1´) a excepción del genotipo En×Egg4. Solo los genotipos En×Egg1 y En×Egg3 presenta en su metabolismo derivados de estilbenos (14´y17´) regulados a la baja, al igual

que los genotipos En1, En2 como se muestra en los modelos OPLS-DA (Figura 4.3.4.), por lo que son los genotipos que presentan mayor semejanza a nivel metabólico con la especie *E. nitens*. La validación de los modelos supervisados para las especies híbridas se obtuvo a través de permutación aleatoria de etiquetas de clase y una validación cruzada interna, mostrando resultados estadísticos aceptables para los parámetros $Q^2 > 0.755$ y $R^2Y>$ 0.997 para los 4 modelos en el conjunto de datos en modo de adquisición negativo (-ESI) (Figura S6).
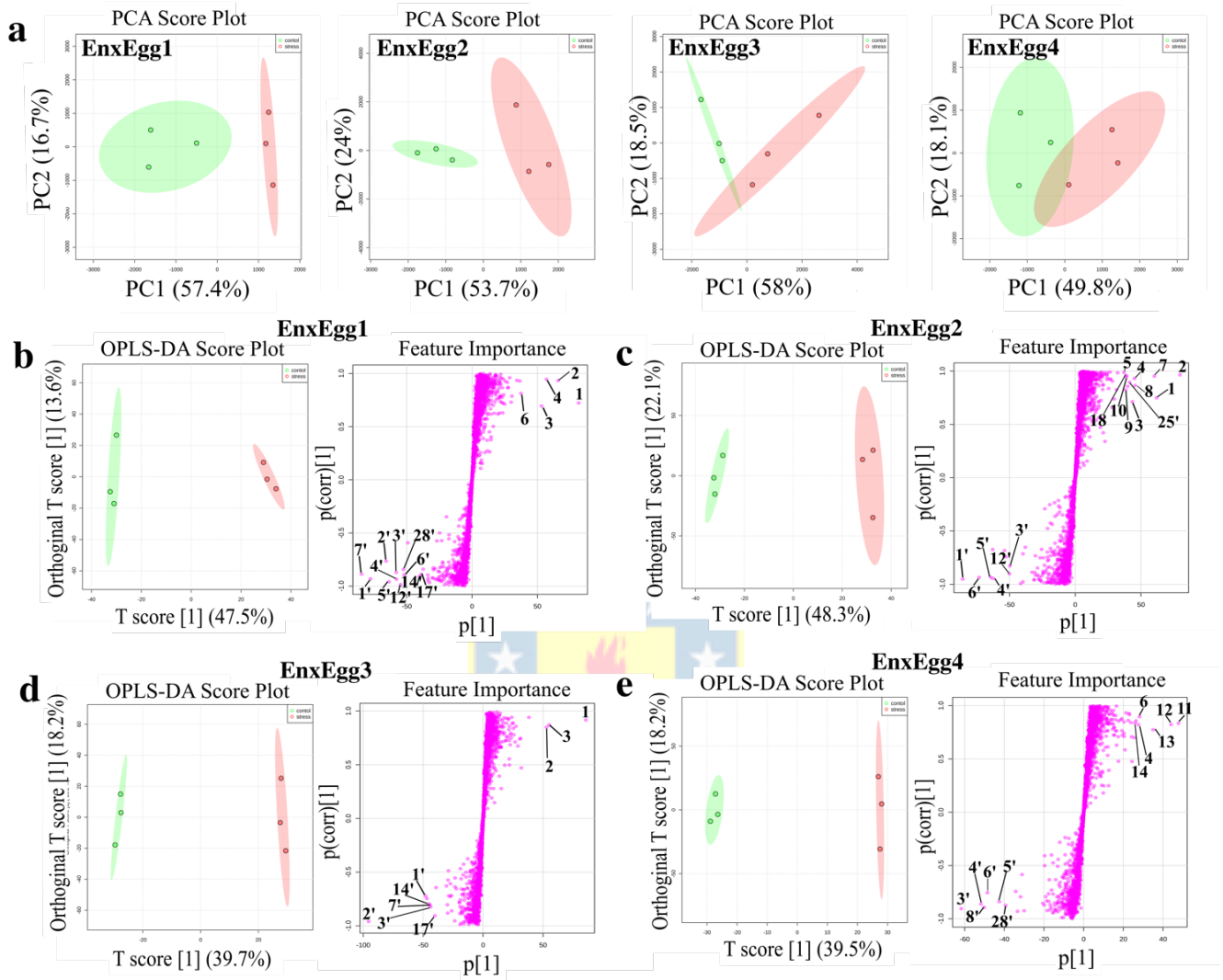
Figura 4.3.5. Modelos estadísticos multivariados para evaluar la variación intra-especie de los cuatro genotipos del híbrido En×Egg frente al estrés por sequía en la instancia de muestreo T1 adquiridos en modo de ionización negativo (ESI-). (**a**) Análisis de Componentes Principales (PCA) para visualizar las tendencias de agrupamiento en cada modelo para cada uno de

los genotipos En×Egg. (**b**, **c**, **d**, **e**) Modelos supervisados OPLS-DA para datos adquiridos en modo de ionización negativa (-ESI) para la selección de metabolitos significativos en plantas de la especie híbrida En×Egg sometidas a estrés por sequía. En los gráficos Score-plot (muestras) se observa la separación de las muestras etiquetadas como control (círculos verdes) de las etiquetadas como estresadas (círculos rojos) a través del primer componente principal (PC1), con sus respectivos intervalos de confianza del 95% (regiones sombreadas de color). Los gráficos de variables (S-plot) de los modelos supervisados fueron utilizados para la identificación de metabolitos significativos, los cuales fueron seleccionados por su alta covarianza > 35 en el componente predictivo, y una correlación ≥ 0.5 en el componente ortogonal para la predicción de clases (Tabla 3).

4.3.4. Discusión

4.3.4.1. Respuesta del metabolismo especializado frente a la sequía y análisis funcional de biomarcadores

Los análisis metabolómicos realizados para las especies de *Eucalyptus* permitieron la identificación de una amplia gama de metabolitos

involucrados en el metabolismo especializado de las hojas de plantas expuestas a estrés por sequía.

En primera instancia se encontró la ruta biosintética del metabolismo del almidón y de la sacarosa con regulación al alza de derivados de glicósidos en plantas posterior al estrés por sequía. El disacárido **1** tiene incrementos de 1.79-fold y esta expresado como significativo (covarianza > 45 y correlación > 0.75) en las hojas de todos los genotipos a excepción de En×Egg4 (Figura 4.3.6a). Sin embargo, el híbrido En×Egg4 sobre-expresa el compuesto hydrangeifolin I (14) (1.114-fold), además del compuesto **6** (1.80-fold), disacárido que también es sobre-expresado en el genotipo En×Egg1 (Figura 4.3.7). Por otra parte, los genotipos Es y Ec×Egg muestran un incremento del compuesto D-(+)-Cellobiose (24) (1.31-fold) y el metabolito **27** (2.068-fold) en sus hojas. Mientras el genotipo Eb muestra sobre-expresado el compuesto Epimelibiose (26) (1.98-fold) en la instancia T1. Se ha reportado que la acumulación de azúcares solubles en hojas de la especie *Eucalyptus* está correlacionado con su función como reguladores osmóticos. Estos ayudan a la disminución del potencial osmótico para mantener una turgencia celular positiva mediante la acumulación de solutos orgánicos en el citosol de la célula vegetal (C. R. Warren, T. Bledy, 2007; Correia et al., 2016). Es

probable que la acumulación de derivados de glicósidos y disacáridos confieran mayor tolerancia a la desecación de la planta a través de su presión osmótica y la estabilización de membranas, organelos y otras macromoléculas (Warren *et al.*, 2011; Kumar *et al.*, 2021).

Por otra parte, se vio una sobreexpresión de la ruta de biosíntesis de terpenos en plantas estresadas por sequía. Los derivados monoterpénicos están sobre-expresados en la especie En1 y Eg, pero principalmente en los híbridos de esta última especie, los genotipos Ec×Egg y En×Egg. Se ha reportado que la especie *E. globulus* es capaz de producir monoterpenos glicósilados conjugados con ácido gálico con capacidad bioactiva (Hasegawa et al., 2008).

En las hojas de plantas estresadas de *Eucalyptus* se encontraron los siguientes monoterpenos: el compuesto Eucaglobulin I (11) con incrementos de 1.38-fold en las hojas de del híbrido Ec×Egg y su isómero Eucaglobulin II (12) con 1.150-fold en las hojas de En1. Los compuestos Cypellocarpin C (18) junto con el compuesto Dihidrocipellocarpin A I (17) tienen un incremento de 3.76-fold y 1.17-fold, respectivamente, en hojas de la especie Eg en instancia de sequía en T1. Pero además el isómero de este último,

Dihidrocipellocarpin A II (9), es regulado al alza en hojas del genotipo En×Egg2 (3.10-fold) (Figura 4.3.7). Estos monoterpenos glicosilados basados en ácido oleuropeico encontrados en *Eucalyptus* (Brezáni & Karel, 2006) poseen importantes roles en actividades como la defensa contra insectos con propiedades repelentes, especialmente por su toxicidad. Además, la glicosilación de las agliconas lipofílicas de estos monoterpenos puede estar relacionada con una funcionalización fisiológica. La glicosilación puede actuar para reducir movilidad de las agliconas lipofílicas en determinadas circunstancias. Puede hacer que los compuestos sean más polares e impedir su difusión libre a través de bicapas lipídicas o entre compartimientos celulares con la necesidad de contener metabolitos potencialmente tóxicos (Goodger & Woodrow, 2013). Por tanto, el estrés hídrico estaría produciendo una acumulación de metabolitos con propiedades fitotóxicas, que pueden actuar como fitoanticipinas frente al ataque de patógenos.

Por otra parte, los monoterpenos glicosilados basados en ácido oleuropeico poseen una alta capacidad antioxidante confiriendo a la planta tolerancia al estrés oxidativo (Goodger & Woodrow, 2013). Se ha reportado que el estrés hídrico severo en plantas puede afectar a nivel celular la producción de

especies reactivas de oxígeno (ROS) (Imadi *et al.*, 2016). Precisamente el genotipo híbrido En×Egg2 regula significativamente al alza el ácido ascórbico (8) con un incremento de 1.69-fold, molécula con la mayor capacidad inhibitoria de ROS en plantas. El incremento significativo de este metabolito puede estar relacionado con una acumulación de compuestos antioxidantes no enzimáticos (secundario) para un posible daño por estrés oxidativo en el individuo En×Egg2 (Huseynova *et al.*, 2013). Se han reportado estudios en *E. globulus* donde altos niveles de estrés por sequía ha alterado la producción de ROS afectando la señalización celular (Shvaleva *et al.*, 2006). Sin embargo, un estado de estrés oxidativo en plantas estresadas en este estudio no se puede asegurar ya que no contamos con resultados necesarios. Además, el genotipo En×Egg2 regula al alza el ácido isocítrico (25´) que está involucrado en el ciclo de los ácidos tricarboxílicos (TCA). Bajo condiciones de restricción hídrica, el ácido isocítrico (25´) incrementó su abundancia en 1.69-fold. Como se ha reportado en los apartados 4.1 y 4.2 de este trabajo de investigación la biosíntesis del ácido isocítrico (25´) se ve regulada a la baja en las especies Eg y En×Egg frente a eventos de herbivoría. Por está razón, una sobreexpresión de este metabolito en plantas con estrés hídrico daría cuenta de una estrategia de conservación de energía, la cual

eventualmente podría utilizarse en la activación de mecanismos de defensa frente a un posible estrés biótico (Imadi et al., 2016; Yang et al., 2018).

Otro importante metabolito expresado en plantas estresadas del genotipo En2, pero que no logra ser significativo en los modelos multivariados el glucosyl salicilate (21), el glucósido de el ácido salicílico (Figura 4.3.7.). El ácido salicílico es una importante fitohormona involucrada en procesos como, crecimiento celular, respiración, cierre de estomas que están correlacionados con el estrés hídrico (Shah, 2003; Loake & Grant, 2007; Rangel Sánchez *et al.*, 2010). Por lo que la expresión del glucósido de **21** daría cuento del deterioro de procesos en la planta.

Por otra parte, durante este estudio se realizó la identificación de metabolitos que podrían tener una funcionalización como fitoanticipinas en la especie *Eucalyptus* en respuesta al estrés hídrico severo. Uno de estos metabolitos es el monoterpeno Vomifoliol glucósido (2) o Reseoside (PubChem CID: 129316932), derivado del metabolismo del ácido abscísico (ABA) (Strauss *et al.*, 1987; Jerkovic *et al.*, 2011). En estudios previos realizados por nuestro grupo de investigación (Campos *et al.*, 2022) (apartado 4.1) se observa una regulación a la baja de Vomifoliol glucósido en árboles de *E. globulus* que

sufren herbivoría por el insecto *G. platensis*. En un segundo trabajo comprendido en el apartado 4.2 de esta tesis doctoral, se aborda el patrón metabólico de este compuesto en árboles de la especie híbrida *E. nitens × globulus* (En×Egg) donde se observa una correlación entre la disminución del contenido de Vomifoliol glucósido (2) con la disminución de severidad del ataque por *G. platensis*. Está molécula (2) es una sustancia inactiva que, ante el estímulo de la herbivoría se hidroliza liberando Vomifoliol como molécula activa. Vomifoliol es la una molécula lipofílica que se encuentra en las cavidades oleosas de las hojas y que podría ejercer un efecto disuasorio directo frente al ataque de insectos. Sin embargo, en plantas bajo estrés hídrico se ha reportado que la forma glicosilada de Vomifoliol se encontró regulado al alza en hojas de lúpulo (Morcol *et al.*, 2020). Situación similar se observó para las especies de *Eucalyptus* incluidas en este estudio, ya que se encuentra sobre-expresado (covarianza > 45 y correlación > 0.75) en plantas bajo estrés por sequía. Este metabolito aumenta su concentración significativamente ($p < 0.05$) en todos los genotipos a excepción del genotipo En×Egg4, el cual no expresa un cambio significativo ($p > 0.05$) en su concentración relativa (Figura 4.3.6b).

La acumulación en hojas de Vomifoliol glucósido en plantas sometidas a estrés hídrico severo daría cuenta de un patrón metabólico distinto de esta molécula frente a un estrés abiótico. Puesto que la regulación al alza de está fitoanticipina y posterior acumulación sería utilizado como un mecanismo de defensa frente a un potencial ataque de patógenos. La estimación de la cantidad de Vomifoliol almacenado en hojas de plantas bajo estrés por sequía puede obtenerse a través de la magnitud del aumento en la concentración de Vomifoliol glucósido (2), dado por el valor de Fold Change (Figura 4.3.6c). Se encontró una interesante variación del contenido de está potencial fitoanticipina por especie, y en el caso de la especie En×Egg una variedad intra-especie dada por los genotipos. Por ejemplo, Vomifoliol glucósido aumentó en las especies Es, Eb en 4.08 y 3.42 veces superando las especies mayormente comercializadas Eg y En (En1 y En2) con valores de 2.62 y 2.06-fold, respectivamente. Para los híbridos En×Egg1, En×Egg2 y En×Egg3 se observaron incrementos de 2.81, 3.25 y 2.54-fold, mientras el híbrido En×Egg4 tiene el menor valor con 1.49-fold (Figura 4.3.6c) lo que se correlaciona con una variación no significativa ($p > 0.05$) en la concentración de dicho compuesto para este genotipo (Figura 4.3.6b).
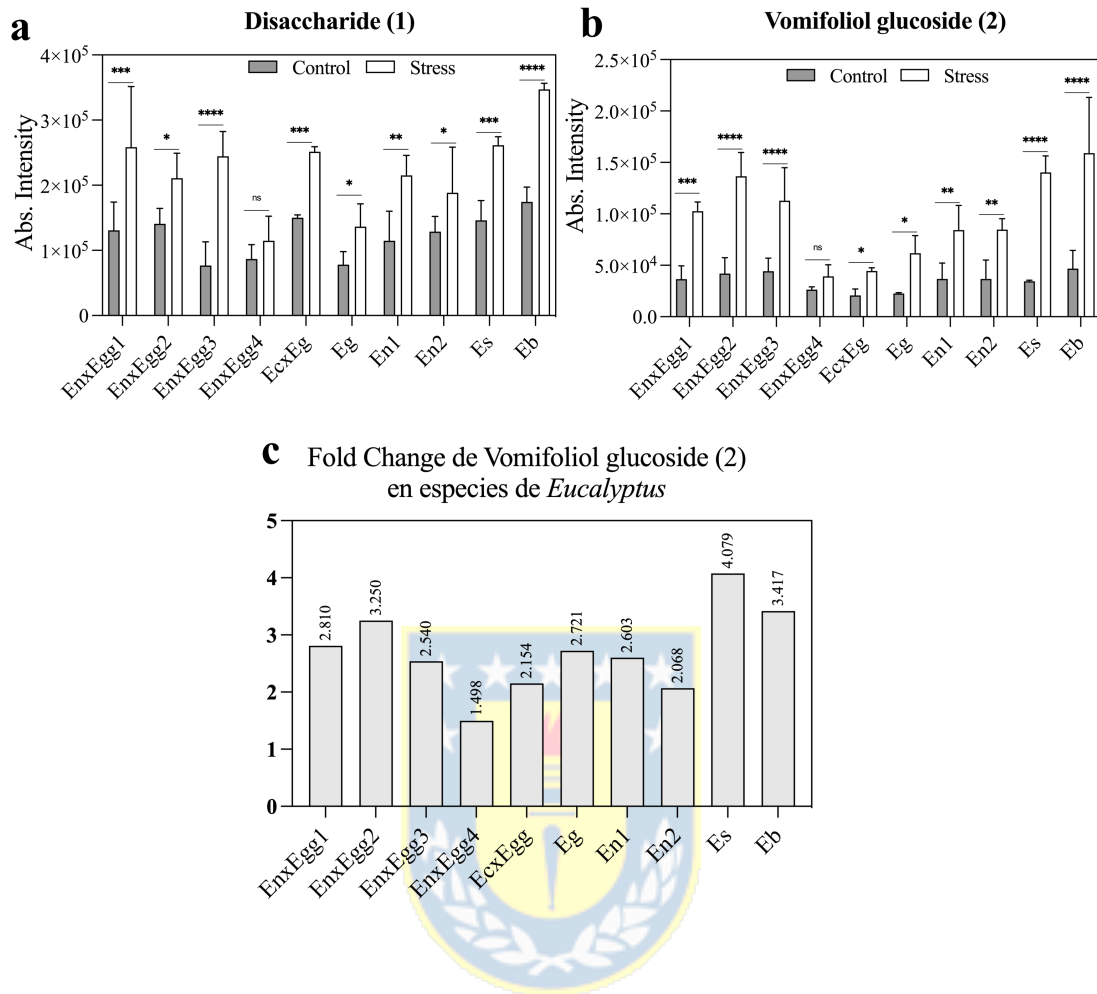
Figura 4.3.6. Gráfico de concentraciones relativas (abs. Intensity) de metabolitos sobre-expresados en respuesta a la sequía en las especies de *Eucalyptu*s. **(a)** Derivado de disacárido y **(b)** Vomifoliol glucósido, metabolitos regulados al alza en todos los genotipos a excepción del híbrido En×Egg4. Se aplicó la prueba de T test múltiple para evaluar diferencias significativas entre medias de intensidades de plantas control y tratamiento sequía (*p* < 0.05). Líneas entre casillas de cada genotipo indica nivel de

241

significancia para los cambios de concentración como significativo (*, 0.01 > p < 0.05), muy significativo (**, 0.001 > p < 0.01), extremadamente significativo (***, 0.0001 > p < 0.001), extremadamente significativo (****, p < 0.0001), y no significativo (ns, p ≥ 0.05). **(c)** Gráfico de Fold Change para Vomifoliol glucósido (2), definido como el cociente de las intensidades medias en plantas bajo estrés por sequía entre la de las mismas plantas antes del estrés por sequía (FC=i_stress/i_control).
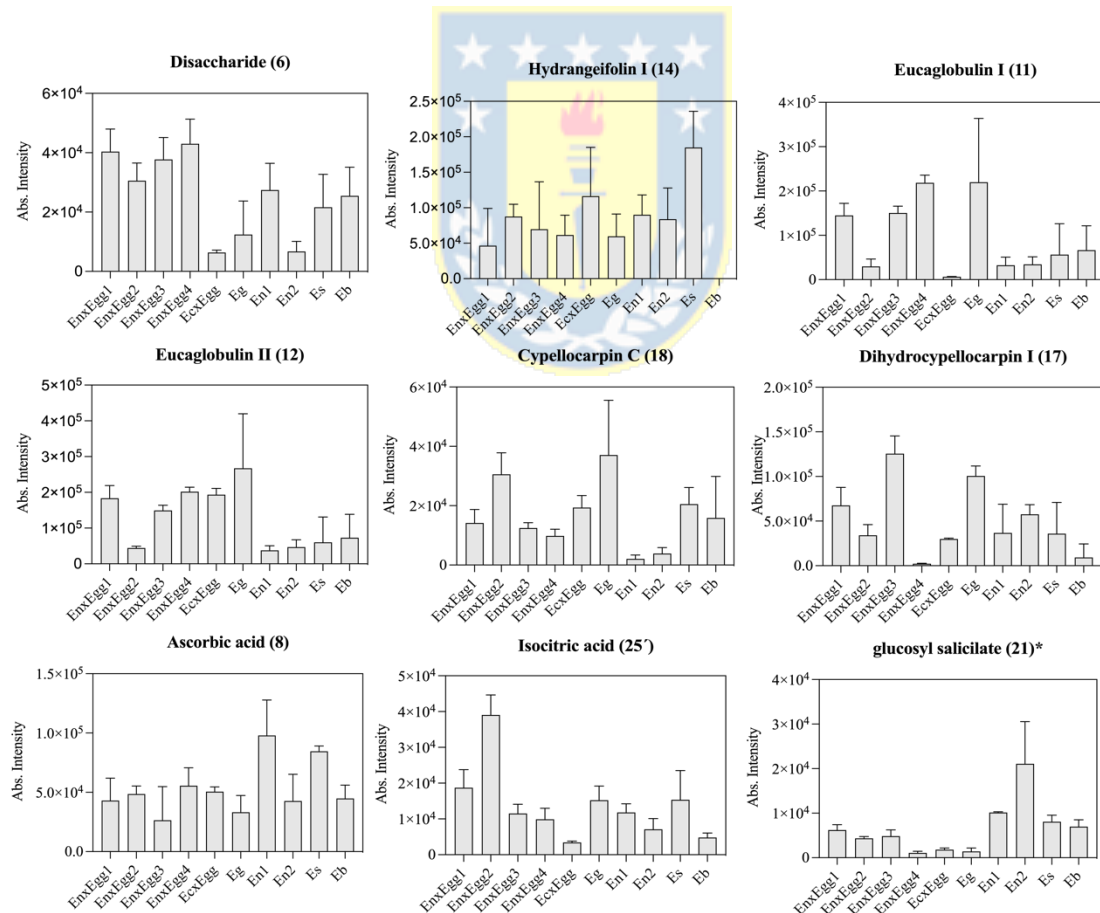
Figura 4.3.7. Gráfico de concentraciones relativas (abs. Intensity) para selección de metabolitos sobre-expresados en respuesta a la sequía en las especies de *Eucalyptus*. Seleccionados en modelos OPLS-DA (alta covarianza > 35 en el componente predictivo y una correlación ≥ 0.5 en el componente ortogonal). Se exponen dos disacáridos (6 y 14), tres monoterpenos glucósidos con una unidad de galato (11, 12 y 17), Cypellocarpin C (18) (glucósido de ácido oleuropeico), dos ácidos orgánicos (8, 25′) y glucosyl salicilate (glucósido de ácido salicílico, *no significativo en modelos multivariados) (Tabla 3).

Por otra parte, el estrés por sequía afectó negativamente importantes rutas biosintéticas en el metabolismo especializado de las plantas de *Eucalyptus*. Una de ellas fue la biosíntesis de fenilpropanoides, metabolitos implicados en la defensa de las plantas contra el estrés biótico (Neilson *et al.*, 2013; Jan *et al.*, 2021). El metabolismo de la ruta de flavonas y flavonoles reguló a la baja ocho flavonoles glicósilados en la especie Eg, y las especies híbridas de esta especie, En×Egg y Ec×Egg. Derivados de Quercetin (3′) (1.50-fold) e Isoquercitrina (4′ y 8′) (4.35-fold) se regularon a la baja en hojas de plantas estresadas con una disminución en su concentración. Junto con 4 derivados

de kaempferol glicosilados (5′, 6′, 10′y 27′) (8.89-fold, 7.39-fold, 1.80-fold y 1.28-fold) y rutina (9′) (1.72-fold). Una posible funcionalización de flavonoides es la constitución de un sistema antioxidante "secundario" en plantas (Huseynova *et al.*, 2013). Los flavonoles glicosilados tienen la capacidad de donar electrones o átomos de hidrógeno para llevar a cabo una actividad reductora, atribuida a los grupos fenólico del anillo B (Agati *et al.*, 2012). Sin embargo, no contamos con resultados suficientes para asegurar un estado de estrés oxidativo en plantas estresadas de este estudio.

En trabajos previos se ha demostrado que una regulación al alza de derivados de flavonoles glucósidos en la especie *E. globulus* se produce como respuesta defensiva frente a la herbivoría generada por *G. platensis* (Campos *et al.*, 2022). A su vez, la acumulación de flavonoles está relacionado con la protección de la planta frente a heridas o herbívora, que actúan como barreras físicas, antimicrobianos o para señalización (Kröner *et al.*, 2012; Jan *et al.*, 2021). Esto daría cuenta del efecto negativo del estrés por sequía en el metabolismo especializado de plantas de *Eucalyptus* en el cual se regulan a la baja metabolitos de defensa contra factores bióticos, principalmente insectos y patógenos.

Por su parte otra importante ruta de la biosíntesis de fenilpropanoides que fue regulada a la baja en respuesta al estrés hídrico fue la biosíntesis de estilbenos. Los genotipos de la especie *E. nitens*, En1 y En2 junto con el genotipo Es y los genotipos de la especie híbrida En×Egg1 y En×Egg3 regulan a la baja una variedad de compuestos de la familia de estilbenos. Se regulan a la baja *trans*-Piceid (14′) que disminuye en 2.45-fold, su isómero geométrico *cis*-Piceid (17′) se regula a la baja en 2.04-fold, junto con la *trans*-Astringin (15′) (1.78-fold). Finalmente, un derivado de resveratrol galloyl-glucósido (18′) disminuye en 3.98-fold para los genotipos En2 y Es. Si bien una de las principales funciones que se les atribuye a los estilbenos en varias familias de plantas es actuar como fitoalexinas (Hain *et al.*, 1990; Dubrovina & Kiselev, 2017), las cuales funcionan como compuestos defensivos de bajo peso molecular producidas en respuesta a una amplia gama de factores (Chong *et al.*, 2009). Es importante mencionar, que se ha demostrado que la acumulación constitutiva de estilbenos y taninos hidrolizables es particular de la especie *E. nitens* y un rasgo heredado para la especie híbrida En×Egg, sugiriendo la existencia de la enzima estilbeno sintasa (STS) (K13232) en ambas especies. Estos metabolitos especializados pueden inhibir la alimentación de *G. platensis* en casi un 30% (Campos et al., 2022)

245

confiriendo protección contra herbívoros. Por tanto, una regulación a la baja de estos metabolitos ocasionada por la restricción hídrica pondría a la planta en una situación de predisposición a la defoliación por parte *G. platensis*.

Junto con la biosíntesis de estilbenos el estrés por sequía también afectó la biosíntesis de taninos hidrolizables. En la mayoría de las especies se reguló a la baja el precursor β-glucogallin I (7´) y su isómero **13´** que muestran un descenso de 4.34-fold y 2.33-fold en los genotipos, En1, En2, Eg, En×Egg1, En×Egg3, Ec×Egg y Eb. Por el contrario, el genotipo En×Egg2 regula al alza un éster de ácido gálico, metabolito **10**, mientras los genotipos Eb y Es sobre-expresan el tanino (22). Está reportado que el precursor **7´** y/o **13´** se producen a partir de la conjugación de ácido gálico y una unidad de UDP-glucosa por acción de la enzima UDP-glucosiltransferasa (K23279) (Ono *et al.*, 2016; Tahara *et al.*, 2018) y se localizan principalmente en las paredes de células del mesófilo de las hojas. La síntesis de derivados de taninos generalmente se asocia a su rol frente a la herbivoría por disuasión y/o toxicidad (Barbehenn & Peter Constabel, 2011; Tahara *et al.*, 2018) y al igual que la familia estilbenos su regulación a la baja en genotipos de la especie *E. nitens* y especie híbrida En×Egg significaría un deterioro del metabolismo de defensa de la planta.

Finalmente, importantes ácidos orgánicos presentaron una disminución en su concentración en los genotipos Eg, En1, Ec×Egg y los híbridos En×Egg1, En×Egg2 y En×Egg3, los cuales son considerados precursores de la ruta de fenilpropanoides. Estos son el ácido quínico (2´) y el ácido shíkimico (1´) que fueron regulados a la baja en 2.33-fold y 2.81-fold, respectivamente. El ácido quínico (2´) es el precursor de la ruta del shikimato y, por tanto, se ve perjudicada la síntesis de fenilpropanoides en plantas de *Eucalyptus* bajo estrés hídrico severo.

4.3.5. Conclusiones

Nuestro análisis metabolómico global en combinación con datos fisiológicos de potencial hídrico foliar han proporcionado nuevos conocimientos para comprender las rutas metabólicas en plantas de 7 especies de *Eucalyptus* bajo condiciones de estrés por sequía. Dentro de las especies de estudio se incluyeron las especies de mayor interés comercial y mayormente plantadas como lo son la especie *E. globulus*, *E. nitens* y la especie híbrida *E. nitens* × *E. globulus* (En×Egg). A modo de conclusión podemos afirmar lo siguiente:

- En este trabajo se realizó la identificación de metabolitos que podrían tener una funcionalización como fitoanticipinas en la especie *Eucalyptus* inducido por el estrés hídrico severo. Este es el caso del metabolito monoterpénico Vomifoliol glucósido (2) o Reseoside (PubChem CID: 129316932), derivado del metabolismo del ácido abscísico (ABA) (Strauss *et al.*, 1987; Jerkovic *et al.*, 2011). Se observó una sobreexpresión de Vomifoliol glucósido (2), compuesto que tendría un efecto disuasorio de la herbivoría en *G. platensis* como se presenta en los resultados del apartado 4.2. de está tesis doctoral. Estos resultados indican que bajo estrés hídrico o sequía se induce la acumulación de este compuesto que podría ser utilizado en mecanismos de defensa frente a un estrés biótico.

- En hojas de plantas bajo estrés hídrico se observaron importantes cambios en la biosíntesis de metabolitos secundarios vegetales. Se observó sobreexpresión del metabolismo del almidón y de la sacarosa. Un aumento en la concentración de azúcares solubles o fotosintatos tiene relación con los ajustes fisiológicos de regulación osmótica en plantas de *Eucalyptus* en situación de estrés hídrico severo.

- Fue detectado un importante metabolito como el glucosyl salicilate (21), en plantas estresadas del genotipo En2, que no alcanza a ser significativo en los modelos multivariados. Este compuesto corresponde al glucósido del ácido salicílico. El ácido salicílico es una importante fitohormona involucrada en procesos de crecimiento celular, respiración, cierre de estomas que están correlacionados con el estrés hídrico (Shah, 2003; Loake & Grant, 2007). Por lo cual, la expresión del glucósido del compuesto **21** daría cuenta del deterioro de procesos vitales en la planta.

- El estrés hídrico reguló al alza importantes vías del metabolismo especializado en plantas de *Eucalyptus*. Se sobre-expresó la biosíntesis de terpenos, compuestos que pueden actuar como repelentes o fitotóxinas frente al ataque de patógenos. Por otra parte, se vio un impacto negativo en ciertas vías biosintéticas. Se observó una regulación a la baja del metabolismo de flavonoles, junto con el metabolismo de estilbenos en plantas estresadas. Compuestos

asociados a respuestas defensivas o denominados como fitoalexinas en

este caso fueron afectados por el estrés hídrico en *Eucalyptus.*

Tabla 3. Datos químicos de metabolitos expresados significativamente en las hojas de especies de *Eucalyptus* sometidas a estrés hídrico severo.

No	Rt (min)	Metabolite name	Metabolite class	Mol. formula	ESI (-) Theor m/z	ESI (-) Found m/z	ESI (+) Theor m/z	ESI (+) Found m/z	m/z error (ppm)[a]	MS/MS ESI (-) fragments m/z [adduct] (int. %)	MS/MS ESI (+) fragments m/z [adduct] (int. %)	UV/ Vis (nm)	InChI-Key	Ident. level (A-D)	Species
										Up-regulated metabolites					
1	1.24	Disaccharide	Disacchaide	$C_{12}H_{22}O_{11}$	377.0855	377.0856 [M+Cl]⁻	n.d.	n.d.	0.25, -	377.08(33), 341.1(100), 215.0(12), 179.0(17), 161.0(2), 119.0(1.3)	n.d.	-	SGQJDTLFQCDZGS-UQEKQVNISA-N	B	En×Egg[1,2,3], Eg, En, Es, Eb, EcxEgg
2	11.27	Vomifoliol glucoside (Reseoside)	Monoterpeno glycoside	$C_{20}H_{32}O_{10}$	431.1922	431.1920 [M+HCOOH-H]⁻	n.d.	n.d.	0.41, -	431.1(25), 385.1(100), 223.1(26), 205.1(22), 179.0(5), 161.0(25), 153.0(25), 119.0(2), 113.0(4)	n.d.	-	SWYRVCGNMNAFEK-FALMWEMVSA-N	B	En×Egg[1,2,3], Eg, En, Es, Eb
3	1.25	Dimer of 1	-	$C_{15}H_{20}O_{10}$	719.2021	719.1994 [2M-H]⁻	n.d.	n.d.	2.73, -	377.0(51), 341.1(100), 215.0(15), 179.0(20)	n.d.	-	-	C	EnxEgg[1,2,3], En, Eb, EcxEgg
4	16.47	7-(6-O-Galloyl-beta-D-glucopyranosyloxy)-p-mentha-1-ene-8-ol	Monoterpene glycoside	$C_{23}H_{32}O_{11}$	483.1871	483.1866 [M-H]⁻	n.d.	n.d.	0.80, -	483.1(100), 169.0(17), 151.0(6.8), 125.0(5), 123.0(7)	n.d.	-	HQIYDBBHSXJRLN-MYMBYEKYSA-N	B	En×Egg[1,2,4], EcxEgg
5	11.53	Isomer of 2	Monoterpene glycoside	$C_{20}H_{32}O_{10}$	431.1922	431.1920 [M-H]⁻	n.d.	n.d.	0.71, -	431.1(43), 225.0(9), 223.1(8), 179.0(100), 161.0(22), 149.0(9), 119.0(16), 113.0(18)	n.d.	-	DLJCQAHSSJRRFF-OUUBHVDSSA-N	B	En×Egg[2], Eb
6	11.86	Methylbutyl 6-O-arabinopyranosyl-glucopyranoside	Disaccharide	$C_{16}H_{30}O_{10}$	381.1766	381.1766 [M-H]⁻	n.d.	n.d.	0.15, -	381.1 (100), 249.1 (62)	n.d.	-	IJPILWLAYQFNOD-UQSUZELCSA-N	B	EnxEgg[1,4]
7	19.70	Flavonol acetyl glycoside	Flavonol acetyl glycoside	$C_{33}H_{32}O_{17}$	699.1557	699.1557 [M-H]⁻	701.1721	701.1721 [M+H]⁺	1.21, 3.41	699.1(91), 547.1(15), 529.1(14), 395.1(100), 275.0(66), 169.0(49), 125.0(8)	701(80), 531(32), 379(95), 277(79), 247(80), 153(57)	-	DHFUUYOJSASGHO-LVWVYJEJSA-N	B	EnxEgg[2]
8	1.32	Ascorbic acid	Tricarboxylic acid	$C_6H_8O_6$	175.0248	175.0248 [M-H]⁻	n.d.	n.d.	0.20, -	175 (13), 137 (72), 115 (100)	n.d.	-	CIWBSHSKHKDKBQ-JLAZNSOCSA-N	B	EnxEgg[2]
9	15.60	Dihydro-cypellocarpin A II	Monoterpene	$C_{23}H_{32}O_{12}$	499.1821	499.1818 [M-H]⁻	n.d.	n.d.	0.63	499.1(100), 169.0(69), 125.0(32)	n.d.	-	RZSYEJWKQPWMQI-PTLWZDEXSA-N	B	EnxEgg[2], En1
10	19.45	7-(4-O,6-O-Digalloyl-glucopyranosyloxy)-p-mentha-1-ene-8-ol	gallate	$C_{30}H_{36}O_{15}$	635.1970	635.1970 [M-H]⁻	619.0911	619.0929 [M+H]⁺	0.9, 2.98	635.1(100), 483.1(54), 465.1(4), 313.0(6), 169.0(26), 125.0(5)	153(100)	-	FWAPFRSXNPLGFB-BCNPCBCGSA-N	B	EnxEgg[2]
11	17.34	Eucaglobulin I	Monoterpene	$C_{23}H_{30}O_{12}$	497.1664	497.1659 [M-H]⁻	n.d.	n.d.	1.14, -	497.1 (25), 169.0(100), 125.0(31)	n.d.	-	GMBUWWLCKJYTTG-	B	EnxEgg[4]

251

#	RT	Name	Class	Formula	Calc. (−)	[M-H]⁻ meas.	Calc. (+)	[M+H]⁺ meas.	log	MS/MS (−)	MS/MS (+)		InChIKey		Source
													UHFFFAOYS A-N		
12	17.41	Eucaglobulin II	Monoterpene	C₂₃H₃₀O₁₂	497.1664	497.1659 [M-H]⁻	n.d.	n.d.	1.04, -	497.1(26), 169.0 (100), 125.0 (31)	n.d.	-	GMBUWWLC KJYTTG-UHFFFAOYS A-N	B	EnxEgg⁴
13	18.21	oxochromen-3-yl]oxymethyl]-4,5-dihydroxy-2-methyloxan-3-yl]oxy-3,4,5-trihydroxyoxan-2-yl]methyl acetate	chromone	C₃₀H₃₄O₁₆	649.1774	497.1768 [M-H]⁻	n.d.	n.d.	1.01, -	649.1 (16), 497.1(100), 313.0(7), 211.0(8), 169.0(24), 151.0(9), 125.0(2)	n.d.	-	FGBBNGLAO SZIHL-MPSWIQRPS A-N	B	EnxEgg⁴
14	11.8	Hydrangeifolin I (Benzyl alcohol-rutinoside)	Disaccharide	C₁₉H₂₈O₁₀	461.1664	461.1663 [M+HCOOH-H]⁻	n.d.	n.d.	0.36, -	415.1(100), 269.1(42), 161.0(5)	n.d.	-	SMUMBCRE XHTKFN-VZOUQOBNS A-N	B	EnxEgg⁴
15	8.52	Biflorin	chromenone	C₁₆H₁₈O₉	353.0877	353.0878 [M-H]⁻	355.1018	355.1023 [M+H]⁺	0.86, 1.53	353.0(59), 233.0(100), 205.0(39), 191.0(2), 163.0(5), 119.0(2)	355(40), 337(47), 235(55),205(100)	-	XTZWWMZD VUKEDJ-SPEJKDPOSA -N	B	Eg, EnxEgg¹
16	18.27	Dihydroxy-oxochromen-oxan-trihydroxybenzoate	Chromone	C₂₆H₂₈O₁₃	547.1457	547.1456 [M-H]⁻	549.1602	549.1606 [M+H]⁺	0.01, 0.6	547.1(16), 395.1(49), 275.0(42), 247.0(11), 169.0(100), 125.0(21), 107.0(4)	549(80), 301(), 277(100), 247(39), 153(7.8)	-	DKDRHLHPR DJJRT-UHFFFAOYS A-N	B	Eg
17	16.33	Dihydro-cypellocarpin A I	Monoterpene gallate glycoside	C₂₃H₃₂O₁₂	499.1821	499.1814 [M-H]⁻	n.d.	n.d.	1.38,	499.2(100), 169.0(36), 151.0(8), 125.0(16)	n.d.	278	RZSYEJWKQ PWMQI-PTLWZDEXS A-N	B	Eg, En2
18	21.11	Cypellocarpin C	Acelated phenol glucoside	C₂₆H₃₂O₁₁	565.1926	565.1933 [M+HCOOH-H]⁻	503.1906	503.1911 [M-H₂O+H]⁺	1.20, 1.12	521 (6), 191 (100)	193(100)	220	OUBDJJFZUQ GQLU-ZHFYLPRNS A-N	B	Eg, EnxEgg²
19	11.53	Sacranoside A	Monoterpene glycoside	C₂₀H₃₂O₁₀	431.1922	431.1920 [M-H]⁻	n.d.	n.d.	0.55,-	431.2(66), 179.0(100), 161.0(26), 119.0(7.8)	n.d	-	YLNYTKXAZ SDTJC-PNRJEVNGS A-N	B	En
20	20.65	Cypellogin C	Flavonol glycoside	C₃₁H₃₆O₁₄	631.2032	631.2026 [M-H]⁻	633.2177	633.2179 [M+H]⁺	0.94, 0.19	631.2(61), 300.0(100), 271.0(11), 255.0(8), 243.0(2), 125.0(1.3)	313(22), 303 (100), 123(205)	-	JZWMWNFZJ XHMLJ-HBAAEAASS A-N	B	En2
21	2.74	Salicylic Acid b-D-glucoside	Organic acid	C₁₃H₁₆O₈	299.0771	299.0772 [M-H]⁻	n.d.	n.d.	0.51, -	255.2(15), 232.2(14), 169.0(17), 137.0(100)	n.d.	-	TZPBMNKOL MSJPF-BZNQNGANS A-N	B	En2
22	22.53	Methyl 3,4-dihydroxy-5-prenylbenzoate 3-glucoside	tannin	C₁₉H₂₆O₉	397.1504	397.1499 [M-H]⁻	399.1649	399.1639 [M+H]⁺	0.06, 2.74	397.1(100), 235.0(85), 219.0(1.5), 207.1(41), 191.0(25), 179.0(3.3), 163.0(6)	237(100), 193(3.8), 181(9.5)	221, 299	OZKMIACEG RRXQA-UHFFFAOYS A-N	B	Es, Eb
23	18.56	Methyl 3,4-dihydroxy-5-prenylbenzoate 3-glucoside	tannin	C₁₉H₂₆O₉	397.1500	397.1504 [M-H]⁻	n.d.	n.d.	0.80, -	397.1(100), 235.0(92), 219.0(7), 207.1(70), 191.0(17), 164.0(6)	n.d.	283	OZKMIACEG RRXQA-UHFFFAOYS A-N	B	Es

#	RT	Name	Class	Formula	m/z (calc)	m/z (exp) [M-H]⁻	m/z (calc)+	m/z (exp) [M+H]⁺	Fold	MS/MS (−)	MS/MS (+)	UV	InChIKey	Level	Source
24	1.23	D-(+)-cellobiose	Disacchaide	C₁₂H₂₂O₁₁	341.1089	341.1081 [M-H]⁻	n.d.	n.d.	2.54,	341.1(97), 297.1(88), 179.0(100), 165.0(61), 161.0(37), 149.0(48), 119.0(57)	n.d.	n.d.	GUBGYTABK SRVRQ-QRZGKKJRS A-N	B	Es, EcxEgg
25	17.74	Quercitrin	Flovonol glysocoside	C₂₁H₂₀O₁₁	447.0932	447.0930 [M-H]⁻	449.1078	449.1089 [M+H]⁺	0.32, 2.34	447.0(100), 300.0(68), 271.0(43), 255.0(29), 243.0(20), 227.0(15), 178.9(3), 151.0(6)	287(100)	266, 323	JPUKWEQWG BDDQB-QSOFNFLRS A-N	B	Es
26	1.34	Epimelibiose	Disaccharide	C₁₂H₂₂O₁₁	341.1089	341.1080 [M-H]⁻	n.d.	n.d.	2.75, -	341.1(100), 297.1(47), 191.0(26), 179.0(44), 175.0(39), 165.0(56), 149.0(53), 133.0(69), 115.0(47)	n.d.	-	DLRVVLDZN NYCBX-OVEBFGLAS A-N	B	Eb
27	1.26	Disaccharide (Dimero of **24**)	Disaccharide	C₂₄H₄₄O₂₂	683.2251	683.2256 [M-H]⁻	n.d.	n.d.	0.67, -	683.2(4), 341.1(100), 179.0(9), 161.0(2), 119.0(6)	n.d.	-	-	C	Es, Eb, EcxEgg
28	18.25	5,7-dihydroxy-2-methylpropyl-chromone-C-(galloyl)glucoside	Chromone gallate-C-glycoside	C₂₆H₂₈O₁₃	547.1471	547.1453 [M-H]⁻	549.1602	549.1606 [M+H]⁺	0.68, 0.6	547.1(14), 395.1(42), 305.1(), 275.1(34), 247.1(14), 169.0(100), 125.0(20)	549(100), 301(7), 277(38), 259(11), 247(9), 153(11)	278	DKDRHLHPR DJJRT-UHFFFAOYS A-N	B	EcxEgg

							Down-regulated metabolites								
1′	1.34	Shikimic Acid	Organic acid	C₇H₁₀O₅	173.0455	173.0454 [M-H]⁻	n.d.	n.d.	0.7, -	173.0(53), 137.0(100), 129.0(34), 111.0(40)	n.d.	-	JXOHGGNKM LTUBP-HSUXUTPPS A-N	A	En×Egg[1,2,3], Eg, En, EcxEgg
2′	1.27	Quinic Acid	Organic acid	C₇H₁₂O₆	191.0561	191.0560 [M-H]⁻	n.d.	n.d.	0.27, -	191.0(100), 173.0(5), 127.0(3.3), 111.0(2.40)	n.d.	-	AAWZDTNX LSGCEK-LNVDRNJUS A-N	A	En×Egg[1,3]
3′	16.35	Quercetin-3-O-glucuronide	flavonol	C₂₁H₁₈O₁₃	477.0674	477.0668 [M-H]⁻	479.0820	479.0833 [M+H]⁺	1.4, 2.75	477.0(28), 301.0(100), 283.0(3), 245.0(6), 211.0(1.2), 178.9(6), 151.0(15), 121.0(3)	303 (100), 257(2.4), 229(3), 113(4.7)	256, 354	DUBCCGAQY VUYEU-ZUGPOPFOS A-N	B	En×Egg[1,2,3,4]
4′	16.19	Isoquercitrin	flavonol	C₂₁H₂₀O₁₂	463.0881	463.0879 [M-H]⁻	465.1027	465.1028 [M+H]⁺	0.63, 0.1	463.0(100), 300.0(83), 271.0(75), 255.0(25), 227.0(3.5), 178.9(1.8), 151.0(6)	465(9), 303 (100), 257 (5), 229(7)	256, 354	OVSQVDMC BVZWGM-QSOFNFLRS A-N	A	En×Egg[1,2,4]
5′	17.18	Kaempferol-7-O-glucoside	flavonol	C₂₁H₂₀O₁₁	447.0932	447.0934 [M-H]⁻	449.1078	449.1088 [M+H]⁺	0.22, 2.07	447.0(100), 284.0(26), 255.0(64), 227.0(85), 211.0(3), 183.0(3.9)	287 (100), 213(4)	265, 350	YPWHZCPM OQGCDQ-HMGRVEAOS A-N	B	En×Egg[1,2,4], EcxEgg
6′	17.60	Kaempferol-3-O-glucoside	flavonol	C₂₁H₂₀O₁₁	447.0932	447.0932 [M-H]⁻	449.1078	449.1078 [M+H]⁺	0.24, 0.03	447.1(100), 284.0(49), 255.0(74), 227.0(227), 211.0(), 183.0(2.4), 151.0(2.6)	287 (100), 213(4)	265, 346	JPUKWEQWG BDDQB-QSOFNFLRS A-N	B	En×Egg[1,2,4], Eg, EcxEgg
7′	3.56	β-Glucogallin I	gallate	C₁₃H₁₆O₁₀	331.0670	331.0675 [M-H]⁻	n.d.	n.d.	1.33, -	331.0(2.2), 169.0(100), 125.0(29)	n.d.	-	GDVRUDXLQ BVIKP-DZWWYZIVSA -N	B	En×Egg[1,3]
8′	16.40	Isoquercitrin (isomer of 4′)	flavonol	C₂₁H₂₀O₁₂	463.0881	463.0879 [M-H]⁻	465.1027	465.1078 [M+H]⁺	0.37, 0.1	463.0(100), 300.0(68), 271.0(59), 255.0(23),	465(9), 303 (100), 257 (5), 229(7)	257,	OVSQVDMCB VZWGM-	A	En×Egg[4], Eg, Ec×Egg

253

										227.0(1.8), 178.9(3), 151.0(4)		354	QSOFNFLRSA-N		
9´	15.92	Rutin	Flavonol glycoside	$C_{27}H_{30}O_{16}$	609.1461	609.1452 [M-H]⁻	611.1534	611.1606 [M+H]⁺	1.56, 1.70	609.1(67), 300.0(100), 271.0(13), 178.9(2)	303(100), 129(7)	255, 354	IKGXIBQEEMLURG-NVPNHPEKSA-N	A	Eg
10´	17.13	Kaempferol-3-rutinoside	Flavonol glycoside	$C_{27}H_{30}O_{15}$	593.1511	593.1509 [M-H]⁻	595.1664	595.1657 [M+H]⁺	0.55, 1.10	593.1(95), 324.0(), 284.0(100), 255.0(20), 229.0(6), 227.0(10), 151.0(21)	449(10), 287(100), 129(3)	265, 346	RTATXGUCZHCSNG-QHWHWDPRSA-N	A	Eg
11´	16.20	Isoquercitrin	Flavonol glycoside	$C_{21}H_{20}O_{12}$	463.0881	463.0878 [M-H]⁻	465.1027	465.1028 [M+H]⁺	0.56, 0.1	463.0(100), 300.0(72), 271.0(66), 255.0(30), 243.0(14), 227.0(3), 151.0(5)	465(9), 303 (100), 257 (5), 229(7)	256, 350	OVSQVDMCBVZWGM-QSOFNFLRSA-N	A	Eg
12´	16.72	O-acyl carbohydrate	O-acyl carbohydrate	$C_{19}H_{24}O_{9}$	395.1347	395.1350 [M-H]⁻	397.1493	397.1496 [M+H]⁺	0.67, 0.83	395.1(100), 305.1(), 275.1(80), 247.1(40), 204.0(79), 191.0(6), 163.0()	397(100), 379(56), 361(45), 277(71), 247(40), 206(49)	277	CDSGJPSZVQMWJQ-SOFGYWHQSA-N	B	EnxEgg[1,2], Eg, EcxEgg
13´	1.88	β-Glucogallin II	gallate	$C_{13}H_{16}O_{10}$	331.0670	331.0673 [M-H]⁻	n.d.	n.d.	1.10, -	331.0(100), 271.0(28), 211.0(12), 169.0(39), 151.0(11), 125.0(6)	n.d.	-	GDVRUDXLQBVIKP-DZWWYZIVSA-N	B	Eg, En, Eb, EcxEgg
14´	15.67	*trans*-Piceid	Stilbene glycoside	$C_{20}H_{22}O_{8}$	389.1241	389.1234 [M-H]⁻	391.1388	391.1387 [M+H]⁺	2.16, 0.06	389.1(0.7), 227.1(100), 185.1(9.6), 143.0(6)	391(20), 229(100)	318	HSTZMXCBWJGKHG-CUYWLFDKSA-N	A	En, Es, EnxEgg[3,1]
15´	13.21	*trans*-Astringin	Stilbene glycoside	$C_{20}H_{22}O_{9}$	405.1191	405.1182 [M-H]⁻	407.1336	407.1327 [M+H]⁺	2.36, 2.27	405.1(8), 243.1(100), 201.1(10), 175.1(1.8), 159.0(8.6)	245(100), 227(8), 199(17), 135(15), 107(14)	323	PERPNFLGJXUDDW-CUYWLFDKSA-N	A	En1 y En2
16´	8.03	*trans*-4-p-coumaroylquinic acid	Organic acid	$C_{16}H_{18}O_{8}$	337.0928	337.0928 [M-H]⁻	n.d.	n.d.	0.16, -	337.1(2.66), 191.1(6.9), 163.0(100), 119.0(14)	n.d.	310	BMRSEYFENKXDIS-OTCYKTEZSA-N	B	En2
17´	17.91	*cis*-Piceid	Stilbene glycoside	$C_{20}H_{22}O_{8}$	389.1241	389.1240 [M-H]⁻	229.0832	229.0862 [M+H]⁺	0.42, 1.30	227.1(100), 185.1(9), 159.1(1), 143.0(7)	229(100), 153(17)	282	HSTZMXCBWJGKHG-BUFXCDORSA-N	B	En1, Es, EnxEgg[3,1]
18´	17.59	Resveratrol-4´-(6´´-galloylglucoside)	Stilbene	$C_{27}H_{26}O_{12}$	541.1424	541.1347 [M-H]⁻	n.d.	n.d.	0.76, -	541.1(100), 313.0(11), 227.1(59), 169.0(46), 151.0(8), 125.0(20)	n.d.	270	HQQSMUBDNVIUPF-FIUJFTFBSA-N	B	En2, Es
19´	15.67	Trans-piceid	Adduct of 14´	$C_{21}H_{24}O_{10}$	435.1296	435.1290 [M+HCOOH-H]⁻	391.1388	391.1387 [M+H]⁺	2.09, 0.06	389.1(17), 227.0(100), 185.1(7.8), 143.0(3)	391(20), 229(100)	318	HSTZMXCBWJGKHG-CUYWLFDKSA-N	B	Es
20´	19.59	Gal(b1-4)Xyl(a)-O-Bn	Alkyl glycoside	$C_{18}H_{26}O_{10}$	401.1453	401.1448 [M-H]⁻	n.d.	n.d.	0.97,	401.1(18), 383.1(20), 263.0(), 239.0(4.4), 221.0(100), 193.0(2.4), 178.0(5), 153.0(2.6), 133.0(2)	n.d.	219	SKUMUKAMXQEGMM-HJVNFEKPASA-N	B	Es, Eb

No.	RT	Name	Class	Formula	Theor. mass [-ESI]	Measured mass [-ESI]	Theor. mass [+ESI]	Measured mass [+ESI]	Mass error (-ESI, +ESI)	MS/MS fragments (-)	MS/MS fragments (+)	UV/Vis	InChI-Key	Level	Source
21´	20.82	Auriculoside	Flavanoid glycoside	C$_{22}$H$_{26}$O$_{10}$	403.1398	403.1393 [M+HCOOH-H]⁻	n.d.	n.d.	1.40, -	241.0(100), 225.0(76), 197.0(3.8)	n.d.	239	IJMWYFHXJWRHQH-PSWNVJQFSA-N		Es
22´	19.67	2,3-Dihydroxy-3-methylbutanoic acid 4-(beta-D-glucopyranosyloxy) benzyl ester	Organic acid	C$_{18}$H$_{26}$O$_{102}$	401.1453	401.1449 [M-H]⁻	n.d.	n.d.	1.15, -	401.1(26), 383.1(15), 315.1(1.7), 239.1(3), 221.1(100), 153.0(5)	n.d.	-	CHRIGVPNNGMWMG-IMBWSVPGSA-N	B	Es, Eb
23´	1.19	Leucrose	Disaccharide	C$_{12}$H$_{22}$O$_{11}$	341.1089	341.1092 [M-H]⁻	n.d.	n.d.	0.78, -	341.1(48), 297.1(42), 179.0(100), 175.0(), 165.0(32), 133.0(), 119.0(32), 115.0(), 113.0(), 101.0()	n.d.	-	DXALOGXSFLZLLN-WTZPKTTFSA-N	B	Eb
24´	19.05	Kaempferol-3-O-rhamnoside	flavonol	C$_{21}$H$_{20}$O$_{10}$	431.0983	431.0985 [M-H]⁻	n.d.	n.d.	0.24, -	431.0(70), 285.0(100), 255.0(63), 227.0(63), 211.0(3,3), 183.0(3,3), 151.0(3)	n.d.	256, 350	SOSLMHZOJATCCP-UHFFFAOYSA-N	B	Eb
25´	1.62	Isocitric acid	Organic acid	C$_{6}$H$_{8}$O$_{7}$	191.0197	191.0198 [M-H]⁻	n.d.	n.d.	0.15, -	191.1(11), 129.0(7.5), 111.0(100)	n.d.	-	ODBLHEXUDAPZAU-UHFFFAOYSA-N	B	Eb, EnxEgg2*
26´	16.97	Methoxy-4-hydroxycinnamoyl]-alpha-L-arabinofuranosyl]-alpha-D-xylopyranosyl]-D-xylopyranose	Coumaroyl derivative	C$_{25}$H$_{34}$O$_{16}$	589.1774	589.1766 [M-H]⁻	n.d.	n.d.	1.44, -	413.1(100), 233.1(84), 175.0(58), 115.0(11)	n.d.	-	GAQJLSKAASWGEF-AOYWDDLQSA-N	B	Eb
27´	17.66	Kaempferol 3-glucuronide	Flavonol glycoside	C$_{21}$H$_{18}$O$_{12}$	461.0725	461.0724 [M-H]⁻	463.0871	463.0878 [M+H]⁺	0.39, 1.53	461.1(14), 285.0(100), 257.0(5), 229.0(10), 213.0(1.3), 175.0(4), 113.0(4)	287(100), 213(4), 113(3)	265, 346	FNTJVYCFNVUBOL-ROQVLGAUSA-N	B	EcxEgg
28´	16.65	Globulusin B	Monoterpene gallate glycoside	C$_{23}$H$_{30}$O$_{12}$	497.1667	497.1672 [M-H]⁻	n.d.	n.d.	1.6, -	497.2(100), 211.0(2.63), 169.0(13), 123.0(8), 107.0(0.7)	n.d.	277	DLZSLMKHPDKBHG-HAJNWZPMSA-N	B	EnxEgg[1,4], EcxEgg

[a]: Mean accurate mass error for -ESI and +ESI; *: Metabolite up-regulated in EnxEgg2; UV/Vis: Absorbance maxima; InChI-Key: IUPAC international identifier for chemical according to PubChem; Identification level (A-D): A-standard or NMR, B-MS/MS, C-MS^E, D-MS only; (I), (II): isobaric compounds with similar MS/MS spectrum, n.d.: no detected.

Referencias

Agati G, Azzarello E, Pollastri S, Tattini M. **2012**. Flavonoids as antioxidants in plants: Location and functional significance. *Plant Science* **196**: 67–76.

Ameglio T, Archer P, Cruiziat P, Daudet FA, Valancogne C, Dayau S, Cohen M. **1997**. A limit in the use of predawn leaf water potential for tree irrigation. *Acta Horticulturae* **449**: 431–437.

Barbehenn R V., Peter Constabel C. **2011**. Tannins in plant-herbivore interactions. *Phytochemistry* **72**: 1551–1565.

Berenguer HDP, Alves A, Amaral J, Leal L, Monteiro P, de Jesus C, Pinto G. **2018**. Differential physiological performance of two *Eucalyptus* species and one hybrid under different imposed water availability scenarios. *Trees - Structure and Function* **32**: 415–427.

Bison O, Ramalho MAP, Rezende GDSP, Aguiar AM, De Resende MDV. **2006**. Comparison between open pollinated progenies and hybrids performance in *Eucalyptus grandis* and *Eucalyptus urophylla*. *Silvae Genetica* **55**: 192–196.

Böcker S, Letzel MC, Lipták Z, Pervukhin A. **2009**. SIRIUS: Decomposing isotope patterns for metabolite identification. *Bioinformatics* **25**: 218–224.

Bowles D, Lim EK, Poppenberger B, Vaistij FE. **2006**. Glycosyltransferases of lipophilic small molecules. *Annual Review of Plant Biology* **57**: 567–597.

Brezáni V, Karel Š. **2006**. Secondary metabolites isolated from the genus *Eucalyptus*. *Current Trends in Mecicinal Chemistry* **1**.

C. R. Warren, T. Bledy MAA. **2007**. Changes in gas exchange versus leaf solutes as a means to cope with summer drought in *Eucalyptus marginata*. : 1–10.

Campos J V., Riquelme S, Pecio Ł, Guedes L, Mardones C, Alzamora R, Arteaga-Pérez LE, Rubilar R, Fiehn O, Pérez AJ. **2022**. Constitutive and inducible defense in *Eucalyptus* determines the feeding host of Gonipterus platensis, denoting specific plant-insect coevolution and a strategy for resistance improvement. *Industrial Crops and Products* **189**.

Chong J, Poutaraud A, Hugueney P. **2009**. Metabolism and roles of stilbenes in plants. *Plant Science* **177**: 143–155.

Chong J, Wishart DS, Xia J. **2019**. Using MetaboAnalyst 4.0 for Comprehensive and Integrative Metabolomics Data Analysis Jasmine. *Current Protocols in Bioinformatics* **68**: 1–128.

Correia B, Valledor L, Hancock RD, Renaut J, Pascual J, Soares AMVM, Pinto G. **2016**. Integrated proteomics and metabolomics to unlock global and clonal responses of *Eucalyptus* globulus recovery from water deficit. *Metabolomics* **12**.

Costa E Silva F, Shvaleva A, Maroco JP, Almeida MH, Chaves MM, Pereira JS. **2004**. Responses to water stress in two *Eucalyptus* globulus clones differing in drought tolerance. *Tree Physiology* **24**: 1165–1172.

Dubrovina AS, Kiselev K V. **2017**. Regulation of stilbene biosynthesis in plants. *Planta* **246**: 597–623.

Dührkop K, Fleischauer M, Ludwig M, Aksenov AA, Melnik A V., Meusel M, Dorrestein PC, Rousu J, Böcker S. **2019**. SIRIUS 4: a rapid tool for turning tandem mass spectra into metabolite structure information. *Nature Methods* **16**: 299–302.

Elisa A, Irar S, Majada JP, Rodríguez A. **2013**. Drought tolerance acquisition in *Eucalyptus globulus* (Labill .): A research on plant morphology , physiology and proteomics. *Journal of Proteomics* **79**: 263–276.

González P, Sossa K, Rodríguez F, Sanfuentes E. **2018**. Rhizobacteria strains as promoters of rooting in hybrids of *eucalyptus nitens × eucalyptus globulus*. *Chilean Journal of Agricultural Research* **78**: 3–12.

Goodger JQD, Woodrow IE. **2013**. *Oleuropeic and menthiafolic acid glucose esters from plants: Shared structural relationships and biological activities*. Copyright © 2013 Elsevier B.V. All rights reserved.

Griffin A, Harbard J, Centurion C, Santini P. **2000**. Breeding *Eucalyptus grandis x globulus* and other inter-specific hybrids with high inviability - problem analysis and experience with Shell Forestry projects in Uruguay and Chile. *In: Dungey H.S., Dieters M.J. and Nikles D.G. (eds), Hybrid Breeding and Genetics of Forest Trees. Proceedings of QFRI/CRC-SPF Symposium, 9–14th April 2000 Noosa, Queensland, Australia. Department of Primary Industries, Brisbane*: 1–13.

Gysling AJ. **2017**. *Anuario forestal 2017*.

Hain R, Bieseler B, Kindl H, Schröder G, Stöcker R. **1990**. Expression of a stilbene synthase gene in Nicotiana tabacum results in synthesis of the phytoalexin resveratrol. *Plant Molecular Biology* **15**: 325–335.

Hasegawa T, Takano F, Takata T, Niiyama M, Ohta T. **2008**. Bioactive monoterpene glycosides conjugated with gallic acid from the leaves of *Eucalyptus globulus*. *Phytochemistry* **69**: 747–753.

Hoffmann MA, Nothias L-F, Ludwig M, Fleischauer M, Gentry EC, Witting M, Dorrestein PC, Dührkop K, Böcker S. **2021**. Assigning confidence to structural annotations from mass spectra with COSMIC. *bioRxiv*: 2021.03.18.435634.

Huseynova IM, Aliyeva DR, Aliyev JA. **2013**. Plant responses to stresses: Role of ascorbate peroxidase in the antioxidant protection. *Peroxidases: Biochemical Characteristics, Functions and Potential Applications*: 142–158.

Imadi SR, Gul A, Dikilitas M, Karakas S, Sharma I, Ahmad P. **2016**. Water stress: Types, causes, and impact on plant growth and development. *Water Stress and Crop Plants: A Sustainable Approach* **2–2**: 343–355.

Jan R, Asaf S, Numan M, Lubna, Kim KM. **2021**. Plant secondary metabolite biosynthesis and transcriptional regulation in response to biotic and abiotic stress conditions. *Agronomy* **11**: 1–31.

Jeandet P, Delaunois B, Conreux A, Donnez D, Nuzzo V, Cordelier S, Clément C, Courot E. **2010**. Biosynthesis, metabolism, molecular engineering, and biological functions of stilbene phytoalexins in plants. *BioFactors* **36**: 331–341.

Jerkovic I, Marijanovic Z, Staver MM. **2011**. Screening of natural organic volatiles from prunus mahaleb L. honey: Coumarin and vomifoliol as nonspecific biomarkers. *Molecules* **16**: 2507–2518.

Kröner A, Marnet N, Andrivon D, Val F. **2012**. Nicotiflorin, rutin and chlorogenic acid: Phenylpropanoids involved differently in quantitative resistance of potato tubers to biotrophic and necrotrophic pathogens. *Plant Physiology and Biochemistry* **57**: 23–31.

Külheim C, Moran GF, Laffan S, Yeoh SH, Wallis IR, Foley WJ. **2011**. The molecular basis of quantitative variation in foliar secondary metabolites in *Eucalyptus globulus*. *New Phytologist* **191**: 1041–1053.

Kumar M, Patel MK, Kumar N, Bajpai AB, Siddique KHM. **2021**. Metabolomics and molecular approaches reveal drought stress tolerance in plants. *International Journal of Molecular Sciences* **22**.

Lanfranco D, Dungey HS. **2001**. Insect damage in *Eucalyptus*: a review of plantations in Chile. *Austral Ecology* **26**: 477–481.

Loake G, Grant M. **2007**. Salicylic acid in plant defence-the players and protagonists. *Current Opinion in Plant Biology* **10**: 466–472.

Madhibha T, Murepa R, Musokonyi C, Gapare W. **2013**. Genetic parameter estimates for interspecific *Eucalyptus* hybrids and implications for hybrid breeding strategy. *New Forests* **44**: 63–84.

Morcol TB, Wysocki K, Sankaran RP, Matthews PD, Kennelly EJ. **2020**. UPLC-QTof-MSEMetabolomics Reveals Changes in Leaf Primary and Secondary Metabolism of Hop (Humulus lupulus L.) Plants under Drought Stress. *Journal of Agricultural and Food Chemistry* **68**: 14698–14708.

Navarrete-Campos D, Le Feuvre R, Balocchi C, Valenzuela S. **2017**. Overexpression of three novel CBF transcription factors from

Eucalyptus globulus improves cold tolerance on transgenic Arabidopsis thaliana. *Trees - Structure and Function* **31**: 1041–1055.

Neilson EH, Goodger JQD, Woodrow IE, Møller BL. **2013**. Plant chemical defense: At what cost? *Trends in Plant Science* **18**: 250–258.

Ono NN, Qin X, Wilson AE, Li G, Tian L. **2016**. Two UGT84 family glycosyltransferases catalyze a critical reaction of hydrolyzable tannin biosynthesis in pomegranate (Punica granatum). *PLoS ONE* **11**: 1–25.

Potts BM, Dungey HS. **2004**. Interspecific hybridization of *Eucalyptus*: Key issues for breeders and geneticists. *New Forests* **27**: 115–138.

Rangel Sánchez G, Castro Mercado E, Beltran Peña E, Reyes de la Cruz H, García Pineda E. **2010**. El acido salicílico y su participación en la resistencia a patógenos en plantas. *Biológicas* **12**: 90–95.

Rezende GDSP, de Resende MD V., de Assis TF. **2014**. *Eucalyptus Breeding for Clonal Forestry*.

Rubilar R, Hubbard R, Emhart V, Mardones O, Quiroga JJ, Medina A, Valenzuela H, Espinoza J, Burgos Y, Bozo D. **2020**. Climate and water availability impacts on early growth and growth efficiency of *Eucalyptus* genotypes: The importance of GxE interactions. *Forest Ecology and Management* **458**: 117763.

Shah J. **2003**. The salicylic acid loop in plant defense. *Current Opinion in Plant Biology* **6**: 365–371.

Shvaleva AL, Costa F, Breia E, Jouve L, Hausman JF, Almeida MH, Maroco JP, Rodrigues ML, Pereira JS, Chaves MM. **2006**.

Metabolic responses to water deficit in two *Eucalyptus globulus* clones with contrasting drought sensitivity. *Tree Physiology* **26**: 239–248.

Singh A, Baker PJ, Kasel S, Trouvé R, Stewart SB, Nitschke CR. **2021**. The role of climatic variability on *Eucalyptus* regeneration in southeastern Australia. *Global Ecology and Conservation* **32**.

Spokevicius A V., Tibbits J, Rigault P, Nolin MA, Müller C, Merchant A. **2017**. Medium term water deficit elicits distinct transcriptome responses in *Eucalyptus* species of contrasting environmental origin. *BMC Genomics* **18**: 1–17.

Strauss CR, Wilson B, Williams PJ. **1987**. 3-oxo-α-ionol, vomifoliol and roseoside in Vitis vinifera fruit. *Phytochemistry* **26**: 1995–1997.

Tahara K, Nishiguchi M, Frolov A, Mittasch J, Milkowski C. **2018**. Identification of UDP glucosyltransferases from the aluminum-resistant tree Eucalyptus camaldulensis forming β-glucogallin, the precursor of hydrolyzable tannins. *Phytochemistry* **152**: 154–161.

Tibbits WN, Hodge GR. **2003**. Genetic Parameters for Cold Hardiness in *Eucalyptus nitens* (Deane & Maiden) Maiden. *Silvae Genetica* **52**: 89–97.

Valdés AE, Irar S, Majada JP, Rodríguez A, Fernández B, Pagès M. **2013**. Drought tolerance acquisition in *Eucalyptus globulus* (Labill.): A research on plant morphology, physiology and proteomics. *Journal of Proteomics* **79**: 263–276.

Villar E, Klopp C, Noirot C, Novaes E, Kirst M, Plomion C. **2011**. RNA-Seq reveals genotype-specific molecular responses to water deficit in *eucalyptus*.

Volker PW, Potts BM, Borralho NMG. **2008**. Genetic parameters of intra- and inter-specific hybrids of *Eucalyptus globulus* and *E. nitens*. *Tree Genetics and Genomes* **4**: 445–460.

Warren CR, Aranda I, Cano FJ. **2011**. Responses to water stress of gas exchange and metabolites in Eucalyptus and Acacia spp.: 1609–1629.

White D a, Beadle CL, Worledge D. **1996**. Seasonal, Drought and Species Effects. *Tree Physiology* **16**: 469–476.

White DA, Crombie DS, Kinal J, Battaglia M, McGrath JF, Mendham DS, Walker SN. **2009**. Managing productivity and drought risk in Eucalyptus globulus plantations in south-western Australia. *Forest Ecology and Management* **259**: 33–44.

Yang L, Fountain JC, Ji P, Ni X, Chen S, Lee RD, Kemerait RC, Guo B. **2018**. Deciphering drought-induced metabolic responses and regulation in developing maize kernels. *Plant Biotechnology Journal* **16**: 1616–1628.

Zeevaart JAD, Creelman RA. **1988**. Metabolism and Physiology of Abscisic Acid. *Annual Review of Plant Physiology and Plant Molecular Biology* **39**: 439–473.

CAPITULO 5: CONCLUSIONES GENERALES

En esta tesis doctoral se estudió el efecto de factores como el estrés por sequía y el daño por herbivoría producida por *Gonipterus platensis* sobre el metabolismo especializado en especies de *Eucalyptus* de gran interés comercial a través de un enfoque metabolómico basado en UHPLC-QTOF-MS/MS.

En primera instancia se determinó la preferencia alimentaria de *G. platensis* por la especie *E. globulus* por sobre *E. nitens*, evidenciando que la ausencia de ciertos metabolitos constitutivos en las hojas de *E. globulus*, especialmente estilbenos y taninos hidrolizables, son responsables de la susceptibilidad de esta especie y de su mayor palatabilidad frente al insecto. Estos resultados demostraron la diferencia constitutiva entre ambas especies, y sugirió la falta de enzimas claves como estilbeno sintasa (STS) y la galato 1-β-glucosiltransferasa en *E. globulus*. Por otra parte, tras la herbivoría no se activó la biosíntesis de estilbenos o galatos en la especie *E. globulus*.

En relación con lo anterior, en un segundo enfoque se determinó que la especie híbrida *E. nitens* × *E. globulus* (En×Egg) posee la capacidad enzimática de producir estilbenos de forma constitutiva heredada por el

264

progenitor resistente, *E. nitens*, un atributo metabólico esencial del cual carece *E. globulus*. Por su parte, se demostró que los genotipos híbridos pueden desplegar su capacidad de biosíntesis de estilbenos para potenciar metabolitos como *trans*-Piceid en respuesta a la herbivoría de forma significativa. En consecuencia, los híbridos de la especie En×Egg pueden mostrar mejor resistencia a la herbivoría de *G. platensis* que *E. globulus,* pero peor que *E. nitens*, lo cual coincide con la severidad de defoliación experimentada por los árboles en campo. Sin embargo, a pesar de dicho rasgo metabólico la imputación de resistencia en los genotipos híbridos no está basada solo en los estilbenos constitutivos o en la acumulación inducida de estos. Sino mas bien se determinó que existía una correlación con la regulación a la baja del compuesto monoterpénico Reseoside (Vomifoliol glucósido) y la severidad de la defoliación causada por *G. platensis*. Vomifoliol glucósido (PubChem CID: 129316932) es un metabolito derivado del metabolismo del ácido abscísico (ABA) y posee una estructura similar a este. En la mayoría de los genotipos híbridos, Vomifoliol glucósido fue significativamente regulado a la baja en respuesta a la herbivoría, lo que sugirió su posible hidrólisis para liberar la molécula activa, Vomifoliol. De este modo, se demostró que entre mayor fue el valor absoluto de Fold-change,

265

mejor fue la protección en contra de la defoliación ocasionada por *G. platensis*. Vomifoliol es un metabolito lipofílico, y es altamente probable que luego de su liberación, este sea secuestrado en las cavidades oleosas de las hojas de *Eucalyptus* como una fitoanticipina con efecto fitotóxico, desde donde ejecuta su efecto disuasorio.

Finalmente, se realizó un análisis metabolómico a seis especies de *Eucalyptus* sometidas a estrés hídrico severo, con el fin de brindar nuevos conocimientos a cerca de rutas metabólicas involucradas en la respuesta al estrés por sequía. En los resultados obtenidos se observó una sobreexpresión del metabolismo del almidón y de la sacarosa, observándose un aumento en la concentración de azúcares solubles o fotosintatos, los cuales participan en ajustes fisiológicos referentes a la regulación osmótica en plantas deshidratadas. Junto con una sobreexpresión de la biosíntesis de terpenos, compuestos reportados por sus características repelentes o fitotóxicas frente al ataque de patógenos. Por otra parte, el estrés por sequía tuvo un impacto negativo en ciertas rutas biosintéticas. Se reguló a la baja la síntesis de flavonoles y estilbenos. Estos compuestos generalmente son asociados a las respuestas defensivas de las plantas.

Junto con estos cambios en el metabolismo de plantas estresadas se evidencio la regulación al alza de la biosíntesis de un metabolito que podría tener funcionalización de fitoanticipina en árboles de la especie *Eucalyptus*, esto inducido por el estrés hídrico severo. Este es el caso de Vomifoliol glucósido (Reseoside), que se vio sobre-expresado en todos los genotipos a excepción del genotipo híbrido EnxEgg4. Como se reportó anteriormente este compuesto tendría un efecto disuasorio de la herbivoría en *G. platensis*. Finalmente, respondiendo a la hipótesis planteada en está tesis doctoral podemos destacar:
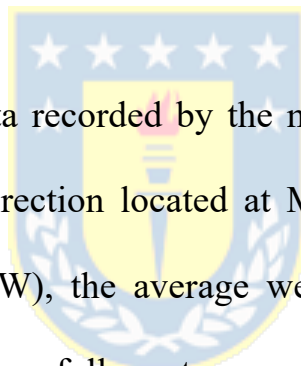
- El estrés hídrico tiene incidencia sobre la biosíntesis de metabolitos secundarios no-volátiles en la planta, afectando la biosíntesis de fenilpropanoides, como flavonoles y estilbenos lo que podría generar una predisposición a la defoliación por *G. platensis.*

- Por otra parte, bajo estrés hídrico o sequía se induce la acumulación del compuesto Vomifoliol glucósido (Reseoside), que podría ser utilizado por la planta en mecanismos de defensa frente a un potencial ataque del insecto defoliador *G. platensis*, lo que sienta las bases de una resistencia adquirida por parte de la especie *Eucalyptus*.

ANEXOS

1. **Supplementary Material: Constitutive and inducible defense in Eucalyptus determines the feeding host of *Gonipterus platensis*, denoting specific plant-insect coevolution and a strategy for resistance improvement.**

Method S1. Climatic conditions during sampling.

According to the data recorded by the meteorological station of the Chilean Meteorological Direction located at María Dolores, Los Angeles (37°24′10.0″S 72°25′21.0″W), the average weather conditions in August 2018 at Nacimiento were as follow: temperatures during the day, 14°C maximum and 3.6°C minimum; 37% of rainfall likelihood, with accumulated rain of 91.2 mm (21.9 mm/24 hours maximum); sunlight periods get longer from beginning to the end of the month, with 2 min and 3 sec of daily increases, and began with 10 hours and 14 min and ended with 11 hours and 15 min length; radiation energy including UV-Visible light ranged between 2.4 kWh m^{-2} and 3.6 kWh m^{-2}; relative humidity was of 89.8%.

Method S2. Biomarker extraction and purification.

Freeze-dried and powdered *E. nitens* leaves (100 g) collected as described in section 2.1 of the manuscript, were subjected to extraction with ethyl acetate under reflux for 2 hours. The obtained solution was filtered, concentrated to dryness, resuspended in distilled water, frozen, and then lyophilized to yield a yellowish powder extract. Five grams of this extract were fractionated using open column chromatography on a 9.5 cm × 4.3 cm i.d. glass column packed with 25-40 μm LiChroprep RP-18 (Merck, Darmstadt, Germany), and eluted with MeOH/H_2O (5:95, 20:80, 80:20, 100:0; 500 ml each, v/v). Fractions eluted with 80% MeOH (F80) and 100% MeOH (F100) were the most abundant, with 44% (2.2 g) and 20% (1.0 g) of the total extract, respectively. The desired composition of the extract and fractions were confirmed after LC-MS analysis under the same conditions as described in section 2.3 of the manuscript (Fig. S1). The major fraction, F80, contained the set of *E. nitens* differential metabolites (**1-12**), with limited interferences of polar and lipophilic substances (Fig. S1b).
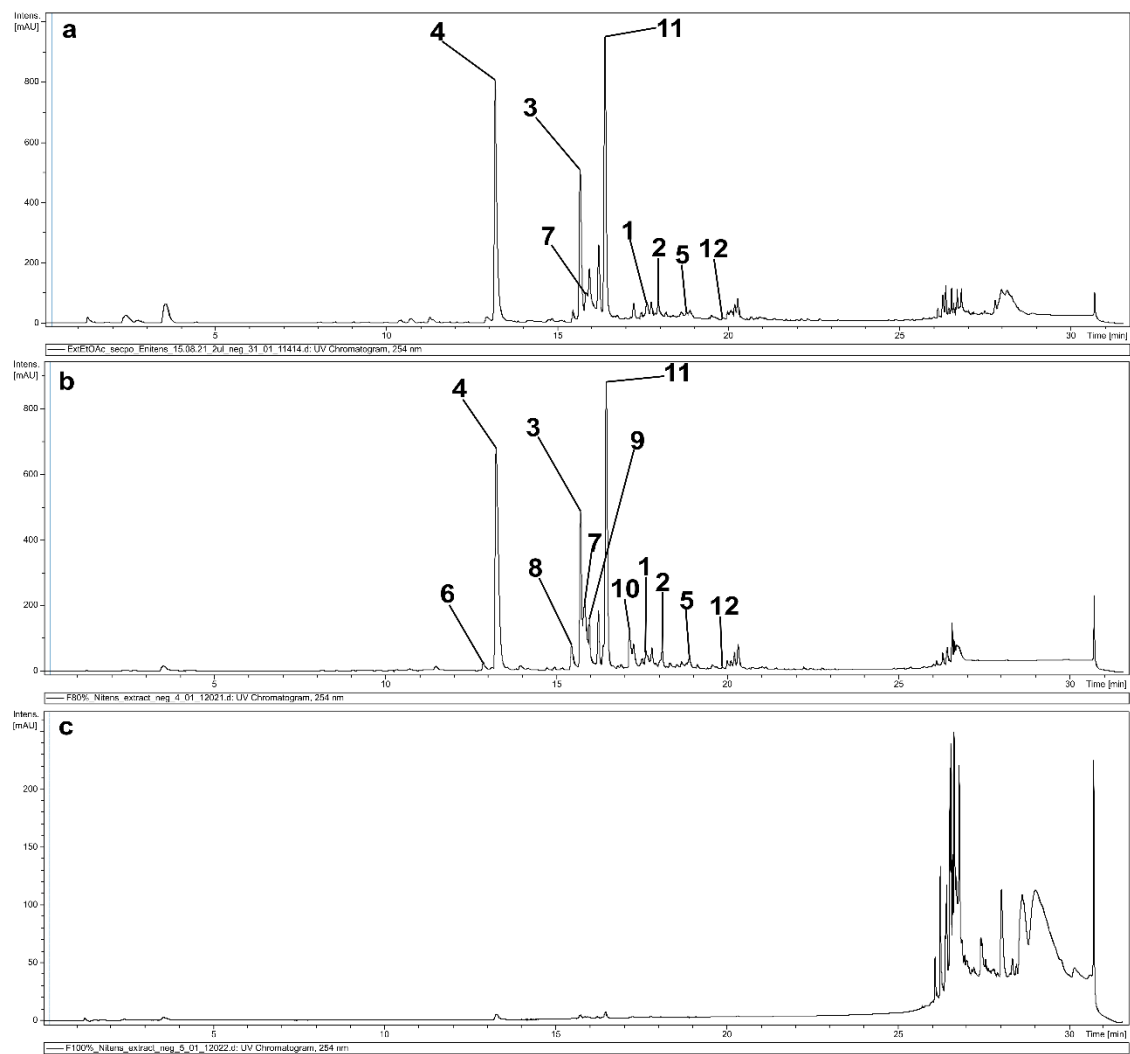
Figure S1. Confirmation of desired composition of the *E. nitens* leaves extract and fractions by LC-MS/UV-Vis analysis. (**a**) LC-UV chromatogram (254 nm) of the ethyl acetate extract with the peaks of significant metabolites labeled according to their assigned number. (**b**) LC-UV chromatogram (254 nm) of fraction F80 containing the desired metabolites without polar substances (earlier retention times) and with reduced amounts of lipophilic

substances (longest retention times). (**c**) LC-UV chromatogram (254 nm) of fraction F100 containing solely the lipophilic substances.

Figure S2. Evaluation of the *G. platensis* feeding choice between *E. globulus* branches containing treated and control leaves. Photos were taken at the end of the assay after 24 h of exposure in a 45×60×45 cm (length/width/height) transparent cage. (**a**) Photo of the whole cage space, with a flask containing twelve sprayed leaves at right, a flask with twelve control leaves at left, and equidistant from them a smaller yellow cage from which 180 weevils were released. (**b**) Photo of the control leaves showing a more significant number of weevils settled in branches and a more massive amount of feces in the ground. (**c**) Photo of the sprayed leaves showing a lower number of weevils and less amount of feces in the ground.

Feeding Inhibition in Branches (24 h)
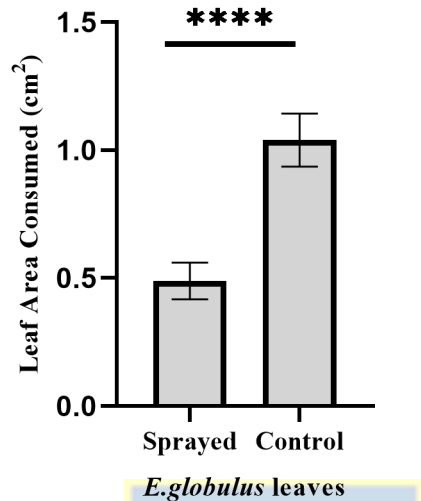
Figure S3. Results of the *G. platensis* feeding choice between *E. globulus* leaves sprayed with purified fraction obtained from *E. nitens* leaves at 20 g l⁻¹, and control leaves, in 24 h. The absolute values for the leaf area consumed by *G. platensis* in cm² are presented along the *y*-axis. Weevil consumption in Treated and Control *E. globulu*s leaves is shown in the *x*-axis as grey bars of mean with SEM, where 0.49 ± 0.072 cm² and 1.04 ± 0.104 cm² were registered in treated and control leaves, respectively. The horizontal line with four asterisks indicates significantly different consumption between treated and control leaves with a *p*-value of 0.0001 for a non-parametric Mann-Whitney test with statistical significance set for $p < 0.05$. Antifeedant index

(AFI) calculated with mean values was 0.36, which indicated a 36% of feeding inhibition in treated leaves.
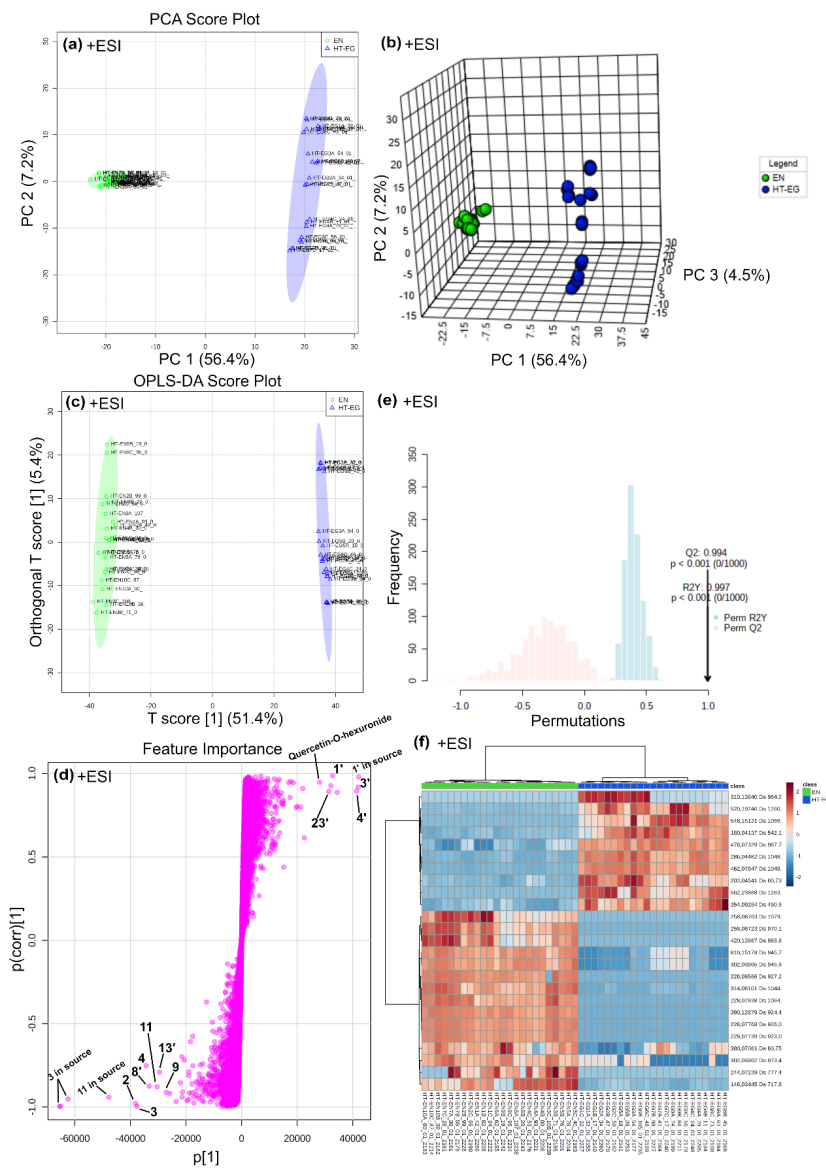
Figure S4. Statistical treatment results of the LC-MS dataset acquired in +ESI mode for distinguishing differential leaves metabolome constitutively

expressed in *E. nitens* (EN) concerning *E. globulus* (HT-EG). (**a**) PCA

score plot showing species-specific cluster pattern between the first two

principal components (PC1 and PC2), where green circles and blue

triangles represent samples from EN and HT-EG, respectively, with their

95% confidence intervals (shadowed regions). (**b**) The same PCA score plot

but incorporating the third PC for a 3D projection of sample distributions.

(**c**) Score plot of the OPLS-DA model showing separation of samples

labeled as EN from that of HT-EG with their 95% confidence intervals

(shadowed regions). The regression method used LC-MS data as the *X*, and

the binary vector *Y* formed with a value of 0 for EN class and 1 for HT-EG

class. The *Y*-predictive component (T score [1]) shown on the *x*-axis

represents the variation in the dataset correlated to class separation, while

the orthogonal component shown on the *y*-axis refers to the uncorrelated

variation for class distinction. (**d**) S-plot of the OPLS-DA model for

visualizing the feature influence in the predictive component, combining

covariance (p[1]) and correlation (p(corr)[1]) loading profiles. Covariance

plotted on the *x*-axis visualizes the contribution to the predictive

component, while correlation on the *y*-axis spans between ±1 as the

reliability has a theoretical minimum of -1 and a maximum of +1 to predict

class 1 (HT-EG). Thus, features visualized on the left-hand side contribute to class separation by high correlation with label EN ($Y = 0$) and the opposite. In this way, significant features were selected by combining high covariance (> |2500|) and high correlation (> |0.5|), and their numbers were assigned according to Table 1. (**e**) Validation of the OPLS-DA model by a random permutation test of class membership with 1000 permutations and internal cross-validation, showing the observed original model statistics (black arrow), cross-validated R^2Y and Q^2 coefficients, and distribution statistics for all permutations. (**f**) Hierarchical cluster analysis presented as a heatmap for the 25 top features according to PLS-DA variable important in projection (VIP) using Euclidean distance for similarity measure and Ward's linkage algorithm for clustering. Colors of cells indicate relative concentration values as high (dark brown) and low (dark blue), with samples in columns and features (exact mass in Da and Rt in seconds) in rows.

(a)　　　　　　　　　　　**(b)**

Figure S5. Results of the cross-validated random permutation test with 1000 permutations for the OPLS-DA models between HT-EG and IT-EG in -ESI (**a**) and +ESI (**b**) acquisition modes.

Pathway	Metabolites
Flavone and flavonol biosynthesis	C05903; C01477; C05623; C01750; C12249; C16911; C00389; C01514; C05625; C19796; C21833; C21854

Pathway	Metabolites
Stilbenoid, diarylheptanoid and gingerol biosynthesis	C00540; C00223; C02947; C10434; C12208; C00852; C00323; C03582; C00406; C10287; C17743

Pathway	Metabolites
Phenylpropanoid biosynthesis	C00082; C00079; C05610; C02666; C00590; C01494; C12208; C02947; C00223; C00852; C05839; C12203; C00482; C05619; C01197; C00811; C00323; C00411; C00406; C12204; C05608; C02325; C12205; C00423; C00540; C10945; C10434; C02646; C05838; C00903; C12206

Figure S6. Metabolite hits in the three most significant pathways according to the functional MS-Peak-to-Pathway analysis based on the -ESI MS data, using *Oryza sativa* as the model plant species. KEGG IDs of mapped metabolites in red were significant hits in the data, those in blue were non-significant hits, and those in grey were not found in the input data. For the pathway of *Stilbenoid, diarylheptanoid and gingerol biosynthesis*, significant hits were *p*-Coumaroyl quinic acid (C12208), Caffeoyl-quinic acid (C00852), and Resveratrol (C03582).

Table S1. Expression data of constitutive differential metabolites in the leaves of *E. nitens* compared to *E. globulus*.

Metabolite number/name	identifier	System code	Fold Change "EN"/"HT-EG"	log2FC	p-value	Type
1	CHEMBL480304	Cl	29,952	4,9046	0,00000010	Metabolomics
2	CHEBI:76155	Ce	204,403	7,6753	0,00000010	Metabolomics
3	CHEBI:8198	Ce	44,399	5,4725	0,00000010	Metabolomics
4	CHEBI:2899	Ce	69,946	6,1282	0,00000010	Metabolomics
5	64898-03-9	Ca	99,021	6,6297	0,00000010	Metabolomics
6	CHEBI:27395	Ce	5,09	2,3477	0,00000010	Metabolomics
7	HZCOWROLPVDVCR-XMPPFBFMSA-N	Ik	84,127	6,3945	0,00000010	Metabolomics
8	CHEBI:17527	Ce	6,498	2,7000	0,00000010	Metabolomics
9	CHEBI:28527	Ce	3,049	1,6083	0,07000000	Metabolomics
10	CHEBI:18082	Ce	7,304	2,8687	0,00000010	Metabolomics
11	CHEBI:8824	Ce	102,903	6,6851	0,00000010	Metabolomics
12	2111182-67-1	Ca	75,156	6,2318	0,00000010	Metabolomics
Gallic acid	CHEBI:30778	Ce	1,684	0,7519	0,00000010	Metabolomics
Glucogallin	CHEBI:15834	Ce	29,952	4,9046	0,00000010	Metabolomics
1,6-diGaGlc	CHEBI:15723	Ce	27,288	4,7702	0,00000010	Metabolomics
Kaempferol	CHEBI:28499	Ce	0,425	-1,2345	0,00000020	Metabolomics
Quercetin	CHEBI:16243	Ce	0,959	-0,0604	0,68100000	Metabolomics
Skimic acid	CHEBI:16119	Ce	0,805	-0,3129	0,13900000	Metabolomics

EN: *Eucalyptus nitens*; HT-EG: *E. globulus* without herbivory.
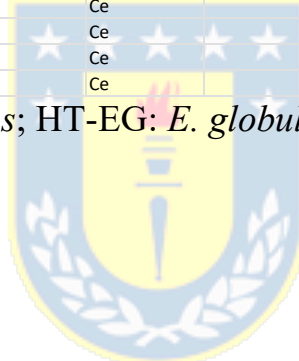
Table S2. Expression data for the metabolites that significantly changed their levels in the leaves of *E. globulus* upon herbivory of *G. platensis*.

Metabolite number/name	Identifier	System code	Fold Change "IT-EG"/"HT-EG"	log2FC	p-value	Type
glucogallin	CHEBI:15834	Ce	0,845	-0,2430	0,0084	Metabolomics
Gallic acid	CHEBI:30778	Ce	2,268	1,1814	0	Metabolomics
Prunasin	CHEBI:25150	Ce	11000	13,4252	0	Metabolomics
11'	BYILEHCAHZEAIX-IHGRRFEYSA-N	Ik	12839	13,6482	0	Metabolomics
Phenylalanine	CHEBI:17295	Ce	1,371	0,4552	0,00048	Metabolomics
eucalmaidin A	COVZIUXOQFAJNB-QUMMREBQSA-N	Ik	2,196	1,1349	0,000001	Metabolomics
Kaempferol	CHEBI:28499	Ce	1,971	0,9789	0,000024	Metabolomics
Quercetin	CHEBI:16243	Ce	2,939	1,5553	0	Metabolomics
Astragalin	CHEBI:30200	Ce	1,195	0,2570	0,400257	Metabolomics
Shikimic acid	CHEBI:16119	Ce	1,14	0,1890	0,278013	Metabolomics
24'	CHEBI:17382	Ce	0,433	-1,2076	0	Metabolomics
pyridoxal	CHEBI:17310	Ce	0,629	-0,6689	0	Metabolomics
pyridoxine	CHEBI:16709	Ce	0,571	-0,8084	0,000001	Metabolomics
tyrosine	CHEBI:17895	Ce	0,595	-0,7490	0	Metabolomics
1'	CHEBI:75721	Ce	0,757	-0,4016	0	Metabolomics
17'	SWYRVCGNMNAFEK-PUVRWCMWSA-N	Ik	0,679	-0,5585	0,000002	Metabolomics
Vomifoliol	CHEBI:28258	Ce	1,702	0,7672	0,003198	Metabolomics
2'	CHEBI:17521	Ce	0,681	-0,5543	0,0034	Metabolomics
12'	CHEBI:4775	Ce	1,302	0,3807	0	Metabolomics
8'	ANUSKTCURGICPQ-JTNJOIGYSA-N	Ik	1,886	0,9153	0,000362	Metabolomics
13'	CHEBI:28299	Ce	1,911	0,9343	0,000043	Metabolomics
15'	PSBFVXDMNYDZMV-SMTCTBLTSA-N	Ik	2,86	1,5160	0	Metabolomics
10'	GUDLVBZWVXAHOX-ZWQPYCCRSA-N	Ik	1,609	0,6862	0,000009	Metabolomics
14'	XJYKKSWBSUUWAV-MJFDLWPTSA-N	Ik	1,729	0,7899	0,000001	Metabolomics
9'	CHEBI:69657	Ce	2,766	1,4678	0,000003	Metabolomics
9	CHEBI:28527	Ce	2,623	1,3912	0	Metabolomics
23'	OUBDJJFZUQGQLU-ZHFYLPRNSA-N	Ik	0,551	-0,860	0,000001	Metabolomics
18' y 19'	GMBUWWLCKJYTTG-UHFFFAOYSA-N	Ik	0,574	-0,801	0,000029	Metabolomics
16'	CHEBI:30887	Ce	0,742	-0,431	0,000001	Metabolomics
6'	QIYRQEHCCPTEPY-VJOHEAABSA-N	Ik	0,808	-0,308	0,190164	Metabolomics
7'	DLZSLMKHPDKBHG-HAJNWZPMSA-N	Ik	1,248	0,320	0,02076	Metabolomics

IT-EG: *Eucalyptus globulus* under herbivory; HT-EG: *E. globulus* without herbivory.
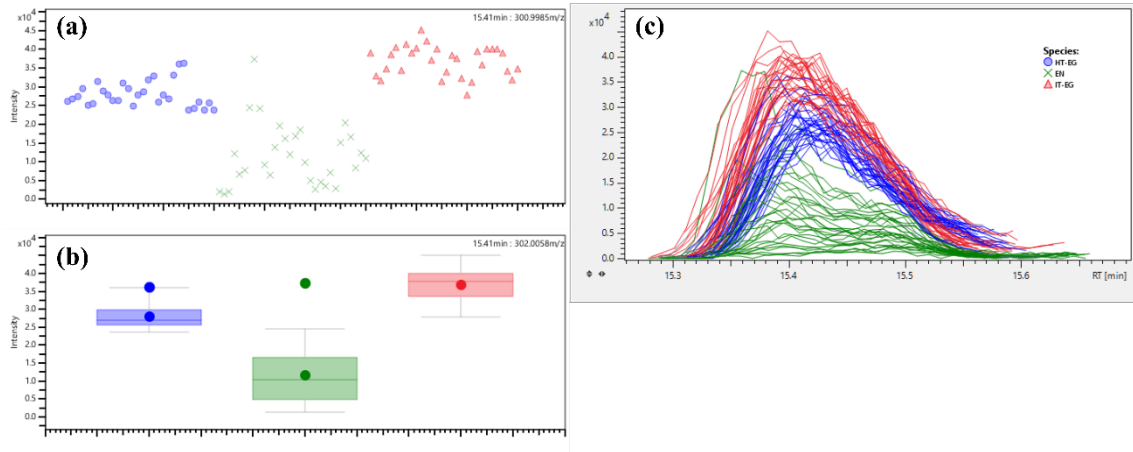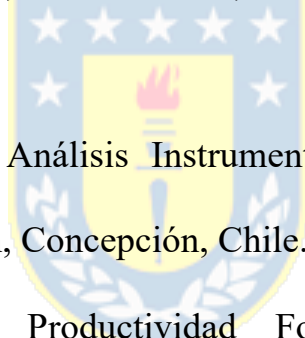
Figure S7. Different plots showing the Ellagic acid (**12′**) accumulation levels in the leaves of both *E. globulus* trees before herbivory (blue) and under herbivory (red), as well as in the leaves of *E. nitens* (green). (**a**) Bucket statistic view showing the absolute ellagic acid ion intensity found in each sample. (**b**) Box plot showing the degree of dispersion and median of ellagic acid content within each group. (**c**) Extracted ion chromatogram for the aligned peaks of Ellagic acid at 15.41 min in each sample.

2. **Supplementary Material: Exploring inherent defensive traits in *Eucalyptus* inter-specific hybrids to combat herbivory by *Gonipterus platensis* and enable genotype selection for building resistance.**

Jasna V. Campos [a], Rafael Rubilar [b], Rosa Alzamora [c], Luis E. Arteaga-Pérez [d], Claudia Mardones [a], Oliver Fiehn [e], Andy J. Pérez [a, *].

[a] Departamento de Análisis Instrumental, Facultad de Farmacia, Universidad de Concepción, Concepción, Chile.

[b] Cooperativa de Productividad Forestal, Departamento de Silvicultura, Facultad de Ciencias Forestales, Universidad de Concepción, Concepción, Chile.

[c] Departamento Manejo de Bosques y Medio Ambiente, Facultad de Ciencias Forestales, Universidad de Concepción, Concepción, Chile.

[d] Laboratory of Thermal and Catalytic Processes (LPTC), Department of Wood Engineering, University of Bío-Bío, Chile.

[e] NIH West Coast Metabolomics Center, UC Davis Genome Center, University of California, Davis, CA 95616, USA.

* Corresponding author E-mail: aperezd@udec.cl (A.J. Pérez). Phone: +56 41 220 3027

Fig. S1. Experimental field located at the nursery garden "Carlos Douglas" owned by Forestal Mininco S.A., from which plant material was collected in 2019. It comprises an area of 4678 m^2, planted in 2017 with different *Eucalyptus* species, including pure *E. nitens*, *E. globulus*, and their

F1 hybrids. Two lines of plants (Buffer lines) were also planted around the field boundary to avoid the border effect on genotypes of interest. The approximate location for the plots of sampled genotypes is shown by their corresponding code (i.e., Eng2 corresponds to *En×Egg*2). Letters A, B, and C represent the replicates.
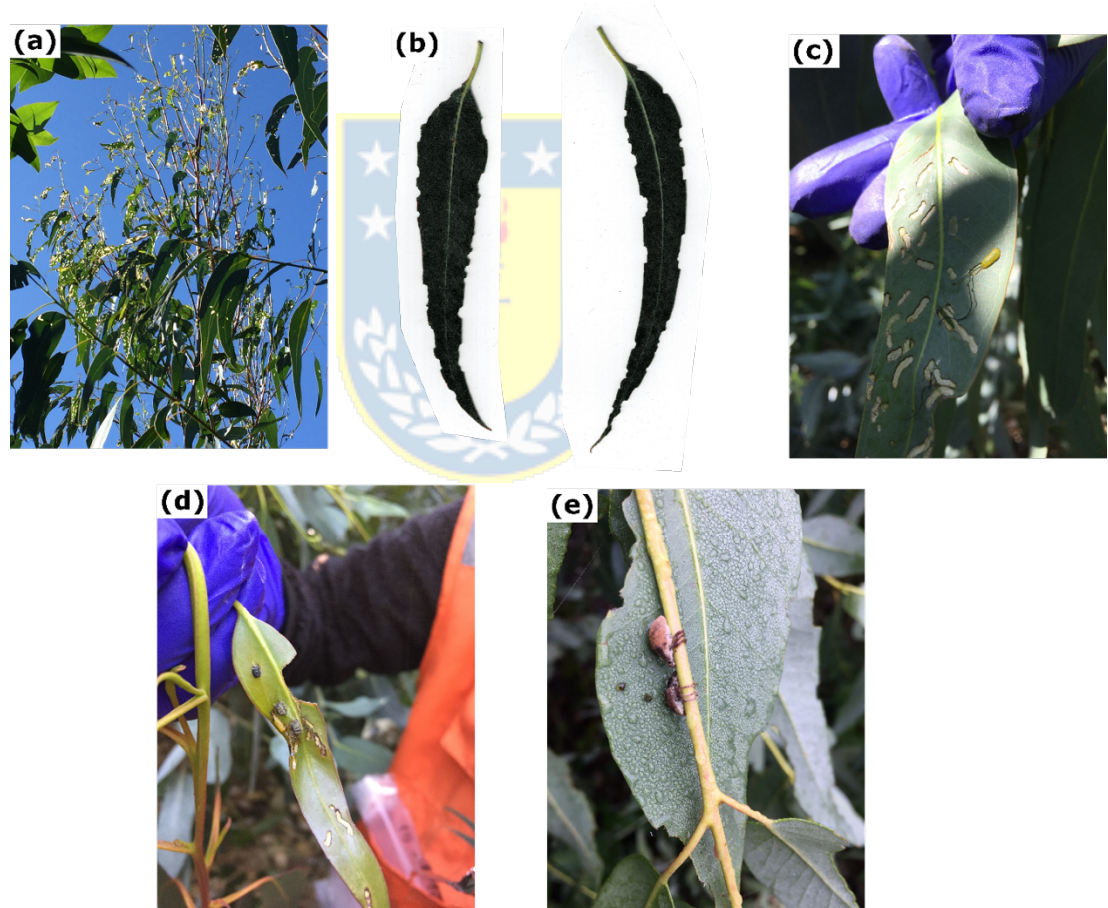
Fig. S2. Photos evidencing the *G. platensis* attack in the experimental field on March 22nd, 2019. **(a)** Tree crown defoliation by adults and larvae.

(b) Scalloped edges of petiolate leaves due to adult feeding. **(c)** Loss of photosynthetic tissues in a leaf due to larvae feeding. **(d)** Three oothecae (greyish capsules which each containing eight eggs approx.) in a leaf surface. **(e)** Two adults sighted in the field.
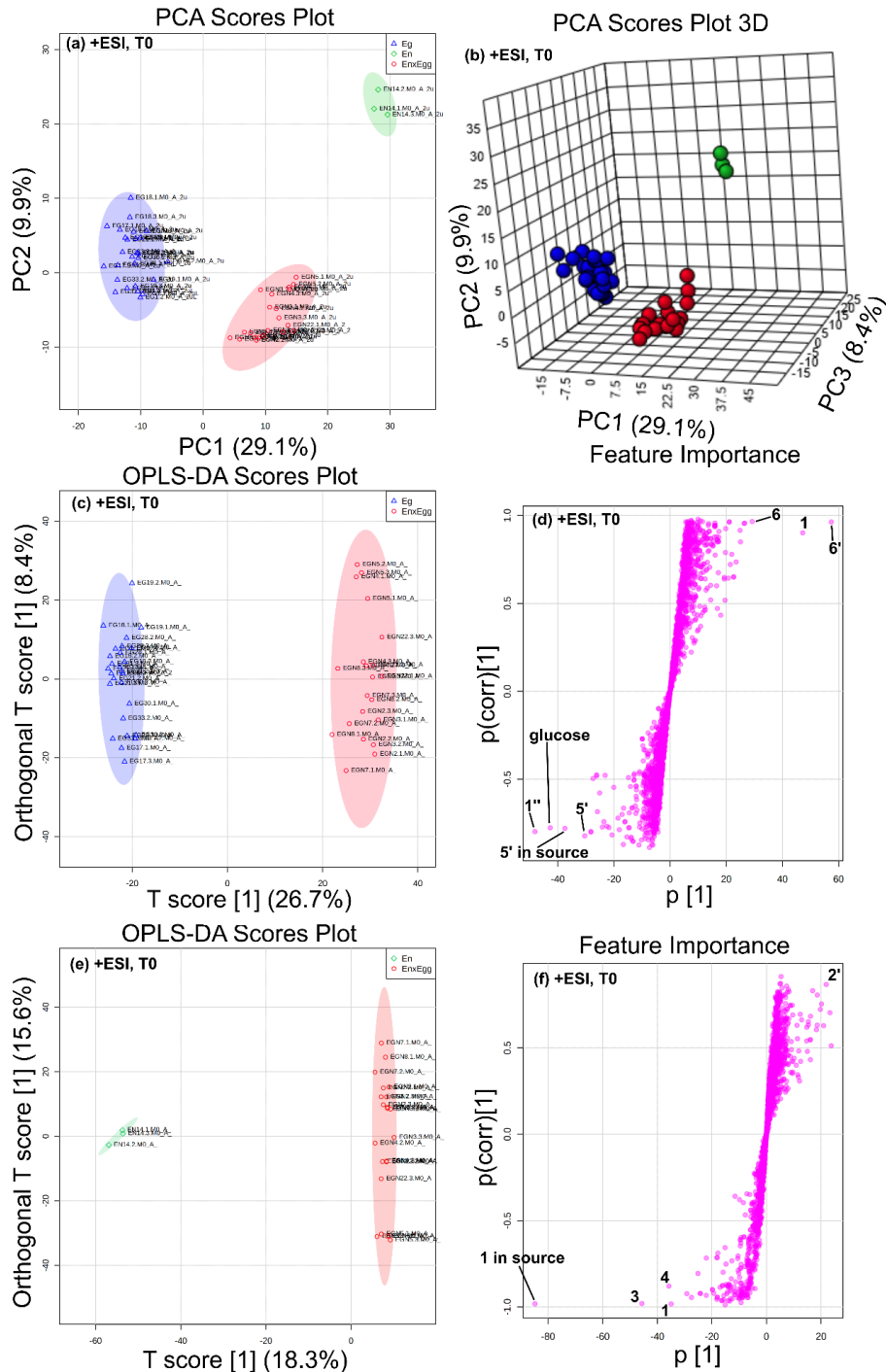
Fig. S3. Results of the multivariate statistical models based on the LC-

MS dataset acquired in +ESI mode for distinguishing differential constitutive

metabolome expressed in the leaves of *En×Egg* genotypes regarding the parent species *Eg* and *En*. (**a**) Scores plot of the PCA model showing species-specific clustering pattern between the first two principal components (PC1 and PC2), where blue triangles, green diamonds, and red circles represent *Eg*, *En*, and *En×Egg* samples with their 95% confidence intervals (shadowed regions), respectively. (**b**) Scores plot of the same PCA model incorporating the third PC for a 3D projection of sample distribution. (**c** and **e**) Scores plot of the OPLS-DA models showing separation of samples labeled as *En×Egg* (red circles) from that of *Eg* (blue triangles) and *En* (green diamonds), with their 95% confidence intervals (shadowed regions). In this regression method, LC-MS data was used as the *X*, and the binary vector *Y* was formed with the value of 0 for *Eg* or *En* class and 1 for *En×Egg*. The *Y*-predictive component (T score [1]) plotted on the *x*-axis represents the variance in the dataset correlated to class separation, while the orthogonal component plotted on the *y*-axis refers to the uncorrelated variance for class distinction. (**d** and **f**) S-plot of the OPLS-DA models for visualizing the feature influence in the predictive component, combining covariance (p[1]) and correlation (p(corr)[1]) loading profiles. Covariance plotted on the *x*-axis indicates the contribution of features to the predictive component, while correlation on the

y-axis spans between ±1 as the reliability has a theoretical minimum of -1 and a maximum of +1 to predict class 1 (*En×Egg*). Features displayed on the right-hand side contribute to class separation by high correlation with label *En×Egg* ($Y = 1$), and those shown on the left-hand side contribute to separation by high correlation with label *Eg* or *En* ($Y = 0$). Thus, significant features were selected by combining the highest possible covariance with correlation >|0.5|. Their numbers were assigned according to Table 2.

Fig. S4. Cross-validated random permutation test with 1000 permutations for OPLS-DA models: (**a**) between *En×Egg* and *Eg* in –ESI mode; (**b**) between *En×Egg* and *Eg* in +ESI mode; (**c**) between *En×Egg* and *En* in –ESI mode; (**d**) between *En×Egg* and *En* in +ESI mode.
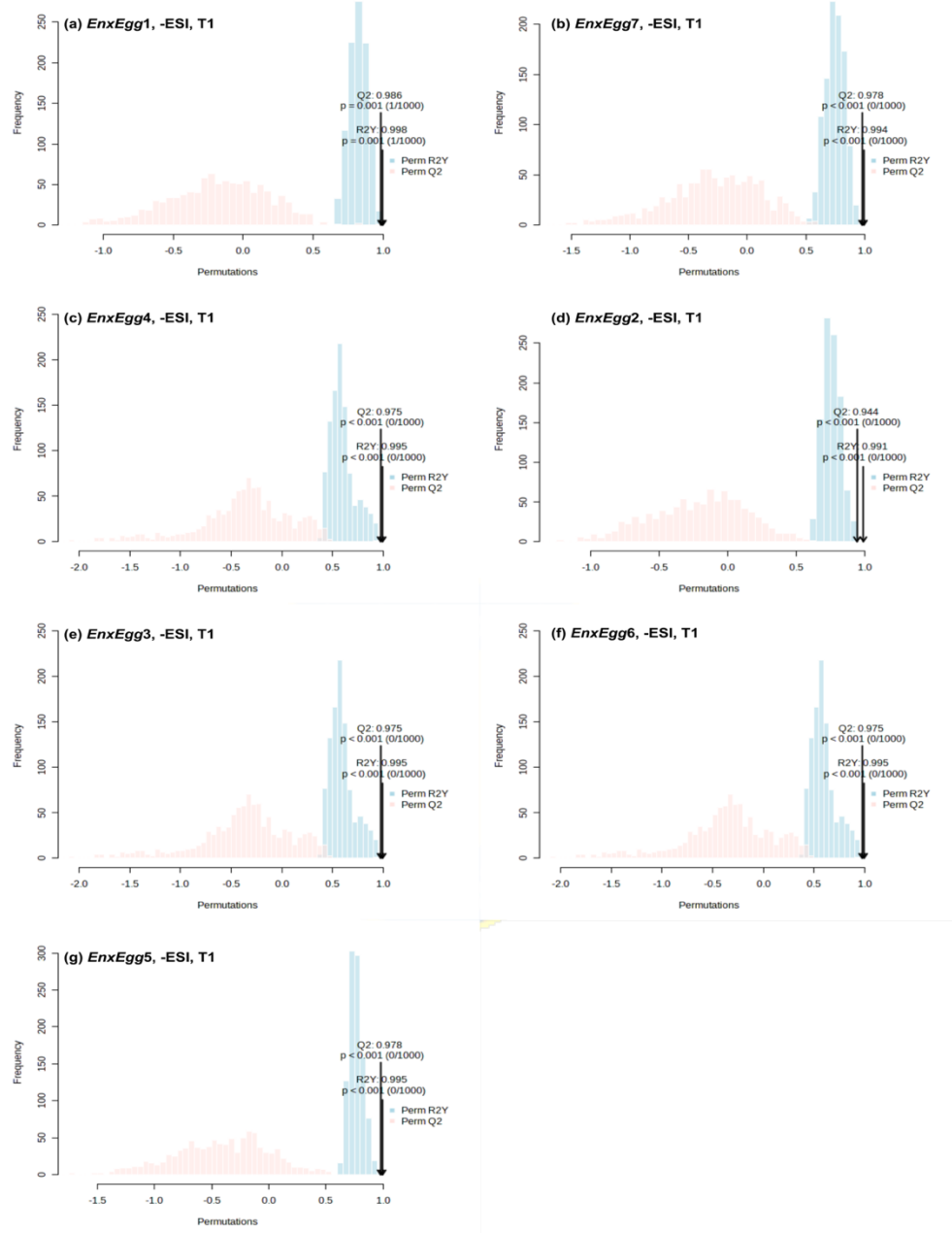
Fig. S5. Cross-validated random permutation tests with 1000 permutations for OPLS-DA models applied to the –ESI dataset of each *En×Egg* genotype.
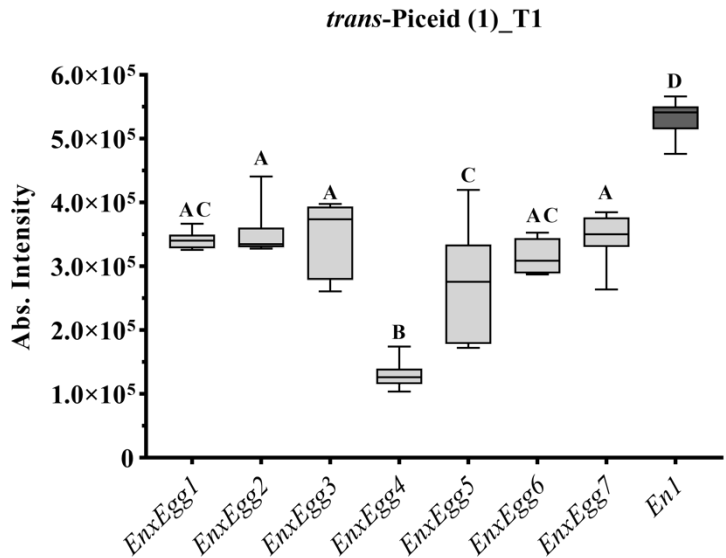
Fig. S6. Comparative levels for the stilbenes *trans*-Piceid (**1**) in the leaves of *En×Egg* genotypes with that in *E. nitens* at T1 (under herbivory). Quantitative data are presented as box-and-whisker diagrams, showing the median of values distribution (horizontal line in the box), the 25% (lower horizontal line of the box) and 75% (upper horizontal line of the box) quartiles, and grey whiskers indicating the extremes lower and upper values. Individual data were first tested for normal Gaussian distribution and then subjected to an ordinary one-way ANOVA to compare the mean level in each genotype with the mean level of every other genotype including *En*1. Tukey's test was used for multiple comparisons of the mean levels, where statistical

significance was set at *p* < 0.05. The same letter over the boxes of a graphic indicates a no-significant difference.
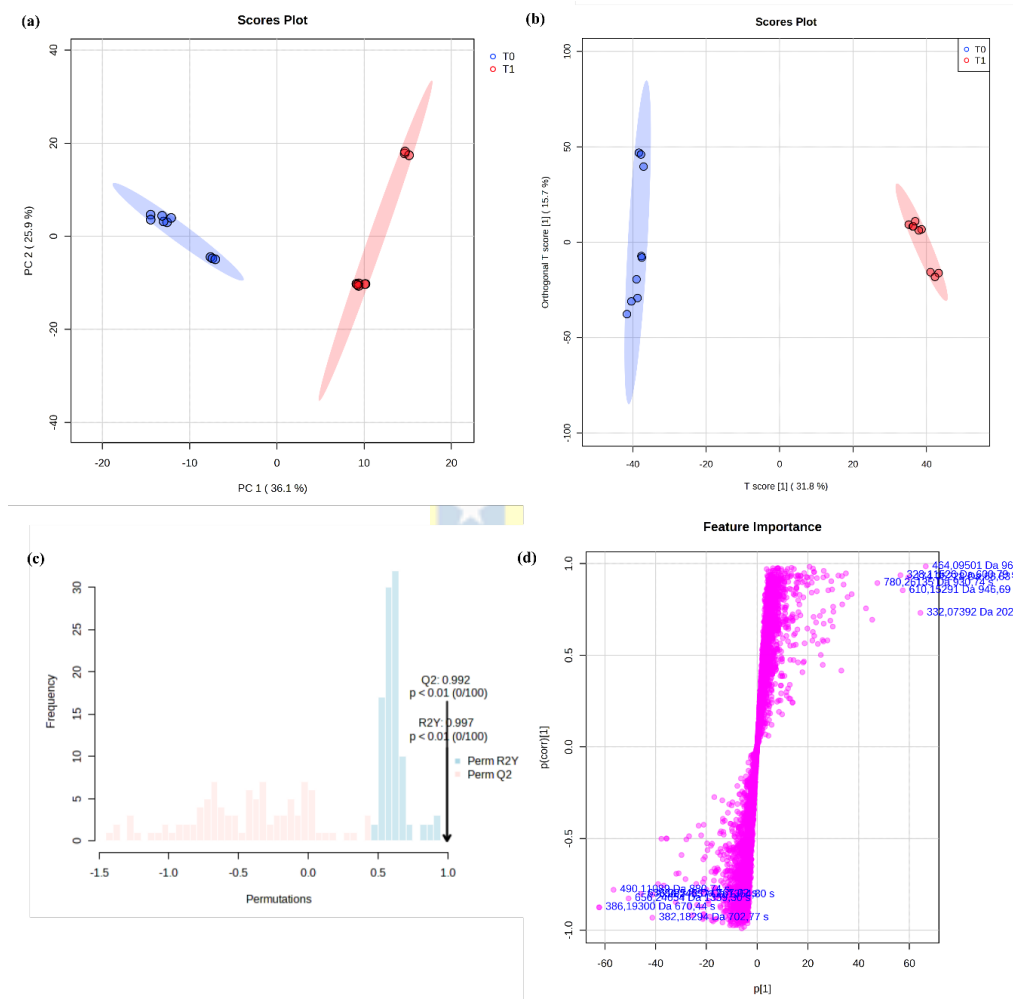
Fig. S7. Results of the multivariate statistical models based on the LC-MS dataset acquired in -ESI mode for distinguishing the metabolome changes in the leaves of *E. nitens* before and after *G. platensis* herbivory (T0 vs T1). (**a**) Scores plot of the PCA model showing clustering pattern between the first

two principal components (PC1 and PC2), where blue and red circles represent samples of the same trees before and under herbivory, respectively, with their 95% confidence intervals (shadowed regions). (**b**) Scores plot of the OPLS-DA model showing separation of samples labeled as T0 from that of T1, with their 95% confidence intervals (shadowed regions). (**c**) Cross-validated random permutation test with 100 permutations for the OPLS-DA model. (**d**) S-plot of the OPLS-DA model for visualizing the feature influence in the predictive component, combining covariance (p[1]) and correlation (p(corr)[1]) loading profiles. Covariance plotted on the *x*-axis indicates the contribution of features to the predictive component, while correlation on the *y*-axis spans between ±1 as the reliability has a theoretical minimum of -1 and a maximum of +1 to predict class 1 (T1). Features displayed on the right-hand side contribute to class separation by high correlation with label T1, and those shown on the left-hand side contribute to separation by high correlation with label T0.

Table S1. Severity of defoliation produced by *G. platensis* in hybrid genotypes and parent selected species [a].

Species	Severity of defoliation [b]	
	T0	T1
*En×Egg*1	0G	2G
*En×Egg*2	0G	3G
*En×Egg*3	0G	2G
*En×Egg*4	0G	3G
*En×Egg*5	0G	3G
*En×Egg*6	0G	2G
*En×Egg*7	0G	1G
En1	0G	0G
Eg1,5,9	0G	4G

[a] 0G: absence of defoliation; 1G: minimum damage; 2G: moderate damage; 3G: intense defoliation; 4G: severe defoliation with the loss of total apex foliage.

[b] Evaluated on February 22nd and March 22nd, 2019, during the first and second sampling times (T0 and T1) (Method S2).

295

Method S1. Weather conditions during sampling.

According to the stations of the Chilean Meteorological Department, located at Los Angeles (37°29'06.3"S 72°21'00.8"W) (code 370033), the weather conditions during the first sampling day, T0, on February 22nd, 2019, were as fallow: mean maximum and minimum temperatures of 26.2 ºC and 12 ºC; mean of relative humidity 59.0 %, with 69.9 % for the day of sampling; rainfall of 0.0 mm for the day of sampling and 0.22 mm accumulated during the month. During second sampling point, T1, on March 22nd, 2019, were as fallow: mean maximin and minimum temperatures of 26.2 ºC and 11.8 ºC; mean of relative humidity 60.5 %, with 65.7% for the day of sampling; rainfall of 0.0 mm for the day of sampling and 5.4 mm accumulate rainfall for the month.

**Method S2.** Visual estimation of defoliation severity caused by *G. platensis*.

The first prospection was done on February 22nd during the first sampling time, T0, where crowns of the trees of all considered *Eucalyptus* species and genotypes were carefully checked to ensure the foliage was

healthy and without weevil-feeding signals. A month later, during the second sampling (T1) on March 22nd (summer season), all trees were inspected again, seeking defoliation signs. According to the empirical records of the Chilean Consortium for Forest Phytosanitary Protection (CPF S.A., https://www.cpf.cl/), one of the massive annual peaks of weevil occurrence and reproduction usually take place in summer between January and April. Indeed, during this second sampling time, different stages of *G. platensis* development were sighted in the field, with severe damage caused in the tree crown of several genotypes. For estimation of defoliation severity, crown foliage of the four central trees of each genotype plot was visually examined for damage caused by adults and larvae. To defoliation percentage observed on the crowns as an average of the four central trees, a scale of the damage was assigned to each genotype. The scale consisted of five levels, where 0G corresponds to 0% of defoliation, 1G to 1-10% (minimum), 2G to 10-20% (moderate), 3G to 20-50% (intense), and 4G to >50% (severe).

3. **Material suplementario: La metabolómica no-dirigida revela la regulación de fitoanticipinas inducida por el estrés hídrico en *Eucalyptus*, sugiriendo la preparación para el ataque de plagas.**

Figura S1. Fotos originales de plantas de *Eucalyptu*s en el invernadero ubicado en la Universidad de Concepción (36°50'05.2"S 73°01'56.9"W) para el experimento de déficit hídrico. (a) plantas al inicio del experimento. (b) plantas después de 20 días de exposición al déficit hídrico. Se incluyen las seis especies de estudio Eg, En (En1 y En2), Es, Eb, Ec×Egg, En×Egg (1– 4), cada planta tratamiento cuenta su planta control.
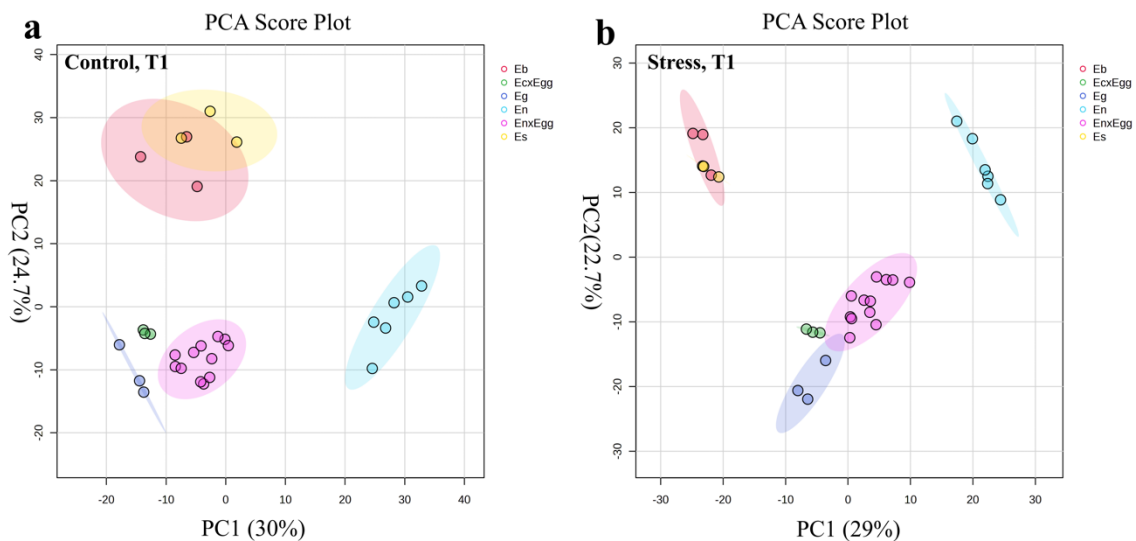
Figura S2. Se utilizó Análisis de Componentes principales (PCA) para las siete especies de *Eucalyptus* en modo de ionización negativa (+ESI) en el experimento de sequía. (**a**) Grupos control correspondiente a plantas sin estrés por restricción hídrica en la instancia de muestreo T1. (**b**) Grupos

tratamiento correspondiente a plantas con estrés severo por restricción hídrica durante 20 días en la instancia de muestreo T1 (2.5MPa). Los ejes *x* e *y* representan el primer y segundo componente principal (PC), y la etiqueta de cada eje incluye el porcentaje de la varianza total explicada por el componente correspondiente.
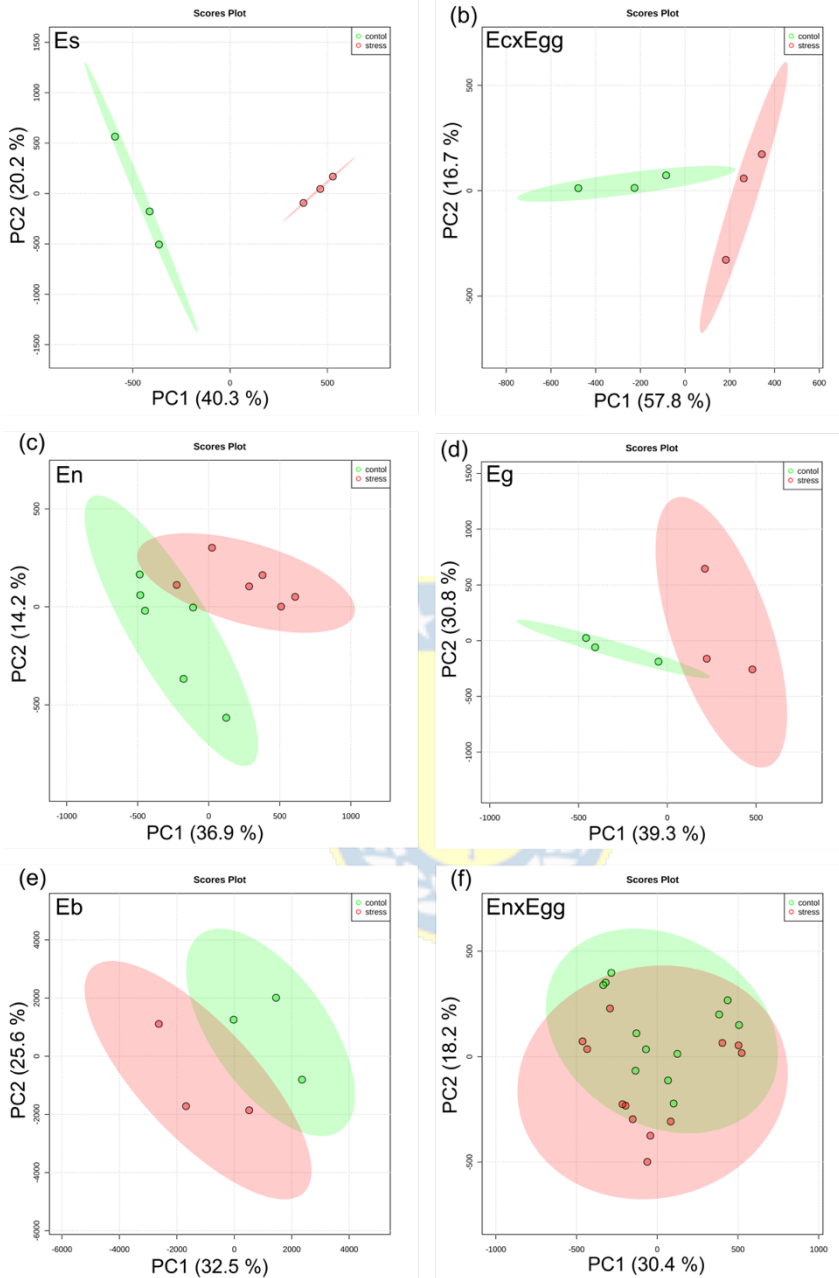
Figura S3. Se utilizó el Análisis de Componentes Principales (PCA) para evaluar las tendencias en la composición química de las especies de

*Eucalyptu*s sometidas a estrés por sequía severa (T1) en el modo de ionización negativa (ESI+). Gráfico de score (muestras) para (a) *E. smithii* (Es), (b) E. *camaldulensis* × *E. globulus* (Ec×Egg), (c) *E. nitens* (En), (d) *E. globulus* (Eg), (e) *E. badjensis* (Eb), (f) *E. nitens* × *E. globulus* (En×Egg).
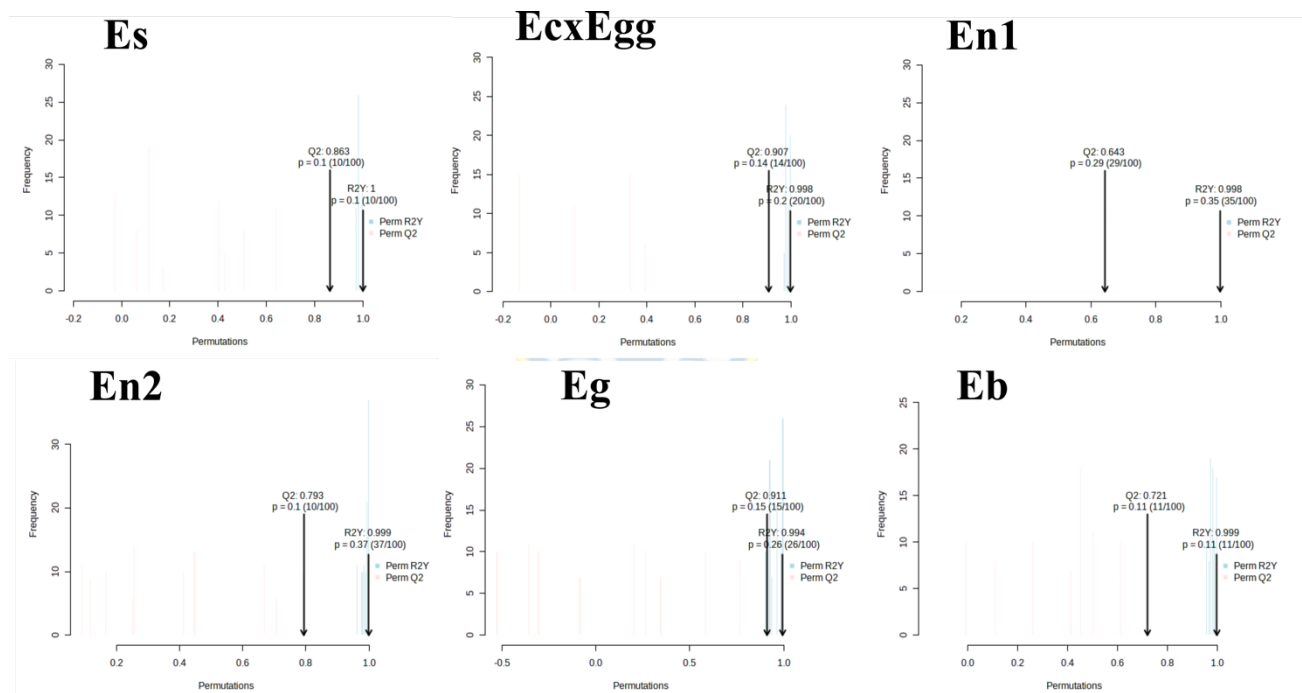

Figura S4. Validación de modelos OPLS-DA para cada una de las especies de E*ucalyptus* mediante la prueba de permutación aleatoria de pertenencia de clases con 100 permutaciones y la validación cruzada interna, que muestra

los parámetros estadísticos $Q^2 > 0.7$ y $R^2Y > 0.993$ para la mayoría de los modelos a excepción del genotipo En1 con $Q^2 = 0.65$.
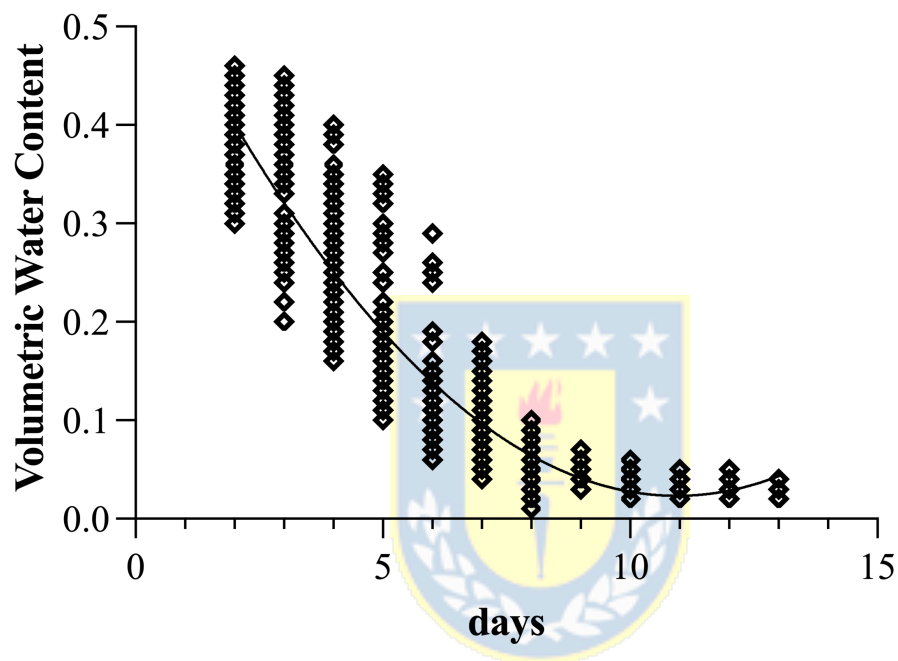
Figura S5. Gráfica del contenido volumétrico de agua para el sustrato de plantas tratamiento sequía *E. smithii* (Es), E. *camaldulensis* × *E. globulus* (Ec×Egg), *E. nitens* (En), *E. globulus* (Eg), *E. badjensis* (Eb), *E. nitens* × *E. globulus* (En×Egg) durante el experimento durante 13 días. Se observa un contenido decreciente de agua.
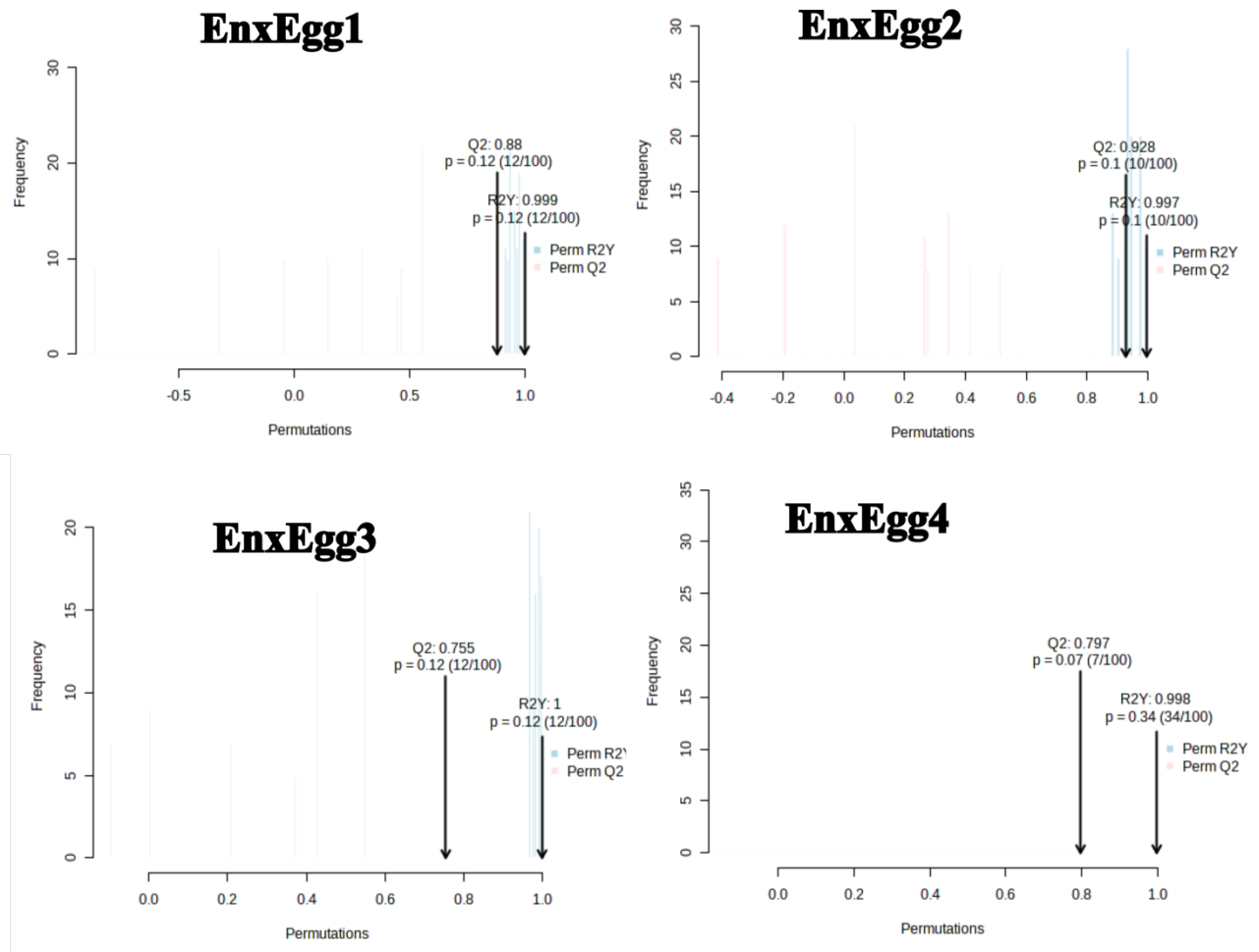
Figura S6. Validación de modelos OPLS-DA para cada una de las especies de E*ucalyptus* mediante la prueba de permutación aleatoria de pertenencia de clases con 100 permutaciones y la validación cruzada interna, que muestra los parámetros estadísticos con valores para $Q^2 > 0.775$ y $R^2Y > 0.997$ para los modelos de las especies híbridas *En×Egg*.